Guiding-center models for edge plasmas and numerical simulations of isolated plasma filaments

Madsen, Jens

Publication date:
2010

Document Version
Publisher's PDF, also known as Version of record

Guiding-center models for edge plasmas and numerical simulations of isolated plasma filaments

Risø-PhD-Report

Jens Madsen
Risø-PhD-65(EN)
September 2010

Risø DTU
National Laboratory for Sustainable Energy

Author: Jens Madsen

Title: Guiding-center models for edge plasmas and numerical simulations of isolated plasma filaments

Department: Plasma Physics and Technology Programme

This thesis is submitted in partial fulfillment of the requirements for the Ph.D. degree at DTU

Report number: Risø-PhD-65(EN)
Publication date: September 2010

Abstract:

The work presented in this thesis falls into two categories: development of reduced dynamical models applicable to edge turbulence in magnetically confined fusion plasmas and numerical simulations of isolated plasma filaments in the scrape-off layer region investigating the influence of finite Larmor radius effects on the radial plasma transport.
The coexistence of low-frequency fluctuations, having length scales comparable to the ion gyroradius, steep pressure gradients and strong E × B-flows in the edge region of fusion plasmas violates the standard gyrokinetic ordering. In this thesis two models are presented that overcome some of the difficulties associated with the development of reduced dynamical models applicable to the edge.
Second order guiding-center coordinates are derived using the phasespace Lie transform method. Using a variational principle the corresponding Vlasov-Maxwell equations expressed in guiding-center coordinates are derived including a local energy theorem. The second order terms describe lowest order finite Larmor radius effects. This set of equations might be relevant for edge plasmas due to the capability of capturing strong E ×B -flows and lowest order finite Larmor radius effects self-consistently.
Next, an extension of the existing gyrokinetic formalism with strong flows is presented. In this work the background electric fields is dynamical, whereas earlier contributions did only incorporate a stationary electric field. In an ordering relevant for edge plasma turbulence, fully electromagnetic second order gyrokinetic coordinates and the corresponding gyrokinetic Vlasov-Maxwell equations are derived, including a local energy theorem. By taking the polarization and magnetization densities in the drift kinetic limit, we present the gyrokinetic Vlasov-Maxwell equations in a more tractable form, which could be relevant for direct numerical simulations of edge plasma turbulence.
Finally, an investigation of the influence of finite Larmor radius effects on the radial transport of isolated plasma filaments (blobs) in the scrape-off region of fusion plasmas is presented. We employ an isothermal electrostatic two-dimensional gyrofluid model to simulate the blob dynamics. The numerical simulations show that, to lowest order, the blob center of mass velocity scales as the acoustic speed times the square root of the ratio of the structure size to the gradient lengthscale of the magnetic field, in agreement with earlier results. However, when the ratio of the thermal ion gyroradius to the structure size exceeds $10 - 20$ % the transport is dramatically enhanced. Having traveled its own initial size 15 times, blobs carry ~ 80 % of their initial density above this threshold but only ~ 20 % below. This observation demonstrate the importance of finite Larmor radius effects in plasma transport modeling.

ISBN 978-87-550-3844-8

Group's own reg. no.:
1710019-35

Sponsorship:
This work was supported financially by The Danish Council for Independent Research, Natural Sciences (FNU). Grant No. 09-062293.

Pages: 151

Guiding-center models for edge plasmas and numerical simulations of isolated plasma filaments

Jens Madsen

Abstract

The work presented in this thesis falls into two categories: development of reduced dynamical models applicable to edge turbulence in magnetically confined fusion plasmas and numerical simulations of isolated plasma filaments in the scrape-off layer region investigating the influence of finite Larmor radius effects on the radial plasma transport.

The coexistence of low-frequency fluctuations, having length scales comparable to the ion gyroradius, steep pressure gradients and strong $\boldsymbol{E} \times \boldsymbol{B}$-flows in the edge region of fusion plasmas violates the standard gyrokinetic ordering. In this thesis two models are presented that overcome some of the difficulties associated with the development of reduced dynamical models applicable to the edge.

Second order guiding-center coordinates are derived using the phase-space Lie transform method. Using a variational principle the corresponding Vlasov-Maxwell equations expressed in guiding-center coordinates are derived including a local energy theorem. The second order terms describe lowest order finite Larmor radius effects. This set of equations might be relevant for edge plasmas due to the capability of capturing strong $\boldsymbol{E} \times \boldsymbol{B}$-flows and lowest order finite Larmor radius effects self-consistently.

Next, an extension of the existing gyrokinetic formalism with strong flows is presented. In this work the background electric fields is dynamical whereas earlier contributions did only incorporate a stationary electric field. In an ordering relevant for edge plasma turbulence, fully electromagnetic second order gyrokinetic coordinates and the corresponding gyrokinetic Vlasov-Maxwell equations are derived, including a local energy theorem. By taking the polarization and magnetization densities in the drift kinetic limit, we present the gyrokinetic Vlasov-Maxwell equations in a more tractable form, which could be relevant for direct numerical simulations of edge plasma turbulence.

Finally, an investigation of the influence of finite Larmor radius effects on the radial transport of isolated plasma filaments (blobs) in the scrape-off region of fusion plasmas is presented. We employ an isothermal electrostatic two-dimensional gyrofluid model to simulate the blob dynamics. The numerical simulations show that, to lowest order, the blob center of mass velocity scales as the acoustic speed times the square root of the ratio of the

structure size to the gradient lengthscale of the magnetic field, in agreement with earlier results. However, when the ratio of the thermal ion gyroradius to the structure size exceeds $10 - 20\,\%$ the transport is dramatically enhanced. Having traveled its own initial size 15 times, blobs carry $\sim 80\,\%$ of their initial density above this threshold but only $\sim 20\,\%$ below. This observation demonstrate the importance of finite Larmor radius effects in plasma transport modeling.

Acknowledgements

First I would like to thank my thesis advisors Volker Naulin, Anders H. Nielsen and Jens Juul Rasmussen, for their continuous support and guidance, and for giving me the opportunity to work on the subjects that interested me the most. Also I would like to thank Taik Soo Hahm for hosting my visit at PPPL and patiently answering my questions.

I would like to acknowledge fruitful discussions with: Odd Erik Garcia, Jeppe Strøm Laursen, Stefan Kragh Nielsen, Morten Stejner Pedersen, Bruce D. Scott and Mirko Salewski.

Finally, I would like to thank my wife, Nanna, for supporting me during this period.

This work was supported financially by The Danish Council for Independent Research, Natural Sciences (FNU). Grant No. 09-062293.

Contents

Chapter 1

Introduction

Two major challenges must be faced in order to solve the present day and future energy supply problem. First, a secure and affordable energy supply must be guaranteed to the ever-growing population of the earth and secondly, the energy consumption must be reduced and energy sources must be found that are not harmful to the environment. Controlled thermonuclear fusion is a potential large scale *green* energy source, releasing no greenhouse gases and impose no hazards to the surrounding environment.

Up until now the most successful setup for thermonuclear fusion is the so-called tokamak device (see Fig. 1.1). The main idea is to confine the plasma in a toroidal chamber using a strong toroidal magnetic field superimposed by a weaker poloidal magnetic field. Historically, this design demonstrated

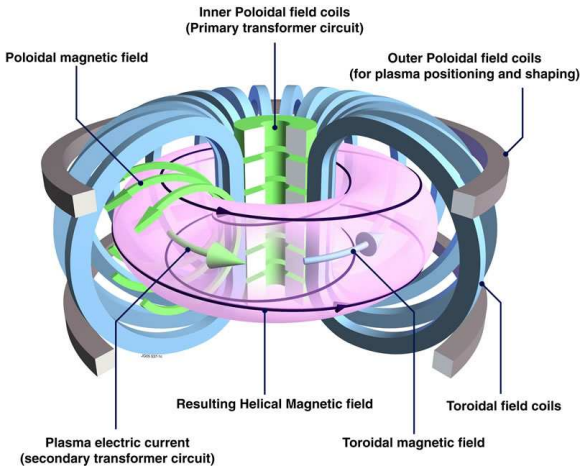

Figure 1.1: Schematic view of the tokamak design.

a rapid progress in achieved energy density but did also reveal that the energy confinement time was much shorter than what was predicted by classical transport theory where the diffusion processes are determined by

collisional processes. Classical transport theory was extended to account for the geometrical effects of the curved magnetic in the *neo-classical* transport theory, but the confinement times according to neo-classical theory were still significantly longer than what was achieved experimentally. It was soon realized that this *anomalous* energy and particle transport was a result of low frequency (in comparison to the plasma frequency) microsinstabilities primarily driven by density and pressure gradients. The notion *microinstabilities* was chosen to distinguish the instabilities from large scale (machine size) MHD instabilities. Microinstabilities lead to an increased fluctuation level (microturbulence) (see review e.g. Wooton[103]). The characteristic temporal scale of the fluctuations is on the order of the diamagnetic frequency $\omega^*/2\pi \sim 10^5\,\mathrm{Hz}$ and the spatial scales are of the order of the ion gyroradius $\rho_i \sim 0.1\,\mathrm{cm}$.

To explain and understand the microturbulence, a theoretical model was needed. Due to high temperatures in fusion plasmas it is safe to consider the plasma as being *collisionless* in most regions of a fusion device, which therefore ruled out classic collisional fluid models. A collsionless plasma is most naturally described by the Vlasov equation which only incorporates particle interaction through grazing collisions described by the corresponding Maxwell equations. However, the Vlasov equation contains very short time (plasma frequency $\omega_{pe}/2\pi \sim 10^{11}\,\mathrm{Hz}$) and spatial scales (Debye length $\lambda_D \sim 10^{-5}\,\mathrm{m}$) which must be seen in relation to the fusion device operation time scale ($\sim 1\,\mathrm{s}$) and the machine size ($\sim 1\,\mathrm{m}$). This shows that the Vlasov equation describes physical mechanisms disparate by several orders of magnitude. A model which is more focused on the relevant temporal and spatial scales is therefore necessary, especially when the dynamics is investigated using numerical methods. The complexity of the highly nonlinear (6+1) dimensional Vlasov equation is way beyond the capability of present day and near future computing power. These observations motivated the development of reduced dynamical models.

When the magnetic field is static and the no electric field is present, the trajectory of a charged particle is a helix centered around a magnetic field line (see Fig. 1.2). The particle motion consists of free streaming along magnetic field lines and a circular *cyclotron* motion in the plane perpendicular to the magnetic field. The magnetic dipole moment $\mu = mv_\perp^2/(2B_0)$ associated with the area traced out by the charged particle in the perpendicular plane is invariant. From the Euler-Lagrange equation[45]

$$\frac{d}{dt}\frac{\partial L}{\partial \dot{q}_j} - \frac{\partial L}{\partial q_j} = 0, \tag{1.1}$$

we make the key observation that if the Lagrangian does not contain the coordinate q_i, the generalized momentum

$$p_i = \frac{\partial L}{\partial \dot{q}_i}, \tag{1.2}$$

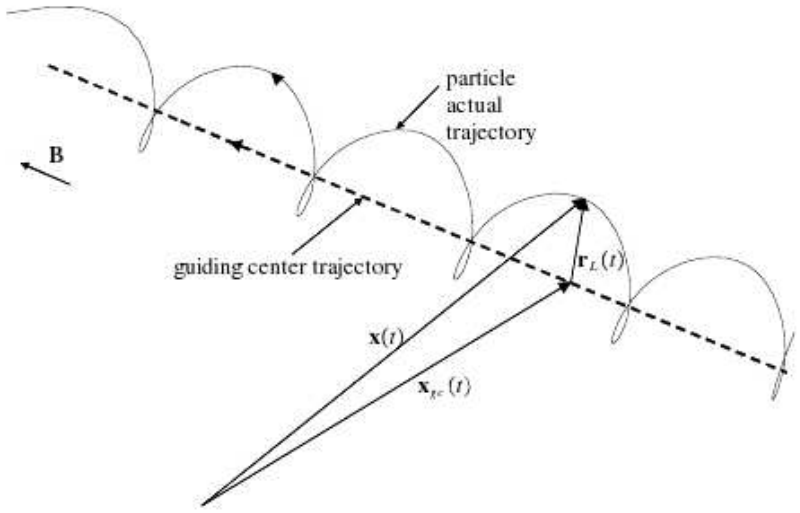

Figure 1.2: Cyclotron motion of a charged particle around a magnetic field line.

conjugate to q_i, is a conserved quantity. Therefore, if the physical conditions in a plasma are such that the magnetic moment is approximately conserved, a coordinate transformation having μ and the conjugate coordinate as coordinates reduce the dimensionality of the problem. In 1940 Alfvén[2] showed that μ is the adiabatic invariant associated with the fast cyclotron motion of charged particles around magnetic field lines, which is conjugate to the phase angle θ of the circular motion in the perpendicular plane. Due to the strong confining toroidal magnetic field in magnetic fusion devices, the angular frequency of the cyclotron motion is relatively high $\Omega = qB/m \sim 10^7 - 10^{11}$ rad/s, at least one order of magnitude larger than the characteristic frequency of the microturbulence associated with the observed anomalous transport.

In this thesis we are concerned with reduced dynamical models which utilize the intrinsic quasi-symmetry of the cyclotron motion to *decouple* the associated fast timescale. In the reduced dynamical models the dynamical evolution of the axis of the helical motion, the *guiding-center*, replace the detailed motion of the particle. That being said, the decoupling is carried out such that the essential physical finite Larmor radius (FLR) effects of the cyclotron motion is retained. The averaged electric field experienced by a particle during a Larmor orbit generally differs from the field at the center of gyration. FLR effects are therefore able to influence the transport properties in regions where the gradient lengthscale of macroscopic quantities is comparable to the (Larmor) radius of the circular motion in the perpendicular plane.

In fusion devices the adiabatic invariant μ is relatively robust. In general the quasi-symmetry persists when: (i) the gradient lengthscale of the low frequency electromagnetic field is long compared to the radius of the circular orbit or (ii) if the fluctuation amplitude is small in comparison with the background fields (not necessarily low frequency). A dynamical reduction based on the assumption of low frequency long gradient scalelength electromagnetic fields leads to so called *guiding-center* models[2, 73]. Models based on a low fluctuation amplitude ordering are denoted *gyrokinetic* models (e.g. Ref. [84, 40]). The development of the latter was motivated by the wish to study the low frequency microturbulence associated with the anomalous transport. The introduction of low frequency, low amplitude, short wavelength fluctuations destroys the guiding-center adiabatic invariant μ. Historically, gyrokinetic models extended existing guiding center models constructing a new adiabatic invariant making up for this shortcoming of guiding-center theories.

Gyrokinetic models[19] play a major role in analytical and numerical investigations of nonlinear low frequency microturbulence. Originally, they were developed to study the confinement region of fusion devices where fluctuation amplitudes are mild and the gradient lengthscales of macroscopic quantities are long compared to the turbulence lengthscale. In the original formulation the theory is not applicable to the edge and scrape off layer (SOL) regions of tokamak plasmas. In the edge region, just inside the last closed flux surface, steep pressure gradients are found[103]. Furthermore, a major part of the particle and energy transport in the SOL region is carried by field aligned *blob* like filaments[4, 71, 72, 93] having high fluctuation amplitudes. Steep gradients and high fluctuation amplitudes violate the gyrokinetic ordering. Nonetheless, experimental measurements of the ratio of ion to electron temperature $\tau = T_i/T_e$ show that typically $\tau \sim 1 - 2$ in the edge and even higher in the SOL region due to rapid parallel losses of energetic electrons[1, 104, 95, 80, 97], showing the potential importance of FLR effects. Therefore, traditional edge/SOL simulations using Braginskii[14] like fluid models are not strictly applicable.

Even more demanding is the modeling of improved confinement modes (H-mode[96]). The H-mode transition is characterized by a steepening of the radial pressure gradient, a significant decrease of the fluctuation levels measured in the SOL region and the formation of transport barriers. Experimental studies have shown that the transition from L-mode (Low confinement) to H-mode (High confinement) operation is associated with the formation of a strong radial sheared electric field E_{0r}, which persists throughout the H-mode[70, 23, 3]. Despite intensive theoretical and experimental research in the role played by E_{0r}, it is still unclear whether E_{0r} is causing or is a consequence of the H-mode. Unfortunately, the H-mode is impeded by quasi-periodic bursts of particles and energy, named edge localized modes (ELM's), deteriorating the plasma profile and are a potential

threat to the plasma facing components.

The high amplitude of E_{0r} violates the gyrokinetic low fluctuation amplitude ordering. Therefore, gyrokinetic theory treat the strong electric field by splitting the total electric field into a strong long gradient lengthscale part and a short wavelength low amplitude part[46, 20, 78, 48]. The disadvantage of dividing the electric field into two parts is that a simultaneous self-consistent solution of both parts becomes doubtful with the gyrokinetic theory available. Strong flows play a central role in the L-H mode transition and the H-mode itself, and it is reasonable to believe that a self-consistent treatment is required in order to reproduce a nonlinear turbulent equilibrium in direct numerical simulations. These observations has motivated other approaches[68] in which only drift kinetic FLR effects are retained but where the strong electrical field can be self-consistently obtained from a Poisson equation which resembles the gyrokinetic counterpart. This resemblance to the traditional gyrokinetic Poisson equation comes at the price of complicating the Hamiltonian and the associated equations of motion.

1.0.1 Contributions

The contributions presented in this work falls into two categories: (i) extensions of existing reduced Vlasov-Maxwell equations and (ii) numerical simulations of the radial transport of isolated plasma filaments in the scrape off layer region of magnetically confined plasmas.

In this thesis Vlasov-Maxwell equations are derived in the guiding-center and the gyrokinetic ordering. The main goal was to extend existing nonrelativistic theories such that they are applicable to edge turbulence. Figure 1.3 illustrates the regimes where the first order guiding-center and gyrokinetic (without background $\boldsymbol{E} \times \boldsymbol{B}$-flows) theories are valid in comparison to the work presented in this thesis. The figure shows the normalized potential $e\Phi/T_i$ as a function of $\epsilon_\perp \sim \rho_i/L_\perp$ which measures the ratio of the ion gyroradius to the perpendicular gradient lengthscales of the electromagnetic fields.

A derivation of second order guiding-center coordinates using the phase-space Lie transform method with time dependent electromagnetic fields is presented. The obtained result is identical to earlier contributions[59] where a more algebraically involved method was applied. The second order perturbation analysis is relevant because the second order terms describe the lowest order finite Larmor radius corrections to the electromagnetic fields. Specifically we identify the Baños [7] term as being an FLR correction to the background magnetic field. The Vlasov-Maxwell equations expressed in second order guiding center coordinates are explicitly derived including a local energy theorem. Earlier works did either not keep the second order contributions[90], derived the equations in the drift kinetic ordering[77] or did not explicitly derive the Maxwell equations[13]. All terms in the Maxwell

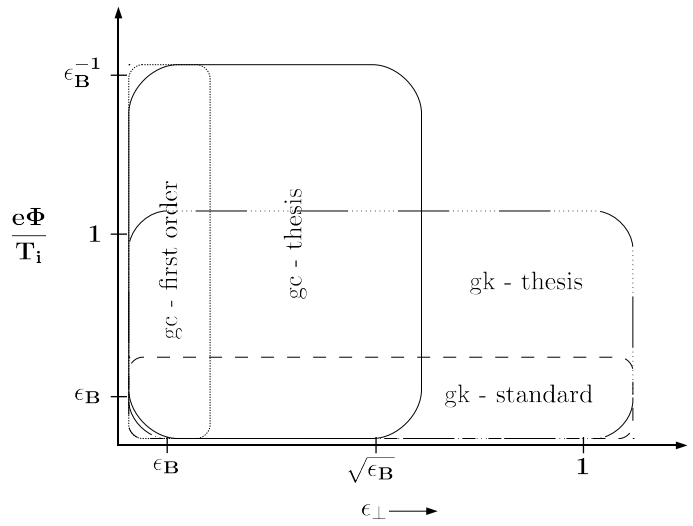

Figure 1.3: Regimes of validity of Vlasov-Maxwell equations expressed in first and second order guiding-center (gc) and in gyrokinetic (gk) coordinates with (this thesis) and without strong $\boldsymbol{E} \times \boldsymbol{B}$-flows. The plot shows the normalized electric potential $e\Phi/T_i$ as a function of $\epsilon_\perp \sim \rho_i/L_\perp$, where $L_\perp$ denotes the characteristic fluctuation lengthscale. $\epsilon_B \sim \rho_i/R$, where R lengthscale of the toroidal magnetic field.

equations are expressed in terms of "free" guiding-center charge, polarization charge and magnetization current, and new terms that arise from the second order analysis are discussed. This work on the guiding-center theory was published in Physics of Plasmas[65].

Another contribution described in this thesis is an extension of existing gyrokinetic theories with strong flows. Existing theories do only describe a stationary background electric field. In this work we include a time varying background electric field into the gyrokinetic theory. Fully electromagnetic perturbations are included in this work as it is believed that magnetic perturbations play a central role in the turbulent radial transport in the edge region[85, 87]. Second order gyrokinetic coordinates are derived in the Hamiltonian and symplectic formulations of gyrokinetics using the elegant phasespace Lie transform method[61]. This is to the knowledge of the author the first derivation of gyrokinetic coordinates with strong flows in the symplectic formulation. Energy conserving Vlasov-Maxwell equations, including a second Poisson equation associated with the background electric field, are derived using a variational principle which also provides the local energy flux density. By taking the polarization and magnetization densities in the long wave length (drift kinetic) limit we obtain Vlasov-Maxwell equations which are numerically tractable. In comparison with earlier con-

tributions several new terms are identified in the Maxwell equations, for example the diamagnetic plasma response to the perturbed magnetic field in the parallel Ampere equation and the polarization current which ensures polarization charge conservation. An article describing some of these results on the gyrokinetic theory is being prepared.

Finally, we present numerical simulations of the radial transport of isolated plasma filaments in the scrape-off layer region of fusion plasmas. Using a simple isothermal gyrofluid model, a parametric study has been performed investigating the influence of finite Larmor radius effects on the blob transport. The numerical simulations show that to lowest order the blob center of mass velocity scales as the acoustic speed times the square root of the ratio of the structure size to the gradient lengthscale of the magnetic field. However, when the ratio of the thermal ion gyroradius to the structure size exceeds $10 - 20\,\%$ the transport is dramatically enhanced. Having traveled its own initial size 15 times, blobs carry $\sim 80\,\%$ of their initial density above this threshold but only $\sim 20\,\%$ below. An article reporting on these findings is in preparation.

1.0.2 Outline

The rest of the thesis is organized as follows. In Chap. 2 the second order guiding-center coordinates are derived using a phasespace Lie transform method. From a variational principle the corresponding Vlasov-Maxwell equations expressed in guiding-center coordinates are derived. Second order fully electromagnetic gyrokinetic coordinates with strong time varying background $\boldsymbol{E} \times \boldsymbol{B}$-flows are presented in Chap. 3. The corresponding Vlasov-Maxwell equations are derived in general terms and in a limiting long wave length form tractable for numerical simulations. Numerical simulations of the radial transport of isolated plasma filaments in the scrape-off region of magnetically confined fusion plasmas are presented in Chap. 4. Conclusions are given in Chap. 5. A review of modern methods of classical mechanics, variational calculus and the Lie transform method is given in App.A. The chapters are self-contained and can in general be read independently.

Chapter 2

Guiding-Center Vlasov-Maxwell Equations

The work in this chapter was published in Physics of Plasmas, issue 17, p. 82107 (2010). I was the sole author of the manuscript. The work is a "by-product" of the effort of including strong dynamical electromagnetic fields into the gyrokinetic formalism. During the work with the gyrokinetic formalism, which is a perturbation of the guiding-center theory, I studied the guiding-center theory and concluded that no previous publication has shown a derivation of the second order guiding center coordinates using the modern phase space Lie transform method. Furthermore, the corresponding Vlasov-Maxwell equations including a local energy theorem was never published including second order terms, which include the lowest order finite Larmor radius corrections to the electromagnetic fields.

Incorporating a strong $\boldsymbol{E}\times\boldsymbol{B}$-flow in the gyrokinetic formalism has some serious disadvantages. The underlying quasi-symmetry of the Larmor orbit cannot exist in the presence of a short wavelength, strong electric field. Therefore, the electrical field is split into a strong long wavelength part and a short wavelength perturbation. Until now no self-consistent solution to the total electric field has been reported and it is questionable whether both parts of the electric field can be determined simultaneously within the present day gyrokinetic theory. Therefore, the guiding center Vlasov-Maxwell equations presented in this chapter could provide an alternative to the gyrokinetic formalism in situations where strong flows are important and the lowest order FLR corrections are sufficient. However, in comparison to the gyrokinetic formalism the resulting Maxwell equations are more complex and are not readily solvable by standard numerical methods.

2.1 Introduction

The motion of a charged particle in an electromagnetic field is in general extremely complex. The equations of motion are nonlinear and are in general not integrable. However, when the electromagnetic fields are "strong" and are changing slowly in space and time compared with the thermal gyroradius ρ_0 and the gyrofrequency Ω_0 respectively, the problem can be substantially simplified. Under such conditions the particle executes a rapid spiraling motion around its "guiding-center" on a time scale which is well separated from the slower time scales of the electromagnetic fields. This "gyromotion" is quasi-periodic and provides an adiabatic invariant $\mu_0 = \frac{mv_\perp^2}{2B}$. Therefore, a perturbative guiding-center coordinate transformation can be obtained which decouples the fast gyromotion and provides a dynamical invariant $\mu = \mu_0 + \cdots$.

Historically, guiding-center coordinates have been derived using different methods: a standard averaging approach, e.g., [73, 69], a "pseudo-canonical" form invariant Hamilton method , e.g., [99], a Darboux/Lie transform method [59] and a Lie transform method , e.g., [13, 20]. Previous results are not all identical. The discrepancies are caused by inherent degrees of freedom in the guiding-center transformation and different orderings of the electrical field E. The *drift ordering* assumes $E/(v_{th}B) \sim \epsilon \ll 1$, where v_{th} denotes thermal velocity, B denotes the magnetic field and $\epsilon \sim \rho_0 k_\perp \sim \omega/\Omega$ is the perturbation parameter where $k_\perp$ and ω are the characteristic inverse perpendicular scale length and frequency, respectively. With this ordering the $\boldsymbol{E} \times \boldsymbol{B}$-drift appears at the same order as the magnetic drifts[61]. The polarization drift does not enter the guiding-center equation of motion and no finite-Larmor-radius (FLR) effects are retained at the order to which the perturbative analysis is carried out. When the *guiding-center* ordering $E/(v_{th}B) \sim 1$ is applied[59] the polarization drift and the lowest order (FLR) corrections to the electromagnetic potentials appear at second order in the perturbation analysis. The *gyrokinetic ordering*[19] describes fluctuating electromagnetic fields assuming $k_\perp \rho_i \sim 1$ and $E/(v_{th}B) \sim \epsilon$ and is therefore not able to describe situations where strong flows are important, which is typically the case in the edge region of tokamak plasmas, e.g.,[23, 48]. To circumvent this problem the electromagnetic fields are split into equillibrium and perturbative parts[46, 78]. This splitting results in very complex equations making self-consistent calculations of the total fields complicated. The present work is motivated by the capability of the guiding-center ordering to treat strong flows and the lowest order FLR effects simultaneously without splitting the electromagnetic fields.

Self-consistent action principles for the Vlasov-Maxwell system were introduced by Low[64]. Expressed in first order guiding-center coordinates the self-consistent Vlasov-Maxwell system was first described by Pfirsch[76] in the drift ordering using the Hamilton-Jacobi equations. Similon[90] used a

mixed Lagrangian Eulerian variational principle to derive covariant Vlasov-Maxwell equations in the guiding-center ordering but only to first order. Boghosian[13] presented a covariant formulation of the Vlasov-Maxwell system in the guiding-center ordering to second order but did not derive explicit Maxwell equations, and treated the second order Baños term[7] different from the result presented here. To the knowledge of the author a self-consistent explicit Vlasov-Maxwell system has not been derived including second order terms in the guiding-center ordering. Earlier results are either derived in the drift ordering , e.g.,[77, 105, 76, 61] or are only taken to first order , e.g.,[100, 90].

In this paper we calculate guiding-center coordinates in the guiding-center ordering using the Lie transform method to second order in the perturbation analysis. The result agrees with Littlejohn[59] where the Darboux/Lie method was used. The derivation of second order guiding center coordinates using the Lie transformation method has not been presented before. We find that the Lie transformation method is the simplest method available. Another advantageous feature of the Lie transform method is that the generating vector fields of the transformation, used in pullback and push-forward representations of fluid moments, are readily available. Also, an explicitly ordered Poisson bracket and the corresponding equations of motion are presented. We discuss the FLR corrections to the electromagnetic fields arising from the second order analysis. We derive self-consistent Vlasov-Maxwell equations explicitly expressed in guiding-center coordinates. All terms arising from the second order perturbation analysis are retained. This extension of the guiding-center Vlasov-Maxwell equations is the principal result of this paper. It is of importance because it provides a set of equations capable of treating strong flows and lowest order FLR corrections to the electromagnetic fields without splitting the fields into equilibrium and perturbative parts. Also, we identify the polarization density and the magnetization and polarization current densities in the Maxwell equations. The system is derived from an action principle which by the Noether method provides us with an energy conservation law. Finally, we propose an ordering which makes the model applicable to the study of the edge regions of tokamak plasmas.

2.2 Single particle guiding-center dynamics

In this section we derive guiding-center coordinates for a single charged particle in an electromagnetic field. The problem is formulated in the Lagrangian phase space formalism introduced in Sec.2.2.1, where prelimenary coordinate transformations are carried out and the subject of gyrogauge invariance is reviewed. In Sec.2.2.2, the guiding-center oneform is derived using the Lie transformation method. In Sec.2.2.3, the Poisson bracket structure and the

equations of motion are obtained from the guiding-center oneform.

2.2.1 Preliminary transformations

The starting point of the derivation is the fundamental phase space Poincaré one-form[39] of a non-relativistic charged particle in an electromagnetic field expressed in canonical coordinates $(\boldsymbol{x}, \boldsymbol{p}, t)$

$$\gamma = \boldsymbol{p} \cdot d\boldsymbol{x} - \big[\frac{1}{2m}(\boldsymbol{p} - q\boldsymbol{A}(\boldsymbol{x}, t))^2 + q\phi(\boldsymbol{x}, t)\big]dt, \tag{2.1}$$

where m and q denote the particle mass and charge, respectively; ϕ is the electric potential and $\boldsymbol{A}$ denotes the magnetic vector potential. Throughout the paper the t-component of γ denotes the Hamiltonian: $-\gamma_t = H$.

Next, a coordinate transformation to the noncanonical *particle* coordinates $(\boldsymbol{x}, \boldsymbol{v}, t)$ is carried out, where $m\boldsymbol{v} = \boldsymbol{p} - q\boldsymbol{A}$. $(\boldsymbol{x}, \boldsymbol{v})$ denote the particle position and velocity respectively. Expressed in the particle coordinates the Poincaré one-form reads

$$\gamma = (q\boldsymbol{A} + m\boldsymbol{v}) \cdot d\boldsymbol{x} - (\frac{1}{2}mv^2 + q\phi)dt. \tag{2.2}$$

A coordinate transformation to *prelimenary* coordinates $(\boldsymbol{x}, \boldsymbol{v}, t) \rightarrow (\boldsymbol{x}, u_0, \mu_0, \theta_0, t)$ is performed in order to define the gyrophase θ_0 and introduce the adiabatic invariant, the magnetic dipole moment μ_0. The particle velocity

$$\boldsymbol{v} = \boldsymbol{D}(\boldsymbol{x}, t) + \hat{\boldsymbol{b}}(\boldsymbol{x}, t)u_0 + \boldsymbol{c}_\perp(\boldsymbol{x}, \mu_0, \theta_0, t) \tag{2.3}$$

is measured in a non-inertial frame moving with: $\boldsymbol{W} = \boldsymbol{D} + \hat{\boldsymbol{b}}u_0$. $\boldsymbol{D} = \frac{\boldsymbol{E}\times\hat{\boldsymbol{b}}}{B}$ denotes the $\boldsymbol{E} \times \boldsymbol{B}$-velocity, where $\boldsymbol{E} = -\nabla\phi - \frac{\partial}{\partial t}\boldsymbol{A}$ and $\boldsymbol{B} = \nabla \times \boldsymbol{A}$ are the electric and magnetic fields, respectively. $\hat{\boldsymbol{b}} = \boldsymbol{B}/B$ is the unit vector following the magnetic field lines; $\boldsymbol{c}_\perp = \sqrt{\frac{2\mu_0 B}{m}}\hat{\perp} = \Omega_0\boldsymbol{\rho}_0 \times \hat{\boldsymbol{b}}$ denotes the co-moving perpendicular velocity; $\Omega_0 = qB/m$ is the cyclotron frequency, and $\boldsymbol{\rho}_0$ denotes the gyroradius vector. The unit vectors $(\hat{\boldsymbol{\theta}}, \hat{\boldsymbol{b}}, \hat{\perp})$ form an orthonormal basis: $\hat{\boldsymbol{\theta}} \times \hat{\boldsymbol{b}} = \hat{\perp} = \frac{\partial\hat{\boldsymbol{\theta}}}{\partial\theta}$, following the particle trajectory. The gyroangle is defined as

$$\theta_0 = \arctan\big(\frac{\hat{\boldsymbol{e}}_1 \cdot \boldsymbol{c}_\perp}{\hat{\boldsymbol{e}}_2 \cdot \boldsymbol{c}_\perp}\big), \tag{2.4}$$

where $\hat{\boldsymbol{e}}_1$ and $\hat{\boldsymbol{e}}_2$ are local fixed orthonormal basis vectors which together with $\hat{\boldsymbol{b}}$ form a local orthonormal triad. The one-form (2.2) expressed in the preliminary coordinates reads

$$\gamma = \big[q\boldsymbol{A} + m\boldsymbol{W} + m\boldsymbol{c}_\perp\big] \cdot d\boldsymbol{x} - \big[\frac{1}{2}mW^2 + \frac{1}{2}m\boldsymbol{c}_\perp^2 + m\boldsymbol{W} \cdot \boldsymbol{c}_\perp + q\phi\big]dt, \tag{2.5}$$

where $\boldsymbol{W} = u_0\hat{\boldsymbol{b}} + \boldsymbol{D}$ is the zeroth order velocity.

The two sets of basis vectors are related as

$$\hat{\perp}(\boldsymbol{x}, \theta_0, t) = -\hat{\boldsymbol{e}}_1(\boldsymbol{x}, t)\sin\theta_0 - \hat{\boldsymbol{e}}_2(\boldsymbol{x}, t)\cos\theta_0, \tag{2.6}$$

$$\hat{\boldsymbol{\theta}}(\boldsymbol{x}, \theta_0, t) = \hat{\boldsymbol{e}}_1(\boldsymbol{x}, t)\cos\theta_0 - \hat{\boldsymbol{e}}_2(\boldsymbol{x}, t)\sin\theta_0. \tag{2.7}$$

Besides the requirements that $\hat{\boldsymbol{e}}_1$ and $\hat{\boldsymbol{e}}_2$ are perpendicular to $\hat{\boldsymbol{b}}$, form an orthonormal basis together with $\hat{\boldsymbol{b}}$ and are defined such that θ is smooth, $\hat{\boldsymbol{e}}_1$ and $\hat{\boldsymbol{e}}_2$ are arbitrary. No physical quantities should depend on the choice of $\hat{\boldsymbol{e}}_1$ and $\hat{\boldsymbol{e}}_2$. To be more specific a rotation of the $(\hat{\boldsymbol{e}}_1, \hat{\boldsymbol{e}}_2, \hat{\boldsymbol{b}})$ frame (a gyrogauge transformation)

$$\hat{\boldsymbol{e}}_1' = \hat{\boldsymbol{e}}_1\cos\alpha + \hat{\boldsymbol{e}}_2\sin\alpha, \tag{2.8}$$

$$\hat{\boldsymbol{e}}_2' = -\hat{\boldsymbol{e}}_1\sin\alpha + \hat{\boldsymbol{e}}_2\cos\alpha, \tag{2.9}$$

should not change physical quantities. α denotes a phaseshift of the gyroangle

$$\theta' = \theta + \alpha(\boldsymbol{x}, t). \tag{2.10}$$

No specific choice of $\hat{\boldsymbol{e}}_1$ and $\hat{\boldsymbol{e}}_2$ will be made here, but we require that all physical quantities are gyrogauge invariant[63].

A phase space vectorfield $\boldsymbol{G}$ is gyrogauge invariant when: $\boldsymbol{G}(f) = \boldsymbol{G}'(f')$, where primed quantities are gyrogauge transformed and f denotes an arbitrary phase space function. Under a gyrogauge transformation only the θ_0 component of $\boldsymbol{G}$ is changed

$$G'_{\theta_0} = G_{\theta_0} + G_1^{\boldsymbol{X}} \cdot \nabla\alpha + G_t\frac{\partial\alpha}{\partial t}. \tag{2.11}$$

A short calculation shows

$$\nabla\alpha = \boldsymbol{R}' - \boldsymbol{R}, \tag{2.12}$$

$$\frac{\partial\alpha}{\partial t} = S' - S, \tag{2.13}$$

where we have introduced the gyrogauge fields

$$\boldsymbol{R} = \nabla\hat{\perp} \cdot \hat{\boldsymbol{\theta}} = \nabla\hat{\boldsymbol{e}}_1 \cdot \hat{\boldsymbol{e}}_2, \tag{2.14}$$

$$S = \hat{\boldsymbol{\theta}} \cdot \frac{\partial\hat{\perp}}{\partial t} = \hat{\boldsymbol{e}}_2 \cdot \frac{\partial\hat{\boldsymbol{e}}_1}{\partial t}, \tag{2.15}$$

measuring the change of triad $(\hat{\boldsymbol{e}}_1, \hat{\boldsymbol{e}}_2, \hat{\boldsymbol{b}})$ in space and time. $\boldsymbol{R}$ and S are θ_0-independent but depend on gyrogauge whereas , e.g., $\nabla \times \boldsymbol{R}$ is gyrogauge invariant.

Combining (2.11)-(2.13) it follows that G_{θ_0} must be of the form[62]

$$G_{\theta_0} = g_{\theta_0} + \boldsymbol{G}_{\boldsymbol{x}} \cdot \boldsymbol{R} + G_t S, \tag{2.16}$$

in order to ensure gyrogauge invariance of $\boldsymbol{G}$. Here, g_θ denotes the gyrogauge invariant part of G_{θ_0}.

Similarly, the coordinate functions of the $\boldsymbol{x}$ and t components of a one-form γ on phase space transforms according to

$$\gamma'_x = \gamma_x - \gamma_{\theta_0} \nabla \alpha, \tag{2.17}$$

$$\gamma'_t = \gamma_t - \gamma_{\theta_0} \frac{\partial \alpha}{\partial t}. \tag{2.18}$$

Therefore the coordinate functions are required to be of the form

$$\gamma_{\boldsymbol{x}} = \bar{\gamma}_{\boldsymbol{x}} - \gamma_\theta \boldsymbol{R}, \tag{2.19}$$

$$\gamma_t = \bar{\gamma}_t - \gamma_\theta S, \tag{2.20}$$

to ensure gyrogauge invariance. $\bar{\gamma}_{\boldsymbol{x}}$ and $\bar{\gamma}_t$ denote the gyrogauge independent parts.

2.2.2 Guiding-center transformation

The main aim of the guiding-center transformation is to find coordinates for which the equations of motion are independent of the gyroangle θ. This is achieved by performing a perturbative coordinate transformation in a small perturbation parameter $\epsilon \ll 1$, from the preliminary coordinates $(\boldsymbol{x}, u_0, \theta_0, \mu_0, t)$ to the guiding-center coordinates $(\boldsymbol{X}, u, \theta, \mu, t)$. The coordinate transformation removes the θ-dependence from the Poincaré one-form, which implies that all derived objects (Poisson bracket, volume element etc.) are also θ-independent. The effective dimensionality of the problem is therefore reduced by one. By removing the gyroangle dependency from the equations of motion the fast time scale associated with the rapid cyclotron motion is decoupled and does not directly enter the problem. Besides removing the gyroangle dependency, the coordinate transformation is constructed such that the conjugated coordinate $\mu = \mu_0 + \cdots$, to θ, is a dynamical invariant: $\dot{\mu} = 0$.

The decoupling relies on an approximate symmetry in the system namely the gyroorbit itself. This "gyrosymmetry" only exists if the projection of the gyroorbit onto the perpendicular plane is nearly periodic over a timeperiod Ω_0^{-1}. Thus, the symmetry only persists when the ratio of the characteristic ion gyroradius ρ_i to the characteristic length scale L of the system is small: $\rho_i/L \sim \epsilon \ll 1$, and only when fluctuations have a low frequency: $\omega/\Omega_0 \sim \epsilon$, where ω is the characteristic fluctuation frequency. The amplitude of the parallel component of the electric field is restricted in order not to destroy the symmetry: $E_\parallel/(v_{th}B) \sim \epsilon$.

Only when the particle is sufficiently strongly tied to the electromagnetic fields the symmetry persists. Specifically the free motion of the particle is considered a perturbation to the coupling of the particle and the electromagnetic potentials

$$\gamma = (q\boldsymbol{A} + \epsilon m\boldsymbol{v}) \cdot d\boldsymbol{x} - (\epsilon\frac{1}{2}mv^2 + q\phi)dt, \tag{2.21}$$

or written in the preliminary coordinates:

$$\gamma = \gamma_0 + \epsilon\gamma_1, \tag{2.22}$$

where

$$\gamma_0 = q\boldsymbol{A} \cdot d\boldsymbol{x} - q\phi dt, \tag{2.23}$$

$$\gamma_1 = (m\boldsymbol{W} + m\boldsymbol{c}_\perp) \cdot d\boldsymbol{x} - (\frac{1}{2}mW^2 + \frac{1}{2}m\boldsymbol{c}_\perp^2 + m\boldsymbol{W} \cdot \boldsymbol{c}_\perp)dt. \tag{2.24}$$

The ordered one-form (2.22) is the starting point of the perturbation analysis in the next section.

The perturbation analysis is only meaningful when the asymptotic expansion converges, i.e., when ϵ is sufficiently small. In section 2.4 we elaborate on the physical significance of ϵ but at this stage the smallness parameter is simply a mathematical placeholder in the perturbation analysis.

Now we discuss the conditions governing the guiding-center transformation. The equations of motion [19] can be written as

$$\frac{dz_j}{dt}(\frac{\partial\gamma_j}{\partial z_i} - \frac{\partial\gamma_i}{\partial z_j}) = \frac{\partial\gamma_i}{\partial t} + \frac{\partial H}{\partial z_i}, \tag{2.25}$$

where z_j denotes the six (non-canonical) phase space coordinates and γ_j the corresponding symplectic components of the Poincaré one-form (not the j'th order one-form). Repeated indices imply summation throughout the paper. A sufficient condition for gyroangle independent equations of motion is

$$\frac{\partial H}{\partial\theta} = \frac{\partial\gamma_l}{\partial\theta} = 0. \tag{2.26}$$

To obtain a sufficient condition for $\dot{\mu} = 0$, consider (2.25) for $z_i = \theta$

$$\dot{\mu}\frac{\partial\gamma_\theta}{\partial\mu} + \dot{y}_l\frac{\partial\gamma_\theta}{\partial y_l} = \frac{\partial\gamma_\theta}{\partial t}, \tag{2.27}$$

where $\boldsymbol{y} = (\boldsymbol{X}, u)$ denotes the remaining coordinates. A sufficient condition for $\dot{\mu} = 0$ [15] is therefore (2.26) combined with the following conditions

$$\frac{\partial\gamma_\theta}{\partial y_l} = \frac{\partial\gamma_\theta}{\partial t} = 0 \quad \text{and} \quad \frac{\partial\gamma_\theta}{\partial\mu} \neq 0. \tag{2.28}$$

To summarize, the guiding-center transformation is governed by (2.26), (2.28), gyrogauge invariance and the goal of obtaining equations of motion that are as simple as possible.

We use the Lie transform method [24, 35] to decouple the fast time scale gyromotion from the slower time scale of the electromagnetic fields. The Lie transform method requires less algebra than other existing methods, it has a clear identification of the governing conditions of the transformation and it can systematically be taken to arbitrary order. More important the pivotal point of the Lie transform method is the Poincaré one-form which is the most fundamental object in the modern formulation of classical mechanics. From the Poincaré one-form, the Poisson bracket, Lagrange bracket, and the volume element are derived[39]. Furthermore, the Lie transform method provides the generating Lie transformation vector fields which are used in pullback and push-forward representations of fluid moments[19].

The Lie transformation method yields an asymptotic expansion in the small parameter ϵ of the functional form of the coordinate functions of differential k-forms and tensor fields expressed in the new coordinates in terms of the coordinate functions expressed in the original coordinates. Here, the relation between the Poincare oneform coordinate function expressed in new Γ and original γ coordinates, respectively, is given to third order:

$$\Gamma_0 = \gamma_0 + dS_0, \tag{2.29}$$

$$\Gamma_1 = \gamma_1 - \mathcal{L}_{\boldsymbol{G_1}}\gamma_0 + dS_1, \tag{2.30}$$

$$\Gamma_2 = \gamma_2 - \mathcal{L}_{\boldsymbol{G}_2}\gamma_0 - \frac{1}{2}\mathcal{L}_{\boldsymbol{G}_1}(\gamma_1 + \Gamma_1) + dS_2, \tag{2.31}$$

$$\Gamma_3 = \gamma_3 - \mathcal{L}_{\boldsymbol{G}_1}\gamma_2 - \mathcal{L}_{\boldsymbol{G}_3}\gamma_0 - \mathcal{L}_{\boldsymbol{G}_2}\Gamma_1 + \frac{1}{3}\mathcal{L}^2_{\boldsymbol{G}_1}(\gamma_1 + \frac{1}{2}\Gamma_1) + dS_3, \tag{2.32}$$

where $\boldsymbol{G}_i$ denotes the i'th order generating vector field and S_n is the n'th order phase space gauge function. $\mathcal{L}_{\boldsymbol{G}}$ denotes the Lie derivative along $\boldsymbol{G}$. When operating on an arbitrary differential form, α, the Lie derivative along $\boldsymbol{G}$ reads[98]: $\mathcal{L}_{\boldsymbol{G}}\alpha = i_{\boldsymbol{G}} \circ d\alpha + d \circ i_{\boldsymbol{G}}\alpha$, where $i_{\boldsymbol{G}}$ denotes interior multiplication (contraction) with $\boldsymbol{G}$ and $\circ$ denotes composition. The equations of motion do not change when adding exact differentials to the one-form[39] so we take:$\mathcal{L}_{\boldsymbol{G}} \doteq i_{\boldsymbol{G}} \circ d$. At all orders we choose not to transform time. Therefore the time components of the Lie transform generating vector fields are set to zero, $G^t_i = 0$.

We outline the Lie transform procedure as follows. Start the derivation at zeroth order. Identify the gyroangle dependent terms. Remove the gyroangle dependent terms by choosing S_n and $\boldsymbol{G}_n$ according to the governing conditions and such that the solutions of the equations of motion are not badly behaved[24]. Repeat the procedure at the next order etc.

The detailed calculations can be found in appendix 2.A. Methodology and notation resemble Brizard[20] which eases verification and comparison

of the rather lengthy expressions. The calculations are algebraically involved because a self-consistent determination of the first and second order generating vector fields requires that the perturbation analysis is taken to third order. However, compared with earlier derivations, e.g., Ref.[99, 59], where the analysis is carried out on the Poisson bracket two tensor, the Lie transformation method requires substantially less algebra.

The resulting second order correct gyrogauge invariant guiding-center one-form reads

$$\Gamma = q\boldsymbol{A}^* \cdot d\boldsymbol{X} + \epsilon^2 \frac{m}{q} \mu d\theta - H dt, \tag{2.33}$$

where

$$\boldsymbol{A}^* = \boldsymbol{A} + \epsilon \frac{m}{q} \boldsymbol{W} - \epsilon^2 \frac{m}{q^2} \mu \bar{\boldsymbol{R}}, \tag{2.34}$$

$$H = q\phi + \epsilon \frac{1}{2} m W^2 + \epsilon \mu B + \epsilon^2 \frac{m\mu}{2q} \hat{\boldsymbol{b}} \cdot \nabla \times \boldsymbol{D} + \epsilon^2 \frac{m\mu}{q} S \tag{2.35}$$

and

$$\bar{\boldsymbol{R}} = \boldsymbol{R} + \frac{1}{2} \hat{\boldsymbol{b}} (\hat{\boldsymbol{b}} \cdot \nabla \times \hat{\boldsymbol{b}}), \quad \boldsymbol{R} = (\nabla \hat{\perp}) \cdot \hat{\boldsymbol{\theta}}, \quad S = \hat{\boldsymbol{\theta}} \cdot \frac{\partial \hat{\perp}}{\partial t} = \hat{\boldsymbol{e}}_2 \cdot \frac{\partial \hat{\boldsymbol{e}}_1}{\partial t}. \tag{2.36}$$

This result is identical to that of Littlejohn[59, Eq.95] who derived the result using a different method namely the Darboux/Lie method. Γ and the generating vector fields $\boldsymbol{G}_i$ given in the appendix also agree with Brizard[20] in the limit: $\partial_t \phi = \partial_t \boldsymbol{A} = 0$. An alternative approach can be found in Ref. [68] where $m\boldsymbol{D} \cdot d\boldsymbol{X}$ is transfered to the Hamiltonian. This implies a very complex Hamiltonian but is motivated by having a linear lowest order polarization density in the Poisson equation which resembles the gyrokinetic counterparts.

The zeroth order terms in Γ describe the electromagnetic potentials at the guiding-center position. The first order term $\frac{m}{q}\boldsymbol{W}$ in the symplectic part of Γ describes the fact that the velocity is measured in a frame moving with velocity $\boldsymbol{W}$. In the Hamiltonian, the first order terms describe the kinetic energy. The decoupled fast time scale term: $m/q\ \mu d\theta$ enter at second order. Therefore the gyrogauge terms, which guarantee gyrogauge invariance of Γ, naturally enter at second order according to (2.19)-(2.20).

The remaining second order terms are closely connected to the lowest order FLR corrections to the electromagnetic potentials $(\phi, \boldsymbol{A})$. The fields at the guiding-center reflect the average fields along the oscillatory gyroorbit in the plane perpendicular to the magnetic field. To lowest order the gyroorbit is circular but the integration path C given by $\boldsymbol{x}(t) : [0, \Omega_0^{-1}] \to \mathbb{R}^3$, is perturbed due to variations in magnetic field amplitude and direction. This

implies that the lowest order FLR corrections (see App. A.3)to the averaged electric potential

$$\langle\phi(\boldsymbol{x})\rangle \doteq \frac{\int_C ds\,\phi}{\int_C ds} = \phi(\boldsymbol{X}) + \frac{m\mu}{2q^2}\hat{\boldsymbol{b}}\cdot\nabla\times\boldsymbol{D} + \mathcal{O}(\epsilon^3) \tag{2.37}$$

reflect variations of ϕ along a circular orbit with radius: $\rho_0 = \Omega_0^{-1}\hat{\boldsymbol{b}}\times\boldsymbol{c}_\perp$, but also variations of the amplitude and direction of the magnetic field:

$$\hat{\boldsymbol{b}}\cdot\nabla\times\boldsymbol{D} = \frac{1}{B}\nabla_\perp^2\phi + \nabla_\perp\phi\cdot\nabla B^{-1} + \frac{1}{B}\hat{\boldsymbol{b}}\cdot\nabla\hat{\boldsymbol{b}}\cdot\nabla_\perp\phi \tag{2.38}$$

Therefore a "gyroaveraged" electric potential is defined

$$\psi = \phi + \frac{m\mu}{2q^2}\hat{\boldsymbol{b}}\cdot\nabla\times\boldsymbol{D}. \tag{2.39}$$

The Baños term [7]

$$\frac{m\mu}{2q^2}\hat{\boldsymbol{b}}\cdot\nabla\times\hat{\boldsymbol{b}} = \frac{\rho_0^2}{4qB}\hat{\boldsymbol{b}}\cdot\big[\nabla(\nabla\cdot\boldsymbol{A}) - \nabla^2\boldsymbol{A}\big], \tag{2.40}$$

contains the lowest order parallel component of the gyroangle average of the magnetic potential (terms arising from $G_2^{\boldsymbol{X}}$ do not contribute because the perpendicular part $G_2^{\boldsymbol{X}}{}_\perp$ [see Eq.(2.98)] is purely oscillatory)

$$\hat{\boldsymbol{b}}\cdot\oint\frac{d\theta}{2\pi}\boldsymbol{A}(\boldsymbol{x}) = A_\parallel(\boldsymbol{X}) + \frac{\rho_0^2}{4B}\hat{\boldsymbol{b}}\cdot\nabla_\perp^2\boldsymbol{A} + \mathcal{O}(\epsilon^3), \tag{2.41}$$

but is also related to FLR corrections to the parallel velocity.

2.2.3 Equations of motion

In this section the equations of motion are derived using the extended phase space formalism[19]. Formally the phase space is extended with an energy coordinate h, and the time coordinate t is treated on equal footing with the remaining coordinates. Phase space trajectories are now parametrized by an unphysical curve parameter τ and the extended phase space one-form reads

$$\Gamma_E = \Gamma - (h + \epsilon^2\frac{m\mu}{q}S)dt - (H - h - \epsilon^2\frac{m\mu}{q}S)d\tau = \hat{\Gamma}_E - \mathcal{H}d\tau, \tag{2.42}$$

where $\mathcal{H} = H - h - \frac{m\mu}{q}S$, denotes the gyrogauge invariant Hamiltonian in extended phase space and $\hat{\Gamma}_E$ is the symplectic part of Γ_E. The gyrogauge term $\frac{m\mu}{q}S$ has been moved to the symplectic part of Γ_E in order to ensure gyrogauge invariance. It should be noted that common practice is to extend the phase space already when expressed in local canonical coordinates $(\boldsymbol{q},\boldsymbol{p})$ and carry the unphysical coordinate h through the subsequent coordinate

transformations. In our opinion extending the phase space after the Lie transform has been carried out simplifies the calculation of the Lie transform.

We define the action[39]

$$S_p = \int \Gamma_E. \tag{2.43}$$

A variation of S_p with respect to the particle trajectories $\boldsymbol{\mathcal{Z}}(t) = (\boldsymbol{X}, u, \mu, \theta, t, h)(t)$ yields the equations of motion

$$\dot{\mathcal{Z}}_a = \{\mathcal{Z}_a, \mathcal{H}\}. \tag{2.44}$$

where $\{\cdot,\cdot\}$ denotes the Poisson bracket in extended phase space. In local coordinates the Poisson bracket equals the inverse coordinate function matrix: $\omega_{ab} = \frac{\partial \hat{\Gamma}_{Eb}}{\partial \mathcal{Z}_a} - \frac{\partial \hat{\Gamma}_{Ea}}{\partial \mathcal{Z}_b}$, of the symplectic two-form $\omega = d\hat{\Gamma}_E$. The Poisson bracket is therefore simply obtained by calculating and inverting ω_{ab} using the block matrix method for anti-symmetric matrices[59] or by using symbolic matrix inversion[102]. Using either method we obtain the extended guiding-center gyrogauge invariant Poisson bracket operating on arbitrary extended phase space functions f and g:

$$\begin{aligned}\{f,g\} = {} & \epsilon^{-2}\frac{q}{m}\Big(\frac{\partial f}{\partial \theta}\frac{\partial g}{\partial \mu} - \frac{\partial f}{\partial \mu}\frac{\partial g}{\partial \theta}\Big) + \epsilon^{-1}\frac{\boldsymbol{B}^*}{mB^*_{\|}}\cdot\Big(\nabla^* f\frac{\partial g}{\partial u} - \nabla^* g\frac{\partial f}{\partial u}\Big) \\ & -\epsilon^0\frac{\hat{\boldsymbol{b}}}{qB^*_{\|}}\cdot\nabla^* f\times\nabla^* g + \epsilon^{-1}\frac{q}{mB^*_{\|}}\boldsymbol{B}^*\cdot\frac{\partial \bar{\boldsymbol{A}}^*}{\partial t}\Big(\frac{\partial f}{\partial u}\frac{\partial g}{\partial h} - \frac{\partial f}{\partial h}\frac{\partial g}{\partial u}\Big) \\ & +\epsilon^0\frac{1}{B^*_{\|}}\hat{\boldsymbol{b}}\times\frac{\partial \bar{\boldsymbol{A}}^*}{\partial t}\cdot\Big(\nabla^* g\frac{\partial f}{\partial h} - \nabla^* f\frac{\partial g}{\partial h}\Big) + \Big(\frac{\partial f}{\partial h}\frac{\partial g}{\partial t^*} - \frac{\partial f}{\partial t^*}\frac{\partial g}{\partial h}\Big),\end{aligned} \tag{2.45}$$

where $\nabla^* = \nabla + \bar{\boldsymbol{R}}\frac{\partial}{\partial \theta}$ and $\frac{\partial}{\partial t^*} = \frac{\partial}{\partial t} + S\frac{\partial}{\partial \theta}$. The gyrogauge invariant generalized potential is defined as

$$\bar{\boldsymbol{A}}^* = \boldsymbol{A} + \epsilon\frac{m}{q}\boldsymbol{W} - \epsilon^2\frac{m}{q^2}\mu\Big[\frac{1}{2}\hat{\boldsymbol{b}}(\hat{\boldsymbol{b}}\cdot\nabla\times\hat{\boldsymbol{b}}) - \nabla\hat{\boldsymbol{b}}\cdot\hat{\boldsymbol{b}}\times\frac{\partial\hat{\boldsymbol{b}}}{\partial t}\Big], \tag{2.46}$$

where the identity

$$-\frac{\partial \boldsymbol{R}}{\partial t} + \nabla S = \nabla\hat{\boldsymbol{b}}\cdot\hat{\boldsymbol{b}}\times\frac{\partial\hat{\boldsymbol{b}}}{\partial t} \tag{2.47}$$

was used to cancel the gyrogauge dependent terms. The volume element is given by: $\mathcal{V} = \sqrt{\mathrm{Det}(\omega_{ab})} = \hat{\boldsymbol{b}}\cdot\nabla\times\boldsymbol{A}^* = m^2B^*_{\|}$[39].

Here we present the $\mathcal{O}(\epsilon^2)$ correct equations of motion. The equations of motion are gyrogauge invariant due to the gyrogauge invariance of the Poisson bracket and the Hamiltonian $\mathcal{H}$. Because the time coordinate t has

not been transformed we trivially get $\dot{t} = 1$, allowing us to replace the orbit parameter τ. The time evolution of the guiding-center $\boldsymbol{X}$ is

$$B_{\parallel}^{*}\dot{\boldsymbol{X}} = u\boldsymbol{B}^{*} + \hat{\boldsymbol{b}} \times \nabla\psi + \frac{\mu}{q}\hat{\boldsymbol{b}} \times \nabla B + \frac{m}{2q}\hat{\boldsymbol{b}} \times \nabla D^{2} + \hat{\boldsymbol{b}} \times \frac{\partial \bar{\boldsymbol{A}}^{*}}{\partial t}. \tag{2.48}$$

Expanding $\boldsymbol{B}^{*}$ and $B_{\parallel}^{*}$ in powers of ϵ yields $\frac{\boldsymbol{B}^{*}}{B_{\parallel}^{*}} = \hat{\boldsymbol{b}} + \epsilon\Omega^{-1}(\nabla \times \boldsymbol{W})_{\perp} + \mathcal{O}(\epsilon^{2})$, which allows us to write the equations of motion in a more familiar form

$$\dot{\boldsymbol{X}} = \boldsymbol{W} + \epsilon\left[\frac{\mu}{qB}\hat{\boldsymbol{b}} \times \nabla B + \frac{1}{\Omega}\hat{\boldsymbol{b}} \times (\boldsymbol{W} \cdot \nabla + \frac{\partial}{\partial t})\boldsymbol{W}\right] + \mathcal{O}(\epsilon^{2}), \tag{2.49}$$

The second term is the ∇B-drift and the last term represent the polarization and the curvature drifts ($\hat{\boldsymbol{b}} \cdot \nabla\hat{\boldsymbol{b}} = -\hat{\boldsymbol{b}} \times \nabla \times \hat{\boldsymbol{b}}$). Written in this form we see that the polarization and the curvature drifts arise due to the fact that the gyroangle θ is measured in a non-inertial reference frame moving with $\boldsymbol{W}$[57, 20]. Also, note that the Baños term does not result in a correction to the parallel velocity. This is a consequence of keeping the Baños term in the symplectic part of Γ which implies that the effective magnetic field $\boldsymbol{B}^{*}$ contains the lowest order FLR correction to $\boldsymbol{A}$.

The parallel acceleration is

$$B_{\parallel}^{*}\dot{u} = -\frac{q\boldsymbol{B}^{*}}{m} \cdot \nabla\psi - \frac{\mu\boldsymbol{B}^{*}}{m} \cdot \nabla B - \frac{\boldsymbol{B}^{*}}{2} \cdot \nabla D^{2} - \frac{q}{m}\boldsymbol{B}^{*} \cdot \frac{\partial \bar{\boldsymbol{A}}^{*}}{\partial t}. \tag{2.50}$$

which expanded in powers of ϵ reads

$$\dot{u} = \epsilon E_{\parallel} - \epsilon\frac{\hat{\boldsymbol{b}}}{m} \cdot (\mu\nabla B + m(\boldsymbol{W} \cdot \nabla)\boldsymbol{W}) + \mathcal{O}(\epsilon^{2}), \tag{2.51}$$

where we recognize the leading order contributions as the acceleration due to a parallel electrical field, the mirror force, and non-inertial forces.

The time evolution of θ

$$\begin{aligned}\dot{\theta} =& \frac{q}{m}\frac{\partial \mathcal{H}}{\partial \mu} + \frac{\boldsymbol{B}^{*}}{mB_{\parallel}^{*}} \cdot \bar{\boldsymbol{R}}\frac{\partial \mathcal{H}}{\partial u} + \frac{\boldsymbol{R}}{qB_{\parallel}^{*}} \cdot \hat{\boldsymbol{b}} \times \nabla\mathcal{H} + \frac{\boldsymbol{R}}{B_{\parallel}^{*}} \cdot \hat{\boldsymbol{b}} \times \frac{\partial \bar{\boldsymbol{A}}^{*}}{\partial t} - S\frac{\partial \mathcal{H}}{\partial h} \\ =& \epsilon^{-1}\Omega_{0} + \epsilon^{0}\big[\boldsymbol{R} \cdot \boldsymbol{W} + S + \frac{1}{2}\hat{\boldsymbol{b}} \cdot \nabla \times \boldsymbol{W}\big] + \mathcal{O}(\epsilon).\end{aligned} \tag{2.52}$$

It is striking (but not surprising) that $\dot{\theta}$ is gyroangle independent and gyrogauge invariant. The gyrogauge invariance is ensured by the $\boldsymbol{R} \cdot \boldsymbol{W} + S$ term. The plane spanned by $(\hat{\boldsymbol{e}}_{1}, \hat{\boldsymbol{e}}_{2})$ is at all times perpendicular to $\hat{\boldsymbol{b}}$. During a gyro orbit the orientation of the perpendicular plane changes if $\nabla \times \boldsymbol{W} \neq 0$. Corrections to the gyrofrequency due to this "wiggling" is described by the $\frac{1}{2}\hat{\boldsymbol{b}} \cdot \nabla \times \boldsymbol{W}$ term. μ is indeed a constant of motion

$$\dot{\mu} = \{\mu, \mathcal{H}\} = \mathcal{O}(\epsilon^{4}), \tag{2.53}$$

because the Hamiltonian is not θ-dependent. Details can be found in the appendix. Due to the explicit time dependence of the electromagnetic potentials the Hamiltonian H is no longer conserved along particle trajectories:

$$\begin{aligned}\dot{h} = \dot{H} =& \frac{\partial \mathcal{H}}{\partial t} - \frac{qu}{B_{\parallel}^{*}} \boldsymbol{B}^{*} \cdot \frac{\partial \bar{\boldsymbol{A}}^{*}}{\partial t} - \epsilon \frac{1}{B_{\parallel}^{*}} \frac{\partial \bar{\boldsymbol{A}}^{*}}{\partial t} \cdot \hat{\boldsymbol{b}} \times \nabla \mathcal{H} \\ =& \epsilon^{0} q \frac{\partial \phi}{\partial t} - q \frac{\partial \boldsymbol{A}}{\partial t} \cdot \boldsymbol{W} + \mathcal{O}(\epsilon^{2}). \end{aligned} \tag{2.54}$$

2.3 Vlasov-Maxwell system

In this section we derive the Vlasov-Maxwell equations and the corresponding local energy equation expressed in guiding-center coordinates using a mixed Eulerian-Lagrangian phase space variational method[64, 31, 105]. The Vlasov-Maxwell equations are obtained from a second order correct guiding center Lagrangian which, to the knowledge of the author, have not previously been presented. This new result is of importance because it provides a set of equations capable of describing physical situations where strong $\boldsymbol{E} \times \boldsymbol{B}$-flows and FLR effects are mutually important. Furthermore, we identify the polarization density and the magnetization and polarization current densities in the Maxwell equations, and give physical interpretations of the new terms originating from the second order analysis.

The Vlasov-Maxwell action

$$I = \int_{-\infty}^{\infty} d\tau \, L_p + L_f, \tag{2.55}$$

is a functional of the fields $(\boldsymbol{\mathcal{Z}}_\alpha, \phi, \boldsymbol{A})$.

We consider a continuum of particles. The particle trajectories in extended phase space $\boldsymbol{\mathcal{Z}}_\alpha = \boldsymbol{\mathcal{Z}}_\alpha(\boldsymbol{\mathcal{Z}}_0, \tau)$, are labeled by their initial position $\boldsymbol{\mathcal{Z}}_0$ at some arbitrary time t_0. The distribution of particles at time t_0 is given by a smooth reference distribution function

$$F_{\alpha 0}(\boldsymbol{\mathcal{Z}}_0) = f_{\alpha 0}(\boldsymbol{Z}_0, t_0) \delta(h_0 - H(\boldsymbol{Z}_0, t_0)). \tag{2.56}$$

where $f_{\alpha 0}$ denotes the reference distribution in phase space at time t_0. Now the particle Lagrangian is defined by

$$L_p = \sum_{\alpha} \int d^8 \boldsymbol{\mathcal{Z}}_{0\alpha} m_\alpha^2 B_{\parallel \alpha 0}^{*} \, F_{\alpha 0}(\boldsymbol{\mathcal{Z}}_{\alpha 0}) \mathcal{L}_p[\boldsymbol{\mathcal{Z}}_\alpha(\boldsymbol{\mathcal{Z}}_0; \tau), \phi(\boldsymbol{X}_\alpha, \tau)] \tag{2.57}$$

where α denotes particle species and

$$\mathcal{L}_{p\alpha} = \hat{\boldsymbol{\Gamma}}_E(\boldsymbol{\mathcal{Z}}_\alpha, \phi) \cdot \dot{\boldsymbol{\mathcal{Z}}}_\alpha - \mathcal{H}(\boldsymbol{\mathcal{Z}}_\alpha, \phi) \tag{2.58}$$

In the following we utilize that the integral of an arbitrary Lagrangian function $g(\boldsymbol{Z}_\alpha(\boldsymbol{Z}_0, t_0), t)$ along all Lagrangian trajectories

$$G = \int d^8 \boldsymbol{\mathcal{Z}}_{0\alpha} m_\alpha^2 B^*_{\parallel\alpha 0}\, F_{\alpha 0}(\boldsymbol{\mathcal{Z}}_0) g(\boldsymbol{\mathcal{Z}}_\alpha(\boldsymbol{\mathcal{Z}}_0; \tau)) \tag{2.59}$$

can be written in the Eulerian coordinates $\mathcal{Z}$

$$G = \int d^8 \boldsymbol{\mathcal{Z}}_{\alpha} m_\alpha^2 B^*_{\parallel\alpha}\, F_{\alpha}(\boldsymbol{\mathcal{Z}}, \tau) g(\boldsymbol{\mathcal{Z}}, \tau) \tag{2.60}$$

where we have defined the Eulerian distribution function

$$m_\alpha^2 B^*_{\parallel_\alpha} F_\alpha(\boldsymbol{Z}, t) = \int d^8 \boldsymbol{\mathcal{Z}}_{0\alpha} m_\alpha^2 B^*_{\parallel 0} F_{\alpha 0} \delta^{(8)}(\mathcal{Z} - \mathcal{Z}_\alpha). \tag{2.61}$$

The Lagrangian of the fields is taken to be of the following form[45]

$$L_f = \int d^3\boldsymbol{r}\, \frac{\epsilon_0 E^2}{2} - \frac{B^2}{2\mu_0}. \tag{2.62}$$

The equations of motion are obtained by varying the action I with respect to the fields $(\boldsymbol{\mathcal{Z}}_\alpha, \phi, \boldsymbol{A})$. In the following we omit the particle labels whenever there is no danger of confusion.

Variation of the action with respect to $\boldsymbol{\mathcal{Z}}_\alpha$, assuming that the variation vanishes at the temporal boundary, implies

$$\dot{\boldsymbol{\mathcal{Z}}}_\alpha = \{\boldsymbol{\mathcal{Z}}_\alpha, \mathcal{H}\}, \tag{2.63}$$

showing that the fields $\boldsymbol{\mathcal{Z}}_\alpha$ indeed obey the single particle equations of motion Eq.(2.44).

2.3.1 Poisson equation

Variation of I with respect to $\phi(\boldsymbol{r}, t)$ yields the Poisson equation given that the variation $\delta\phi$ vanishes at the temporal and spatial boundaries

$$\epsilon_0 \nabla \cdot \boldsymbol{E} = \rho_f - \nabla \cdot \boldsymbol{P}, \tag{2.64}$$

where the guiding-center charge density is

$$\rho_f = \sum_\alpha \int d^6 \boldsymbol{Z} m^2 B^*_\parallel q F \delta^{(3)}(\boldsymbol{r} - \boldsymbol{X}). \tag{2.65}$$

The polarization vector is defined as

$$\boldsymbol{P} = \sum_\alpha \int d^6 \boldsymbol{Z} m^2 B^*_\parallel \boldsymbol{\mathcal{P}} \tag{2.66}$$

where the polarization density is

$$\boldsymbol{\mathcal{P}} = \sum_{\alpha} \int d^6\boldsymbol{Z} m^2 B_{\parallel}^{*}\, \delta^{(3)}(\boldsymbol{r}-\boldsymbol{X}) \Big(\frac{m}{B}\hat{\boldsymbol{b}} \times (\dot{\boldsymbol{X}} - \boldsymbol{D}) \\ -\frac{\mu}{2\Omega}[\nabla_{\perp} + \hat{\boldsymbol{b}} \times \nabla \times \hat{\boldsymbol{b}}] \Big) F. \tag{2.67}$$

The first term represents the "classical" polarization due to the charge and/or mass dependent $\mathcal{O}(\epsilon)$ drifts, whereas the last term represents the lowest order FLR correction to the guiding-center density (2.65). The polarization charge is not associated with bound charge in the classical sense, but describes the difference between particle- and guiding-center charge. This residual charge arises because the charge is not located at the guiding-center but at the real particle position. The "bound charge" associated with the polarization is therefore moving with the free guiding-center charge ρ_f.

2.3.2 Ampère's equation

A variation of I with respect to $\boldsymbol{A}(\boldsymbol{r},t)$ yields Ampère's equation given that the variation, $\delta\boldsymbol{A}$, vanishes at the temporal and spatial boundaries

$$\frac{1}{\mu_0}\nabla \times \boldsymbol{B} - \epsilon_0 \frac{\partial}{\partial t}\boldsymbol{E} = \boldsymbol{J} + \nabla \times \boldsymbol{M} + \frac{\partial}{\partial t}\boldsymbol{P} \tag{2.68}$$

where

$$\boldsymbol{J} = \sum_{\alpha} \int d^6\boldsymbol{Z} m_{\alpha}^2 B_{\parallel}^{*}\, qF\delta^{(3)}(\boldsymbol{r}-\boldsymbol{X})\dot{\boldsymbol{X}} \tag{2.69}$$

denotes the guiding-center current. The magnetization $\nabla \times \boldsymbol{M}$ and polarization $\frac{\partial}{\partial t}\boldsymbol{P}$ currents arise because charges are not carried by guiding-centers but by particles. This difference between guiding-center and particle charges gave rise to a polarization charge in the Poisson equation (2.64). Therefore the magnetization is split into an intrinsic contribution

$$\boldsymbol{M}_{\mu} = \sum_{\alpha} \int d^6\boldsymbol{Z} m^2 B_{\parallel}^{*} \, -\mu F \delta(\boldsymbol{r}-\boldsymbol{X}) \big[\hat{\boldsymbol{b}} + \frac{(\nabla \times \boldsymbol{W})_{\perp}}{2\Omega_0} + \frac{(\dot{\boldsymbol{X}}_{\perp} - \boldsymbol{D})}{2\Omega_0} \hat{\boldsymbol{b}} \cdot \nabla \times \hat{\boldsymbol{b}} \big] \\ + \delta(\boldsymbol{r}-\boldsymbol{X}) \frac{E_{\parallel}}{B^2} \hat{\boldsymbol{b}} \times \nabla \times \big(\hat{\boldsymbol{b}} \frac{m\mu F}{2q} \big) \tag{2.70}$$

and a contribution

$$\boldsymbol{M}_{p} = \sum_{\alpha} \int d^6\boldsymbol{Z} m^2 B_{\parallel}^{*} \boldsymbol{\mathcal{P}} \times \boldsymbol{W} - \delta(\boldsymbol{r}-\boldsymbol{X}) \frac{mFE_{\parallel}}{B^2} \hat{\boldsymbol{b}} \times (\dot{\boldsymbol{X}} - \boldsymbol{W}) \tag{2.71}$$

originating from the comoving polarization charge[52, 54].

In comparison with earlier results several new terms appear in Ampère's equation[105, 77]. All new terms originate from the second order terms in L_p. New higher order terms in $\boldsymbol{M}_p$ appear because $\boldsymbol{\mathcal{P}}$ contains higher order terms. In $\boldsymbol{M}_p$ the last term is small but must be kept to maintain consistency. We also note that the new contributions to the polarization current $\frac{\partial}{\partial t}\boldsymbol{P}$ and $\boldsymbol{M}_p$ contain the lowest order FLR correction to the guiding center current. The term $-\frac{1}{2}\mu F\Omega_0^{-1}(\nabla\times\boldsymbol{W})_\perp$ in $\boldsymbol{M}_\mu$ is a correction to the classical magnetization term $-\mu F\hat{\boldsymbol{b}}$. The correction is a non-inertial centrifugal effect arising because the perpendicular velocity components are measured in a frame moving with non-constant $\boldsymbol{W}$. The remaining terms in $\boldsymbol{M}_\mu$ are small but are kept in order to maintain consistency.

2.3.3 Vlasov equation

By construction the Eulerian distribution function (2.61) satisfies the equation

$$\frac{\partial}{\partial\boldsymbol{\mathcal{Z}}}\cdot(B_\parallel^*\dot{\boldsymbol{\mathcal{Z}}}F)=0 \tag{2.72}$$

which together with the Liouville theorem[61]

$$\frac{\partial}{\partial\boldsymbol{\mathcal{Z}}}\cdot(B_\parallel^*\dot{\boldsymbol{\mathcal{Z}}})=0 \tag{2.73}$$

yields the Vlasov equation

$$\dot{\boldsymbol{\mathcal{Z}}}\cdot\frac{\partial F}{\partial\boldsymbol{\mathcal{Z}}}=0 \tag{2.74}$$

As F is gyroangle independent[36] and $\dot{\mu}=0$, (2.72) can be written as

$$\begin{aligned}\frac{\partial}{\partial t}B_\parallel^*F+\nabla\cdot\big[(u\boldsymbol{B}^*+\hat{\boldsymbol{b}}\times\nabla\psi+\frac{\mu}{q}\hat{\boldsymbol{b}}\times\nabla B+\frac{m}{2q}\hat{\boldsymbol{b}}\times\nabla D^2+\hat{\boldsymbol{b}}\times\frac{\partial\bar{\boldsymbol{A}}^*}{\partial t})F\big]\\ +\frac{\partial}{\partial u}\big[(-\frac{q\boldsymbol{B}^*}{m}\cdot\nabla\psi-\frac{\mu\boldsymbol{B}^*}{m}\cdot\nabla B-\frac{\boldsymbol{B}^*}{2}\cdot\nabla D^2+\frac{q}{m}\boldsymbol{B}^*\cdot\frac{\partial\bar{\boldsymbol{A}}^*}{\partial t})F\big]=0.\end{aligned} \tag{2.75}$$

where we have inserted (2.48) and (2.51).

2.3.4 Energy theorem

The energy density is found using the Noether method[90, 45]. From the time translation invariance (the laws of physics do not change with time) we obtain the local energy balance equation

$$\frac{\partial\mathcal{E}}{\partial t}+\nabla\cdot\boldsymbol{S}=0 \tag{2.76}$$

where

$$\mathcal{E} = \frac{\epsilon_0 E^2}{2} + \frac{B^2}{2\mu_0} + \sum_\alpha \left[\boldsymbol{P} \cdot \boldsymbol{E} + \int d^6\boldsymbol{Z} m^2 B_\parallel^* F \delta^{(3)}(\boldsymbol{r} - \boldsymbol{X})(H - q\phi) \right] \tag{2.77}$$

is the energy density, and

$$\boldsymbol{S} = \frac{\boldsymbol{E} \times \boldsymbol{B}}{\mu_0} + \sum_\alpha \left[\boldsymbol{M} \times \boldsymbol{E} + \int d^6\boldsymbol{Z} m^2 B_\parallel^* F \delta^{(3)}(\boldsymbol{r} - \boldsymbol{X})(H - q\phi)\dot{\boldsymbol{X}} \right] \tag{2.78}$$

denotes the energy flux.

2.4 Discussion

So far we only vaguely defined the physical meaning of the smallness parameter ϵ. The traditional guiding-center ordering[100, 59] is a perturbation in the length scale separation smallness parameter

$$\rho_i |\nabla \ln E| \sim \rho_i |\nabla \ln B| \sim \epsilon_\perp, \tag{2.79}$$

where ρ_i is the thermal ion gyroradius. This ordering applies to the results shown here. Simply replace ϵ according to: $\epsilon^m \to \epsilon_\perp^{m-1}$, where $m \in \mathbb{Z}$. Now the electromagnetic potentials $(\boldsymbol{A}, \phi)$, enter the Lagrangian at $\mathcal{O}(\epsilon_\perp^{-1})$ such that $\boldsymbol{B} \sim \mathcal{O}(1)$ and $\boldsymbol{E}/(v_{th}B) \sim \mathcal{O}(1)$.

The gyrokinetic formalism[19], on the other hand, is an expansion in the fluctuation amplitude smallness parameter

$$\frac{E}{v_{th}B} \sim \epsilon_\delta. \tag{2.80}$$

Contrary to the guiding-center ordering, the gyrokinetic ordering assumes: $k_\perp \rho_i \sim \epsilon_\perp \sim 1$; $k_\perp$ denotes a characteristic inverse fluctuation length scale in the perpendicular plane.

When $\epsilon_\perp \sim \epsilon_\delta \sim 1$, the gyrosymmetry no longer exists. The gyrokinetic formalism has been extendeded to such conditions by splitting the electromagnetic fields into equilibrium strong long wavelength (guiding-center or drift kinetic) and fluctuating (gyrokinetic) short wavelength parts, eg.[48, 78]. The extension of standard gyrokinetics is motivated by the necessity of treating the edge region of tokamak plasmas. The edge region is characterized by having large fluctuation amplitudes $\epsilon_\delta \sim 0.1 - 1$, strong sheared flows $\boldsymbol{D}/v_{th} \sim 1$, steep profile gradients: $\rho_i/L \lesssim 1$, and unfortunately a fluctuation power spectrum that peaks near but below ρ_i^{-1}[48].

Motivated by the presence of the lowest order FLR corrections to $(\phi, \boldsymbol{A})$, we propose an ordering that resembles the long wavelength limit[46] of nonlinear gyrokinetics: $(k_\perp \rho_i)^2 \ll 1$, which allows strong $\boldsymbol{E} \times \boldsymbol{B}$-flows and

non-constant magnetic field without splitting the electromagnetic fields into equilibrium and fluctuating parts. We assume

$$\epsilon_E^2 \sim \epsilon_B \tag{2.81}$$

where $\epsilon_E \sim \rho_i |\nabla \ln \boldsymbol{E}|$. This ordering is relevant for the edge region of tokamak plasmas where $\rho_i/L_E \sim L_E/L_B$. Formally we substitute $\epsilon^m \to \epsilon_E^{m-1}$ in terms involving ϕ and substitute according to $\epsilon^m \to \epsilon_E^{m-2}$, wherever $\boldsymbol{A}$ enters the guiding-center one-form (2.33). This implies that we retain $\frac{E}{v_{th}B} \sim 1$.

With this ordering the result should be thought of as a $\mathcal{O}(1)$ guiding-center theory with $\mathcal{O}(\sqrt{\epsilon_B})$ finite Larmor radius corrections to the electric potential ϕ. This model could is a first step towards a nonlinear turbulence model with self-consistently determined electromagnetic fields for edge plasmas.

2.5 Conclusions

The second order gyrogauge invariant guiding-center coordinates were derived using the Lie transformation method, which is clearer and simpler than other methods previously used. Previous results are identical but have not been derived using the Lie transform method. The Poisson bracket and the corresponding equations of motion were presented where we emphasized the finite-Larmor-corrections to the electromagnetic fields contained in the second order terms. An energy conserving Vlasov-Maxwell system expressed in the guiding-center coordinates has been derived from a mixed Lagrangian Eulerian variational principle. The guiding center Vlasov-Maxwell equations have not previously been derived from the second order correct guiding center Lagrangian. New terms originating from the second order analysis mainly describe lowest order FLR effects. Therefore the Vlasov-Maxwell equations presented here are applicable to systems where FLR effects and strong flows are important. Also, in the Maxwell equations the polarization density and the magnetization and polarization current densities were explicitly identified. This system of equations was accompanied by a local energy theorem which provides important physical insight and is an important validation tool in numerical simulations. Finally, we suggested an ordering which makes the Vlasov-Maxwell system suitable for some regimes of edge turbulence.

2.A Detailed guiding-center calculations

In this appendix we present the detailed calculations of the guiding-center coordinate transformation. The Lie transform method described in section 2.2.2 is used on the fundamental Poincaré one-form γ.

2.A.1 Zeroth order analysis

The zeroth order one-form (2.29) is not gyroangle dependent so we choose: $\Gamma_0 = \gamma_0$, and take $S_0 = 0$.

2.A.2 First order analysis

The first order guiding-center one-form Γ_1 is calculated using (2.30). If the coordinate matrix of $d\gamma_0$ has an inverse, $\boldsymbol{G}_1$ can be determined uniquely. Unfortunately, $d\gamma_0$ has only rank two. Therefore $\boldsymbol{G}_1$ cannot self-consistently be determined from the first order analysis. Only the two components of ${G_1^{\boldsymbol{X}}}_\perp$ are found at this order

$$\begin{aligned}\Gamma_1 = \big[m\boldsymbol{W} + m\boldsymbol{c}_\perp + qG_1^{\boldsymbol{X}} \times (\nabla \times \boldsymbol{A})\big] \cdot d\boldsymbol{X} \\ -\big[\frac{1}{2}mW^2 + \frac{1}{2}mc_\perp^2 + m\boldsymbol{W} \cdot \boldsymbol{c}_\perp + qG_1^{\boldsymbol{X}} \cdot \boldsymbol{E}\big]dt,\end{aligned} \tag{2.82}$$

where $S_1 = 0$ has been used. Only the $\boldsymbol{c}_\perp$ terms are gyroangle dependent. The gyroangle dependency is removed from the first term solving: $m\boldsymbol{c}_\perp + qG_1^{\boldsymbol{X}} \times (\nabla \times \boldsymbol{A}) = 0$, for $G_1^{\boldsymbol{X}}$

$${G_1^{\boldsymbol{X}}}_\perp = -\boldsymbol{\rho}_0 = \frac{\boldsymbol{c}_\perp \times \hat{\boldsymbol{b}}}{\Omega_0}. \tag{2.83}$$

Inserting (2.83) into the Hamiltonian all θ-dependent terms in the Hamiltonian cancel

$$\Gamma_1 = m\boldsymbol{W} \cdot d\boldsymbol{X} - (\frac{1}{2}mW^2 + \mu B)dt. \tag{2.84}$$

2.A.3 Second order

The second order analysis follows from (2.31). We start by calculating:

$$\begin{aligned}i_{\boldsymbol{G}} \circ d\Gamma_1 = \big[-mG_1^{\boldsymbol{X}} \times (\nabla \times \boldsymbol{W}) + mG_1^u \hat{\boldsymbol{b}}\big] \cdot d\boldsymbol{X} - G_1^{\boldsymbol{X}} \cdot \hat{\boldsymbol{b}} du \\ -\big[mG_1^{\boldsymbol{X}} \frac{\partial \boldsymbol{W}}{\partial t} + \frac{1}{2}(G_1^{\boldsymbol{X}} \cdot \nabla)W^2 + muG_1^u - BG_1^\mu - \mu G_1^{\boldsymbol{X}} \cdot \nabla B\big]dt,\end{aligned} \tag{2.85}$$

and note that: $i_G \circ d\gamma_1 = i_G \circ d\Gamma_1 + i_G \circ d(m\boldsymbol{c}_\perp \cdot d\boldsymbol{X} - m\boldsymbol{W} \cdot \boldsymbol{c}_\perp dt)$, so we only have to calculate

$$\begin{aligned}&i_{\boldsymbol{G}} \circ d(m\boldsymbol{c}_\perp \cdot d\boldsymbol{X} - m\boldsymbol{W} \cdot \boldsymbol{c}_\perp dt) \\ &\quad = [-mG_1^{\boldsymbol{X}} \times (\nabla \times \boldsymbol{c}_\perp) + m\frac{\partial \boldsymbol{c}_\perp}{\partial \mu} + mG_1^\theta \frac{\partial \boldsymbol{c}_\perp}{\partial \theta}] \cdot d\boldsymbol{X} \\ &\qquad - mG_1^{\boldsymbol{X}} \cdot \frac{\partial \boldsymbol{c}_\perp}{\partial \mu} d\mu - mG_1^{\boldsymbol{X}} \cdot \frac{\partial \boldsymbol{c}_\perp}{\partial \theta} d\theta \\ &\qquad - \big[mG_1^{\boldsymbol{X}} \cdot \frac{\partial \boldsymbol{c}_\perp}{\partial t} + mG_1^{\boldsymbol{X}} \cdot (\nabla \boldsymbol{W}) \cdot \boldsymbol{c}_\perp + mG_1^u \frac{\partial \boldsymbol{W}}{\partial u} \cdot \boldsymbol{c}_\perp \\ &\qquad + mG_1^{\boldsymbol{X}} \cdot (\nabla \boldsymbol{c}_\perp) \cdot \boldsymbol{W} + mG_1^\mu \frac{\partial \boldsymbol{c}_\perp}{\partial \mu} \cdot \boldsymbol{W} + mG_1^\theta \frac{\partial \boldsymbol{c}_\perp}{\partial \theta} \cdot \boldsymbol{W}\big]dt,\end{aligned} \tag{2.86}$$

in order to obtain $i_G \circ d\gamma_1$. The remaining term is given by

$$i_{\boldsymbol{G}_2} \circ d\gamma_0 = -qG_2^{\boldsymbol{X}} \times \boldsymbol{B} \cdot d\boldsymbol{X} + qG_2^{\boldsymbol{X}} \cdot \boldsymbol{E}dt. \tag{2.87}$$

Now collecting all terms, the coordinate functions of the second order guiding-center one-form are

$$\begin{aligned}\Gamma_2^{\boldsymbol{X}} &= qG_2^{\boldsymbol{X}} \times \boldsymbol{B} + mG_1^{\boldsymbol{X}} \times (\nabla \times \boldsymbol{W}) - m\hat{\boldsymbol{b}}G_1^u \\ &\quad + \frac{1}{2}mG_1^{\boldsymbol{X}} \times (\nabla \times \boldsymbol{c}_\perp) - \frac{1}{2}mG_1^\mu \frac{\partial \boldsymbol{c}_\perp}{\partial \mu} - \frac{1}{2}mG_1^\theta \frac{\partial \boldsymbol{c}_\perp}{\partial \theta} + \frac{\partial S_2}{\partial \boldsymbol{x}}, \qquad (2.88)\\ \Gamma_2^u &= mG_1^{\boldsymbol{X}} \cdot \hat{\boldsymbol{b}} + \frac{\partial S_2}{\partial u}, \qquad (2.89)\\ \Gamma_2^\mu &= \frac{m}{2}G_1^{\boldsymbol{X}} \cdot \frac{\partial \boldsymbol{c}_\perp}{\partial \mu} + \frac{\partial S_2}{\partial \mu} = \frac{\partial S_2}{\partial \mu}, \qquad (2.90)\\ \Gamma_2^\theta &= \frac{m}{2}G_1^{\boldsymbol{X}} \cdot \frac{\partial \boldsymbol{c}_\perp}{\partial \theta} + \frac{\partial S_2}{\partial \theta} = \frac{m\mu}{q} + \frac{\partial S_2}{\partial \theta}, \qquad (2.91)\\ \Gamma_2^t &= -qG_2^{\boldsymbol{X}} \cdot \boldsymbol{E} + mG_1^{\boldsymbol{X}} \cdot \frac{\partial \boldsymbol{W}}{\partial t} + \frac{m}{2}(G_1^{\boldsymbol{X}} \cdot \nabla)W^2 + muG_1^u + BG_1^\mu \\ &\quad + \mu G_1^{\boldsymbol{X}} \cdot \nabla B + \frac{m}{2}G_1^{\boldsymbol{X}} \cdot \frac{\partial \boldsymbol{c}_\perp}{\partial t} + \frac{m}{2}G_1^{\boldsymbol{X}} \cdot (\nabla \boldsymbol{W}) \cdot \boldsymbol{c}_\perp + \frac{m}{2}G_1^u \frac{\partial \boldsymbol{W}}{\partial u} \cdot \boldsymbol{c}_\perp \\ &\quad + \frac{m}{2}G_1^{\boldsymbol{X}} \cdot (\nabla \boldsymbol{c}_\perp) \cdot \boldsymbol{W} + \frac{m}{2}G_1^\mu \frac{\partial \boldsymbol{c}_\perp}{\partial \mu} \cdot \boldsymbol{W} + \frac{m}{2}G_1^\theta \frac{\partial \boldsymbol{c}_\perp}{\partial \theta} \cdot \boldsymbol{W} + \frac{\partial S_2}{\partial t}. \qquad (2.92)\end{aligned}$$

We must determine the generating vector fields $\boldsymbol{G}$ according to (2.26) and (2.28). We choose $S_2 = 0$ and readily see that $\Gamma_2^\mu = 0$. Also, $\Gamma_2^\theta = \frac{m}{q}\mu$ such that the conditions in (2.28) are fulfilled. Furthermore we set: $\hat{\boldsymbol{b}} \cdot G_1^{\boldsymbol{X}} = 0$, such that: $\Gamma_2^u = 0$.

More work must be put into the remaining component Γ_2^t and $\Gamma_2^{\boldsymbol{X}}$. Besides removing the gyroangle dependency we must ensure that Γ_2^t and $\Gamma_2^{\boldsymbol{X}}$ retain their gyrogauge invariant forms (according to (2.19) and (2.20)) since $\Gamma_2^\theta \neq 0$. In order to ease the notation and a comparison with [20] the following abbreviations are introduced:

$$g_u = G_1^u - G_1^{\boldsymbol{X}} \cdot \nabla \hat{\boldsymbol{b}} \cdot \boldsymbol{c}_\perp = G_1^u - \frac{\mu}{q}\big[\hat{\boldsymbol{b}} \cdot \nabla \times \hat{\boldsymbol{b}} - (\hat{\boldsymbol{\theta}}\hat{\perp} + \hat{\perp}\hat{\boldsymbol{\theta}}) : \nabla \hat{\boldsymbol{b}}\big], \tag{2.93}$$

$$g_\mu = G_1^\mu + \mu G_1^{\boldsymbol{X}} \cdot \nabla \ln B. \tag{2.94}$$

Next, the second and fourth terms in (2.88) are rewritten using the identities:

$$\begin{aligned}\frac{m}{2}G_1^{\boldsymbol{X}} \times (\nabla \times \boldsymbol{c}_\perp) =& -\frac{\mu \boldsymbol{R}}{q} + \frac{\mu}{q}\hat{\boldsymbol{\theta}}(\hat{\boldsymbol{\theta}} \cdot \boldsymbol{R}) \\ &+ \frac{\mu}{q}\hat{\boldsymbol{b}}(\hat{\boldsymbol{\theta}} \cdot \nabla \hat{\perp} \cdot \hat{\boldsymbol{b}}) - \frac{m}{4}\boldsymbol{c}_\perp (G_1^{\boldsymbol{X}} \cdot \nabla \ln B), \qquad (2.95)\\ G_1^{\boldsymbol{X}} \times (\nabla \times \boldsymbol{W}) =& \Omega^{-1}\hat{\boldsymbol{b}}(\boldsymbol{c}_\perp \cdot \nabla \times \boldsymbol{W}) + G_1^{\boldsymbol{X}} \times \hat{\boldsymbol{b}}(\hat{\boldsymbol{b}} \cdot \nabla \times \boldsymbol{W}), \qquad (2.96)\end{aligned}$$

which allows us to separate the perpendicular and a parallel parts of $\Gamma_2^{\boldsymbol{X}}$

$$\begin{aligned}\Gamma_2^{\boldsymbol{X}} =& -\frac{m}{q}\mu\boldsymbol{R} - \frac{m}{2}\big[\frac{\partial \boldsymbol{c}_\perp}{\partial\mu} + \frac{\partial \boldsymbol{c}_\perp}{\partial\theta}\big] \\ & - \boldsymbol{B}\times\big[qG_2^{\boldsymbol{X}} + \frac{m}{B}G_1^{\boldsymbol{X}}(\hat{\boldsymbol{b}}\cdot\nabla\times\boldsymbol{W})\big] \\ & - \hat{\boldsymbol{b}}\big[mg_u + \frac{1}{2}G_1^{\boldsymbol{X}}\cdot\nabla\hat{\boldsymbol{b}}\cdot\boldsymbol{c}_\perp - \frac{m}{\Omega}(\boldsymbol{c}_\perp\cdot\nabla\times\boldsymbol{W})\big]. \end{aligned} \tag{2.97}$$

The first term in (2.97), $-\Gamma_\theta\boldsymbol{R}$, is gyroangle independent and ensures gyrogauge invariance of Γ as expected from (2.19). The perpendicular part of the remaining terms are all purely oscillatory. Taking the cross product of (2.97) with $\hat{\boldsymbol{b}}$ we solve for

$$G_2^{\boldsymbol{X}}{}_\perp = \frac{1}{2\Omega}g_\mu\hat{\boldsymbol{b}}\times\frac{\partial\boldsymbol{c}_\perp}{\partial\mu} - \Omega^{-1}G_1^{\boldsymbol{X}}(\hat{\boldsymbol{b}}\cdot\nabla\times\boldsymbol{W}) + \frac{1}{2\Omega}g_\theta\hat{\boldsymbol{b}}\times\frac{\partial\boldsymbol{c}_\perp}{\partial\theta}. \tag{2.98}$$

The gyroangle dependency in the parallel part of $\Gamma_2^{\boldsymbol{X}}$ can be removed through g_u. We rewrite the last parenthesis in (2.97) using the identity

$$G_1^{\boldsymbol{X}}\cdot\nabla\hat{\boldsymbol{b}}\cdot\boldsymbol{c}_\perp = \frac{m\mu}{q}(\hat{\boldsymbol{b}}\cdot\nabla\times\hat{\boldsymbol{b}} - (\hat{\boldsymbol{\theta}}\hat{\perp} + \hat{\boldsymbol{\theta}}\hat{\perp}) : \nabla\hat{\boldsymbol{b}}), \tag{2.99}$$

and observe that the $\hat{\boldsymbol{b}}\cdot\nabla\times\hat{\boldsymbol{b}}$ term is gyroangle independent. The remaining gyroangle dependent terms are absorbed into g_u:

$$g_u = \frac{\mu}{2q}(\hat{\boldsymbol{\theta}}\hat{\perp} + \hat{\perp}\hat{\boldsymbol{\theta}}) : \nabla\hat{\boldsymbol{b}} + \Omega^{-1}\boldsymbol{c}_\perp\cdot\nabla\times\boldsymbol{W}, \tag{2.100}$$

and we get

$$\Gamma_2^{\boldsymbol{X}} = -\frac{m}{q}\mu\boldsymbol{R} - \frac{m}{2q}\mu\hat{\boldsymbol{b}}(\hat{\boldsymbol{b}}\cdot\nabla\times\hat{\boldsymbol{b}}). \tag{2.101}$$

Because the Baños term: $-\frac{m}{2q}\mu\hat{\boldsymbol{b}}(\hat{\boldsymbol{b}}\cdot\nabla\times\hat{\boldsymbol{b}})$, contains the lowest order FLR correction to the magnetic potential it is kept in (2.101). It could have been absorbed in $< g_u >$ and would then appear in the Hamiltonian instead.

Similarly the second order guiding-center Hamiltonian can be simplified

$$\begin{aligned}\Gamma_2^t =& \frac{m}{2}(G_1^{\boldsymbol{X}}\cdot\nabla)W^2 - qG_2^{\boldsymbol{X}}\cdot\boldsymbol{E} + Bg_\mu + mug_u \\ & + \frac{m}{2}uG_1^{\boldsymbol{X}}\cdot\nabla\hat{\boldsymbol{b}}\cdot\boldsymbol{c}_\perp + \frac{m}{2}g_\mu\boldsymbol{W}\cdot\frac{\partial\boldsymbol{c}_\perp}{\partial\mu} + \frac{m}{2}g_\theta\boldsymbol{W}\cdot\frac{\partial\boldsymbol{c}_\perp}{\partial\theta} \\ & + \frac{m}{2}G_1^{\boldsymbol{X}}\cdot\nabla\boldsymbol{W}\cdot\boldsymbol{c}_\perp + \frac{m}{2}G_1^{\boldsymbol{X}}\cdot\frac{\partial\boldsymbol{c}_\perp}{\partial t} + mG_1^{\boldsymbol{X}}\cdot\frac{\partial\boldsymbol{W}}{\partial t}. \end{aligned} \tag{2.102}$$

When inserting $G_2^{\boldsymbol{X}}{}_\perp$ into (2.102) the $g_\theta\frac{\partial\boldsymbol{c}_\perp}{\partial\theta}$ and $g_\mu\frac{\partial\boldsymbol{c}_\perp}{\partial\mu}$ terms combine:

$$-qG_2^{\boldsymbol{X}}\cdot\boldsymbol{E} + \frac{m}{2}g_\mu\boldsymbol{W}\cdot\frac{\partial\boldsymbol{c}_\perp}{\partial\mu} + \frac{m}{2}g_\theta\boldsymbol{W}\cdot\frac{\partial\boldsymbol{c}_\perp}{\partial\theta} = \frac{m}{B}(\boldsymbol{\rho}\cdot\nabla\phi)\hat{\boldsymbol{b}}\cdot\nabla\times\boldsymbol{W}. \tag{2.103}$$

Inserting g_u and collecting terms yields

$$\begin{aligned}\Gamma_2^t =&\frac{m}{2}(G_1^{\boldsymbol{X}}\cdot\nabla)W^2+\frac{m}{B}(\boldsymbol{\rho}\cdot\nabla\phi)\hat{\boldsymbol{b}}\cdot\nabla\times\boldsymbol{W}+B\tilde{g}_\mu\\&+\frac{mu}{\Omega}\boldsymbol{c}_\perp\cdot\nabla\times\boldsymbol{W}+mG_1^{\boldsymbol{X}}\cdot\frac{\partial\boldsymbol{W}}{\partial t}-\frac{m\mu}{2q}((\hat{\boldsymbol{\theta}}\hat{\perp}+\hat{\boldsymbol{\theta}}\hat{\perp}):\nabla\boldsymbol{W})\\&+\frac{m}{2}G_1^{\boldsymbol{X}}\cdot\frac{\partial\boldsymbol{c}_\perp}{\partial t}+\frac{mu\mu}{q2}\hat{\boldsymbol{b}}\cdot\nabla\times\hat{\boldsymbol{b}}+\frac{m\mu}{2q}\hat{\boldsymbol{b}}\cdot\nabla\times\boldsymbol{W}+B<g_\mu>,\end{aligned}\tag{2.104}$$

where g_μ has been divided into a gyroangle independent $< g_\mu >$ and oscillating $\tilde{g}_\mu$ parts. The six first terms are purely oscillatory. These terms are removed from Γ_2^t by choosing

$$\tilde{g}_\mu=\frac{-m}{B}G_1^{\boldsymbol{X}}\cdot(\boldsymbol{W}\cdot\nabla)\boldsymbol{W}+\frac{\mu}{2\Omega}(\hat{\boldsymbol{\theta}}\hat{\perp}+\hat{\perp}\hat{\boldsymbol{\theta}}):\nabla\boldsymbol{W}-\frac{m}{2B}G_1^{\boldsymbol{X}}\cdot\frac{\partial\boldsymbol{W}}{\partial t},\tag{2.105}$$

where vector identity: $\nabla(\boldsymbol{A}\cdot\boldsymbol{B})=\boldsymbol{A}\times(\nabla\times\boldsymbol{B})+\boldsymbol{B}\times(\nabla\times\boldsymbol{A})+(\boldsymbol{A}\cdot\nabla)\boldsymbol{B}+(\boldsymbol{B}\cdot\nabla)\boldsymbol{A}$, has been used to combine the $\boldsymbol{W}$-terms. The last four terms in (2.104) are gyro-angle independent

$$\Gamma_2^t=-H_2=\frac{m\mu}{q}S+\frac{mu\mu}{q2}\hat{\boldsymbol{b}}\cdot\nabla\times\hat{\boldsymbol{b}}+\frac{m\mu}{2q}\hat{\boldsymbol{b}}\cdot\nabla\times\boldsymbol{W}+B<g_\mu>.\tag{2.106}$$

$< g_\mu >$ is not determined at this stage. It turns out that in order to ensure $\dot{\mu}=0$ to third order in ϵ, $< g_\mu >$ must be determined from third order calculations.

Collecting the terms the guiding-center one-form to second order reads

$$\Gamma_2=\big[-\frac{m}{q}\mu\boldsymbol{R}-\frac{m}{2q}\mu\hat{\boldsymbol{b}}(\hat{\boldsymbol{b}}\cdot\nabla\times\hat{\boldsymbol{b}})\big]\cdot d\boldsymbol{X}+\frac{m}{q}\mu d\theta-H_2dt.\tag{2.107}$$

2.A.4 Third order

$< g_\mu >$, g_θ and $\hat{\boldsymbol{b}}\cdot G_2^{\boldsymbol{X}}$ are determined from the third order calculations. Furthermore third order analysis is necessary to ensure: $\dot{\mu}=\mathcal{O}(\epsilon^4)$. The calculations are governed by (2.26) and (2.28). A sufficient choice is therefore $\Gamma_3^u=\Gamma_3^\theta=\Gamma_3^\mu=0$, assuming that $\Gamma_3^{\boldsymbol{X}}$ and Γ_3^t are gyro angle independent..

The third order calculations are long and cumbersome but it is sufficient considering only Γ_3^u, Γ_3^μ and Γ_3^θ. In (2.32) the most complex term is the $\frac{1}{3}\mathcal{L}_{\boldsymbol{G}}^2(\gamma_1+\frac{1}{2}\Gamma_1)$. Luckily, as $\hat{\boldsymbol{b}}\cdot G_1^{\boldsymbol{X}}=0$, a short calculation shows that only $\mathcal{L}_{\boldsymbol{G}}^2(\boldsymbol{c}_\perp\cdot d\boldsymbol{x})$ contributes. Terms that do not contribute to Γ_3^u, Γ_3^μ and Γ_3^θ are

not written out explicitly:

$$\begin{aligned}\mathcal{L}^2_{\boldsymbol{G}}(\boldsymbol{c}_\perp\cdot d\boldsymbol{x}) =&\big[G_1^{\boldsymbol{X}}\cdot\frac{\partial G_1^{\boldsymbol{X}}}{\partial\theta}\times(\nabla\times\boldsymbol{c}_\perp)-\frac{1}{2\mu}G_1^\mu G_1^{\boldsymbol{X}}\cdot\frac{\partial\boldsymbol{c}_\perp}{\partial\theta}\\&-G_1^{\boldsymbol{X}}\cdot\frac{\partial\boldsymbol{c}_\perp}{\partial\theta}\frac{\partial G_1^\theta}{\partial\theta}+\frac{1}{2\mu}G_1^\mu G_1^{\boldsymbol{X}}\cdot\boldsymbol{c}_\perp-G_1^{\boldsymbol{X}}G_1^{\boldsymbol{X}}\cdot\frac{\partial\boldsymbol{c}_\perp}{\partial\theta}\\&-G_1^\mu\frac{\partial\boldsymbol{c}_\perp}{\partial\theta}\cdot\frac{\partial G_1^{\boldsymbol{X}}}{\partial\theta}-G_1^{\boldsymbol{X}}\cdot\nabla G_1^{\boldsymbol{X}}\cdot\frac{\partial\boldsymbol{c}_\perp}{\partial\theta}\big]d\theta\\&+\big[-G_1^\theta\frac{\partial^2\boldsymbol{c}_\perp}{\partial\theta\partial\mu}\cdot G_1^{\boldsymbol{X}}-G_1^{\boldsymbol{X}}\cdot\frac{\partial\boldsymbol{c}_\perp}{\partial\theta}\frac{\partial G_1^\theta}{\partial\mu}-G_1^\theta G_1^{\boldsymbol{X}}\cdot\frac{\boldsymbol{c}_\perp}{2\mu}\\&+G_1^\theta\frac{\partial\boldsymbol{c}_\perp}{\partial\theta}\cdot\frac{\partial G_1^{\boldsymbol{X}}}{\partial\mu}\big]d\mu-G_1^{\boldsymbol{X}}\cdot\frac{\partial\boldsymbol{c}_\perp}{\partial\theta}\frac{\partial G_1^\theta}{\partial u}du+\cdots\end{aligned}\tag{2.108}$$

Collecting all contributing terms from (2.32) we get

$$\begin{aligned}\Gamma_3^\theta=-\frac{m}{q}<g_\mu>&-\frac{m\mu}{q\Omega}\hat{\boldsymbol{b}}\cdot\nabla\times\boldsymbol{W}-\frac{2}{3}\frac{m\mu}{q}\frac{\partial g_\theta}{\partial\theta}\\&-\frac{m}{q}\tilde{g}_\mu-\frac{2}{3}\frac{m\mu}{q}G_1^{\boldsymbol{X}}\cdot\nabla\ln B+\frac{\partial S_3}{\partial\theta},\end{aligned}\tag{2.109}$$

Only the second term is gyro angle independent which leads to

$$<g_\mu>=-\frac{\mu}{\Omega}\hat{\boldsymbol{b}}\cdot\nabla\times\boldsymbol{W}.\tag{2.110}$$

We further define $S_3=\frac{2}{3}\frac{m\mu}{q}g_\theta+s_3$ such that

$$\Gamma_3^\theta=-\frac{m}{q}\tilde{g}_\mu-\frac{2}{3}\frac{m\mu}{q}G_1^{\boldsymbol{X}}\cdot\ln B+\frac{\partial s_3}{\partial\theta}.\tag{2.111}$$

Then

$$\Gamma_3^u=mG_2^{\boldsymbol{X}}\cdot\hat{\boldsymbol{b}}+\frac{\partial s_3}{\partial u}\tag{2.112}$$

and we readily see that $G_2^{\boldsymbol{X}}\cdot\hat{\boldsymbol{b}}=-\frac{1}{m}\frac{\partial s_3}{\partial u}$ and

$$\Gamma_3^\mu=\frac{m}{q}g_\theta+\frac{\partial s_3}{\partial\mu},\tag{2.113}$$

which determines

$$g_\theta=-\frac{q}{m}\frac{\partial s_3}{\partial\mu}\tag{2.114}$$

from the requirement $\Gamma_3^\mu=0$. Now what is left is to solve $\Gamma_\theta^3=0$ from (2.111). Using the identity $\frac{\partial(\hat{\boldsymbol{\theta}}\hat{\boldsymbol{\theta}})}{\partial\theta}=\frac{1}{2}\frac{\partial}{\partial\theta}(\hat{\boldsymbol{\theta}}\hat{\boldsymbol{\theta}}-\hat{\perp}\hat{\perp})=\hat{\boldsymbol{\theta}}\hat{\perp}+\hat{\boldsymbol{\theta}}\hat{\perp}$, inserting (2.105) and by choosing s_3 to be purely oscillatory we integrate and get

$$s_3=\frac{m}{\Omega}\boldsymbol{\rho}\times\hat{\boldsymbol{b}}\cdot\big[(\boldsymbol{W}\cdot\nabla)\boldsymbol{W}+\frac{1}{2}\frac{\partial\boldsymbol{W}}{\partial t}-\frac{2}{3}\frac{\Omega\mu}{q}\nabla\ln B\big]+\frac{m\mu}{2q\Omega}\hat{\boldsymbol{\theta}}\hat{\boldsymbol{\theta}}:\nabla\boldsymbol{W}\tag{2.115}$$

and

$$G_2^{\boldsymbol{X}} \cdot \hat{\boldsymbol{b}} = -\frac{1}{\Omega}\boldsymbol{\rho} \times \hat{\boldsymbol{b}} \cdot \big[(\hat{\boldsymbol{b}} \cdot \nabla)\boldsymbol{W} + (\boldsymbol{W} \cdot \nabla)\hat{\boldsymbol{b}} + \frac{1}{2}\frac{\partial \hat{\boldsymbol{b}}}{\partial t}\big] - \frac{\mu}{2q\Omega}\hat{\boldsymbol{\theta}}\hat{\boldsymbol{\theta}} : \nabla \hat{\boldsymbol{b}}. \tag{2.116}$$

Chapter 3

Gyrokinetics

3.1 Introduction

The gyrokinetic theory describes the guiding-center dynamics when self-consistent low frequency, perpendicular, short wavelength electromagnetic perturbations are introduced. Treating the perturbed electromagnetic fields is of importance in fusion plasmas because the experimental observed anomalous transport is believed to be driven by electromagnetic microturbulence[103]. Experimental measurements show that the fluctuation frequency is at least one order of magnitude slower than the ion gyro frequency, which holds true in the core, edge and scrape off layer (SOL) regions of most fusion plasma devices. The fluctuations are highly anisotropic having wavelengths parallel to the magnetic field that are much longer than the perpendicular wavelengths $k_\parallel/|\boldsymbol{k}_\perp| \ll 1$, where $\boldsymbol{k}_\perp$ and $k_\parallel$ denotes the characteristic inverse perpendicular and parallel length scales respectively. In the plane perpendicular to the magnetic field the fluctuation spectrum is found to be nearly isotropic $\Delta k_r/\Delta k_\theta \sim 1-2$, where k_r and k_θ denote the characteristic inverse length scales in the radial and poloidal directions respectively. At fixed frequency the characteristic perpendicular wavelength is found to be $k_\theta \rho_s \sim 0.05-0.1$ in the edge region whereas $k_\theta \rho_s \sim 0.1-1$ in the core region; ρ_s denotes the ion gyroradius at electron temperature. Since the ion temperature is usually comparable to the temperature of the electrons, the ion gyroradius ρ_i is a typical scale length of the perpendicular turbulence. In the core region the fluctuation amplitude is $\tilde{n}/n \sim 0.01$, but increases going towards the edge where $\tilde{n}/n \sim 0.1$[103, 38]. When the fluctuations are carried by blobs in the SOL[12, 109, 93] the fluctuation amplitude can get even higher $\tilde{n}/n \sim 0.25-0.50$. Fluctuations are found in all macroscopic quantities including magnetic field and the fluctuation amplitudes vary differently for different quantities at different radial positions (see Ref. [103] for a list of references).

In the edge region steep pressure gradients are found just inside the last

closed flux surface (LCFS). The steep pressure profile is accompanied by a strong radial electrical field E_r[23, 70]. When operating tokamaks in enhanced confinement modes (H-mode) the pressure gradient is particularly steep and the gradient length scales of the radial electrical field and the pressure are compareable $L_p \sim L_E$, which in turn is comparable to the poloidal gyroradius $\rho_\theta = \rho_i B/B_\theta$. This implies that $\rho_i/L_p > L_p/R$, where R denotes the major radius, showing the interesting situation where the ratio of a microscopic and a macroscopic quantity is greater than the ratio between two macroscopic scale lengths[48]. Whereas most background macroscopic quantities evolve on transport time scale, $1-100\,\mathrm{ms}$, in steady state L-mode operation, the evolution of macroscopic quantities in the L-H mode transition is faster $\sim 1 - 100\,\mu$s[107]. The H-mode operation is characterized by quasi-periodic bursts of edge localized modes (ELMs) which infer momentarily losses of particles and energy which take place on a timescale of $\sim 100 - 200\,\mu$s[56, 74]. A valid theoretical/numerical description of the L-H mode transition and H-mode operation must therefore account for temporal variations of the background quantities on a timescale comparable to the turbulence time scale.

A dynamical reduction of the Vlasov-Maxwell equations relies on the identification of a physical smallness parameter quantifying the perturbation in the perturbation analysis. In strongly magnetized plasmas the perturbative analysis relies on the existence of the quasi-symmetry of the Larmor orbit around magnetic field lines. Guiding center dynamics (see Sec. 2) is an asymptotic expansion in the ratio of the gyroradius to the gradient lengthscale of the electromagnetic fields. In standard gyrokinetic the expansion parameter is the perturbation amplitude normalized to the background fields. An extension of the gyrokinetic formalism to the edge region is therefore quite challenging because a strong electric fields, and steep pressure gradients coexist with short lengthscale fluctuations. A perturbative analysis is therefore only possible by splitting the electrical field into a perturbed short wavelength part and a background part having longer length scales.

Originally, the aim of the gyrokinetic theory was to study linear low frequency, loosely defined, kinetic drift-Alfvén waves with wave length comparable to the ion gyroradius[84]. In the early studies the main focus was to derive the gyroaveraged Vlasov equation, the so-called "gyrokinetic equation", using an iterative averaging approach. Later, the theory was extended to the nonlinear regime retaining the nonlinear coupling terms in the Vlasov equation[40]. However, the early works did not consider the conservation properties (phase space volume, energy etc.) of the gyrokinetic theory and did not recognize the importance of self consistent polarization effects in the Maxwell equations. Lee[58] recognized the importance of the gyrokinetic polarization density in numerical turbulence simulations. Littlejohn[61, 60, 59] formulated the guiding-center problem in terms of Hamiltonian mechanics and derived the guiding-center coordinates using the asymptotic Lie trans-

formation method[101, 30, 35, 24], where phasespace volume conservation and energy conservation is asymptotically guaranteed. Based on the work of Littlejohn, Dubin[36] derived self-consistent electrostatic gyrokinetic Vlasov-Maxwell equations including a self-consistent energy theorem, using the Darboux-Lie method[59]. This work was then formulated in general "coordinate free" form by Hahm[49] using the phasespace Lie transform method[61] which to date is the clearest and most efficient method. The modern formulation was extended to include magnetic perturbations by Hahm[47] (shear Aflvénic dynamics in slab geometry) and Brizard[15](generalized geometry including compressional Alfvén dynamics). The inclusion of magnetic perturbations is motivated by measurements of significant magnetic fluctuations levels[103]. Theoretical and numerical studies have identified the importance of incoorporating magnetic fluctuations in the theoretical description of various plasmas phenomena, for example linear ion temperature gradient instabilitites and nonlinear zonal flow generation[87, 82, 22, 85, 108, 86]..

These contributions were all focused on treating core like turbulence having small fluctuation amplitudes and only fluctuating flows. With the discovery of improved confinement modes and the observations of sheared strong poloidal flows the gyrokinetic theory was extended to include these effects. Expressed in the modern gyrokinetic formalism Brizard[20] included strong flows in terms of a background plasma (ion) flow in the gyrokinetic coordinate transformation and Hahm[46] derived the corresponding Poisson equation and energy theorem but included the strong background flows using a background electric potential. Recently, the gyrokinetic theory including background flows was extended by Hahm[48] to include magnetic perturbations. In these contributions the background flow was static and therefore not able to describe the dynamical evolution of the strong gradients in the edge region. Table 3.1 summarize the evolution of the modern gyrokinetic theory.

The main contribution of this chapter is an extension of the existing gyrokinetic theory with strong flows[48], which allows time variations in the background potential $\phi_0(\boldsymbol{x}, t)$. Invoking the edge turbulence ordering by Hahm[48], second order fully electromagnetic gyrokinetic coordinates, including a time dependent background electric potential, are derived in the Hamiltonian and the symplectic formulations of gyrokinetics. We discuss the importance of ordering the amplitude of the flows associated with the background electric potential smaller than the thermal velocity in order to obtain tractable gyrokinetic coordinates. Using the so-called pullback representation, general Vlasov-Maxwell equations and the corresponding local energy theorem are presented, including a Poisson equation associated with the strong background electric potential. We conclude that the time dependence of the background electric potential does not alter the gyrokinetic theory dramatically. The most significant implication is the introduction of polarization drifts and the time dependence of the volume element. Due to

	ϕ	$A_\parallel$	$\boldsymbol{A}_\perp$	$\boldsymbol{D}$	$\boldsymbol{D}(t)$	Maxwell	$\mathcal{E}$	S
Hahm 1988[49]	x					x	x	
Hahm et al 1988[47]	x	h,s				h,s	h,s	
Brizard 1989[15]	x	h,s	h,s			h	h	
Brizard 1995[20]	x	h		s				
Hahm 1996[46]	x	h		s		h	h	
Brizard 2000[21]	x	h	h			h	h	h
Qin 2007[78]	x	h	h	s	s	†		
Hahm 2009[48]	x	h	h	s		h	h	
Miyato2009[68]				h	h	h	h	
This work	x	h,s	h,s	s	s	h,s	h,s	h,s

Table 3.1: Progress in the gyrokinetic formulation with strong flows. The top row describes items possibly included in the paper in the first column: ϕ electrostatic perturbations, $A_\parallel$ and $\boldsymbol{A}_\perp$ refer to shear and compressional Alfvén magnetic fluctuations respectively, $\boldsymbol{D}$ and $\boldsymbol{D}(t)$ denotes static and dynamical background $\boldsymbol{E}\times\boldsymbol{B}$-flows, "Maxwell", "$E_{tot}$" and "$S$" refer to the possible derivation of gyrokinetic Maxwell equations, gyrokinetic global energy theorem and local energy theorem including the energy flux respectively. In the interior of the table "h" and "s" refer to the Hamiltonian and symplectic formulation of gyrokinetics and "x" refer to both formulations if possible. Vacant slots indicate that the specific item is not considered in the particular paper. † only electrostatic

the vast complexity of the general gyrokinetic Vlasov-Maxwell equations we derive the equations in a limiting form. We approximate all terms quadratic in the fluctuating electromagnetic fields by imposing the long wavelength (drift kinetic) limit to the second order Hamiltonian. In this limit we derive the Vlasov-Maxwell equations in both gyrokinetic formulations and categorize all terms in the Maxwell equations as being associated with "free" gyrocenter charge or "bound" polarization charge and magnetization currents. In comparison with earlier contributions we identify several new terms in the Maxwell equations. Most interesting is the identification of an intrinsic magnetization current which represents the diamagnetic plasma response to magnetic perturbations perpendicular to the toroidal background magnetic field. Furthermore, we derive an explicit local energy theorem, which differs from earlier results, mainly due to the polarization associated with the background potential. Finally, by assuming that the ratio of the ion gyroradius to gradient scale length of the background electric field $\epsilon_E \sim \rho_i/L_E$, is bigger than the fluctuation amplitude, we obtain a solution to the generating function of the first order transformation in powers of ϵ_E. By expressing the Vlasov-Maxwell equations in these coordinates, we identify several new terms. Most significant is: the identification of the polarization associated with the inductive electrical field and the identification of the polarization current in the Ampere equation which ensures polarization charge conservation.

This chapter is organized as follows. In Sec. 3.2 the gyrokinetic coordinate transformation is derived. Next, in Sec. 3.3 the gyrokinetic Vlasov-

Maxwell equations and the corresponding local energy theorem are presented. By taking the second order Hamiltonian in the long wave length limit we present the Maxwell equations explicitly identifying the polarization and magnetization vectors in Sec. 3.4. The work presented in this chapter is summarized and discussed in Sec. 3.5.

3.2 Single particle dynamics

In this section the single particle gyrokinetic (gk) coordinates are derived. When low frequency, short wavelength, low amplitude fluctuations are introduced to the guiding-center dynamics (see Chap. 2) the fast cyclotron motion time scale is re-introduced and the guiding-center adiabatic invariant μ is destroyed. The gyrokinetic transformation decouples the fast time scale reintroduced by the fluctuations in such a way that the essential effects of low frequency electromagnetic fluctuations with length scales comparable to the gyration orbit radius are captured. By construction the phase coordinate "$\bar{\theta}$" of the gyrating motion is removed from the equations and the new gyrocenter magnetic moment coordinate "$\bar{\mu}$" is by construction a constant of motion $\dot{\bar{\mu}} = 0$.

In recent publications [78, 55] a method has been used which removes the gyrophase dependence from the background and perturbed dynamics in only one step. In the standard approach, used in this section, the guiding-center transformation decouples the fast timescale associated with the background dynamics, followed by the gyrokinetic coordinate transformation which is a perturbative expansion in the fluctuation amplitude. Using only one coordinate transformation has some disadvantages. First of all, the algebra gets more complicated, mainly because the calculations cannot be formulated in the Poisson bracket formalism. Secondly, by only using one coordinate transformation, the derivation is also limited to only *one* formal expansion parameter. Therefore more delicate/detailed orderings [46, 48] where the guiding-center and gyrokinetic smallness parameters are not identical cannot be used. Furthermore, we show in Sec. (3.2.2) that with the "maximal" ordering proposed in Ref.[78], no "simple" gyrokinetic coordinate transformation can be obtained. In this section we therefore choose to derive the gyrokinetic coordinates in two steps[19].

We emphasize that in this work all electromagnetic potentials except the background magnetic potential $\boldsymbol{A}_0$ are time dependent. The amplitude of magnetic fluctuations in running tokamak devices are much smaller than the externally imposed toroidal magnetic field. A time dependent toroidal magnetic field would only complicate the calculations. All time dependent magnetic fluctuations are therefore captured by the fluctuating magnetic potential $\boldsymbol{A}$.

The starting point of this two-step derivation is the Poincaré one-form[39]

γ of a charged particle in extended phasespace expressed in canonical coordinates $(\boldsymbol{x}, \boldsymbol{p}, k, t)$

$$\gamma_c = \boldsymbol{p} \cdot d\boldsymbol{x} - kdt - (h^c - k)d\tau = \gamma_a dz_a - (h^c - k)d\tau, \tag{3.1}$$

where h^c denotes the Hamiltonian

$$h^c = q\phi_0(\boldsymbol{x}, t) + \epsilon_\delta q\phi(\boldsymbol{x}, t) - \frac{1}{2m}(\boldsymbol{p} - q\boldsymbol{A}_0(\boldsymbol{x}) - \epsilon_\delta q\boldsymbol{A}(\boldsymbol{x}, t))^2, \tag{3.2}$$

and γ_a denotes the coordinate functions of the symplectic part of the Poincaré one-form. k is an energy coordinate "anti-conjugated" to the time coordinate t. τ is an unphysical curve parameter. ϵ_δ denotes the smallness parameter describing the small amplitude of the perturbations(see Sec. 3.2.2).

The extended phasespace formalism is advantageous when dealing with time dependent Hamiltonians[59, 19] as can be seen by considering the Poincaré one-form expressed in arbitrary coordinates $(\boldsymbol{y}, \tau)$

$$\gamma = \gamma_{y_i}(\boldsymbol{y}, \tau) \cdot dy_i - [H(\boldsymbol{y}, \tau) - k]d\tau. \tag{3.3}$$

A variation of the action[39]

$$S = \int_{\tau_1}^{\tau_2} \gamma, \tag{3.4}$$

with respect to y_i yields the form invariant equation of motion

$$\frac{dy_a}{d\tau} = \omega_{ab}^{-1} \frac{\partial}{\partial z_b}(H - k) = \{y_a, H - k\}, \tag{3.5}$$

where

$$\omega_{ab} = \frac{\partial \gamma_b}{\partial z_a} - \frac{\partial \gamma_a}{\partial z_b}, \tag{3.6}$$

denotes the coordinate matrix of the exterior derivative of the symplectic part of the Poincaré one-form $\omega = d\boldsymbol{\gamma}$ and $\omega_{ab}^{-1} = \{y_a, y_b\}$ denotes the inverse matrix also known as the Poisson bracket matrix. A short review of the formulation of classical mechanics in symplectic geometry can be found in App. A.1.

Next, we change coordinates to the more physical, but non-canonical, coordinates $(\boldsymbol{x}, \boldsymbol{v}, k, t)$

$$\boldsymbol{v} = \frac{1}{m}(\boldsymbol{p} - q\boldsymbol{A}_0). \tag{3.7}$$

The velocity coordinate $\boldsymbol{v}$ describes the particle velocity and $\boldsymbol{x}$ is the particle position. In the $(\boldsymbol{x}, \boldsymbol{v}, k, t)$ coordinates the one-form Eq. (3.1) reads

$$\gamma = (q\boldsymbol{A}_0 + m\boldsymbol{v}) \cdot d\boldsymbol{x} - kdt - (h_0 + \epsilon_\delta h_1 + \epsilon_\delta^2 h_2)d\tau, \tag{3.8}$$

where the Hamiltonian has been divided into unperturbed, h_0 and perturbed, $h_1 + h_2$ parts

$$h_0 = (q\phi_0 + \frac{1}{2}mv^2 - k)d\tau, \tag{3.9}$$

$$h_1 = q\phi(\boldsymbol{x}, t) - q\boldsymbol{v} \cdot \boldsymbol{A}d\tau, \tag{3.10}$$

$$h_2 = \frac{q^2}{2m}\boldsymbol{A} \cdot \boldsymbol{A}d\tau. \tag{3.11}$$

3.2.1 Guiding center dynamics

We now present the guiding-center transformation. We emphasize that the background electric potential ϕ_0 is time dependent. The guiding-center transformation treats the unperturbed part of the Hamiltonian (3.9). The purpose of the guiding-center transformation is to construct coordinates in which the fast timescale of the gyromotion is decoupled from the slower drift dynamics. Furthermore, the new coordinate μ conjugated to the gyrophase θ is by construction a constant of motion $\dot{\mu} = 0$. A derivation of the guiding-center transformation $T_{\epsilon_B}(\boldsymbol{z}) = \boldsymbol{Z}$ correct to order $\mathcal{O}(\epsilon_B)$ including time dependence of $\boldsymbol{A}_0$ is found in Chapter 2. The result is obtained using a second order Lie transform method. The resulting extended phasespace guiding-center one-form γ_0 reads:

$$\begin{aligned}\gamma_0 &= \boldsymbol{\gamma}_0^E \cdot d\boldsymbol{Z} - \mathcal{H}_0 d\tau \\ &= q\boldsymbol{A}^* \cdot d\boldsymbol{X} + \frac{m}{q}\mu d\theta - (k + \frac{m\mu}{q}S)dt - (\mathcal{H}_0 - \frac{m\mu}{q}S)d\tau,\end{aligned} \tag{3.12}$$

where $\boldsymbol{\gamma}^E$ denotes the symplectic coordinate functions and $\mathcal{H}_0 = h_0 - k$ is the extended Hamiltonian. The generalized magnetic potential is defined as

$$\boldsymbol{A}^* = \boldsymbol{A}_0 + \frac{m}{q}\boldsymbol{W} - \frac{m}{q^2}\mu\bar{\boldsymbol{R}}, \tag{3.13}$$

and the guiding-center Hamiltonian is given by

$$h_0 = q\phi_0 + \frac{1}{2}mW^2 + \mu B + \frac{m\mu}{2q}\hat{\boldsymbol{b}} \cdot \nabla \times \boldsymbol{D} + \frac{m\mu}{q}S. \tag{3.14}$$

The zeroth order guiding-center velocity is

$$\boldsymbol{W} = \boldsymbol{D} + \hat{\boldsymbol{b}}u \tag{3.15}$$

where $\boldsymbol{D} = \frac{\hat{\boldsymbol{b}} \times \nabla\phi_0}{B}$ denotes the background $\boldsymbol{E} \times \boldsymbol{B}$ velocity. In the symplectic part we have retained the terms

$$-\frac{m}{q^2}\mu\bar{\boldsymbol{R}} = -\frac{m}{q^2}\mu(\boldsymbol{R} + \frac{1}{2}\hat{\boldsymbol{b}}(\hat{\boldsymbol{b}} \cdot \nabla \times \hat{\boldsymbol{b}})) \tag{3.16}$$

In the plane perpendicular to the magnetic field the unit vectors $(\hat{\boldsymbol{e}}_1, \hat{\boldsymbol{e}}_2)$ are not fixed a priori. Only are the unit vector required to vary smoothly in space and time. This freedom (gyrogauge freedom) has no physical meaning. The first term $\boldsymbol{R} = \nabla\hat{\boldsymbol{e}}_1 \cdot \hat{\boldsymbol{e}}_2$ in (3.16) enters in order to ensure that the physics is left gyrogauge invariant. Similarly the term $\frac{m\mu}{q}S$ ensures gyrogauge invariance when the perpendicular unit vector have explicit time dependence. Note that this term has been transfered from the Hamiltonian to the t-component of γ_0 in order to ensure a gyro-gauge invariant conserved energy.

The $\frac{m\mu}{2q}\hat{\boldsymbol{b}}\cdot\nabla\times\boldsymbol{D}$ term describes[20] the lowest order FLR (Finite Larmor Radius) correction to ϕ_0

$$\frac{1}{2\pi}\oint d\theta\,\phi_0(\boldsymbol{x}) = \phi_0(\boldsymbol{X}) + \frac{m\mu}{2q^2}\hat{\boldsymbol{b}}\cdot\nabla\times\boldsymbol{D} + \cdots, \tag{3.17}$$

where the integral is along the gyroorbit for one quasi-period Ω^{-1}. Recall that an alternative definition of the curl operator is

$$\hat{\boldsymbol{b}}\cdot\nabla\times\boldsymbol{D}(\boldsymbol{X}) = \lim_{A\to 0}\frac{\oint_C \boldsymbol{D}\cdot d\boldsymbol{l}}{A} \tag{3.18}$$

where $C = \partial A$ is the positively oriented boundary curve of an arbitrary surface with area A. A short discussion of this type of gyroaverage is given in App. A.3. The FLR correction gives rise to an FLR correction of the $\boldsymbol{E}\times\boldsymbol{B}$-drift. A similar calculation (see Sec. 2) shows that the Baños[7] term, second term in Eq. (3.16), is the lowest order FLR correction to the background magnetic field (in Coulomb gauge $\nabla\cdot\boldsymbol{A} = 0$). The Baños term appears in the symplectic part of the Poincaré one form which implies that the parallel direction is "FLR corrected".

The guiding-center Poisson bracket is found by inverting the coordinate matrix of the exterior derivative of the symplectic part of the guiding-center one-form

$$\begin{aligned}\{f,g\}_0 = {}& \epsilon^{-2}\frac{q}{m}\Big(\frac{\partial f}{\partial\theta}\frac{\partial g}{\partial\mu} - \frac{\partial f}{\partial\mu}\frac{\partial g}{\partial\theta}\Big) + \epsilon^{-1}\frac{\boldsymbol{B}^*}{mB_\parallel^*}\cdot\Big(\nabla^* f\frac{\partial g}{\partial u} - \nabla^* g\frac{\partial f}{\partial u}\Big)\\ & -\epsilon^0\frac{\hat{\boldsymbol{b}}}{qB_\parallel^*}\cdot\nabla^* f\times\nabla^* g + \epsilon^{-1}\frac{q}{mB_\parallel^*}\boldsymbol{B}^*\cdot\frac{\partial\bar{\boldsymbol{A}}^*}{\partial t}\Big(\frac{\partial f}{\partial u}\frac{\partial g}{\partial h} - \frac{\partial f}{\partial h}\frac{\partial g}{\partial u}\Big)\\ & +\epsilon^0\frac{1}{B_\parallel^*}\hat{\boldsymbol{b}}\times\frac{\partial\bar{\boldsymbol{A}}^*}{\partial t}\cdot\Big(\nabla^* g\frac{\partial f}{\partial h} - \nabla^* f\frac{\partial g}{\partial h}\Big) + \Big(\frac{\partial f}{\partial h}\frac{\partial g}{\partial t^*} - \frac{\partial f}{\partial t^*}\frac{\partial g}{\partial h}\Big),\end{aligned} \tag{3.19}$$

where $\nabla^* = \nabla + \bar{\boldsymbol{R}}\frac{\partial}{\partial\theta}$ and $\frac{\partial}{\partial t^*} = \frac{\partial}{\partial t} + S\frac{\partial}{\partial\theta}$. The volume element $\mathcal{V}$ is given by $\mathcal{V} = \sqrt{\mathrm{Det}(\omega_{ab})} = m^2\hat{\boldsymbol{b}}\cdot\nabla\times\boldsymbol{A}^* = m^2B_\parallel^*$[39]. The Equations of motion (EOM) are found according to (3.5) as

$$\frac{d}{d\tau}Z_i = \{Z_i, \mathcal{H}_0\}_0. \tag{3.20}$$

Explicit expressions of the guiding-center equation of motion can be found in Sec. 2.2.3.

In the process of deriving the guiding-center coordinates the amplitude of the background magnetic $\boldsymbol{A}_0$ and electric ϕ_0 potential are formally assumed to be of $\mathcal{O}(\epsilon_B^{-1}, \epsilon_E^{-1})$, and the spatial inhomogeneity parameters $\frac{\rho_i}{L_E} \sim \epsilon_E$ and $\frac{\rho_i}{R} \sim \epsilon_B$ of the electric and magnetic fields are assumed comparable. This ordering is the most relaxed under which the adiabatic gyrosymmetry persists. In the edge region [48], but also in internal transport barrier regions [46], the ordering must be altered. In the edge region strong radial pressure gradients are found in both L-mode and H-mode plasmas[75, 104]. The typical length scale of the pressure gradient L_p is comparable to the ion poloidal gyroradius $\rho_{\theta i} = \frac{v_{th} m_i}{q_i B_\theta}$. The pressure gradients are a source of free energy which can be the main contributor to the background radial electric field E_{0r}[70, 23, 81]. From the radial force balance equation $E_{0r} \sim \frac{1}{(e_i n_i)} \partial_r P_i$, it is plausible to assume that the scale lengths of the radial pressure L_p and of the radial electrical field L_E are comparable $L_E \sim L_p$. This implies that the amplitude of background $\boldsymbol{E} \times \boldsymbol{B}$-drift is of order $D \sim \epsilon_E v_{th}$ and similar for the electric potential $e\phi_0/T_i \sim 1$. Often the situation will be such that

$$\frac{\rho_i}{L_p} > \frac{L_p}{R} \tag{3.21}$$

This implies that the background electrical inhomogeneity parameter ϵ_E is smaller than the typical guiding-center smallness parameter:

$$\epsilon_E^2 > \epsilon_B \tag{3.22}$$

It is therefore important to keep the $\mathcal{O}(\epsilon_E^2)$ terms in the guiding-center one-form (3.12) in order to have a valid model for the edge region. One could argue that it would have been more relevant to use a drift kinetic $e\phi_0/T_i \sim 1$ ordering as the basis of the gyrokinetic perturbative calculations instead. This however, would require full third order calculations in order to get the interesting FLR correction of the background electrical potential (see Eq. (3.17)).

3.2.2 Gyrokinetic Lie transform

In this section we derive the gyrokinetic coordinate transformation $T_\epsilon \boldsymbol{Z} = \bar{\boldsymbol{Z}}$, which removes the gyroangle dependency reintroduced by the perturbative parts of the Hamiltonian h_1 and h_2 and construct a new magnetic dipole moment constant of motion coordinate $\bar{\mu}$. The gyrokinetic coordinate transformation is derived in the presence of a time dependent strong perpendicular electric field having spatial scales that are considerable shorter than the background magnetic field.

We start by defining physical relevant ordering parameters. We consider only low frequency fluctuations described by the time scale ordering

parameter

$$\frac{\omega}{\Omega_i} \sim \epsilon_\omega \ll 1, \tag{3.23}$$

where ω is the characteristic fluctuation frequency and Ω is the ion cyclotron frequency. Experimental observations show that $k_\perp \rho_i \sim 0.1 - 1.0$ in the confinement region and $k_\perp \rho_i \sim 0.1$ in the edge region[103]; $k_\perp$ denotes the characteristic inverse length scale of the fluctuating field perpendicular to the magnetic field. We encompass these observations by retaining the full FLR effects described by the perpendicular length scale ordering parameter $\epsilon_\perp$

$$k_\perp \rho_i \sim \epsilon_\perp \sim 1. \tag{3.24}$$

The restriction to low frequency dynamics implies $k_\parallel \sim \omega / v_{th}$ and therefore

$$\frac{k_\parallel}{k_\perp} \sim \frac{\epsilon_\omega}{\epsilon_\perp}, \tag{3.25}$$

where $k_\parallel$ is the characteristic inverse length scale of the fluctuating field parallel to the magnetic field. The smallness parameter of the gyrokinetic perturbation analysis is the amplitude smallness parameter

$$\frac{e\phi}{T_i} \sim \frac{e v_{th} A}{T_i} \sim \frac{\delta f}{f_0} \sim \epsilon_\delta, \tag{3.26}$$

which implies

$$\frac{E}{v_{th} B_0} \sim \frac{B}{B_0} \sim \epsilon_\delta \epsilon_\perp, \tag{3.27}$$

where δf and f_0 are the fluctuating and equilibrium parts of the distribution function respectively. Furthermore, we assume that the nonlinear coupling term is comparable to the linear drive term in the Vlasov equation

$$\frac{\delta f}{f_0} \sim \frac{1}{L_p k_\perp}, \tag{3.28}$$

which is equivalent[48] to $\epsilon_\delta \sim \epsilon_E$ for $\epsilon_\perp \sim 1$. This assumption implies that long wavelength strong $\boldsymbol{E} \times \boldsymbol{B}$-flows are solely described by ϕ_0

$$\frac{|\boldsymbol{D}|}{|\boldsymbol{u}_E|} \sim \epsilon_\perp^{-1}. \tag{3.29}$$

We stress that as $\epsilon_E^2 \sim \epsilon_\delta^2 \gtrsim \epsilon_B \ll 1$, the asymptotic expansion leading to the gyrokinetic coordinates in the presence of high amplitude fluctuations only converge if all second order terms are kept.

In most low $\beta = \mu_0 P/B^2$ tokamaks this ordering overestimates the relative fluctuation amplitude of $\boldsymbol{B}$. For low β tokamaks a more realistic ordering would be $\boldsymbol{E}/(v_{th}B_0) \gg \boldsymbol{B}_\perp/B_0 \gg B_\parallel/B_0$. We stress that compressional magnetic perturbations in low β plasmas cannot be described by the gyrokinetic formalism when $\epsilon_\perp \sim 1$. The simple dispersion relation (zero pressure MHD) of the fast (compressional) Alfvén waves $\omega^2 = v_A^2 k_\perp$, and the corresponding wave equation[8] $\partial_{tt} B_\parallel = v_A^2 \nabla^2 B_\parallel$, where $v_A^2 = B^2/(\mu_0 n m_i)$ is the Alfvén speed, implies[19] $\omega/\Omega \sim \epsilon_\perp/\sqrt{\beta}$. The ordering is therefore maximal for the magnetic perturbations and is kept as such for its generality and relevance for high β plasmas.

General gyrokinetic expressions

We now derive the gyrokinetic Poincaré one-form using the phase space Lie transformation method (see App. A.2). There are different derivation paths which lead to identical results but vary in the level algebraic complexity. The gyrokinetic transformation is governed by the requirement of decoupling the cyclotron times scale from the slower time scale of the electromagnetic fluctuations by making the Poincaré one-form gyroangle independent. This is achieved by choosing appropriate generating vectorfields and functions of the Lie transformation. The gyroangle independence condition does not uniquely fix the coordinate transformation. Therefore, gyroangle independent gyrokinetic coordinates come in different versions. In this section we present the two most common formulations differing only in the way the magnetic perturbations are treated: (i) in the Hamiltonian formulation the magnetic perturbation is retained in the Hamiltonian. The parallel gyrocenter velocity is therefore "canonical": $\hat{\boldsymbol{b}} \cdot \dot{\boldsymbol{X}} \simeq \bar{u} + q/mA_\parallel$. (ii) In the symplectic formulation of gyrokinetic the magnetic perturbation is transformed to the symplectic part of the Poincaré one-form. This imply that the gyrocenter velocity in this formulation corresponds to the physical velocity. All in all the symplectic formulation eventually results in physically more intuitive equations.

The Lie transform method (see App. A.2) establish a functional relation between the unperturbed guiding-center one-form γ_0, the perturbations $\gamma_{1,2}$ and the new gyrokinetic one-form Γ. Order by order the relations are

$$\Gamma_0 = \gamma_0 + dS_0, \tag{3.30}$$

$$\Gamma_1 = \gamma_1 - \mathcal{L}_{\boldsymbol{G_1}}\gamma_0 + dS_1, \tag{3.31}$$

$$\Gamma_2 = \gamma_2 - \mathcal{L}_{\boldsymbol{G_1}}\gamma_1 + \left(\frac{1}{2}\mathcal{L}^2_{\boldsymbol{G_1}} - \mathcal{L}_{\boldsymbol{G_2}}\right)\gamma_0 + dS_2. \tag{3.32}$$

$\mathcal{L}_{\boldsymbol{G}}$ denotes the Lie derivative along the $\boldsymbol{G}$. When operating on an arbitrary differential form, α, the Lie derivative along $\boldsymbol{G}$ reads[98]: $\mathcal{L}_{\boldsymbol{G}}\alpha = i_{\boldsymbol{G}} \circ d\alpha + d \circ i_{\boldsymbol{G}}\alpha$, where $i_{\boldsymbol{G}}$ denotes interior multiplication (contraction) with $\boldsymbol{G}$ and $\circ$

denotes composition. The equations of motion do not change when adding exact differentials to the one-form so we take $\mathcal{L}_{\boldsymbol{G}} \doteq i_{\boldsymbol{G}} \circ d$.

Consider the first order relation Eq. (3.31). It involves the term

$$\mathcal{L}_{\boldsymbol{G_1}} \gamma_0 = i_{\boldsymbol{G}_1} \circ d\gamma_0 = i_{\boldsymbol{G}_1} \circ \omega_0, \tag{3.33}$$

where ω_0 denotes the guiding-center symplectic two-form. As discussed earlier the corresponding coordinate matrix has an inverse, namely the guiding-center Poisson bracket matrix Eq. (3.19). Contracting the first order relation Eq. (3.31) with the Poisson matrix yields the following equations

$$G_{1c} = \gamma_{1a}\{z_a, z_c\}_0 - \Gamma_{1a}\{z_a, z_c\}_0 + \{S_1, z_c\}_0, \tag{3.34}$$

$$H_1 + \{S_1, \mathcal{H}_0\}_0 = h_1 + \Gamma_{1a} \cdot \{Z_a, \mathcal{H}_0\}_0 - \gamma_{1a}\{Z_a, \mathcal{H}_0\}_0, \tag{3.35}$$

which provides an explicit expression for the first order generating vector field $\boldsymbol{G}_1$ and an equation from which the generating function S_1 of the first order Lie transform can be determined. A well behaved solution is ensured by choosing[24] the first order gyrokinetic Hamiltonian as the gyroaverage of the right-hand side of (3.35)

$$H_1 = \langle h_1 + \Gamma_{1a}\{Z_a, \mathcal{H}_0\}_0 - \gamma_{1a}\{Z_a, \mathcal{H}_0\}_0 \rangle, \tag{3.36}$$

where

$$\langle \cdot \rangle = \frac{1}{2\pi} \int_0^{2\pi} d\theta \, \cdot, \tag{3.37}$$

denotes gyroangle integration. The solution of S_1 is found from Eq. (3.35). It is interesting to note that in Eq. (3.34)-(3.35) only Γ_1 can be chosen freely. In passing we note that the Poisson bracket formulation in Eq.(3.35) is only possible because the gyrokinetic coordinate transformation is a perturbation of the "equilibrium" guiding-center dynamics. It is the non-degeneracy of the guiding-center two-form ensuring that the corresponding coordinate matrix has an inverse. The guiding-center transformation can be viewed as a perturbation theory by considering the "free motion" as a perturbation to the strong coupling to the magnetic field. However, the magnetic field part of the one-form, $\boldsymbol{A}_0 \cdot d\boldsymbol{x}$ is not invertible which implies that the problem cannot be expressed in terms of Poisson brackets and eventually makes the transformation harder.

Similarly, the second order relation (3.32) can be expressed in terms of Poisson bracket

$$G_{2c} = \omega_{bc}^{-1}\Big[\frac{\partial S_2}{\partial z_b} - \frac{1}{2}G_{1a}(\omega_{1ab} + \bar{\omega}_{1ab}) - \Gamma_{2b} + \gamma_{2b}\Big] \tag{3.38}$$

$$\begin{aligned} H_2 + \{S_2, \mathcal{H}_0\}_0 =& h_2 + (\Gamma_{2a} - \gamma_{2a})\{z_a, \mathcal{H}_0\}_0 \\ &+ \frac{1}{2}\omega_{da}^{-1}(\gamma_{1d} - \Gamma_{1d} + \frac{\partial S_1}{\partial z_d})(\omega_{1ab} + \bar{\omega}_{1ab})\{z_b, \mathcal{H}_0\}_0 \\ &- \frac{1}{2}(\gamma_{1a} - \Gamma_{1a} + \frac{\partial S_1}{\partial z_a})\{z_a, h_1 + H_1\}_0 \end{aligned} \tag{3.39}$$

where $\omega_{1ab} = \partial_a\gamma_{1b} - \partial_b\gamma_{1a}$ and $\bar{\omega}_{1ab} = \partial_a\Gamma_{1b} - \partial_b\Gamma_{1a}$. The second order Hamiltonian must again be the gyroaverage of the RHS of (3.39)

$$H_2 = \langle RHS \rangle, \tag{3.40}$$

in order ensure that S_2 is well behaved.

A common approach, different form what was just presented, is to determine the generating vectorfields directly from Eq. (3.30)-(3.32) and determine the generating functions subsequently[49, 79]. This approach is quite algebraically involved because the generating vector fields must be solved for one by one. In the approach presented here explicit algebraic expressions for the generating vectorfields are found. Therefore, only the generating functions must be solved for at each order, which all in all significantly simplifies the derivation path[15, 18]. Solutions of the generating functions are derived in Sec. 3.2.2. The derivation can be simplified further. In most previous derivations[15, 19, 48] the magnetic perturbation $\boldsymbol{A}$ was taken as a perturbation of the symplectic part of the Poincaré one-form. Here, the magnetic perturbation in Eq. (3.10)-(3.11) is not transfered to the symplectic part because only the background magnetic potential is part of the guiding-center kinetic velocity $\boldsymbol{v}$ defined in Eq. (3.7). In the Hamiltonian formulation of gyrokinetic the magnetic perturbation is kept in the Hamiltonian. It is therefore no surprise that the derivation is simplified by *not* moving the perturbation to the symplectic part and move it back again to the original position afterwards. Also, the derivation of the gyrokinetic equations in the symplectic formulation turns out to be simplified. This approach was also used in Ref. [92].

Hamiltonian formulation In the Hamiltonian formulation of gyrokinetics we take $\Gamma_1 = \Gamma_2 = 0$ which implies that the perturbed magnetic field $\boldsymbol{A}$ is kept in the Hamiltonian. Therefore, the magnetic perturbation acts as a potential alongside the electric potential ϕ and is not a part of the generalized magnetic field. The inductive part of the electric field $\frac{\partial}{\partial t}\boldsymbol{A}$ does not enter the equations of motion explicitly but appear as current density terms in the Amperes equation instead.

The governing equation of the first order transformation is obtained from Eq. (3.35)

$$H_1 + \{S_1, \mathcal{H}_0\}_0 = h_1. \tag{3.41}$$

A well behaved solution is obtained by choosing the gyrokinetic Hamiltonian to the gyroaverage of the RHS side of (3.41)

$$H_1 = \langle h_1 \rangle = q\langle \phi - \boldsymbol{v}\cdot\boldsymbol{A} \rangle = q\langle \psi \rangle. \tag{3.42}$$

The formal solution of S_1 obtained from (3.41) can be expressed as

$$S_1 = \big(\frac{d^0}{d\tau}\big)^{-1}\big[h_1 - \langle h_1 \rangle\big] = \big(\frac{d^0}{d\tau}\big)^{-1}\tilde{h}_1, \tag{3.43}$$

where $(d^0/d\tau)^{-1}$ denotes integration along an unperturbed guiding-center orbit. This shows that S_1 carries the gyroangle dependent part of the perturbation h_1. Therefore, the gyroangle dependent part of h_1 along unperturbed orbits $\{S_1, \mathcal{H}_0\}_0$ is subtracted from h_1 in (3.41) leaving only the gyroangle independent part $\langle H_1 \rangle$.

The second order relation (3.39) is relatively simple

$$H_2 + \{S_2, \mathcal{H}_0\}_0 = h_2 - \frac{1}{2}\{S_1, h_1 + H_1\}_0, \tag{3.44}$$

because $\gamma_1 = \Gamma_1 = 0$ and therefore $\omega_1 = \bar{\omega}_1 = 0$. We choose

$$H_2 =< h_2 - \frac{1}{2}\{S_1, h_1 + H_1\}_0 >= \frac{q^2}{2m}\langle A^2 \rangle - \frac{q}{2} < \{S_1, \psi\}_0 >, \tag{3.45}$$

where we have used the constraint $\langle S_1 \rangle = 0$.

To summarize, the gyrokinetic Poincaré one-form in the Hamiltonian formulation is

$$\Gamma = \gamma_0 - [q\langle \psi \rangle + \frac{q^2}{2m}\langle A^2 \rangle - \frac{q}{2} < \{S_1, \psi\}_0 >]d\tau. \tag{3.46}$$

The Poisson bracket is identical to the guiding-center Poisson bracket (3.19) as the symplectic part of the Poincaré one-form is unchanged. Therefore, the equations of motion are given by

$$\dot{\bar{Z}}_i = \{\bar{Z}_i, H - k\}_0. \tag{3.47}$$

Symplectic formulation In the symplectic formulation of gyrokinetics the magnetic perturbation is transformed to the symplectic part of the gyrokinetic Poincaré one-form. This formulation is physically more "natural" because the background and perturbed magnetic vector potentials are both in the symplectic part of the Poincaré one-form which in turn implies that the generalized magnetic field contains the background and perturbed magnetic field. Also, the inductive part of the electric field $\frac{\partial}{\partial t}\boldsymbol{A}$ appear explicitly in the equations of motion and the parallel gyrocenter velocity $\hat{\boldsymbol{b}} \cdot \dot{\boldsymbol{X}}$ is the actual gyrocenter velocity.

In order to transfer the magnetic perturbation to the symplectic part of the gyrokinetic Poincaré one-form we choose

$$\Gamma_{1\boldsymbol{X}} = q\langle \boldsymbol{A} \rangle \cdot d\boldsymbol{X}, \tag{3.48}$$

such that (3.35) now reads

$$H_1 + \{S_1, \mathcal{H}_0\}_0 = h_1 + q\langle \boldsymbol{A} \rangle \cdot \boldsymbol{v}_0, \tag{3.49}$$

where the unperturbed guiding-center velocity is defined as

$$\boldsymbol{v}_0 = \{\boldsymbol{X}, \mathcal{H}_0\}_0. \tag{3.50}$$

Again, H_1 equals the gyroaverage of the RHS of Eq. (3.49)

$$H_1 = q\langle \phi - (\boldsymbol{v} - \boldsymbol{v}_0)\cdot \boldsymbol{A}\rangle. \tag{3.51}$$

The formal solution of S_1 , obtained from (3.49), can be expressed as

$$S_1 = \big(\frac{d^0}{d\tau}\big)^{-1}\big[h_1 + q\langle A\rangle\cdot \boldsymbol{v}_0 - \langle h_1 + q\langle A\rangle\cdot \boldsymbol{v}_0\rangle\big] = \big(\frac{d^0}{d\tau}\big)^{-1}\tilde{h}_1, \tag{3.52}$$

showing that the solution of S_1 does not depend on Γ_1 and is identical to the corresponding solution in the Hamiltonian formulation.

We choose $\Gamma_2 = 0$ in order not to make the Poisson bracket too complex. Any choice of a finite Γ_2 would include at least quadratic terms in the fluctuating potentials, which would simplify the Amperes equations but complicate the Poisson bracket. Therefore, it is in some sense more correct to denote the symplectic formulation: "first order symplectic", because the second and higher order parts are retained in the Hamiltonian and are not moved to the symplectic part of the gyrokinetic one-form. The second order governing equation (3.39) is then given by

$$\begin{aligned} H_2 + \{S_2, h_0\}_0 = h_2 + \frac{1}{2}\omega_{da}^{-1}(-\Gamma_{1d} + \frac{\partial S_1}{\partial z_d})\bar{\omega}_{1ab}\{z_b, \mathcal{H}_0\}_0 \\ - \frac{1}{2}(-\Gamma_{1a} + \frac{\partial S_1}{\partial z_a})\{z_a, h_1 + H_1\}_0. \end{aligned} \tag{3.53}$$

In passing we note that in the traditional approach[15] the symplectic derivation is cumbersome as 4 extra terms must be calculated in Eq. (3.39).

The second order Hamiltonian is defined as the gyroaverage of the RHS of Eq. (3.53)

$$\begin{aligned} H_2 = \frac{q^2}{2m}\langle A^2\rangle + \frac{1}{2}\Gamma_1\cdot\{\boldsymbol{X},\boldsymbol{X}\}_0\cdot\{\Gamma_1,\mathcal{H}_0\}_0 - \Gamma_1\cdot\{\boldsymbol{X},\Gamma_1\}_0\cdot\boldsymbol{v}_0 \\ +\Gamma_1\cdot\{\boldsymbol{X},H_1\}_0 - \frac{1}{2}\Gamma_1\cdot\{\boldsymbol{X},\boldsymbol{v}_0\}_0\cdot\Gamma_1 - \frac{1}{2}\langle\{S_1,h_1\}_0\rangle, \end{aligned} \tag{3.54}$$

where the identity

$$\langle h_1\rangle = H_1 - \boldsymbol{\Gamma}_1\cdot\boldsymbol{v}_0, \tag{3.55}$$

was used.

To summarize, the gyrokinetic Poincaré one-form in the symplectic formulation is

$$\Gamma = \gamma_0 + q\langle \boldsymbol{A}\rangle\cdot d\bar{\boldsymbol{X}} - [q\langle\phi - (\boldsymbol{v}-\boldsymbol{v}_0)\cdot\boldsymbol{A}\rangle + H_2]d\tau. \tag{3.56}$$

In comparison with the guiding-center and the Hamiltonian formulation of gyrokinetics the $\boldsymbol{X}$-component of symplectic part of the Poincaré one-form is changed: $\Gamma_X = q\boldsymbol{A}^* + q\langle A\rangle \doteq q\boldsymbol{A}^{**}$. Therefore, the Poisson bracket

is altered

$$\{f,g\}^S = \frac{q}{m}(\frac{\partial f}{\partial\theta}\frac{\partial g}{\partial\bar{\mu}} - \frac{\partial f}{\partial\bar{\mu}}\frac{\partial g}{\partial\bar{\theta}}) + \frac{\boldsymbol{B}^{**}}{mB_\parallel^{**}}\cdot(\bar{\nabla}^{**}f\frac{\partial g}{\partial\bar{u}} - \bar{\nabla}^{**}g\frac{\partial f}{\partial\bar{u}})$$
$$-\frac{\hat{\boldsymbol{b}}}{qB_\parallel^{**}}\cdot\bar{\nabla}^{**}f\times\bar{\nabla}^{**}g + \frac{q}{mB_\parallel^{**}}\boldsymbol{B}^{**}\cdot\frac{\partial\boldsymbol{A}^{**}}{\partial t}(\frac{\partial f}{\partial\bar{u}}\frac{\partial g}{\partial k} - \frac{\partial f}{\partial k}\frac{\partial g}{\partial\bar{u}})$$
$$+\frac{\hat{\boldsymbol{b}}}{B_\parallel^{**}}\cdot\Big\{\frac{\partial f}{\partial k}(\frac{\partial\boldsymbol{A}^{**}}{\partial t}\times\bar{\nabla}^{**}g) - \frac{\partial g}{\partial k}(\frac{\partial\boldsymbol{A}^{**}}{\partial t}\times\bar{\nabla}^{**}f)\Big\} + (\frac{\partial f}{\partial k}\frac{\partial g}{\partial t^*} - \frac{\partial f}{\partial t^*}\frac{\partial g}{\partial k}), \tag{3.57}$$

where

$$\bar{\nabla}^{**} = \bar{\nabla}^{*} - \frac{q^2}{m}\frac{\partial}{\partial\bar{\mu}}\boldsymbol{A}^{**}\frac{\partial}{\partial\bar{\theta}} \tag{3.58}$$

Also, the volume element $\mathcal{V}$ becomes: $\mathcal{V} = \sqrt{\mathrm{Det}(\omega_{ab})} = m^2\hat{\boldsymbol{b}}\cdot\nabla\times\boldsymbol{A}^{**} = m^2B_\parallel^{**}$. The equations of motion are obtained from the new Poisson bracket

$$\dot{\bar{\boldsymbol{Z}}} = \{\bar{\boldsymbol{Z}}, H-k\}^S. \tag{3.59}$$

Iterative solution of the first order generating function S_1

Until now we have only shown the governing equation Eq. (3.41) and have given the formal solution Eq. (3.43) of the first order generating function of the Lie transform S_1. In order to determine the first order gyrokinetic coordinate transformation and the second order gyrokinetic Poincaré one-form an explicit solution of S_1 must be obtained.

We follow the standard approach[19] and solve for S_1 iteratively. It is convenient to repeat the governing equation (3.41) for S_1

$$\{S_1,\mathcal{H}_0\}_0 = \widetilde{\psi}. \tag{3.60}$$

to observe that the integration constant can always be chosen such that $\langle S_1\rangle = 0$. To obtain an iterative solution to S_1 we expand the Poisson bracket

$$\dot{\boldsymbol{Z}}\cdot\frac{\partial S_1}{\partial\boldsymbol{Z}} = \epsilon_E\boldsymbol{D}\cdot\nabla S_1 + \Omega\frac{\partial S_1}{\partial\theta} + \epsilon_\omega\frac{\partial S_1}{\partial t} + \mathcal{O}(\epsilon_E^3,\epsilon_B) = \tilde{\psi}. \tag{3.61}$$

The leading order solution is

$$S_1^0 = \frac{1}{\Omega}\int_0^\theta d\theta'\, q(\phi - u\widetilde{A_\parallel - \boldsymbol{c}_\perp}\cdot\boldsymbol{A}_\perp). \tag{3.62}$$

Note that the $-\boldsymbol{A}_\perp\cdot\boldsymbol{D}$ part of $\tilde{\psi}$ is not included in S_1^0 because it is of $\mathcal{O}(\epsilon_E\epsilon_\delta)$. It is also clear that the time dependence of the background electric potential ϕ_0 does change the lowest order solution S_1^0 of the first order generating function.

From Eq. (3.61), the importance of ordering the amplitude of the background $\boldsymbol{E} \times \boldsymbol{B}$-flow smaller than the thermal velocity unity is seen. If the background $\boldsymbol{E} \times \boldsymbol{B}$-flow is comparable to the thermal velocity, no simple solution of S_1^0 can be obtained because the $\Omega\partial_\theta S_1$ term is not dominating

$$\frac{|\boldsymbol{D} \cdot \nabla S_1|}{|\Omega \partial_\theta S_1|} \sim \epsilon_\perp,$$

when $\epsilon_\perp \sim 1$. In Ref. [78, 33] the background $\boldsymbol{E} \times \boldsymbol{B}$-flow is ordered $D \sim v_{th}$ and the characteristic frequency of the fluctuating fields is assumed comparable to the gyrofrequency $\omega/\Omega \sim 1$. Invoking this more relaxed ordering does not destroy the Larmor orbit quasi-symmetry but it hinders an iterative solution of S_1. Anyhow, in Ref. [78, 33] the, $\Omega\partial_\theta S_1$ term is assumed being the dominating term in the governing equation (3.41), and iterative solutions of S_1 resembling Eq. (3.62) are derived in conflict with the ordering used.

3.3 Vlasov-Maxwell system

In this contribution a self-consistent Maxwell-Vlasov system will be derived using variational techniques. Various variational methods are available [106, 26]. We have chosen to apply the mixed Eulerian-Lagrangian extended phase-space action[64, 32, 90]. We consider this method to be simpler and more intuitive than the Eulerian e.g. Ref. [26] and the Hamilton-Jacobi methods e.g. Ref. [77]. Naturally, all methods lead to identical results when applied to identical problems.

The Vlasov-Maxwell system is obtained by considering a smooth continuum of particles (trajectories) $\boldsymbol{z}_\alpha = \boldsymbol{z}_\alpha(\boldsymbol{z}_0, \tau)$ in extended phase space; α denotes species. All particles in the continuum are labeled by their initial position $\boldsymbol{z}_0 = \boldsymbol{z}_\alpha(\boldsymbol{z}_0, t_0)$ and the particle trajectories are parametrized by τ. The density of initial configurations is given by a *smooth* labeling function $f_{0\alpha} = f_{0\alpha}(\boldsymbol{z}_0, t)$, one for each species α. This leads to the particle Lagrangian L_p of the Vlasov-Maxwell system expressed in arbitrary coordinates

$$L_{p\alpha} = \int d^8\boldsymbol{z}_0 \mathcal{J}_0 \, f_{0\alpha}^E(\boldsymbol{z}_0)\mathcal{L}(z_\alpha(\boldsymbol{z}_0, t), \phi, \boldsymbol{A}), \tag{3.63}$$

where $\mathcal{J}_0$ denotes the Jacobian of a coordinate transformation from canonical to arbitrary coordinates $(\boldsymbol{x}, \boldsymbol{p}, k, t)_\alpha \to \boldsymbol{z}_\alpha$ at initial time t_0; the labeling function in extended phasespace f_0^E is defined as

$$f_{0\alpha}^E = f_{0\alpha}\delta(t_0 - t_1)\delta(k_0 - h(\boldsymbol{z}_0, t_0)), \tag{3.64}$$

and the particle Lagrangian density is

$$\mathcal{L}_\alpha = \gamma_i \dot{z}_i - (H - k). \tag{3.65}$$

$\mathcal{L}_\alpha$ is the Lagrangian counterpart to the single particle Poincaré one-form

$$\gamma_i dz_{\alpha i} - (h-k)d\tau = [\gamma_i \dot{z}_{\alpha i} - (h-k)]d\tau = Ld\tau. \tag{3.66}$$

The Vlasov-Maxwell action S is now defined as

$$S = \int_{t_1}^{t_2} d\tau \left\{ \sum_\alpha L_{p\alpha} + \int_{-\infty}^{\infty} d^3r\, \mathcal{L}_f \right\}, \tag{3.67}$$

where the Eulerian electromagnetic field energy Lagrangian density $\mathcal{L}_f$ is

$$\mathcal{L}_f = \frac{\epsilon_0 E^2}{2} - \frac{B^2}{2\mu_0}, \tag{3.68}$$

and the electric and magnetic fields are

$$\boldsymbol{E} = -\nabla\Phi - \frac{\partial}{\partial t}\boldsymbol{\mathcal{A}}, \tag{3.69}$$

$$\boldsymbol{B} = \nabla \times \boldsymbol{\mathcal{A}}. \tag{3.70}$$

$\Phi = \phi_0 + \phi$ denotes the total electric potential and $\boldsymbol{\mathcal{A}} = \boldsymbol{A}_0 + \boldsymbol{A}$ is the total magnetic vector potential.

In previous works the inductive part of the electric field has been neglected[21, 92]. Neglecting this term leads to Amperes equation (i.e. no Maxwell correction $\epsilon_0 \frac{\partial}{\partial t}\boldsymbol{E}$). As pointed out in Ref. [28], neglecting the inductive electric field destroys the gauge invariance and leads to unphysical terms in the energy flux[21]. We refer the reader to Ref. [28] on how to construct the field Lagrangian such that the Ampere's equation is obtained but also on how to implement quasi-neutrality into the variational principle in a consistent way.

In the following we utilize that the integral of an arbitrary Lagrangian function $g(\boldsymbol{z}_\alpha(\boldsymbol{z}_0, t_0), \tau)$ along all Lagrangian trajectories

$$G = \int d^8\boldsymbol{z}_{0\alpha} \mathcal{J}_{0\alpha}\, f^E_{0\alpha}(\boldsymbol{z}_0) g(\boldsymbol{z}_\alpha(\boldsymbol{z}_0;\tau)), \tag{3.71}$$

can be written in the Eulerian coordinates $\boldsymbol{z}$

$$G = \int d^8\boldsymbol{z} \mathcal{J}_\alpha\, f^E_\alpha(\boldsymbol{z},\tau) g(\boldsymbol{z},\tau), \tag{3.72}$$

where we have defined the Eulerian distribution function

$$\mathcal{J}_\alpha f^E_\alpha(\boldsymbol{z},t) = \int d^8\boldsymbol{z}_{0\alpha} \mathcal{J}_{0\alpha} f^E_{\alpha 0} \delta^{(8)}(\boldsymbol{z} - \boldsymbol{z}_\alpha). \tag{3.73}$$

We note that the Eulerian coordinates $\boldsymbol{z}$ carry no subscript in order to avoid confusion with the Lagrangian particle trajectories $\boldsymbol{z}_\alpha$, but in the gyrokinetic coordinates are indeed species dependent as different species have different

mass and charge. The Eulerian distribution function satisfy by construction the equation

$$\frac{\partial}{\partial \boldsymbol{z}} \cdot (\dot{\boldsymbol{z}} \mathcal{J}_\alpha f_\alpha^E) = 0. \tag{3.74}$$

Using that the volume $\mathcal{J}$ is conserved along Hamiltonian flows (see Sec. A.1.4)

$$\frac{\partial}{\partial z_a}(\dot{z}_a \mathcal{J}) = 0, \tag{3.75}$$

we obtain the Vlasov equation

$$\dot{\boldsymbol{z}} \cdot \frac{\partial}{\partial \boldsymbol{z}} f = 0. \tag{3.76}$$

The equations of motion are obtained by varying the action S assuming that the fields $(\boldsymbol{z}_\alpha, \phi, \boldsymbol{A})$ vanish at the integration boundaries.

Vlasov-Maxwell system in particle coordinates

So far the Maxwell-Vlasov action was presented in arbitrary coordinates. However, an interesting consistency check of the validity of the variational principle is a derivation in kinetic particle coordinates $(\boldsymbol{x}, \boldsymbol{v})$. In kinetic coordinates $(\boldsymbol{x}, \boldsymbol{v})$ the particle Lagrangian density becomes

$$\mathcal{L}^k_{p\alpha} = (q\boldsymbol{A} + m\boldsymbol{v}_\alpha) \cdot \dot{\boldsymbol{x}}_\alpha - k_\alpha \dot{t}_\alpha - [q\phi(\boldsymbol{x}_\alpha, t) + \frac{1}{2} m v_\alpha^2 - k_\alpha], \tag{3.77}$$

and the volume element is $\mathcal{J} = m^3$. A variation the action S with respect to the fields $\boldsymbol{z}_\alpha$ shows that the fields evolve according to the one particle equations of motion Eq. (3.5). Variation of S with respect to $\phi(\boldsymbol{r}, t)$ and $\boldsymbol{A}(\boldsymbol{r}, t)$ yields the Poisson and Amperes equations respectively

$$\epsilon_0 \nabla \cdot \boldsymbol{E} = \sum_\alpha \int d^6 z_{0\alpha} m_\alpha^3 f_{0\alpha 0}\, q_\alpha \delta^{(3)}(\boldsymbol{r} - \boldsymbol{x}_\alpha), \tag{3.78}$$

$$\frac{1}{\mu_0} \nabla \times \boldsymbol{B} = \epsilon_0 \frac{\partial \boldsymbol{E}}{\partial t} + \sum_\alpha \int d^6 z_0 m_\alpha^3 f_0\, q \dot{\boldsymbol{x}}_\alpha \delta^{(3)}(\boldsymbol{r} - \boldsymbol{x}_\alpha). \tag{3.79}$$

The charge and current densities are expressed in the Lagrangian picture. However, multiplying the Maxwell equations by

$$1 = \int d^6 z\, \delta^{(6)}(\boldsymbol{z} - \boldsymbol{z}_\alpha) \tag{3.80}$$

the charge and current densities can be expressed in terms of the Eulerian distribution function Eq. (3.73)

$$\int d^6 z_{0\alpha} m_\alpha^3 f_{0\alpha 0}\, q_\alpha \delta^{(3)}(\boldsymbol{r} - \boldsymbol{x}_\alpha) = \int d^6 z m_\alpha^3\, f(\boldsymbol{z}, t) q_\alpha \delta^{(3)}(\boldsymbol{r} - \boldsymbol{x}), \tag{3.81}$$

$$\int d^6 z_0 m_\alpha^3 f_0\, q \dot{\boldsymbol{x}}_\alpha \delta^{(3)}(\boldsymbol{r} - \boldsymbol{x}_\alpha) = \int d^6 z m_\alpha^3\, f(\boldsymbol{z}, t) q \dot{\boldsymbol{x}} \delta^{(3)}(\boldsymbol{r} - \boldsymbol{x}), \tag{3.82}$$

which are the well known Maxwell equations of the Vlasov-Maxwell system[64].

3.3.1 General gyrokinetic Vlasov-Maxwell equations

Before presenting the gyrokinetic Vlasov-Maxwell equations it is helpful to elaborate a little on how phasespace functions transforms under a coordinate transformation $T_\epsilon y = z$

$$f(y) = F(z) = F(T_\epsilon y) = \delta T_\epsilon F(y), \tag{3.83}$$

where δT_ϵ denotes the pullback[39] of F under T_ϵ. When the coordinate transformation is given by an asymptotic expansion in a small parameter ϵ the pullback can be considered an operator simply by Taylor expanding around $\epsilon = 0$ and collect terms with equal powers of ϵ. Similarly, using the inverse coordinate transformation $T_\epsilon^{-1} z = y$ the transformation of phase-space functions can be given in terms of the push-forward map δT_ϵ^{-1}

$$f(y) = F(z) = f(T_\epsilon^{-1} z) = \delta T_\epsilon^{-1} f(z). \tag{3.84}$$

Similarly, a one-form γ expressed in local coordinates $\boldsymbol{y}$

$$\begin{aligned} \gamma &= \gamma_i(z) dy_i = \gamma_i(y) \frac{\partial y_i}{\partial z_l} dz_l = \Gamma_l(z) d\boldsymbol{z}_l \\ &= \gamma(T_\epsilon^{-1}\boldsymbol{z}) \cdot d(T_\epsilon^{-1}\boldsymbol{z}) = \delta T_\epsilon^{-1}[\gamma_l(z) dz_l]. \end{aligned} \tag{3.85}$$

Therefore, the gyrokinetic Poincaré one-form Γ derived in section (3.2.2) can be written as

$$\begin{aligned} \Gamma(\bar{\boldsymbol{Z}}, t) = \gamma(\boldsymbol{z}, t) = \delta T_{\epsilon_B}^{-1} \delta T_\epsilon^{-1} \Big[(q\boldsymbol{A}_0 + m\boldsymbol{W} + m\boldsymbol{c}_\perp) \cdot d\boldsymbol{x} \\ -(q\Phi + \frac{1}{2} m W^2 + \frac{1}{2} m c_\perp^2 + m\boldsymbol{W} \cdot \boldsymbol{c}_\perp - q\boldsymbol{v} \cdot \boldsymbol{A} + \frac{q^2}{2m} A^2 - k_0) d\tau \Big]. \end{aligned} \tag{3.86}$$

where $T_{\epsilon_B}^{-1}$ denotes the inverse guiding-center transformation. The particle one-form is expressed in the zeroth order preliminary coordinates (see Sec. 2.2.1) and all functions are evaluated in gyrokinetic coordinates e.g.

$$\boldsymbol{v}(\bar{\boldsymbol{Z}}) = \bar{u} \hat{\boldsymbol{b}}(\bar{\boldsymbol{X}}) + \boldsymbol{D}(\bar{\boldsymbol{X}}, t) + \boldsymbol{c}_\perp(\bar{\boldsymbol{Z}}, t). \tag{3.87}$$

Formally, the gyrokinetic Vlasov-Maxwell action is given by

$$S = \int_{t_1}^{t_2} d\tau \big\{ \sum_\alpha \bar{L}_{p\alpha} + \int_{-\infty}^{\infty} d^3 r \, \mathcal{L}_f \big\}, \tag{3.88}$$

where the gyrokinetic particle Lagrangian is

$$\bar{L}_p = \int d^8 \bar{\boldsymbol{Z}}_0 \bar{\mathcal{J}}_0 \, \bar{F}_{0\alpha}^E(\bar{\boldsymbol{Z}}_0) \big(\Gamma_i \dot{\bar{\boldsymbol{Z}}}_{\alpha i} - [H(\bar{\boldsymbol{Z}}_\alpha, t) - \bar{k}_{\alpha 0}] \big), \tag{3.89}$$

and

$$H = h_0 + H_1 + H_2 \tag{3.90}$$

is the gyrokinetic Hamiltonian. Alternatively, the gyrokinetic particle Lagrangian can be expressed in terms of the guiding-center and gyrokinetic pullbacks as in Eq. (3.86). The advantage of the pullback representation of the gyrokinetic one-form Γ is the simplified derivation of general gyrokinetic Maxwell equations. As an example consider the functional variation of the gyrokinetic particle Lagrangian with respect to the electric potential $\phi(\boldsymbol{r})$

$$\begin{aligned}
&\frac{\delta}{\delta\phi(\boldsymbol{r})}\int d\tau \bar{L}_p(\bar{\boldsymbol{Z}}_\alpha, \phi(\bar{\boldsymbol{Z}}_\alpha)) \\
=&\frac{\delta}{\delta\phi(\boldsymbol{r})}\int d\tau \int d^8\boldsymbol{z}_0 m^3\, f_0^E L_p(\boldsymbol{z}_\alpha, \phi(\boldsymbol{z}_\alpha)) \\
=&-\int d\tau d^3\boldsymbol{r}\int d^8\boldsymbol{z}_0 m^3\, f_0^E q\delta(\boldsymbol{r}-\boldsymbol{x}_\alpha) \\
=&-\int d\tau d^3\boldsymbol{r}\int d^8\boldsymbol{z} m^3\, f^E(\boldsymbol{z},\tau) q\delta(\boldsymbol{r}-\boldsymbol{x}) \\
=&-\int d\tau d^3\boldsymbol{r}\int d^8\bar{\boldsymbol{Z}}\mathcal{J}\,\bar{F}^E q\delta T_{\epsilon_B}^{-1}\delta T_\epsilon^{-1}\delta^{(3)}(\boldsymbol{r}-\bar{\boldsymbol{X}}),
\end{aligned} \tag{3.91}$$

where we change to the Eulerian description going from line three to four. Naturally, the explicit a cumbersome pullback transformation must be carried out in practical application. However, the method is useful in theoretical manipulations.

Gyrokinetic equations of motion

Now we are ready to derive the gyrokinetic equations of motion. The particle trajectories are obtained by varying the gyrokinetic action Eq. (3.88) with respect to $\bar{\boldsymbol{Z}}_\alpha$

$$\dot{\bar{\boldsymbol{Z}}}_\alpha = \{\bar{\boldsymbol{Z}}_\alpha, H - \bar{k}_\alpha\}, \tag{3.92}$$

where the Poisson bracket is given by Eq. (3.19) (Hamiltonian) or Eq. (3.57) (Symplectic). This shows that the fields $\bar{\boldsymbol{Z}}_\alpha$ indeed follow the gyrokinetic single particle trajectories.

A variation of the gyrokinetic action with respect to $\phi(\boldsymbol{r})$ or $\phi_0(\boldsymbol{r})$ yields the general gyrokinetic Poisson equation

$$\epsilon_0\nabla\cdot\boldsymbol{E} = \sum_\alpha q\int d^6\bar{\boldsymbol{Z}}\mathcal{J}\,\bar{F}\delta T_{\epsilon_B}^{-1}\delta T_\epsilon^{-1}\delta^{(3)}(\boldsymbol{r}-\bar{\boldsymbol{X}}). \tag{3.93}$$

Note that when varying with respect to ϕ_0, terms including $\boldsymbol{D}$ in the symplectic part of the particle one-form expressed in preliminary guiding-center

coordinates are canceled by kinetic energy terms in the Hamiltonian, leaving only the pullback of the variation of the potential term, $q\phi_0$ in the Poisson equation. This shows that splitting the electric potential into background and perturbed parts in general leads to an underdetermined system. From this formal expression of the gyrokinetic Poisson equation, both parts of the electrical field cannot be determined simultaneously. Only if the Poisson equations really express different parts of the solution both electrical potentials can be obtained. The most natural way to accomplish this task is to perform a filtering operation[50] in agreement with the ordering of the electrical fields, meaning splitting the equation into a long wavelength high amplitude part responsible for ϕ_0 and an equation for low amplitude short wavelength governing ϕ. Such a consistent splitting has not been derived in this work.

However, in the following sections we derive the Vlasov-Maxwell equations from the simplified Poincaré one-form Eq. (3.107) and (3.109) in various limiting forms. Here, terms of order $\mathcal{O}(\epsilon_B, \epsilon_E^3, \epsilon_E\epsilon_\omega)$ are neglected in the perturbed fields $(\phi, \boldsymbol{A})$, which implies that two different Poisson equations are derived. We have not examined whether both ϕ_0 and ϕ can be determined from these equations, but we have chosen to show both equations in the coming sections anyway. We need both Poisson equations in order to rewrite the energy theorem which can be compared to earlier results. Also, until the question whether both potentials can be determined simultaneously is settled, having two equations gives the opportunity to pick the Poisson equation which is most practical in a given situation.

A variation with respect to $\boldsymbol{A}$ gives the Amperes equation

$$\frac{1}{\mu_0}\nabla\times\boldsymbol{B} = \epsilon_0\frac{\partial \boldsymbol{E}}{\partial t} + \sum_\alpha \int d^6\bar{\boldsymbol{Z}}\,\mathcal{J}\,\bar{F}\delta T_{\epsilon_B}^{-1}\delta T_\epsilon^{-1}\big\{\delta(\boldsymbol{r}-\bar{\boldsymbol{X}})(\frac{q}{m}\boldsymbol{A}(\bar{\boldsymbol{X}},t)-\boldsymbol{v}(\bar{\boldsymbol{Z}}))\big\}. \tag{3.94}$$

Energy theorem

An arbitrary variation of the action S Eq. (3.88) satisfying the equations of motion Eq. (3.92)-(3.94) is given by

$$\begin{aligned}\delta S = &\int d^4\boldsymbol{r}\Big\{\delta\phi\big[\epsilon_0\nabla\cdot\boldsymbol{E} - \sum_\alpha\int d^6\bar{\boldsymbol{Z}}\mathcal{J}\,\delta T_{\epsilon_B}^{-1}\delta T_\epsilon^{-1}q\delta(\boldsymbol{r}-\bar{\boldsymbol{X}})\big]\\ &+\int d^4\boldsymbol{r}\Big\{\delta\phi_0\big[\epsilon_0\nabla\cdot\boldsymbol{E} - \sum_\alpha\int d^6\bar{\boldsymbol{Z}}\mathcal{J}\,\delta T_{\epsilon_B}^{-1}\delta T_\epsilon^{-1}q\delta(\boldsymbol{r}-\bar{\boldsymbol{X}})\big]\\ &+\delta\boldsymbol{A}\big[\epsilon_0\partial_t\boldsymbol{E} - \frac{1}{\mu_0}\nabla\times\boldsymbol{B}\\ &+\sum_\alpha\int d^6\bar{\boldsymbol{Z}}\mathcal{J}\,q\delta T_{\epsilon_B}^{-1}\delta T_\epsilon^{-1}\big\{\delta(\boldsymbol{r}-\bar{\boldsymbol{X}})(\frac{q}{m}\boldsymbol{A}(\bar{\boldsymbol{X}})-\boldsymbol{v}(\bar{\boldsymbol{Z}})\big\}\big]\\ &-\frac{\partial}{\partial t}\big[\epsilon_0\delta\boldsymbol{A}\cdot\boldsymbol{E}\big] - \nabla\cdot\big[\epsilon_0(\delta\phi+\delta\phi_0)\boldsymbol{E}+\frac{1}{\mu_0}\delta\boldsymbol{A}\times\boldsymbol{B}\big]\\ &+\int dt\sum_\alpha\int d^6\bar{\boldsymbol{Z}}\mathcal{J}\,\delta Z_a\big[\dot{Z}_b\omega_{ab}-\frac{\partial}{\partial t}\Gamma_a-\frac{\partial}{\partial Z_a}H\big]+\frac{d}{dt}\big(\Gamma_b\delta Z_b\big),\end{aligned} \tag{3.95}$$

where $d^4\boldsymbol{r} \doteq dtd^3\boldsymbol{r}$. We note that even though the variations with respect to ϕ_0 and ϕ result in identical Poisson equations both potentials contribute to the boundary terms. The laws of physics do not change with time so the system is invariant to time translations $t \to t+s$

$$\delta S = \int d^4\boldsymbol{r}\frac{\partial}{\partial t}\mathcal{L}_f + \int dt\int d\Lambda\frac{\partial}{\partial t}L_p. \tag{3.96}$$

Identifying Eq. (3.95) and Eq. (3.96) and using the equations of motion yields the local energy equation

$$\int d^4\boldsymbol{r}\frac{\partial}{\partial t}\mathcal{E} + \nabla\cdot\boldsymbol{S} = 0, \tag{3.97}$$

where the local energy density is

$$\mathcal{E} = \frac{\epsilon_0 E^2}{2} + \frac{B^2}{2\mu_0} - \Phi\epsilon_0\nabla\cdot\boldsymbol{E} + \int d^6\bar{\boldsymbol{Z}}\mathcal{J}\,\bar{F}H\delta(\boldsymbol{r}-\bar{\boldsymbol{X}}), \tag{3.98}$$

and the local energy density flux is given as

$$\boldsymbol{S} = \frac{1}{\mu_0}\boldsymbol{E}\times\boldsymbol{B} - \Phi\boldsymbol{J}^{tot} + \int d^6\bar{\boldsymbol{Z}}\mathcal{J}\,\bar{F}H\dot{\bar{\boldsymbol{X}}}\delta(\boldsymbol{r}-\bar{\boldsymbol{X}}). \tag{3.99}$$

The total current $\boldsymbol{J}_{tot}$ is

$$\boldsymbol{J}_{tot} = \int d^6\bar{\boldsymbol{Z}}\bar{\mathcal{J}}\,\bar{F}q\delta T_{\epsilon_B}^{-1}\delta T_\epsilon^{-1}\big\{\delta(\boldsymbol{r}-\bar{\boldsymbol{X}})(\frac{q}{m}\boldsymbol{A}(\bar{\boldsymbol{X}})-\boldsymbol{v}(\bar{\boldsymbol{Z}})\big\}. \tag{3.100}$$

In order to move the particle Lagrangian under the spatial integration with respect to $\boldsymbol{r}$ the following identity has been used

$$\int dt \int d^6\bar{\boldsymbol{Z}}\mathcal{J}\,\frac{d}{dt}(\bar{F}H) = \int d^4\boldsymbol{r}\int d^6\bar{\boldsymbol{Z}}\mathcal{J}\,\frac{\partial}{\partial t}\big[\bar{F}(\bar{\boldsymbol{Z}},t)\delta^{(3)}(\boldsymbol{r}-\bar{\boldsymbol{X}})H[\phi(\boldsymbol{r},t),\boldsymbol{A}(\boldsymbol{r},t),\cdots]\big] + \nabla\cdot\big[\dot{\bar{\boldsymbol{X}}}\bar{F}(\bar{\boldsymbol{Z}},t)\delta^{(3)}(\boldsymbol{r}-\bar{\boldsymbol{X}})H[\phi(\boldsymbol{r},t),\boldsymbol{A}(\boldsymbol{r},t),\cdots]\big]. \tag{3.101}$$

In the energy density function(3.98) the Poisson equations can be inserted in the $-\Phi\epsilon_0\nabla\cdot\boldsymbol{E}$ term. This eliminates the electric potentials ϕ and ϕ_0 from the particle Hamiltonian. A similar cancellation of the $\Phi\boldsymbol{J}^{tot}$ and the electric potential terms in the Hamiltonian also exists.

Maxwell equations in terms of free and bound charge

The Maxwell equations (3.93)-(3.94) take forms that are rather lengthy and complicated. A better understanding of the gyrokinetic Maxwell equations is gained by formulating the source terms in terms of "free" and "bound" charge and current as suggested by classical electrodynamics [52]

$$\epsilon_0\nabla\cdot\boldsymbol{E} = \bar{\rho} - \nabla\cdot\boldsymbol{P}, \tag{3.102a}$$

$$\frac{1}{\mu_0}\nabla\times\boldsymbol{B} = \bar{\boldsymbol{J}} + \boldsymbol{J}_{pol} + \boldsymbol{J}_M + \epsilon_0\frac{\partial\boldsymbol{E}}{\partial t}, \tag{3.102b}$$

where $(\bar{\rho},\bar{\boldsymbol{J}})$ denotes the free gyrocenter charge and current respectively; $-\nabla\cdot\boldsymbol{P} = \rho_{pol}$ is the polarization charge; $\boldsymbol{J}_{pol} = \frac{\partial}{\partial t}\boldsymbol{P}$ denotes the polarization current and $\boldsymbol{J}_M = \nabla\times\boldsymbol{M}$ is the magnetization current. In the classical sense all particles in a fully ionized plasma are considered free particles. The free "gyrocenter charge" is associated with the charge carried by the gyrocenters having unperturbed (gc) gyroorbits. Similarly, the polarization charge is not bound charge but describes the charge accumulation due to deviations from the unperturbed guiding-center dynamics caused by the perturbations $(\phi,\boldsymbol{A})$. This identification can be seen by rewriting the general Poisson equation (3.93) as

$$\epsilon_0\nabla\cdot\boldsymbol{E} = \sum_\alpha q_\alpha\int d^6\bar{Z}\bar{\mathcal{J}}\big[\bar{F}\delta(\boldsymbol{r}-T^{-1}_{\epsilon_B}\bar{\boldsymbol{X}}) + \bar{F}(\delta T^{-1}_\epsilon - 1)\delta(\boldsymbol{r}-T^{-1}_{\epsilon_B}\bar{\boldsymbol{X}})\big], \tag{3.103}$$

where the first term corresponds to the "free gyrocenter charge" and the last term is the polarization charge. The polarization charge is therefore not bound in the classical sense but is bound to the free gyrocenter charge. Similarly, the free and bound parts of the current density can be identified using the pullback representation[18]. This shows that the magnetization

current consists of two parts: an intrinsic contribution due to the intrinsic magnetization dipole moment which arise from the fast cyclotron motion $\boldsymbol{M}_{intr} \propto \mu$, and a contribution due to the comoving polarization charge Ref. [52][(chap. 6.7)] $\boldsymbol{M}_P \propto \boldsymbol{P} \times \dot{\bar{\boldsymbol{X}}}$.

With these identifications we see that under the assumption of quasineutrality $\bar{\rho} - \nabla \cdot \boldsymbol{P} = 0$, the free gyrocenter charge

$$\frac{\partial}{\partial t}\bar{\rho} = \nabla \cdot \frac{\partial}{\partial t}\boldsymbol{P} = -\nabla \cdot \bar{\boldsymbol{J}} \tag{3.104}$$

and the polarization charge

$$\frac{\partial}{\partial t}\rho_{pol} + \nabla \cdot \boldsymbol{J}_{pol} = 0 \tag{3.105}$$

are conserved. In the gyrokinetic equations the polarization vector is explicitly time dependent through the perturbed potential $(\phi, \boldsymbol{A})$ which therefore leads to a finite polarization current. Under the gyrokinetic ordering presented in Sec. (3.2.2) we expect the polarization current to appear at $\mathcal{O}(\epsilon_\delta \epsilon_\omega \epsilon_\perp)$. The gyrokinetic Maxwell equations are not derived to this order in previous contributions so the polarization current has not been explicitly derived. However, seen in the light of the central role played by the polarization current in the conservation laws of free gyrocenter and polarization charge, the identification and derivation is of theoretical interest. An explicit derivation will be given in the long wavelength limit in Sec. (3.4.4).

The polarization current $\frac{\partial}{\partial t}\boldsymbol{P}$ should not be confused with the current arising from the polarization drift $\boldsymbol{v}_p = \frac{1}{\Omega}\hat{\boldsymbol{b}} \times \frac{d}{dt}\dot{\bar{\boldsymbol{X}}}$. Remember that the polarization vector vanishes when $\epsilon_\delta \to 0$, whereas the polarization drift does not. The polarization drift is a result of being in a non-inertial reference frame moving with $\boldsymbol{W}$ whereas the polarization current is due to an explicit time dependence of the polarization vector. However, in the symplectic formulation the perturbed potentials are moved to the symplectic part of the one-form which gives rise to a "$\langle \boldsymbol{A} \rangle$" polarization drift making the distinction more difficult. In passing we note that from Eq. (3.103) no polarization density due to ϕ_0 should be expected in the gyrokinetic Poisson equation simply because the last term vanishes as $\epsilon \to 0$. The gyrokinetic polarization charge arise due to deviations from the guiding-center dynamics when the perturbed fields are introduced. Therefore, the polarization charge due to ϕ_0 resides in the gyrokinetic volume element, which contains the term $\hat{\boldsymbol{b}} \cdot \nabla \times \boldsymbol{D} = B^{-1}\nabla_\perp^2 \phi_0 + \mathcal{O}(\epsilon_B)$.

This analog to classical electrodynamics has been demonstrated for the guiding-center Vlasov-Maxwell system in e.g. Ref. [90, 105] and in generalized terms for the gyrokinetic Vlasov-Maxwell system in Ref. [19, 18].

3.4 Long wave length limit of H_2

In their most general forms the gyrokinetic Vlasov-Maxwell equations (see sections 3.2.2,3.2.2 and 3.3.1) are often too complex and complicated for most practical applications. Especially the quadratic terms in the gyrokinetic Hamiltonian are cumbersome in numerical simulations. The quadratic terms are the generators of polarization and magnetization in the Maxwell equations and must be kept. It is therefore common practice to simplify the gyrokinetic model by introducing additional approximations. In general the simplifications of the quadratic terms fall into two categories: (i) in the linearized approach the Maxwell equations are linearized assuming a Maxwellian background distribution function in μ, $\bar{F}_0 \propto \exp(-\mu B/T)$ in the polarization charge and in the magnetization and polarization currents. In this approach the full FLR effects $k_\perp \rho_i \sim 1$ are retained. First examples of the linearized gyrokinetic model can be found in Ref. [36, 58] (electrostatic, slab geometry). In Ref. [47] the linearized equations are presented including shear Alfvénic fluctuations and lately the linearized gyrokinetic equations including a time independent background electric potential ϕ_0 and compressional Alfvénic perturbation were presented in Ref. [48]. (ii) By taking the gyrokinetic second order Poincaré one-form in the long wavelength limit (LWL) $\epsilon_\perp^3 \ll 1$, equations are obtained which are able to describe the evolution of an arbitrary distribution function $\bar{F}$, but at the expense of retaining only the FLR effects to the lowest orders $\epsilon_\perp^3 \ll 1$ in the polarization and magnetization vectors. The LWL is feasible for global descriptions where full FLR effects are assumed to be less important. This limiting form of the gyrokinetic Vlasov-Maxwell equations could be feasible for edge/SOL turbulence where the fluctuation amplitudes $\delta n/n \sim 0.1 - 0.5$ approaches unity and $k_\perp \rho_i \lesssim 0.1$[94, 11, 103]. However, the importance of keeping full FLR effects in the polarization and magnetization densities in edge turbulence models is yet unclear[87].

In this section we derive the gyrokinetic Vlasov-Maxwell equations in the limit where second order terms in the gyrokinetic one-form are taken in the LWL. As already mentioned no second order perturbations are transfered to the symplectic part of the gyrokinetic Poincaré one-form in either formulation of gyrokinetic, leaving the original Hamiltonian Eq. (3.19) and symplectic Eq. (3.57) Poisson brackets unchanged. All approximations are carried out on the gyrokinetic Poincaré one-form, such that all equations of motion and the corresponding energy theorem follow from variations of the same Poincaré one-form which guarantees energetic consistency automatically. An alternative approach is to apply the approximations in the pullback representations of the gyrokinetic Maxwell equations. Following this approach, the derivation of an energy theorem consistent with the equations of motion is not automatically guaranteed.

The remaining part of this section is organized as follows. In Sec. 3.4.1 we

invoke common approximations to the gyrokinetic Hamiltonian, consistent with the gyrokinetic ordering. Next, we present the gyrokinetic Vlasov-Maxwell equation taking the Hamiltonian in the long wave length limit. In Sec. 3.4.2 we present the Vlasov-Maxwell equations in the Hamiltonian formulation of gyrokinetics. The corresponding equations in the symplectic formulation of gyrokinetic are found in Sec. 3.4.3. Lastly, in Sec. 3.4.4 we present the Vlasov-Maxwell equations in a version which includes the polarization current in the Amperes equation. Details of the long wavelength calculations can be found in Appendix 3.A.1.

3.4.1 Simplified Hamiltonians

The gyrokinetic Hamiltonians $H_{1,2}$ are in their most general form very complex. For practical purposes the gyrokinetic one-form is approximated. We will make the following approximations which are widely applied in the literature.[49, 15, 36, 48]

1. In the fluctuating potentials $(\phi, \boldsymbol{A})$ we neglect the $\mathcal{O}(\epsilon_B, \epsilon_E^2)$ part of the guiding-center transformation $\boldsymbol{x} - (\boldsymbol{X} + \boldsymbol{\rho}_0) = \mathcal{O}(\epsilon_B, \epsilon_E^2)$. An $\mathcal{O}(\epsilon_E^2)$ term $\propto \boldsymbol{\rho}\hat{\boldsymbol{b}} \cdot \nabla \times \boldsymbol{D}$ enters the guiding-center transformation. Discarding these higher order corrections is in agreement with the ordering $\epsilon_\delta \sim \epsilon_E$.

2. The zeroth order velocity $\boldsymbol{v}_0$ appearing in the first and second order gyrokinetic transformation is approximated as $\boldsymbol{v}_0 = \boldsymbol{W} + \boldsymbol{c}_\perp$, thus neglecting $\mathcal{O}(\epsilon_B, \epsilon_E\epsilon_\omega, \epsilon_E^3)$ contributions in the $\mathcal{O}(\epsilon_\delta)$ equations.

3. In the second order Hamiltonians Eq. (3.45) and Eq. (3.54), only the leading order term $\{\theta, \mu\}$, in $\frac{1}{2}\langle\{S_1, h_1\}\rangle$ is retained. The magnitude of the $\{\bar{\boldsymbol{X}}, \bar{\boldsymbol{X}}\}$ term is comparable to the $\{\theta, \mu\}$ term, but the $\{\bar{\boldsymbol{X}}, \bar{\boldsymbol{X}}\}$ term leads to terms in the Maxwell equations which are at least $\mathcal{O}(\epsilon_E)$ smaller than the terms kept, and is therefore neglected (see App. (3.A.1)).

4. The $\mathcal{O}(\epsilon_E\epsilon_\delta)$ term, $-q\langle \boldsymbol{A}_\perp \cdot \boldsymbol{D}\rangle$ is kept in the second order Hamiltonian.

Hamiltonian formulation Invoking these approximations the explicit expression of the Poincaré one-form in the Hamiltonian formulation is given by

$$\bar{\Gamma} = \gamma_0^E \cdot d\bar{\boldsymbol{Z}} - \big[\mathcal{H}_0 + H_1 + H_2\big]d\tau \tag{3.106}$$

where the first and second order Hamiltonian are defined as

$$H_1 = q\langle \phi - \boldsymbol{A} \cdot (\hat{\boldsymbol{b}}\bar{u} + \boldsymbol{c}_\perp)\rangle = q\langle\psi_0\rangle - q\langle \boldsymbol{A} \cdot \boldsymbol{c}_\perp\rangle, \tag{3.107a}$$

$$H_2 = -q\langle \boldsymbol{A}_\perp \cdot \boldsymbol{D}\rangle + \frac{q^2}{2m} < \delta\boldsymbol{A} \cdot \delta\boldsymbol{A} > -\frac{q^2}{2m}\frac{\partial}{\partial\bar{\mu}} < \tilde{\psi}\frac{\partial S_1}{\partial\bar{\theta}} > . \tag{3.107b}$$

This result is in agreement with the previous results in Refs. [48, 19] in the limit where $\frac{\partial}{\partial t}\phi_0 = 0$. We note that in the Hamiltonian formulation the magnetic perturbation retains the "canonical" form $q\boldsymbol{A}\cdot\boldsymbol{v}$ and acts as a potential in line with the electric potential ϕ.

Symplectic formulation In the symplectic formulation the explicit expression for the Poincaré one-form reads

$$\bar{\Gamma} = \gamma_0^E \cdot d\bar{\boldsymbol{Z}} + q\langle A\rangle \cdot d\bar{\boldsymbol{X}} - \big[\mathcal{H}_0 + H_1 + H_2\big]d\tau, \tag{3.108}$$

where the first and second order Hamiltonian reads

$$H_1 = q\langle \phi - \boldsymbol{A}\cdot\boldsymbol{c}_\perp\rangle, \tag{3.109a}$$

$$\begin{aligned} H_2 =& \frac{q^2}{2m}\langle A^2\rangle - \frac{q^2}{2m}\langle A_\parallel\rangle^2 - \frac{q^2}{2m}\frac{\partial}{\partial\bar{\mu}} < \tilde{\psi}\frac{\partial S_1}{\partial\bar{\theta}} > + \frac{1}{B}\langle \boldsymbol{A}_\perp\rangle\cdot\hat{\boldsymbol{b}}\times\nabla H_1 \\ &+ \frac{q}{B}\hat{\boldsymbol{b}}\times\langle\boldsymbol{A}_\perp\rangle\cdot\nabla\langle\boldsymbol{A}\rangle\cdot\boldsymbol{W} - \frac{q}{2B}\boldsymbol{D}\cdot\nabla\langle\boldsymbol{A}_\perp\rangle\cdot\hat{\boldsymbol{b}}\times\langle\boldsymbol{A}_\perp\rangle. \end{aligned} \tag{3.109b}$$

This does *not* fully agree with previous results. The result should agree with Ref. [19] in the limit $\boldsymbol{D}\to 0$. In this limit the second last term: $\frac{qu}{B}\hat{\boldsymbol{b}}\times\langle\boldsymbol{A}_\perp\rangle\cdot\nabla\langle A_\parallel\rangle$, does not appear in eq.(173) Ref. [19]. However, considering the general expression for H_2 Eq. (129) in Ref. [19] we find that the expression is identical to (3.39). This can be seen using the Jacobi identity. The last term in this general expression for H_2 eq.(129) of Ref. [19] gives us the missing term.

In the following these approximated Hamiltonians form the basis of the derivations in the long wave length limit.

3.4.2 Hamiltonian formulation of gyrokinetics

In the long wave length limit discarding terms of $\mathcal{O}(\epsilon_\perp^3, \epsilon_E^3)$ or higher, the second order Hamiltonian H_2, Eq. (3.107b), reads

$$\begin{aligned} H_2 =& -q\big[\boldsymbol{A}_\perp + \frac{\rho_0^2}{4}\nabla_\perp^2\boldsymbol{A}_\perp\big]\cdot\boldsymbol{D} + \frac{q^2}{2m}(A_\parallel^2 + \frac{\rho_0^2}{2}A_\parallel\nabla_\perp^2 A_\parallel) \\ &- \frac{m}{2B^2}|\nabla_\perp\psi_0|^2 + \frac{\bar{\mu}}{2B}(B_\parallel^2 + B_\perp^2) - \frac{q}{B}\hat{\boldsymbol{b}}\times\nabla\psi_0\cdot\boldsymbol{A}_\perp, \end{aligned} \tag{3.110}$$

where

$$\nabla_\perp\psi_0 \doteq \nabla_\perp\phi - u\nabla_\perp A_\parallel, \tag{3.111}$$

and the perturbed magnetic fields are defined as

$$B_\parallel = \hat{\boldsymbol{b}}\cdot\nabla_\perp\times\boldsymbol{A}_\perp, \tag{3.112}$$

$$\boldsymbol{B}_\perp = \nabla A_\parallel\times\hat{\boldsymbol{b}}. \tag{3.113}$$

The zeroth and first order parts of the gyrokinetic one-form $\bar{\Gamma}$ Eq. (3.106) retain full FLR effects and are not modified.

The third second term in H_2 is the collisionless skin depth term which is an artifact of the Hamiltonian formulation of gyrokinetics[19]. This term does not introduce turbulence at the skin depth scale but can cause cancellations problems in the parallel Amperes equation in numerical simulations[67, 47]. The fourth term represents the lowest order FLR correction to the skin depth term and might get important as the physical important part of the skindepth term is small and only appears after a cancellation of two large terms in the parallel current and in the skin depth term itself. The FLR correction to the skin depth term has not been derived in previous contributions.

In the Hamiltonian formulation of gyrokinetic's, magnetic perturbations are retained in the Hamiltonian which implies that the magnetic perturbations and the electric potential form the generalized potential $\psi = q^{-1}H_1$. The generalized potential results in the perpendicular drifts $(B^{-1}\hat{\boldsymbol{b}} \times \nabla\langle\psi\rangle)$ (see Eq. (3.116b)). The energies associated to these perpendicular drifts, except the modified grad-B drift which is of $\mathcal{O}(\epsilon_\perp^4)$, are contained in the $|\nabla_\perp \psi_0|^2$ term. The first order perturbed perpendicular currents interact with the perpendicular magnetic perturbation described by the term $-q/B\hat{\boldsymbol{b}}\times \nabla\psi_0 \cdot \boldsymbol{A}_\perp$.

Due to the perturbed magnetic fields we get a correction $\bar{\mu}/(2B)(B_\parallel^2 + B_\perp^2)$ to the fluctuating perpendicular energy $\bar{\mu}B = mc_\perp^2/2 + \cdots$, appearing in the guiding-center Hamiltonian h_0. The correction due to $B_\parallel$ appears on a different form in comparison with other works e.g.Ref. [19, 18], because there the correction is calculated from the first order Hamiltonian taken in the LWL. The correction due to the perpendicular magnetic field has to the knowledge of the author never been presented before. As we show in this section this term is responsible for intrinsic magnetization, originating from the cyclotron motion, in the parallel Amperes equation.

Now we derive the Maxwell equations by varying the gyrokinetic action

$$S = \int d\tau \int d^3\boldsymbol{r}\mathcal{L}_f + \int d\tau \int d^8\bar{\boldsymbol{Z}} m^2 B_\parallel^* \bar{F}^E \big[\gamma_0^E \cdot \dot{\bar{\boldsymbol{Z}}} - H\big], \tag{3.114}$$

where the total gyrokinetic Hamiltonian is defined as

$$H = \mathcal{H}_0 - H_1 - H_2, \tag{3.115}$$

with the second order Hamiltonian taken in LWL Eq. (3.110).

Equations of motion The equations of motion follow from the general expression Eq. (3.47)

$$\dot{\bar{\boldsymbol{X}}} = \frac{\boldsymbol{B}^*}{mB_\parallel^*}\frac{\partial H}{\partial \bar{u}} + \frac{1}{qB_\parallel^*}\hat{\boldsymbol{b}}\times\nabla H + \frac{1}{B_\parallel^*}\hat{\boldsymbol{b}}\times\frac{\partial \boldsymbol{A}^*}{\partial t}, \tag{3.116a}$$

$$\dot{\bar{u}} = -\frac{\boldsymbol{B}^*}{mB_\parallel^*}\cdot\nabla H - \frac{q}{mB_\parallel^*}\boldsymbol{B}^*\cdot\frac{\partial \boldsymbol{A}^*}{\partial t}. \tag{3.116b}$$

To lowest order the equations of motion equal the guiding-center counterparts (see Sec.(2.2.3)) including the polarization drift $(\Omega^{-1}\hat{\boldsymbol{b}}\times(\partial_t+\boldsymbol{W}\cdot\nabla)\boldsymbol{D})$ of the background electric field. The most important contribution of the perturbed electromagnetic potentials is the term $(1/B_\parallel^*)\hat{\boldsymbol{b}}\times\nabla\psi$, which consists of the following perturbed particle drifts responsible for the radial turbulent transport:

- electrostatic perturbed $\boldsymbol{E}\times\boldsymbol{B}$-drift: $B_\parallel^{*-1}\hat{\boldsymbol{b}}\times\nabla\langle\phi\rangle$,
- the magnetic flutter drift: $-uB_\parallel^{*-1}\hat{\boldsymbol{b}}\times\nabla\langle A_\parallel\rangle$,
- and the perturbed grad-B drift: $-B_\parallel^{*-1}\hat{\boldsymbol{b}}\times\nabla\langle\boldsymbol{c}_\perp\cdot\boldsymbol{A}_\perp\rangle = \bar{\mu}/(qB)\hat{\boldsymbol{b}}\times\nabla B_\parallel + \cdots$.

As a consequence of keeping the perturbed potentials in the Hamiltonian the corresponding polarization drifts do not appear to the order retained here.

Poisson equation Variation of the action S (3.67) with respect to $\phi(\boldsymbol{r})$ yields the Poisson equation

$$\epsilon_0\nabla\cdot\boldsymbol{E} = \sum_\alpha q\bar{N}_\alpha - \nabla\cdot\boldsymbol{P}_\alpha^\phi, \tag{3.117}$$

where the gyroaveraged gyrocenter density is

$$\bar{N} = \int d^6\bar{\boldsymbol{Z}}m^2B_\parallel^*\,\bar{F}\langle\delta(\boldsymbol{r}-\bar{\boldsymbol{X}}-\boldsymbol{\rho}_0)\rangle, \tag{3.118}$$

and $\boldsymbol{P}^\phi$ denotes the polarization vector

$$\boldsymbol{P}^\phi = \int d^6\bar{\boldsymbol{Z}}m^2B_\parallel^*\,\boldsymbol{\mathcal{P}}^\phi, \tag{3.119}$$

where

$$\boldsymbol{\mathcal{P}}^\phi = -\bar{F}\delta(\boldsymbol{r}-\bar{\boldsymbol{X}})[\frac{m}{B^2}\nabla_\perp\psi_0 + \frac{q}{B}\boldsymbol{A}_\perp\times\hat{\boldsymbol{b}}] \tag{3.120}$$

is the polarization density vector. We note that only the gyroaveraged density "$\bar{N}$" contains ($\bar{\mu}$-dependent) FLR corrections. The polarization vector

in the LWL describes finite inertia effects. The first term $\nabla_\perp \psi_0$ is the gyrokinetic realization of the polarization drift as a shielding term here also including the magnetic perturbations as they appear as potentials in the Hamiltonian. The second term $(-\nabla \cdot (\bar{F}q/B\boldsymbol{A}_\perp \times \hat{\boldsymbol{b}}) = NB_\parallel/B)$ appears because the velocity coordinates in the Hamiltonian formulation are canonical $\boldsymbol{v}_\perp \simeq \boldsymbol{c}_\perp + q/m\boldsymbol{A}_\perp$, and is not a gyrokinetic shielding term representing the perpendicular inductive electrical field as claimed in Ref. [48, 18, 19]. In the long wavelength limit the total time derivative of the gyrokinetic Poisson equation (assuming quasi-neutrality) resembles the drift fluid vorticity equation(see Chap.(4.3))[16, 9, 89]. Rederiving the vorticity equation in terms of the canonical velocity component show exactly this term. Also, the term does not appear in the the symplectic formulation of gyrokinetic (see Sec. 3.4.3), where the velocity coordinates are not canonical. The inductive part of the $\boldsymbol{E} \times \boldsymbol{B}$-drift should appear at $\mathcal{O}(\epsilon_\delta \epsilon_\perp \epsilon_\omega)$ which is not retained here. Actually, the last term represents a part of the inductive $\boldsymbol{E} \times \boldsymbol{B}$-flow as we will demonstrate in Sec. 3.4.4.

Poisson equation II Variation of the action S (3.67) with respect to $\phi_0(\boldsymbol{r})$ yields the Poisson equation

$$\epsilon_0 \nabla \cdot \boldsymbol{E} = \sum_\alpha q\bar{N}_{0\alpha} - \nabla \cdot \boldsymbol{P}^{\phi_0}_\alpha, \tag{3.121}$$

where the background FLR-corrected density is

$$\bar{N}_0 = \int d^6\bar{\boldsymbol{Z}} B^*_\parallel \, q\bar{F}\delta(\boldsymbol{r} - \bar{\boldsymbol{X}}) + \nabla \cdot \big(\frac{\hat{\boldsymbol{b}}}{B} \times \nabla \times \big[\hat{\boldsymbol{b}} \frac{m\mu\bar{F}\delta(\boldsymbol{r} - \bar{\boldsymbol{X}})}{2q}\big]\big), \tag{3.122}$$

and the polarization vector $\boldsymbol{P}^{\phi_0}$ is given by

$$\begin{aligned} \boldsymbol{P}^{\phi_0} = \int d^6\bar{\boldsymbol{Z}} m^2 B^*_\parallel \, & \frac{m\bar{F}\delta(\boldsymbol{r} - \bar{\boldsymbol{X}})}{B} \hat{\boldsymbol{b}} \times (\dot{\bar{\boldsymbol{X}}} - \boldsymbol{D}) \\ & - \frac{q\bar{F}\delta(\boldsymbol{r} - \bar{\boldsymbol{X}})}{B} \big[\boldsymbol{A}_\perp + \frac{\rho_0^2}{4}\nabla^2_\perp \boldsymbol{A}_\perp\big] \times \hat{\boldsymbol{b}} \end{aligned} \tag{3.123}$$

We notice that no terms of $\mathcal{O}(\epsilon_E)$ appear in $\boldsymbol{P}^{\phi_0}$ because the $\boldsymbol{D}$-part of $\dot{\bar{\boldsymbol{X}}}$ is canceled: $\hat{\boldsymbol{b}} \times (\dot{\bar{\boldsymbol{X}}} - \boldsymbol{D}) \sim \mathcal{O}(\epsilon_\delta, \epsilon_E^3, \epsilon_B)$. The second term is a reminiscence of the Hamiltonian formulation of gyrokinetics and arise because the velocity component is canonical.

As we discussed in Sec. 3.3.1 we have not clarified whether ϕ_0 and ϕ can be simultaneously determined in the current framework. Furthermore, ϕ_0 cannot easily be determined from (3.121). In most applications quasi neutrality is assumed. The leading order ϕ_0 dependent term is the $\mathcal{O}(\epsilon_E^3)$ order polarization drift current term in the $m\bar{F}/B\hat{\boldsymbol{b}} \times (\dot{\bar{\boldsymbol{X}}} - \boldsymbol{D})$ term, which

is nonlinear in ϕ_0 and is not easily solved in numerical simulations. Furthermore the equation gets quite involved because the full $\dot{\bar{\boldsymbol{X}}}$ must be retained in the first term in order to ensure energetic consistency. This is a consequence of having moved the background $\boldsymbol{E}\times\boldsymbol{B}$-drift $\boldsymbol{D}$ into the symplectic part of $\bar{\Gamma}$. If the frame of reference is not moving with $\boldsymbol{D}$ a shielding term $\bar{F}\nabla_\perp\phi_0$, similar to what appears in (3.117) would appear in the polarization vector $\boldsymbol{P}^{\phi_0}$[68]. In some sense Eq. (3.121) is more suitable for determining the perturbed potentials $(\phi,\boldsymbol{A})$ as the the first term in $\boldsymbol{P}^{\phi_0}$ contains a term $\nabla\cdot(m\bar{F}/B\nabla_\perp\psi_0)$. All in all we are not very confident that the Poisson equation Eq. (3.121) is a helpful expression for a self consistent determination of the strong background electric field ϕ_0, but future investigation will hopefully clarify this. The main argument for showing the result is that the polarization vector $\boldsymbol{P}^{\phi_0}$ is used to rewrite the energy theorem on a form which resembles earlier contributions.

Parallel Amperes equation Variation of the action S Eq. (3.67) with respect to $A_\parallel(\boldsymbol{r})$ yields

$$\begin{aligned}-\epsilon_0\frac{\partial E_\parallel}{\partial t}+\frac{1}{\mu_0}\hat{\boldsymbol{b}}\cdot\nabla\times\boldsymbol{B}&=\bar{J}_\parallel+J_{M\parallel}\\&-\frac{q^2}{m}\big[NA_\parallel+\frac{P_\perp}{m\Omega^2}\nabla_\perp^2A_\parallel+A_\parallel\nabla_\perp^2(\frac{P_\perp}{2m\Omega^2})\big],\end{aligned}\tag{3.124}$$

where $\bar{J}_\parallel$ denotes the gyroaveraged parallel current

$$\bar{J}_\parallel=\int d^6\bar{\boldsymbol{Z}}m^2B_\parallel^*\,\bar{F}\bar{u}\delta(\boldsymbol{r}-\bar{\boldsymbol{X}}-\boldsymbol{\rho}_0),\tag{3.125}$$

and $J_{M\parallel}$ is the parallel part $(\hat{\boldsymbol{b}}\cdot\nabla\times\boldsymbol{M})$ of the magnetization current

$$J_{M\parallel}=\nabla_\perp\cdot\int d^6\bar{\boldsymbol{Z}}m^2B_\parallel^*\,\bar{F}\delta(\boldsymbol{r}-\bar{\boldsymbol{X}})\big(-\boldsymbol{\mathcal{P}}^\phi u+\frac{\mu B}{B^2}\hat{\boldsymbol{b}}\times\boldsymbol{B}_\perp\big).\tag{3.126}$$

The perpendicular pressure enters the last two terms and is defined as

$$P_\perp=\int d^6\bar{\boldsymbol{Z}}m^2B_\parallel^*\,\bar{F}\mu B\delta(\boldsymbol{r}-\bar{\boldsymbol{X}})\tag{3.127}$$

The first term in $J_{M\parallel}$ is the magnetization current due to the comoving polarization charge (see Ref. [52][(chap. 6.7)])

$$\begin{aligned}&\nabla_\perp\cdot\int d^6\bar{\boldsymbol{Z}}m^2B_\parallel^*\,\bar{F}\delta(\boldsymbol{r}-\bar{\boldsymbol{X}})\big(-\boldsymbol{\mathcal{P}}^\phi u\big)\\&=\hat{\boldsymbol{b}}\cdot\nabla\times\int d^6\bar{\boldsymbol{Z}}m^2B_\parallel^*\,\bar{F}\boldsymbol{\mathcal{P}}^\phi\times u\hat{\boldsymbol{b}}+\mathcal{O}(\epsilon_B^2)\end{aligned}\tag{3.128}$$

and the last term is the parallel intrinsic magnetization current: $\hat{\boldsymbol{b}} \cdot \nabla \times \boldsymbol{M}_{intr} = \nabla \cdot (\boldsymbol{M}_{intr} \times \hat{\boldsymbol{b}}) + \mathcal{O}(\epsilon_B)$. This terms represents the diamagnetic response of the cyclotron motion to the perpendicular magnetic perturbations. The intrinsic magnetization did not appear in previous contributions, e.g.[48, 19]. The last three terms is the collisionless skin depth term with lowest order FLR corrections. The polarization current $\partial_t \boldsymbol{P}^\phi$ does not appear in the parallel Amperes equation because the polarization vector vanishes in parallel direction to the order considered here.

Perpendicular Amperes equation Variation of the action S Eq. (3.67) with respect to $\boldsymbol{A}_\perp(r)$ yields

$$-\epsilon_0 \frac{\partial \boldsymbol{E}_\perp}{\partial t} + \frac{1}{\mu_0}(\nabla \times \boldsymbol{B})_\perp = \bar{\boldsymbol{J}}_D + \boldsymbol{J}_{\psi_0} + \boldsymbol{J}_{M\mu} + \boldsymbol{J}_{pol}, \tag{3.129}$$

where

$$\bar{\boldsymbol{J}}_D = \int d^6\bar{\boldsymbol{Z}} m^2 B_\parallel^* \left[q\bar{F}\boldsymbol{D} + \nabla_\perp^2(\bar{F}\boldsymbol{D}\frac{\bar{\mu}B}{2B\Omega})\right]\delta(\boldsymbol{r} - \bar{\boldsymbol{X}}), \tag{3.130}$$

is the gyroaveraged current of the strong $\boldsymbol{E} \times \boldsymbol{B}$-drift $\boldsymbol{D}$, and

$$\boldsymbol{J}_{\psi_0} = \int d^6\bar{\boldsymbol{Z}} m^2 B_\parallel^* \frac{q\bar{F}}{B}\hat{\boldsymbol{b}} \times \nabla\psi_0, \tag{3.131}$$

is the current due to the perturbed potentials. The intrinsic magnetization current is

$$\boldsymbol{J}_{M\mu} = \int d^6\bar{\boldsymbol{Z}} m^2 B_\parallel^* \bar{F}\langle\delta(\boldsymbol{r} - \bar{\boldsymbol{X}} - \boldsymbol{\rho}_0)\boldsymbol{c}_\perp\rangle - \nabla \times \big(\frac{\bar{F}\delta(\boldsymbol{r} - \bar{\boldsymbol{X}})\hat{\boldsymbol{b}}B_\parallel\bar{\mu}}{B}\big). \tag{3.132}$$

The first term contains the classical dia-magnetic dipole moment $-\mu\hat{\boldsymbol{b}}$. The magnetization current due to the comoving polarization charge, $\propto \nabla\times(\boldsymbol{\mathcal{P}}^\phi \times \boldsymbol{D})$ is of $\mathcal{O}(\epsilon_E\epsilon_\delta)$ and enters at next order in the perturbation analysis. It is interesting to note that the polarization drift current ($\propto \hat{\boldsymbol{b}} \times (\partial_t + \boldsymbol{D} \cdot \nabla)\boldsymbol{D}$) does not appear in the perpendicular Amperes equation as the term is of $\mathcal{O}(\epsilon_E\epsilon_\omega, \epsilon_E^3)$. The "missing" polarization drift current is a consequence of the simplifications made to the Hamiltonians in Sec. 3.4.1, where only zeroth order guiding-center drifts ($\dot{\boldsymbol{X}} \simeq \boldsymbol{v}_0$) were retained when appearing in combination with the perturbed fields.

Energy Theorem The local energy density is obtained from Eq. (3.98)

$$\begin{aligned}\mathcal{E} =& \frac{\epsilon_0 E^2}{2} + \frac{B^2}{2\mu_0} - \nabla\phi \cdot \boldsymbol{P}^\phi - \nabla\phi_0 \cdot \boldsymbol{P}^{\phi_0} \\ &+ \int d^6\bar{\boldsymbol{Z}} m^2 B_\parallel^* \bar{F}\delta(\bar{\boldsymbol{X}} - \boldsymbol{r})[H - q\phi_0 - \frac{m\mu}{2q}\hat{\boldsymbol{b}} \cdot \nabla \times \boldsymbol{D} - q\langle\phi\rangle),\end{aligned} \tag{3.133}$$

where partial integration and the Poisson equations have been inserted to eliminate the, $\Phi\epsilon_0\nabla\cdot\boldsymbol{E}$ term. The energy density can be put on a form which resembles earlier results by inserting the explicit expressions of polarization vectors Eq. (3.120) and Eq. (3.123)

$$\begin{aligned}\mathcal{E} =&\frac{\epsilon_0 E^2}{2}+\frac{B^2}{2\mu_0}+\int d^6\bar{\boldsymbol{Z}}m^2B_\parallel^*\,\delta(\boldsymbol{r}-\bar{\boldsymbol{X}})\bar{F}\Big\{\mu B+\frac{1}{2}mW^2\\&-qu\langle A_\parallel\rangle-q\langle\boldsymbol{c}\cdot\boldsymbol{A}_\perp\rangle+\frac{q^2}{2m}(A_\parallel^2+\frac{\rho_0^2}{2}A_\parallel\nabla_\perp^2A_\parallel)+\frac{\mu}{2B}(B_\parallel^2+B_\perp^2)\\&+\frac{1}{2}mu_E^2-\frac{mu^2}{2B^2}B_\perp^2-\frac{qu}{B}\boldsymbol{A}_\perp\cdot\boldsymbol{B}_\perp+m\boldsymbol{D}\cdot[\dot{\boldsymbol{X}}-\boldsymbol{D}]\Big\}.\end{aligned}\tag{3.134}$$

This result resembles the results of earlier contributions[19, 48] but there are some differences. Naturally, the inclusion of new terms in the LWL second order Hamiltonian result in new terms in the energy theorem. However, we also find other differences that are associated with the usage of the Poisson equation Eq. (3.121). We notice that all electric potential terms are no longer present in the Hamiltonian. This also includes the lowest order FLR correction $\frac{m\mu}{2q}\hat{\boldsymbol{b}}\cdot\nabla\times\boldsymbol{D}$ of ϕ_0. In earlier contribution this term appears in the energy theorem whereas it is canceled by the $\phi_0\nabla\cdot\boldsymbol{P}^{\phi_0}$ term in this paper. Similarly, terms originating from the term, $-\langle\boldsymbol{A}_\perp\cdot\boldsymbol{D}\rangle$ do not appear in the energy density $\mathcal{E}$ but persists in Ref. [48], which again can be ascribed the elimination of potential like terms by inserting the Poisson equation associated with ϕ_0 Eq. (3.121).

Including the boundary terms which appear due to partial integration when the explicit polarization vectors were inserted into the general energy expression Eq. (3.133) the energy flux density $\boldsymbol{S}$ Eq. (3.99) reads

$$\begin{aligned}\boldsymbol{S} =&\frac{1}{\mu_0}\boldsymbol{E}\times\boldsymbol{B}-(\phi_0+\phi)\boldsymbol{J}^{tot}+\int d^6\bar{\boldsymbol{Z}}\mathcal{J}\,\bar{F}H\dot{\bar{\boldsymbol{X}}}\delta(\boldsymbol{r}-\bar{\boldsymbol{X}})\\&+\frac{\partial}{\partial t}\Big[\boldsymbol{P}_\phi\phi+\boldsymbol{P}_{\phi_0}\phi_0+\boldsymbol{D}\times\big(\hat{\boldsymbol{b}}\frac{m\mu\bar{F}\delta(\boldsymbol{r}-\bar{\boldsymbol{X}})}{2q}\big)\\&-\phi_0\frac{\hat{\boldsymbol{b}}}{B}\times\nabla\times\big(\hat{\boldsymbol{b}}\frac{m\mu F\delta(\boldsymbol{r}-\bar{\boldsymbol{X}})}{2q}\big)\Big],\end{aligned}\tag{3.135}$$

where the total current is

$$\boldsymbol{J}^{tot}=\hat{\boldsymbol{b}}(\bar{J}_\parallel+\bar{J}_{M\parallel})+\bar{\boldsymbol{J}}+\boldsymbol{J}_{\psi_0}+\boldsymbol{J}_M,\tag{3.136}$$

which is the sum of the currents in the parallel (see Eq. (3.124)) and perpendicular (see Eq. (3.129)) Amperes equations. We note that

$$\frac{1}{\mu_0}\boldsymbol{E}\times\boldsymbol{B}-\Phi\boldsymbol{J}_M=\frac{1}{\mu_0}\boldsymbol{E}\times\boldsymbol{B}+\nabla\Phi\times\boldsymbol{M}\approx\boldsymbol{E}\times\boldsymbol{H}\tag{3.137}$$

where $\boldsymbol{H}=\frac{1}{\mu_0}\boldsymbol{B}-\boldsymbol{M}$, denotes the auxiliary magnetic field. The "missing" $\frac{\partial}{\partial t}\boldsymbol{A}\times\boldsymbol{M}$ term is of $\mathcal{O}(\epsilon_\delta^2\epsilon_\omega)$ and is expected to be found if the calculations are taken to $\mathcal{O}(\epsilon_\delta^3)$.

3.4.3 Symplectic formulation of gyrokinetics

Now we derive the gyrokinetic Vlasov-Maxwell equations as they appear in the symplectic formulation of gyrokinetics (see Sec. 3.4.1). Again, we take the second order Hamiltonian in the long wave length limit discarding all terms of order $\mathcal{O}(\epsilon_E^2, \epsilon_\perp^2)$ or higher

$$H_2 = -\frac{m}{2B^2}|\nabla\psi_0|^2 + \frac{\mu}{2B}(B_\parallel^2 + B_\perp^2) + \frac{\mu}{B}\boldsymbol{A}_\perp \cdot \hat{\boldsymbol{b}} \times \nabla B_\parallel. \tag{3.138}$$

We refer the reader to appendix 3.A.1 for details of the calculations. In comparison with the LWL second order Hamiltonian in the Hamiltonian formulation Eq. (3.110), H_2 is simplified. This is a result of moving parts of the magnetic perturbations to the symplectic part of the Poincaré one-form (see Sec. 3.2.2). Only the fourth term ($\mu/B\boldsymbol{A}_\perp \cdot \hat{\boldsymbol{b}} \times \nabla B_\parallel$) is new and describes the nonlinear interaction of the gyroaveraged perpendicular magnetic perturbation ($\langle A \rangle$), which resides in the symplectic part of the Poincaré one-form, and the modified grad-B drift ($\mu/B\hat{\boldsymbol{b}} \times \nabla B_\parallel$) which appear in the first order Hamiltonian through the term,$-\langle \boldsymbol{A}_\perp \cdot \boldsymbol{c}_\perp \rangle$.

Now we derive the Maxwell equations by varying gyrokinetic action

$$S = \int d\tau \int d^3\boldsymbol{r}\mathcal{L}_f + \int d\tau \int d^8\bar{\boldsymbol{Z}} m^2 B_\parallel^{**} \bar{F}^E \left[(\gamma_0^E + \bar{\Gamma}_1) \cdot \dot{\bar{\boldsymbol{Z}}} - H\right], \tag{3.139}$$

where the Hamiltonian is given by

$$H = \mathcal{H}_0 - H_1 - H_2, \tag{3.140}$$

with the second order Hamiltonian taken in LWL Eq. (3.138).

Equations of motion The equations of motion follow from the general expression Eq. (3.59)

$$\dot{\bar{\boldsymbol{X}}} = \{\bar{\boldsymbol{X}}, H\}_S = \frac{\boldsymbol{B}^{**}}{mB_\parallel^{**}}\frac{\partial H}{\partial \bar{u}} + \frac{1}{qB_\parallel^{**}}\hat{\boldsymbol{b}} \times \nabla H + \frac{1}{B_\parallel^{**}}\hat{\boldsymbol{b}} \times \frac{\partial \boldsymbol{A}^{**}}{\partial t}, \tag{3.141a}$$

$$\dot{\bar{u}} = -\frac{\boldsymbol{B}^{**}}{mB_\parallel^{**}} \cdot \nabla H - \frac{q}{mB_\parallel^{**}}\boldsymbol{B}^{**} \cdot \frac{\partial \boldsymbol{A}^{**}}{\partial t}. \tag{3.141b}$$

To lowest order the equations of motion equal the guiding-center equations of motion (see Sec.(2.2.3)). In the symplectic formulation the perturbed $\boldsymbol{E} \times \boldsymbol{B}$-drift ($B_\parallel^{**-1}\hat{\boldsymbol{b}} \times \nabla\langle\phi\rangle$) and the perturbed grad-B drift ($B_\parallel^{**-1}\hat{\boldsymbol{b}} \times \nabla\langle \boldsymbol{c}_\perp \cdot \boldsymbol{A}_\perp \rangle$) are the leading order perturbed drifts. The magnetic perturbations are contained in the generalized magnetic field $\boldsymbol{B}^{**}$ and appear as "polarization drifts" or more correct as the perturbed inductive $\boldsymbol{E} \times \boldsymbol{B}$-drift ($B_\parallel^{**-1}\hat{\boldsymbol{b}} \times \frac{\partial\langle \boldsymbol{A} \rangle}{\partial t}$). The parallel acceleration contains the inductive part of the electric field $-q/m\partial_t\langle A_\parallel \rangle$. Inductive terms are not desirable in many

numerical schemes especially Particle in Cell (PIC) codes[29]. Common practice in PIC codes is to formulate the Vlasov equation as a system of ordinary differential equations (ODE's) using the method of characteristics. In order to apply the method of characteristics (here considering only shear Alfvén dynamics, $\boldsymbol{A}_\perp = 0$) the inductive term is replaced by the parallel electric field $-\partial_t A_\parallel = E_\parallel$, which can be solved for in a generalized Ohm's law. The generalized Ohm's law is not easily solved numerically, because the cancellation problem of the parallel Amperes equation in the Hamiltonian formulation of gyrokinetic now appears in the generalized Ohm's law. Also, the generalized Ohm's law requires the calculation of various higher order moments which is numerically demanding. However, these observed disadvantages might not be a problematic in continuum Vlasov solvers and in gyrofluid models.

Poisson equation I Variation with respect to ϕ yields

$$\epsilon_0 \nabla \cdot \boldsymbol{E} = q\bar{N} - \nabla \cdot \boldsymbol{P}_S^\phi, \tag{3.142}$$

where $\bar{N}$ (see Eq. (3.118)) is the gyroaveraged gyrocenter density and $\boldsymbol{P}_S^\phi$ denotes the polarization vector

$$\boldsymbol{P}_S^\phi = \int d^6 \bar{\boldsymbol{Z}} m^2 B_\parallel^{**} \boldsymbol{\mathcal{P}}_S^\phi, \tag{3.143}$$

where

$$\boldsymbol{\mathcal{P}}_S^\phi = -\delta(\boldsymbol{r} - \bar{\boldsymbol{X}}) \frac{m\bar{F}}{B^2} \nabla_\perp \psi_0 \tag{3.144}$$

is the polarization vector density. As expected, the canonical momentum term which appears in the Hamiltonian Poisson equation (3.120) does not appear because the magnetic perturbations are transfered to the symplectic part of the gyrokinetic one-form. The physical interpretation of the individual terms can be found in Sec. 3.4.2.

Poisson equation II Variation with respect to ϕ_0 gives the Poisson equation

$$\epsilon_0 \nabla \cdot \boldsymbol{E} = q\bar{N}_{gc}^S - \nabla \cdot \boldsymbol{P}_S^{\phi_0}, \tag{3.145}$$

which resembles the corresponding Poisson equation in the Hamiltonian formulation Eq. (3.121). The Poisson equations differs only due to different volume elements. The gyrocenter density with lowest order FLR correction is

$$\bar{N}_{gc}^S = \int d^6 \bar{\boldsymbol{Z}} m^2 B_\parallel^{**} F \delta(\boldsymbol{r} - \boldsymbol{X}) + \nabla \cdot \big(\frac{\hat{\boldsymbol{b}}}{B} \times \nabla \times \big[\frac{\hat{\boldsymbol{b}} m \mu F \delta(\boldsymbol{r} - \boldsymbol{X})}{2q} \big] \big), \tag{3.146}$$

and the polarization vector is defined as

$$\boldsymbol{P}_S^{\phi_0} = \int d^6\bar{\boldsymbol{Z}} m^2 B_\parallel^{**} \frac{m\bar{F}\delta(\boldsymbol{r}-\bar{\boldsymbol{X}})}{B}\hat{\boldsymbol{b}}\times(\dot{\bar{\boldsymbol{X}}}-\boldsymbol{D}) \tag{3.147}$$

Parallel Maxwell equation A variation with respect to $A_\parallel$ yields

$$\frac{1}{\mu_0}\hat{\boldsymbol{b}}\cdot\nabla\times\boldsymbol{B}-\epsilon_0\frac{\partial}{\partial t}E_\parallel = \bar{J}_\parallel + J_{M\parallel}, \tag{3.148}$$

where

$$\bar{J}_\parallel = \int d\Lambda\, qF\langle\delta(\boldsymbol{r}-\boldsymbol{X}-\boldsymbol{\rho})\rangle\hat{\boldsymbol{b}}\cdot\dot{\boldsymbol{X}}, \tag{3.149}$$

is the parallel current and the parallel magnetization current is

$$J_{M\parallel} = \nabla_\perp\cdot\int d^6\bar{\boldsymbol{Z}} m^2 B_\parallel^*\bar{F}\delta(\boldsymbol{r}-\bar{\boldsymbol{X}})\big(-\boldsymbol{\mathcal{P}}^\phi u+\frac{\mu B}{B^2}\hat{\boldsymbol{b}}\times\boldsymbol{B}_\perp\big), \tag{3.150}$$

which consists of the contribution due to the comoving polarization charge and an intrinsic magnetization respectively.

The perpendicular Maxwell equation A variation with respect to $\boldsymbol{A}_\perp$ yields

$$-\epsilon_0\frac{\partial\boldsymbol{E}_\perp}{\partial t}+\frac{1}{\mu_0}(\nabla\times\boldsymbol{B})_\perp = \bar{\boldsymbol{J}}_\perp+\boldsymbol{J}_{M\mu} \tag{3.151}$$

where

$$\bar{\boldsymbol{J}}_\perp = \int d^6\bar{\boldsymbol{Z}} m^2 B_\parallel^{**}\bar{F}q\langle\delta(\boldsymbol{r}-\bar{\boldsymbol{X}}-\boldsymbol{\rho})\dot{\bar{\boldsymbol{X}}}\rangle, \tag{3.152}$$

is the *total* perpendicular gyrocenter current. The gyrocenter current contains the full gyrocenter dynamics $\dot{\bar{\boldsymbol{X}}}$ including the polarization *drift* current associated with $\boldsymbol{D}$. The intrinsic magnetization current is given by

$$\begin{aligned}\boldsymbol{J}_{M\mu} = \int d^6\bar{\boldsymbol{Z}} m^2 B_\parallel^{**}\bar{F}q\langle\delta(\boldsymbol{r}-\bar{\boldsymbol{X}}-\boldsymbol{\rho})\boldsymbol{c}_\perp\rangle - B_\parallel\nabla\times\big(\hat{\boldsymbol{b}}\frac{\bar{F}\bar{\mu}}{B}\big)\\ +\nabla\times\big(\hat{\boldsymbol{b}}\nabla\cdot[\boldsymbol{A}_\perp\times\hat{\boldsymbol{b}}\frac{\bar{F}\bar{\mu}}{B}]\big)\end{aligned} \tag{3.153}$$

The leading order contribution of the last two terms in $\boldsymbol{J}_{M\mu}$ can be shown to be $\mu\bar{F}/B\hat{\boldsymbol{b}}\times\nabla B_\parallel$ which is the current of the modified grad-B drift.

Energy Theorem The local energy density is obtained from Eq. (3.98)

$$\mathcal{E} = \frac{\epsilon_0 E^2}{2} + \frac{B^2}{2\mu_0} - \nabla\phi \cdot \boldsymbol{P}_S^{\phi} - \nabla\phi_0 \cdot \boldsymbol{P}_S^{\phi_0} + \int d^6\bar{\boldsymbol{Z}} m^2 B_{\parallel}^{**} \bar{F}\delta(\bar{\boldsymbol{X}} - \boldsymbol{r})[H - q\phi_0 - \frac{m\mu}{2q}\hat{\boldsymbol{b}} \cdot \nabla \times \boldsymbol{D} - q\langle\phi\rangle), \quad (3.154)$$

where partial integration and the Poisson equations have been inserted to eliminate the $\Phi\epsilon_0\nabla \cdot \boldsymbol{E}$ term. The energy density can be put on a form which resembles the Hamiltonian counterpart (see Eq. (3.134)) and earlier results[47] by inserting the explicit expressions of the polarization vectors Eq. (3.144) and Eq. (3.147)

$$\mathcal{E} = \frac{\epsilon_0 E^2}{2} + \frac{B^2}{2\mu_0} + \int d^6\bar{\boldsymbol{Z}} m^2 B_{\parallel}^{**}\, \delta(\boldsymbol{r} - \boldsymbol{X}) F \Big[\mu B + \frac{1}{2} m W^2 - qF\langle \boldsymbol{c}_\perp \cdot \boldsymbol{A}_\perp\rangle + \frac{\mu}{2B}(B_\perp^2 + B_\parallel^2) + \frac{1}{2} m u_E^2 - \frac{mu^2}{2B^2} B_\perp^2 + \frac{\mu}{B}\boldsymbol{A}_\perp \cdot \hat{\boldsymbol{b}} \times \nabla B_\parallel\Big]. \quad (3.155)$$

The corresponding energy density flux is

$$\boldsymbol{S} = \frac{1}{\mu_0}\boldsymbol{E} \times \boldsymbol{B} - (\phi_0 + \phi)\boldsymbol{J}^{tot} + \int d^6\bar{\boldsymbol{Z}} m^2 B_{\parallel}^{**}\, \bar{F} H \dot{\bar{\boldsymbol{X}}}\delta(\boldsymbol{r} - \bar{\boldsymbol{X}}) + \frac{\partial}{\partial t}\big[\boldsymbol{P}_S^{\phi}\phi + \boldsymbol{P}_S^{\phi_0}\phi_0 + \boldsymbol{D} \times \big(\hat{\boldsymbol{b}}\frac{m\mu\bar{F}\delta(\boldsymbol{r} - \bar{\boldsymbol{X}})}{2q}\big) - \phi_0\frac{\hat{\boldsymbol{b}}}{B} \times \nabla \times \big(\hat{\boldsymbol{b}}\frac{m\mu F\delta(\boldsymbol{r} - \bar{\boldsymbol{X}})}{2q}\big)\big]. \quad (3.156)$$

Comparing the formulations of gyrokinetics

We have derived the Vlasov-Maxwell equations taking the second order Hamiltonian in the long wavelength limit in the Hamiltonian (Sec.3.4.2) and symplectic (Sec.3.4.3) formulations of gyrokinetics. The long wavelength limit could be a relevant description of edge region plasmas where[103] $k_\perp\rho_s \lesssim 0.1$ is often satisfied, but this limiting form also gives physical insight into the forest of terms appearing in the general gyrokinetic equations. Unless $k_\perp\rho_i \gtrsim 1$, we can determine the dominating physical effects of the general gyrokinetic system from the long wavelength limit equations which can be quite a difficult task considering the vast complexity of the general gyrokinetic equations.

Different formulations of gyrokinetics describe identical physics but have different strengths and weaknesses in theoretical and numerical applications. In table 3.2 highlights of the differences and similarities of the Hamiltonian and symplectic formulations of gyrokinetics are shown. In the symplectic formulation the physical interpretation of various terms is in some sense intuitively clear. Background and perturbed magnetic potentials are grouped

Table 3.2: Comparison of the gyrokinetic Vlasov-Maxwell equations in the Hamiltonian and symplectic formulations.

Equation	Hamiltonian	Symplectic
Vlasov	Time dependent volume element: $\partial_t B_\parallel^* \simeq m/(qB)\partial_t \nabla_\perp^2 \phi_0$	Time dependent volume element: $\partial_t B_\parallel^{**} = \partial_t B_\parallel^* + \nabla \times \langle \partial_t \boldsymbol{A} \rangle$
	Magnetic flutter drifts: $uB_\parallel^{*-1}\hat{\boldsymbol{b}} \times \nabla\langle A_\parallel \rangle + B_\parallel^{*-1}\hat{\boldsymbol{b}} \times \nabla \boldsymbol{A}_\perp \cdot \boldsymbol{D}$.	Inductive $\boldsymbol{E} \times \boldsymbol{B}$-drift: $\hat{\boldsymbol{b}} \times \partial_t \langle \boldsymbol{A}_\perp \rangle$.
	Perturbed grad-B drift: $\bar{\mu}/(qB)\hat{\boldsymbol{b}} \times \nabla B_\parallel$	Perturbed grad-B drift: $\bar{\mu}/(qB)\hat{\boldsymbol{b}} \times \nabla B_\parallel$
		Inductive electric field $\dot{\bar{u}} = q/m\partial_t \langle A_\parallel \rangle + \cdots$.
	Polarization drift: $\propto \hat{\boldsymbol{b}} \times \frac{d}{dt}\boldsymbol{D}$	Polarization drift: $\propto \hat{\boldsymbol{b}} \times \frac{d}{dt}\boldsymbol{D}$
Poisson	Canonical term $\propto NB_\parallel$	
Ampere $\parallel$	Skin depth term with FLR corrections: $\propto NA_\parallel$	
	Intrinsic magnetization $-\hat{\boldsymbol{b}} \cdot \nabla \times (\boldsymbol{B}_\perp \bar{F}\bar{\mu}B/B^2)$	Intrinsic magnetization $-\hat{\boldsymbol{b}} \cdot \nabla \times (\boldsymbol{B}_\perp \bar{F}\bar{\mu}B/B^2)$
	$\bar{J}_\parallel \propto \langle \bar{F} \rangle \bar{u}$	$\bar{J}_\parallel \propto \langle \bar{F} \rangle \hat{\boldsymbol{b}} \cdot \dot{\bar{\boldsymbol{X}}}$
Ampere $\perp$	$\perp$ "free" currents: $\boldsymbol{J}_D \propto q\langle \bar{F} \rangle \boldsymbol{D}$ and $J_{\psi_0} \propto \bar{F}\hat{\boldsymbol{b}} \times \nabla \psi_0$	$\perp$ "free" current $\boldsymbol{J}_\perp \propto q\langle \bar{F} \rangle \dot{\bar{\boldsymbol{X}}}$

together which implies that the inductive part of the electric field appears naturally. The parallel velocity coordinate $\bar{u}$, is indeed the parallel velocity of gyrocenters. Also, the Amperes equations contain the total currents. The symplectic formulation is therefore useful in theoretical applications of the gyrokinetic theory. The physical intuitive features of the symplectic formulation makes it less useful in particle in cell simulations[29, 19] and in kinetic simulations in general (when $\phi_0 = 0$) because the volume element is time dependent via the inclusion of the perturbed magnetic potential in the symplectic part of the Poincaré one-form. Similar problems seems not to appear in gyrofluid equations[16] derived from symplectic gyrokinetics. The main advantage of the symplectic gyrofluid equations is the "missing" skin depth term in the parallel Amperes equation[87].

Keeping the magnetic potentials in the Hamiltonian implies that the gyrokinetic parallel velocity coordinate $\bar{u}$ describes parallel gyrocenter velocity *and* the perturbed magnetic potential. The Hamiltonian formulation results in equations having terms which are not readily understandable but has the advantage that the magnetic perturbations appear as potentials together with the electric potential. Therefore, the inductive part of the electric field potential $-\partial_t \boldsymbol{A}$ does not enter the equations and the perturbed perpendicular drifts appear explicitly. Furthermore the volume element is only time dependent through background $\boldsymbol{E} \times \boldsymbol{B}$-drift $\boldsymbol{D}$.

3.4.4 Gyrokinetics including the polarization current

In this section we present a version of the gyrokinetic Maxwell equations in which the polarization current $\partial_t \boldsymbol{P}^\phi$ appears explicitly; *not* to be confused

with the polarization drift current, $\propto \Omega^{-1}\hat{\boldsymbol{b}} \times [\partial_t + \boldsymbol{W} \cdot \nabla]\boldsymbol{D}$. As discussed in Sec.3.3.1 the gyrokinetic equations conserve the gyrocenter and polarization charge to the order of the perturbative analysis (see Eq. (3.104) and Eq. (3.105) respectively). By including the polarization current explicitly we conserve the corresponding polarization charge

$$\frac{\partial}{\partial t}\rho_{pol} = -\nabla \cdot \boldsymbol{J}_{pol} = -\nabla \cdot \frac{\partial}{\partial t}\boldsymbol{P}^{\phi}. \tag{3.157}$$

Also, we obtain the magnetization current, $\propto \nabla \times (\boldsymbol{P}^{\phi} \times \boldsymbol{D})$ due to the comoving polarization charge. In other words, we identify and derive the currents associated with a given polarization charge $-\nabla \cdot \boldsymbol{P}^{\phi}$, as suggested by classical electrodynamics Ref. [52][(chap. 6.7)]. Specifically, we explicitly identify the currents associated with the polarization charge of the Hamiltonian formulation of gyrokinetics, where the second order Hamiltonian is taken in the long wavelength limit.

Considering the polarization vector $\boldsymbol{P}^{\phi}$ in Eq. (3.118) it is clear that in order to obtain the corresponding magnetization and polarization currents the perturbative analysis must be extended such that terms of at least $\mathcal{O}(\epsilon_{\delta}^2\epsilon_E, \epsilon_{\delta}^2\epsilon_{\omega})$ enter the second order Hamiltonian Eq. (3.110). The polarization charge in gyrokinetics mainly originates from the, $\frac{1}{2}\langle\{S_1, h_1\}\rangle$ term in the second order Hamiltonian. As the gyrokinetic theory is an asymptotic expansion in the amplitude smallness parameter ϵ_{δ}, we must take the iterative solution of the first order generating function S_1 to higher orders. Formally, we assume $\epsilon_E^2 \gtrsim \epsilon_{\delta}$ and solve iteratively for S_1 in powers of ϵ_E. In passing, this kind of ordering could be relevant when describing internal transport barriers[46] where higher order ϵ_E terms might be important in the Maxwell equations.

This ordering implies that the term, $\boldsymbol{D} \cdot \boldsymbol{A}_{\perp}$ must be retained in the first order Hamiltonian

$$h_1 = q\phi - \boldsymbol{A} \cdot (\boldsymbol{W} + \boldsymbol{c}_{\perp}). \tag{3.158}$$

The governing equation for the generating function Eq. (3.41) reads

$$\{S_1, \mathcal{H}_0\}_0 = \widetilde{\psi}. \tag{3.159}$$

To obtain an iterative solution for S_1 we expand the Poisson bracket keeping only the leading order terms

$$\epsilon_E \boldsymbol{D} \cdot \nabla S_1 + \Omega \frac{\partial S_1}{\partial \theta} + \epsilon_{\omega}\frac{\partial}{\partial t}S_1 + \mathcal{O}(\epsilon_E^3, \epsilon_B) = \tilde{\psi}. \tag{3.160}$$

The $\mathcal{O}(\epsilon_E^0)$ order solution S_1^0 for S_1 reads

$$S_1^0 = \frac{1}{\Omega}\int_0^{\theta} d\theta'\, q(\phi - u\widetilde{A_{\parallel}} - \boldsymbol{c}_{\perp} \cdot \boldsymbol{A}_{\perp}), \tag{3.161}$$

the $\mathcal{O}(\epsilon_E^1)$ solution S_1^1 is

$$S_1^1 = -\frac{1}{\Omega}\int_0^\theta d\theta' \boldsymbol{D}\cdot\nabla S_1^0 + \widetilde{\boldsymbol{D}\cdot\boldsymbol{A}_\perp}, \tag{3.162}$$

and the $\mathcal{O}(\epsilon_E^2)$ solution S_1^2 reads

$$S_1^2 = -\frac{1}{\Omega}\int_0^\theta d\theta' \boldsymbol{D}\cdot\nabla S_1^1 - \frac{\partial}{\partial t}S_1^0, \tag{3.163}$$

where we have formally ordered $\epsilon_\omega \sim \epsilon_E^2$. We know that the polarization vector will contain terms of $\mathcal{O}(\epsilon_\delta\epsilon_\perp\epsilon_E)$ which implies that the second order Hamiltonian must retain terms of $\mathcal{O}(\epsilon_\delta\epsilon_\perp^2\epsilon_E\epsilon_\omega)$. The iterative solution of S_1 is therefore taken to third order

$$S_1^3 = -\frac{1}{\Omega}\int_0^\theta d\theta' \boldsymbol{D}\cdot\nabla S_1^2 - \frac{\partial}{\partial t}S_1^1, \tag{3.164}$$

which in principle should also contain parallel acceleration terms, polarization current terms etc., but we simply choose S_1^3 as given above because it turns out that it contains terms entering the polarization current.

Including the new contributions from Eq. (3.162), Eq. (3.163) and Eq. (3.164) the second order gyrokinetic Hamiltonian reads

$$\begin{aligned}
H_2 =& \frac{q^2}{2m}(A_\parallel^2 + \frac{\rho_0^2}{2}A_\parallel\nabla_\perp^2 A_\parallel) - \frac{m}{2B^2}|\nabla_\perp\psi_0|^2 + \frac{\mu}{2B}(B_\parallel^2 + B_\perp^2) \\
&- \frac{q}{B}\hat{\boldsymbol{b}}\times\nabla\psi_0\cdot\boldsymbol{A}_\perp + \frac{m}{2B^2}(\boldsymbol{D}\cdot\nabla\nabla_\perp\psi_0\cdot\boldsymbol{A}_\perp - \boldsymbol{D}\cdot\nabla\boldsymbol{A}_\perp\cdot\nabla_\perp\psi_0) \\
&+ \frac{q}{2B}\hat{\boldsymbol{b}}\cdot\boldsymbol{A}_\perp\times(\boldsymbol{D}\cdot\nabla)\boldsymbol{A}_\perp + \frac{m}{2B^2}[(\boldsymbol{D}\cdot\nabla)^2\boldsymbol{A}_\perp]\cdot\boldsymbol{A}_\perp \\
&+ \frac{q}{2B}\hat{\boldsymbol{b}}\cdot\boldsymbol{A}_\perp\times\frac{\partial}{\partial t}\boldsymbol{A}_\perp + \frac{m}{2B^2}(\boldsymbol{A}_\perp\cdot\frac{\partial}{\partial t}\nabla_\perp\psi_0 - \nabla_\perp\psi_0\cdot\frac{\partial}{\partial t}\boldsymbol{A}_\perp) \\
&+ \frac{m}{2B^2}(\boldsymbol{D}\cdot\nabla\frac{\partial}{\partial t}\boldsymbol{A}_\perp\cdot\boldsymbol{A}_\perp + \frac{\partial}{\partial t}(\boldsymbol{D}\cdot\nabla\boldsymbol{A}_\perp)\cdot\boldsymbol{A}_\perp + \boldsymbol{A}_\perp\cdot\frac{\partial^2}{\partial t^2}\boldsymbol{A}_\perp),
\end{aligned} \tag{3.165}$$

where all terms of $\mathcal{O}(\epsilon_\perp^3)$ or higher have been discarded and where the generalized potential is defined as

$$\nabla_\perp\psi_0 \doteq \nabla_\perp\phi - u\nabla_\perp A_\parallel - \nabla_\perp\boldsymbol{A}_\perp\cdot\boldsymbol{D}. \tag{3.166}$$

In agreement with the ordering $\epsilon_E^2 \sim \epsilon_\omega$ we rewrite some terms in H_2 to

avoid irrelevant higher orders terms in the Maxwell equation

$$\begin{aligned}
&\int dt \int d^6\bar{\boldsymbol{Z}} m^2 B_\parallel^* \bar{F}\Big[\frac{m}{2B^2}[(\boldsymbol{D}\cdot\nabla)^2\boldsymbol{A}_\perp]\cdot\boldsymbol{A}_\perp \\
&+\frac{m}{2B^2}(\boldsymbol{A}_\perp\cdot\frac{\partial}{\partial t}\nabla_\perp\psi_0 - \nabla_\perp\psi_0\cdot\frac{\partial}{\partial t}\boldsymbol{A}_\perp) \\
&+\frac{m}{2B^2}(\boldsymbol{D}\cdot\nabla\frac{\partial}{\partial t}\boldsymbol{A}_\perp\cdot\boldsymbol{A}_\perp + \frac{\partial}{\partial t}(\boldsymbol{D}\cdot\nabla\boldsymbol{A}_\perp)\cdot\boldsymbol{A}_\perp + \boldsymbol{A}_\perp\cdot\frac{\partial^2}{\partial t^2}\boldsymbol{A}_\perp)\Big] \\
&\approx \int dt\int d^6\bar{\boldsymbol{Z}} m^2 B_\parallel^*\nabla\cdot\big(\boldsymbol{D}\frac{m\bar{F}}{2B^2}\boldsymbol{D}\cdot\nabla\boldsymbol{A}_\perp\big)\cdot\boldsymbol{A}_\perp + \nabla\psi_0\cdot\boldsymbol{A}_\perp\nabla\cdot\big(\boldsymbol{D}\frac{m\bar{F}}{2B^2}\big) \\
&-\frac{m\bar{F}}{B^2}\nabla_\perp\psi_0\cdot\frac{\partial}{\partial t}\boldsymbol{A}_\perp + \boldsymbol{A}_\perp\nabla\cdot\big(\boldsymbol{D}\frac{m\bar{F}}{B^2}\frac{\partial}{\partial t}\boldsymbol{A}_\perp\big) + \frac{1}{B_\parallel^*}\boldsymbol{A}_\perp\cdot\frac{\partial}{\partial t}\big(\frac{m\bar{F}B_\parallel^*}{2B^2}\frac{\partial\boldsymbol{A}_\perp}{\partial t}\big),
\end{aligned} \tag{3.167}$$

where partial integration and the pre-Vlasov equation Eq. (3.74) was used. With these modifications the gyrokinetic action reads

$$\begin{aligned}
S = &\int d\tau\int d^3\boldsymbol{r}\mathcal{L}_f + \int d\tau\int d^8\boldsymbol{Z}B_\parallel^*\Big[\bar{F}^E(\gamma_0^E\cdot\dot{\bar{\boldsymbol{Z}}} - \mathcal{H}_0 - H_1) \\
&-\Big\{\frac{q^2\bar{F}^E}{2m}(A_\parallel^2 + \frac{\rho_0^2}{2}A_\parallel\nabla_\perp^2 A_\parallel) - \frac{m\bar{F}^E}{2B^2}|\nabla_\perp\psi_0|^2 + \frac{\mu\bar{F}^E}{2B}(B_\parallel^2 + B_\perp^2) \\
&-\frac{q\bar{F}^E}{B}\hat{\boldsymbol{b}}\times\nabla\psi_0\cdot\boldsymbol{A}_\perp + \frac{m\bar{F}^E}{2B^2}(\boldsymbol{D}\cdot\nabla\nabla_\perp\psi_0\cdot\boldsymbol{A}_\perp - \boldsymbol{D}\cdot\nabla\boldsymbol{A}_\perp\cdot\nabla_\perp\psi_0) \\
&+\frac{q\bar{F}^E}{2B}\hat{\boldsymbol{b}}\cdot\boldsymbol{A}_\perp\times(\boldsymbol{D}\cdot\nabla)\boldsymbol{A}_\perp + \nabla\cdot\big(\boldsymbol{D}\frac{m\bar{F}^E}{2B^2}\boldsymbol{D}\cdot\nabla\boldsymbol{A}_\perp\big)\cdot\boldsymbol{A}_\perp \\
&+\frac{q\bar{F}^E}{2B}\hat{\boldsymbol{b}}\cdot\boldsymbol{A}_\perp\times\frac{\partial}{\partial t}\boldsymbol{A}_\perp + \nabla\psi_0\cdot\boldsymbol{A}_\perp\nabla\cdot\big(\boldsymbol{D}\frac{m\bar{F}^E}{2B^2}\big) - \frac{m\bar{F}^E}{B^2}\nabla_\perp\psi_0\cdot\frac{\partial}{\partial t}\boldsymbol{A}_\perp \\
&+\boldsymbol{A}_\perp\nabla\cdot\big(\boldsymbol{D}\frac{m\bar{F}^E}{B^2}\frac{\partial}{\partial t}\boldsymbol{A}_\perp\big) + \frac{1}{B_\parallel^*}\boldsymbol{A}_\perp\cdot\frac{\partial}{\partial t}\big(\frac{m\bar{F}^E B_\parallel^*}{2B^2}\frac{\partial\boldsymbol{A}_\perp}{\partial t}\big)\Big\}\Big].
\end{aligned} \tag{3.168}$$

From this action we now derive the Maxwell equations.

Poisson equation I A variation with respect to ϕ yields

$$\epsilon_0\nabla\cdot\boldsymbol{E} = q\bar{N} - \nabla\cdot\boldsymbol{P}^\phi, \tag{3.169}$$

where the polarization vector is

$$\boldsymbol{P}^\phi = \int d^6\bar{\boldsymbol{Z}} m^2 B_\parallel^*\boldsymbol{\mathcal{P}}^\phi, \tag{3.170}$$

and

$$\boldsymbol{\mathcal{P}}^\phi = -\bar{F}\delta(\boldsymbol{r}-\bar{\boldsymbol{X}})\frac{m}{B^2}(\nabla_\perp\psi_0 + \boldsymbol{D}\cdot\nabla\boldsymbol{A}_\perp + \frac{\partial}{\partial t}\boldsymbol{A}_\perp) - \frac{q}{B}\boldsymbol{A}_\perp\times\hat{\boldsymbol{b}}, \tag{3.171}$$

denotes the polarization density vector. A direct consequence of keeping $\mathcal{O}(\epsilon_\delta^2\epsilon_\omega)$ terms in the second order Hamiltonian the polarization vector now contains the contribution from the perpendicular inductive electrical field $(-m/B^2\partial_t \boldsymbol{A}_\perp)$. Notice that no inductive perturbed $\boldsymbol{E}\times\boldsymbol{B}$-drift enter the gyrocenter velocity. The, $\boldsymbol{D}\cdot\boldsymbol{A}_\perp$ term in ψ_0 can be combined with the second term in $\boldsymbol{\mathcal{P}}^\phi$

$$-\nabla\cdot\big(\frac{Fm}{B^2}[-\nabla_\perp\boldsymbol{A}_\perp\cdot\boldsymbol{D}+\boldsymbol{D}\cdot\nabla_\perp\boldsymbol{A}_\perp]\big)=-\nabla\cdot\big(\frac{B_\parallel}{B}\frac{F}{\Omega}\frac{\nabla_\perp\phi_0}{B}\big), \quad (3.172)$$

which looks like a polarization density associated with ϕ_0 when field lines are compressed. The second term $(-\bar{F}m/B^2\boldsymbol{D}\cdot\nabla\boldsymbol{A}_\perp)$ in $\boldsymbol{\mathcal{P}}^\phi$ did not appear in earlier contributions[48].

Poison equation II Variation of the action with respect to $\phi_0(\boldsymbol{r})$ yields the Poisson equation

$$\epsilon_0\nabla\cdot\boldsymbol{E}=\sum_\alpha q\bar{N}_{0\alpha}-\nabla\cdot\boldsymbol{P}^{\phi_0}_\alpha \quad (3.173)$$

where the background FLR-corrected density is

$$\bar{N}_0=\int d^6\bar{\boldsymbol{Z}}\mathcal{J}\,q\bar{F}\delta(\boldsymbol{r}-\boldsymbol{X})+\nabla\cdot\big(\frac{\hat{\boldsymbol{b}}}{B}\times\nabla\times\big[\hat{\boldsymbol{b}}\frac{m\mu\bar{F}\delta(\boldsymbol{r}-\bar{\boldsymbol{X}})}{2q}\big]\big) \quad (3.174)$$

and the polarization vector $\boldsymbol{P}^{\phi_0}$

$$\begin{aligned}
\boldsymbol{P}^{\phi_0}=&\int d^6\bar{\boldsymbol{Z}}m^2B^*_\parallel\frac{m\bar{F}\delta(\boldsymbol{r}-\bar{\boldsymbol{X}})}{B}\hat{\boldsymbol{b}}\times(\dot{\bar{\boldsymbol{X}}}-\boldsymbol{D})-\frac{q\bar{F}\delta(\boldsymbol{r}-\bar{\boldsymbol{X}})}{B}\langle\boldsymbol{A}_\perp\rangle\times\hat{\boldsymbol{b}}\\
&-\frac{m\bar{F}\delta(\boldsymbol{r}-\bar{\boldsymbol{X}})}{B^3}\hat{\boldsymbol{b}}\times[\nabla_\perp\psi_0\cdot\nabla]\boldsymbol{A}_\perp-\frac{q\bar{F}\delta(\boldsymbol{r}-\bar{\boldsymbol{X}})}{B^2}\hat{\boldsymbol{b}}\times[(\boldsymbol{A}_\perp\times\hat{\boldsymbol{b}})\cdot\nabla]\boldsymbol{A}_\perp\\
&-\frac{m\bar{F}\delta(\boldsymbol{r}-\bar{\boldsymbol{X}})}{2B^2}A_{m\perp}\hat{\boldsymbol{b}}\times\nabla_\perp\nabla_{m\perp}\psi_0-\frac{\hat{\boldsymbol{b}}\times\nabla_l\boldsymbol{A}_\perp}{B}\nabla\cdot\big(\boldsymbol{D}A_l\frac{m\bar{F}\delta(\boldsymbol{r}-\bar{\boldsymbol{X}})}{2B^2}\big)\\
&+\frac{m\bar{F}\delta(\boldsymbol{r}-\bar{\boldsymbol{X}})}{2B^3}\hat{\boldsymbol{b}}\times\nabla A_{m\perp}\nabla_{m\perp}\psi_0-\frac{m\bar{F}\delta(\boldsymbol{r}-\bar{\boldsymbol{X}})}{2B^3}\hat{\boldsymbol{b}}\times([(\boldsymbol{D}\cdot\nabla)\boldsymbol{A}_\perp]\cdot\nabla)\boldsymbol{A}_\perp\\
&-\frac{q\bar{F}\delta(\boldsymbol{r}-\bar{\boldsymbol{X}})}{2B}\hat{\boldsymbol{b}}\times\nabla A_{s\perp}(\hat{\boldsymbol{b}}\times\boldsymbol{A}_\perp)_s+\frac{m\bar{F}\delta(\boldsymbol{r}-\bar{\boldsymbol{X}})}{2B^2}\frac{\hat{\boldsymbol{b}}}{B}\times\nabla A_l\boldsymbol{D}\cdot\nabla A_l\\
&+\frac{\hat{\boldsymbol{b}}}{B}\times(\boldsymbol{A}_\perp\cdot\nabla)\boldsymbol{A}_\perp\nabla\cdot\big(\boldsymbol{D}\frac{m\bar{F}}{2B^2}\big)+\frac{m\bar{F}}{2B^2}\frac{\hat{\boldsymbol{b}}}{B}\times\nabla(\boldsymbol{A}_\perp\cdot\nabla\psi_0)\\
&+\frac{m\bar{F}\delta(\boldsymbol{r}-\bar{\boldsymbol{X}})}{B^3}\hat{\boldsymbol{b}}\times\big(\frac{\partial\boldsymbol{A}_\perp}{\partial t}\times\nabla\times\boldsymbol{A}_\perp\big) \quad (3.175)
\end{aligned}$$

Note that all terms in $\boldsymbol{P}^{\phi_0}$ except the first vanish when $\boldsymbol{A}_\perp=0$. The second term is of order $\mathcal{O}(\epsilon_\delta)$ and is a reminiscence of the Hamiltonian formulation of gyrokinetic where the velocity component is canonical. The remaining terms are of $\mathcal{O}(\epsilon_\delta^2)$ or higher.

Parallel Ampere equation Variation with respect to $A_\parallel$ yields

$$-\epsilon_0\frac{\partial E_\parallel}{\partial t}+\frac{1}{\mu_0}\hat{\boldsymbol{b}}\cdot\nabla\times\boldsymbol{B}=\bar{J}_\parallel+J_{M\parallel}$$
$$-\frac{q^2}{m}\big[NA_\parallel+\frac{P_\perp}{m\Omega^2}\nabla_\perp^2A_\parallel+A_\parallel\nabla_\perp^2(\frac{P_\perp}{2m\Omega^2})\big], \tag{3.176}$$

where $\bar{J}_\parallel$ denotes the gyroaveraged parallel current. $J_{M\parallel}$ denotes the parallel part $\hat{\boldsymbol{b}}\cdot\nabla\times\boldsymbol{M}$ of the magnetization current

$$J_{M\parallel}=\nabla_\perp\cdot\int d^6\bar{\boldsymbol{Z}}B_\parallel^*\big(-\boldsymbol{\mathcal{P}}^\phi u+\bar{F}\delta(\boldsymbol{r}-\bar{\boldsymbol{X}})\frac{\mu B}{B^2}\hat{\boldsymbol{b}}\times\boldsymbol{B}_\perp\big). \tag{3.177}$$

Perpendicular Ampere equation Variation of the action with respect to $\boldsymbol{A}_\perp(\boldsymbol{r})$ yields

$$-\epsilon_0\frac{\partial\boldsymbol{E}_\perp}{\partial t}+\frac{1}{\mu_0}(\nabla\times\boldsymbol{B})_\perp=\bar{\boldsymbol{J}}_D+\boldsymbol{J}_{\psi_0}+\boldsymbol{J}_M+\boldsymbol{J}_{pol}, \tag{3.178}$$

where

$$\bar{\boldsymbol{J}}_D=\int d^6\bar{\boldsymbol{Z}}m^2B_\parallel^*\,q\bar{F}\langle\delta(\boldsymbol{r}-\bar{\boldsymbol{X}}-\boldsymbol{\rho}_0)\boldsymbol{D}\rangle. \tag{3.179}$$

The current due to the perturbed potentials in the Hamiltonian is

$$\boldsymbol{J}_{\psi_0}=\int d^6\bar{\boldsymbol{Z}}m^2B_\parallel^*\,qF\delta(\boldsymbol{r}-\bar{\boldsymbol{X}})\bigg[\frac{\hat{\boldsymbol{b}}\times(\nabla\phi+\partial_t\boldsymbol{A}_\perp)}{B}$$
$$-\frac{\bar{u}}{B}\hat{\boldsymbol{b}}\times\nabla A_\parallel-\frac{\hat{\boldsymbol{b}}\times\nabla\boldsymbol{A}_\perp\cdot\boldsymbol{D}}{B}\bigg], \tag{3.180}$$

where the first term is the $\boldsymbol{E}\times\boldsymbol{B}$-current including the inductive contribution. The magnetization current due to the comoving polarization charge is

$$\boldsymbol{J}_{MW}=\int d^6\bar{\boldsymbol{Z}}m^2B_\parallel^*\,\nabla\times(\boldsymbol{\mathcal{P}}^\phi\times\boldsymbol{D}), \tag{3.181}$$

and

$$\boldsymbol{J}_{M\mu}=\int d^6\bar{\boldsymbol{Z}}m^2B_\parallel^*\,q\bar{F}\langle\delta(\boldsymbol{r}-\bar{\boldsymbol{X}}-\boldsymbol{\rho}_0)\boldsymbol{c}_\perp\rangle-\nabla\times\big(\frac{\bar{F}\delta(\boldsymbol{r}-\bar{\boldsymbol{X}})\hat{\boldsymbol{b}}B_\parallel\bar{\mu}}{B}\big), \tag{3.182}$$

is the intrinsic magnetization current. The polarization current is given as

$$\boldsymbol{J}_{pol}=\frac{\partial}{\partial t}\bigg(\int d^6\bar{\boldsymbol{Z}}m^2B_\parallel^*\,\bar{F}\delta(\boldsymbol{r}-\bar{\boldsymbol{X}})\boldsymbol{\mathcal{P}}^\phi\bigg)$$
$$+\int d^6\bar{\boldsymbol{Z}}m^2B_\parallel^*\,\epsilon_{ijk}A_{\perp j}\big[\frac{1}{B_\parallel^*}\frac{\partial}{\partial t}(\hat{b}_k\frac{q\bar{F}B_\parallel^*}{2B})+\nabla\cdot(\boldsymbol{D}\hat{b}_k\frac{q\bar{F}}{2B})\big]. \tag{3.183}$$

The last two terms can be shown to cancel using the pre-Vlasov equation Eq. (3.74) to the order considered her but are kept to ensure energy conservation. We have there succeeded in obtained the gyrokinetic Maxwell equation written in terms of "free" and "bounded" charge.

The energy theorem follows from Eq. (3.133) and the explicit expressions can be worked out by inserting the explicit expression for the polarization vectors.

3.5 Summary

In this chapter we have presented an extension of the gyrokinetic coordinate transformations. For the first time fully electromagnetic second order gyrokinetic coordinates have been derived with a time varying strong, long wavelength electrical field potential $e\phi_0/T_i \sim 1$ present. An ordering relevant for edge region plasmas in tokamaks is presented. The results are derived in the so-called Hamiltonian and symplectic formulations of gyrokinetics. We discussed the necessity of ordering the amplitude of the strong background flow smaller than the the thermal velocity in order to obtain useful gyrokinetic coordinates. In comparison to the static case the main implication of the time dependent background potential is the explicit time dependent volume element and the introduction of the polarization drift in the equations of motion.

Next, we presented the general Vlasov-Maxwell equations derived from an Eulerian-Lagrangian variational principle which also provides a local energy theorem. A Poisson equation associated with the strong electrical potential was derived, which plays an important in the energy theorem. We discussed the formulation of the Maxwell equations in terms of "free" gyrocenter charge and currents and "bound" polarization charge and magnetization current. The discussion also regarded the difference between polarization and polarization drift currents.

Finally, we presented the Vlasov-Maxwell equations in the limit where the second order Hamiltonian, the generator of polarization and magnetization, was taken in the long wavelength limit (drift kinetic). All terms in the Maxwell's equation were expressed in terms of "free" gyrocenter charge and polarization and magnetization density vectors. This limiting form gives physical insight and is relevant for numerical simulations of edge turbulence. The equations are derived in both formulations of gyrokinetics. As a consequence of systematically keeping all terms in the long wavelength limit new terms appear in the Ampere equation. Most significant is the intrinsic magnetization current in the parallel Ampere equation which describes the diamagnetic response of the cyclotron motion to the perpendicular magnetic perturbations. The explicit local energy theorem is presented. A comparison to earlier results show some differences which can be ascribed the usage of the

Poisson equation associated with the strong background electric potential, in the process of eliminating potential like terms in the energy theorem. Lastly, the Vlasov-Maxwell equations in the Hamiltonian formulation are derived in a version where the polarization current appears in the Ampere equation. Formally, we iteratively solve for the first order generating function of the Lie transformation in powers of the background electrical field inhomogeneity smallness parameter. Furthermore, the polarization due to the inductive part of the electric field is identified in the Poisson equation. This ordering could be relevant in studies of internal transport barriers.

3.A Appendix

3.A.1 Details of the long wavelength limit calculations

In this section details of the calculations leading to the long wave length limit of the second order gyrokinetic Hamiltonians. The most algebraically involved term in the calculation is

$$\frac{q}{2} < \{S_1, \psi\}_0 > \simeq \frac{q^2}{2m}\frac{\partial}{\partial \bar{\mu}} < \tilde{\psi}\frac{\partial S_1}{\partial \bar{\theta}} > = \frac{q^2}{2B}\frac{\partial}{\partial \bar{\mu}} < \tilde{\psi}^2 > + \mathcal{O}(\epsilon_\delta^2 \epsilon_E), \quad (3.184)$$

which appears in both the Hamiltonian and the symplectic formulation of gyrokinetics. When evaluating this we are going to use that

$$< \tilde{\psi}^2 > = < \psi^2 > - < \psi >^2 . \quad (3.185)$$

Our calculations involve gyroaverages of various functions. It is often an advantage to Fourier transform the gyroaveraged functions because the gyroaveraging operation is a Bessel function in Fourier space. We state the following Bessel function identities that will become handy in the subsequent calculations. The n'th order Bessel function can be defined as[91]

$$J_n(z) = \frac{1}{2\pi i^n}\int_0^{2\pi} e^{iz\cos\theta} e^{i\theta n}, \quad (3.186)$$

as the series expansion

$$J_n(z) = \sum_{l=0}^{\infty} \frac{(-1)^l}{2^{2l+n} l!(n+l)!} z^{2l+n}, \quad (3.187)$$

or

$$e^{iz\cos\theta} = J_0(z) + 2\sum_{l=1}^{\infty} J_l(z) i^l \cos[l(\theta - \alpha)]. \quad (3.188)$$

We define the wave vector $\boldsymbol{k}$ in Fourier space as

$$\boldsymbol{k} = \hat{\boldsymbol{b}} k_\parallel + k_\perp(\hat{\boldsymbol{e}}_1 \cos\alpha + \hat{\boldsymbol{e}}_2 \sin\alpha), \quad (3.189)$$

such that

$$\boldsymbol{k}\cdot\boldsymbol{\rho} = k_\perp \rho\cos(\theta+\alpha). \tag{3.190}$$

In general the gyroaverage of a function $f(\boldsymbol{x})$ can expressed in terms of the zeroth order Bessel function J_0(we suppress the normalization factor$(2\pi)^{-3/2}$ for simplicity)

$$\begin{aligned}
< f(\boldsymbol{x}) > &= \int d^3k e^{i\boldsymbol{k}\cdot\boldsymbol{R}} f_{\boldsymbol{k}} \frac{1}{2\pi}\int_0^{2\pi} d\theta\, e^{ik_\perp\rho\cos(\theta+\alpha)} \\
&= \int d^3k e^{i\boldsymbol{k}\cdot\boldsymbol{R}} f_{\boldsymbol{k}} \Big[J_0(k_\perp\rho) + 2\sum_{l=1}^{\infty} J_l(k_\perp\rho) i^l \frac{1}{2\pi}\int_0^{2\pi} d\theta \cos[l(\theta+\alpha)] \Big] \\
&= \int d^3k e^{i\boldsymbol{k}\cdot\boldsymbol{R}} f_{\boldsymbol{k}} \Big[J_0(k_\perp\rho) + 2\sum_{l=1}^{\infty} J_l(k_\perp\rho) i^l \frac{1}{2\pi}\int_0^{2\pi} d\theta \cos l\theta\cos l\alpha + \sin l\theta \sin l\alpha \Big] \\
&= \int d^3k e^{i\boldsymbol{k}\cdot\boldsymbol{R}} f_{\boldsymbol{k}} J_0(k_\perp\rho) = f(\boldsymbol{R}) + \frac{\rho^2}{4}\nabla_\perp^2 f + \mathcal{O}(\epsilon_\perp^4),
\end{aligned} \tag{3.191}$$

where all terms including Bessel functions of orders higher than zero vanish because they are purely oscillatory. In order to obtain the LWL of $\langle \boldsymbol{c}_\perp \cdot \boldsymbol{A}_\perp \rangle$ we calculate

$$\begin{aligned}
< \hat{\perp}\cdot\boldsymbol{A} > &= -\int d^3k e^{i\boldsymbol{k}\cdot\boldsymbol{R}} \frac{1}{2\pi}\int_0^{2\pi} d\theta \left[A_1(\boldsymbol{k})\sin\theta + A_2(\boldsymbol{k})\cos\theta \right] e^{ik_\perp\rho\cos(\theta+\alpha)} \\
&= -\int d^3k e^{i\boldsymbol{k}\cdot\boldsymbol{R}} \frac{1}{2\pi}\int_0^{2\pi} d\theta \left[A_1(\boldsymbol{k})\sin\theta + A_2(\boldsymbol{k})\cos\theta \right] \times \\
&\qquad \left[J_0(k_\perp\rho) + 2\sum_{l=1}^{\infty} J_l(k_\perp\rho) i^l \cos[l(\theta+\alpha)] \right] \\
&= -\int d^3k e^{i\boldsymbol{k}\cdot\boldsymbol{R}} \frac{1}{2\pi}\int_0^{2\pi} d\theta \left[A_1(\boldsymbol{k})\sin\theta + A_2(\boldsymbol{k})\cos\theta \right] \times \\
&\qquad \left[2\sum_{l=1}^{\infty} J_l(k_\perp\rho) i^l (\cos l\theta\cos l\alpha - \sin l\theta\sin l\alpha) \right] \\
&= \int d^3k e^{i\boldsymbol{k}\cdot\boldsymbol{R}} \left[\hat{\boldsymbol{e}}_1\cdot\boldsymbol{A} J_1(\lambda)\sin\alpha - \hat{\boldsymbol{e}}_2\cdot\boldsymbol{A} J_1(\lambda)\cos\alpha \right] \\
&= -\frac{\rho}{2} B_\parallel + \mathcal{O}(\epsilon_\perp^3).
\end{aligned} \tag{3.192}$$

Similarly, we get

$$
\begin{aligned}
< (\boldsymbol{c}_\perp \cdot \boldsymbol{A})^2 > &= \rho^2\Omega^2 < (\hat{\boldsymbol{e}}_1 \cdot \boldsymbol{A})^2 \sin^2\theta + (\hat{\boldsymbol{e}}_2 \cdot \boldsymbol{A})^2 \cos^2\theta - 2(\hat{\boldsymbol{e}}_1 \cdot \boldsymbol{A})(\hat{\boldsymbol{e}}_2 \cdot \boldsymbol{A}) \sin\theta\cos\theta > \\
&= \rho^2\Omega^2 \int d^3k e^{i\boldsymbol{k}\cdot\boldsymbol{R}} \big[(\hat{\boldsymbol{e}}_1 \cdot \boldsymbol{A})^2(\boldsymbol{k}) (\frac{J_0(\lambda)}{2} + \frac{J_2(\lambda)}{2}\cos 2\alpha) \\
&+ (\hat{\boldsymbol{e}}_2 \cdot \boldsymbol{A})^2(\boldsymbol{k}) (\frac{J_0(\lambda)}{2} - \frac{J_2(\lambda)}{2}\cos 2\alpha) + J_2(\lambda)(\hat{\boldsymbol{e}}_1 \cdot \boldsymbol{A})(\hat{\boldsymbol{e}}_2 \cdot \boldsymbol{A}) \sin 2\alpha \big] \\
&= \rho^2\Omega^2 \int d^3k e^{i\boldsymbol{k}\cdot\boldsymbol{R}} \Big\{ A_\perp^2(\boldsymbol{k}) \big[\frac{1}{2} - \frac{\lambda^2}{16}\big] - \frac{\lambda^2}{8} \big[(\hat{\boldsymbol{e}}_1 \cdot \boldsymbol{A})^2(\boldsymbol{k}) \sin^2\alpha \\
&+ (\hat{\boldsymbol{e}}_2 \cdot \boldsymbol{A})^2(\boldsymbol{k}) \cos^2\alpha - 2(\hat{\boldsymbol{e}}_1 \cdot \boldsymbol{A})(\hat{\boldsymbol{e}}_2 \cdot \boldsymbol{A}) \sin\alpha\cos\alpha \big] \\
&= \rho^2\Omega^2 \big[\frac{A_\perp^2}{2} + \frac{\rho^2}{16}\nabla_\perp^2 A_\perp^2 + \frac{\rho^2}{8} B_\parallel^2 + \mathcal{O}(\epsilon_\perp^3) \big], \qquad (3.193)
\end{aligned}
$$

and

$$
< \hat{\mathbb{1}}_\perp \cdot \boldsymbol{A}\psi_0 >= -\frac{\rho}{2}\hat{\boldsymbol{b}} \cdot \nabla \times (\boldsymbol{A}_\perp \psi_0) + \mathcal{O}(\epsilon_\perp^3). \qquad (3.194)
$$

using double angle formulas and various geometric identities.

The $\{\boldsymbol{X}, \boldsymbol{X}\}$ term in H_2 The reason why the $\{\bar{\boldsymbol{X}}, \bar{\boldsymbol{X}}\}$ part of $-q/2\{S_1, h_1\}$ has been neglected can be seen by

$$
\begin{aligned}
&\frac{\delta}{\delta\phi(\boldsymbol{r})} \int dt d\Lambda \frac{F}{2B_\parallel^*} \langle \hat{\boldsymbol{b}} \cdot \nabla_{\bar{\boldsymbol{X}}} S_1 \times \nabla_{\bar{\boldsymbol{X}}} \tilde{\psi} \rangle \\
&\quad = \int d^4\boldsymbol{r} d\Lambda \frac{F}{2B_\parallel^*} \langle \hat{\boldsymbol{b}} \times \nabla_{\bar{\boldsymbol{X}}} S_1 \cdot \nabla_{\bar{\boldsymbol{X}}} \delta^{(3)}(\widetilde{\boldsymbol{r} - \bar{\boldsymbol{X}}} - \rho_0) \delta\phi(\boldsymbol{r}) \\
&\quad - \hat{\boldsymbol{b}} \times \nabla_{\bar{\boldsymbol{X}}} \tilde{\psi} \cdot \nabla_{\bar{\boldsymbol{X}}} \int_0^\theta d\theta' \delta^{(3)}(\widetilde{\boldsymbol{r} - \bar{\boldsymbol{X}}} - \boldsymbol{\rho}) \delta\phi(\boldsymbol{r}) \rangle \\
&\quad = \int d^4\boldsymbol{r} \delta\phi(\boldsymbol{r}) \int d\Lambda \langle -\nabla_{\bar{\boldsymbol{X}}} \cdot [\frac{F}{2B_\parallel^*} \hat{\boldsymbol{b}} \times \nabla_{\bar{\boldsymbol{X}}} S_1] \delta^{(3)}(\widetilde{\boldsymbol{r} - \bar{\boldsymbol{X}}} - \rho_0) \\
&\quad + \nabla_{\bar{\boldsymbol{X}}} \cdot [\frac{F}{2B_\parallel^*} \hat{\boldsymbol{b}} \times \nabla_{\bar{\boldsymbol{X}}} \tilde{\psi}] \int_0^\theta d\theta' \delta^{(3)}(\widetilde{\boldsymbol{r} - \bar{\boldsymbol{X}}} - \boldsymbol{\rho}) \rangle \qquad (3.195)
\end{aligned}
$$

Naturally $\nabla \cdot [\hat{\boldsymbol{b}} \times \nabla S_1] \sim \mathcal{O}(\epsilon_B)$. The last term ($\nabla_{\bar{\boldsymbol{X}}} F \cdot \hat{\boldsymbol{b}} \times \nabla_{\bar{\boldsymbol{X}}} S_1$ is $\mathcal{O}(\epsilon_E)$ smaller than the leading order terms in the $\{\bar{\theta}, \bar{\mu}\}$ contribution to H_2.

3.A.2 Non-inertial reference frames and the polarization drift

Consider the one-form of a free particle [57]

$$
\gamma_f = mv dx - \frac{1}{2} m v^2 dt. \qquad (3.196)
$$

Now, change to a non-inertial reference frame moving with $u = u(t)$ and change coordinate to comoving (r, w) where $r = x - R$, $w = \dot{x} - u$

$$\gamma_f = m(w+u)dr - (\frac{1}{2}mw^2 - \frac{1}{2}mu^2). \tag{3.197}$$

The equations of motion are simply

$$\dot{r} = w, \tag{3.198}$$

$$\dot{w} = -\frac{\partial}{\partial t}u. \tag{3.199}$$

Two observations should be made from this simple system. I) The "free" particle experiences a fictitious force $-\frac{\partial}{\partial t}u$ II) the kinetic energy which corresponds to the motion of the non-inertial frame $-\frac{1}{2}m_u^2$ appears with a negative sign in the Hamiltonian.

In a magnetized plasma we have the standard interpretation that every force $\boldsymbol{F}$ gives rise to a drift $\boldsymbol{v}_D = \frac{1}{qB}\boldsymbol{F} \times \hat{\boldsymbol{b}}$. From the definition of the lowest order guiding-center coordinates we notice that the perpendicular velocity components (μ, θ) are measured in a frame moving with $\boldsymbol{W} = u\hat{\boldsymbol{b}} + \boldsymbol{D}$, where as the particle position is measured in the lab frame. The grad-B and the polarization drifts can therefore be interpreted as fictitious forces

$$\boldsymbol{D} + \boldsymbol{v}_{\nabla \times \hat{\boldsymbol{b}}} = -\frac{m}{qB}\hat{\boldsymbol{b}} \times \frac{d}{dt}\boldsymbol{W}. \tag{3.200}$$

However, we also notice that the kinetic energy term of the comoving frame in the Hamiltonian comes with a positive sign. This surprising situation is due to the weirdness of the guiding-center/gyrokinetic coordinates. In some sense we have made a coordinate transformation that follows the position $\bar{\boldsymbol{X}}$ and the parallel velocity of the non-inertial frame whereas the perpendicular velocity components (μ, θ) are measured in the comoving frame. Following this picture we also get a better understanding why the energy of perturbed ExB drift enters the Hamiltonian with a negative sign.

We now take a close look at the symplectic part of the guiding-center one-form. Besides the background magnetic potential $\boldsymbol{A}_0$ the $\boldsymbol{X}$-component of the coordinate function $\Gamma_{\boldsymbol{X}}$ of the Poincaré one-form includes the term $m\boldsymbol{W}$, meaning that the frame of reference in which (μ, θ) are measured is moving with the non constant velocity $\boldsymbol{W}$. Therefore, the perpendicular velocity components are measured in a noninertial reference frame. Fictitious forces proportional to $\sim \frac{d}{dt}\boldsymbol{W}$ are expected to enter the equations of motion. This is naturally nothing but the $\nabla \times \hat{\boldsymbol{b}}$ and the polarization drifts: $\boldsymbol{v}_{noninertial} = \frac{1}{\Omega}\hat{\boldsymbol{b}} \times \frac{d}{dt}\boldsymbol{W}$. However, the parallel velocity u is measured in the laboratory frame and the position coordinate $\boldsymbol{X}$ is the position of the comoving reference frame. The guiding-center coordinates is indeed a weird construction.

Chapter 4

Gyrofluid Blobs

4.1 Introduction

Experimental observations have revealed that the transport in the edge and scrape-off-layer (SOL) of toroidally magnetized plasmas is strongly intermittent and involves large outbreaks of hot plasma[4, 103, 93]. These structures, often referred to as blobs, are formed near the last closed flux surface (LCFS) and propagate far into the SOL, see e.g., Ref. [71, 72] for references. They have a profound influence on the pressure profiles in the SOL, the ensuing parallel flows, and the power deposition on plasma facing components. It is therefore crucial to understand the blob dynamics in order to improve the confinement in present day and future plasma fusion devices, where they are potentially harmful to the plasma facing components.

The blobs have a characteristic spatial size perpendicular to the magnetic $\sigma \sim 1\,\mathrm{cm}$, their radial speeds are up to 10% of the acoustic speed c_s and are large amplitudes. Edge/SOL temperature measurements report that $\tau = T_i/T_e \sim 1-10$[1, 104, 95, 80, 97]. Measured in units of the ion gyroradius the characteristic blob size is usually $\sigma \sim 5-20\sqrt{\tau}\rho_s$, where $\rho_s = \sqrt{T_e/m_i}$ is the cold ion acoustic gyroradius. Finite Larmor radius effects might therefore be of imprtance to the blob dynamics. The basic blob dynamics was well described in terms of nonlinear interchange motions in the limit of cold ions [10, 41, 43], but the cold ion models fail to macth the spatial blob structure and did not consider the blob coherence. The impact of the power deposition on the plasma facing component by the blob structures strongly depends on whether the blob is fragmented or remains compact.

In the present chapter we are presenting an investigation of the influence of ion temperature on the motion of isolated filaments in a toroidally confined plasma. The investigation is carried out using an isothermal electrostatic gyrofluid model. Gyrofluid models are derived from the gyrokinetic formalism presented in chapter3, by taking gyrofluid moments of the Vlasov equation expressed in gyrokinetic coordinates. Gyrokinetic coordinates are

constructed such that the fast timescale of the gyromotion is asymptotically decoupled from the drift motion time scale. This results in an effective reduction of the dimensionality of the system because the phase angle of the gyromotion in the perpendicular plane becomes an ignorable coordinate and the conjugated coordinate becomes an invariant As the orderings of drift fluid equations and gyrokinetics are compatible drift fluid equations can be derived from the gyrofluid equations[89]. However, FLR (Finite Larmor Radius) effects enter the gyrofluid models more naturally and results in algebraically simpler models because the fast gyromotion has been decoupled at the kinetic level. Especially the troublesome *gyroviscous cancellation*[16, 9, 27, 51] and the corresponding correction appear naturally in the gyrofluid description.

Gyrofluid models are inherently collisionless as they are derived from the gyrokinetic Vlasov equation. However, in the SOL region collisional dissipation and viscosity play important roles. Furthermore, all numerical simulation must add similar effects in order to compensate the finite resolution of the numerical discretization. In the gyrokinetic description efforts was made[66, 17] to derive self-consistent gyrokinetic collision operators but these contributions are not yet fully developed. In this chapter we are instead adding collisional effects in an ad-hoc manner. When adding dissipation and viscosity one must avoid that artificial charges and currents are set up. This requirement is a priori not simple in a gyrofluid model because the gyrofluid moments are mixtures of physical quantities; number density, charge, vorticity etc.

Variations of the ion temperature change the thermal energy and the characteristic radius of the ion Larmor motion. When the plasma is anisotropic the fast Larmor motion effectively perform an averaging operation which implies that electrons and ions are advected differently, but does also imply that the ions contribute to the charge balance as rings of charge instead of point charges. In order to separate the FLR effects from variations in the thermal energy we have performed a parameter scan varying the ion temperature and the characteristic length scale of the blob in numerical simulation of isolated blob structures. The simulations reveal that when the ion temperature has a huge impact on the blob dynamics. The controlling parameter of the FLR effect is the ratio of the thermal ion gyroradius to the blob length scale $\lambda = \rho_{it}/\sigma$.

This chapter is outlined as follows: in Section 4.2 we derive the isothermal electrostatic gyrofluid model; collisional dissipation and viscosity is added to the model inherently collisionless gyrofluid model in Section 4.3. In Section 4.4 the results from the numerical simulations of isolated blob structures are presented,

4.2 Isothermal gyrofluid model

We apply a simple one moment gyrofluid model to investigate the influence of finite ion temperature on the motion of isolated blobs structures. This model is in some sense the simplest self-consistent model available for nonlinear evolution of interchange motion in a finite ion temperature plasma. The single moment model is a subset of more general higher moment gyrofluid and gyrokinetic models. However, choosing this simple model allows us the isolate the effects of finite ion temperature on the interchange motion of isolated blob structures. In this work we choose free parameters that resemble the characteristic physical properties in the SOL region of fusion plasmas. This implies low dissipation and viscosity coefficients which are very numerically challenging and demands a simple model. Furthermore, the single moment model resembles the Oberbeck-Boussinesq two-field model in the cold ion limit used in earlier contributions [42, 43, 41].

Gyrofluid equations are fluid moment equations derived from gyrokinetic theory[19](see Sec. 3). Gyrokinetic theory decouples the fast gyromotion time scale from the remaining dynamics by performing an asymptotic coordinate transformation in a smallness parameter $\epsilon \ll 1$. The smallness parameter is related to the existence of a quasi symmetry of the gyroorbit and a corresponding adiabatic invariant $\bar{\mu}$. When the following physical relations hold the gyroorbit is quasi-symmetric and the fast gyroorbit timescale can be decoupled:

$$\frac{\omega}{\Omega_i} \sim \frac{k_\parallel}{k_\perp} \sim \frac{e\phi}{T_e} \sim \frac{\rho_i}{L} \sim= \mathcal{O}(\epsilon) \quad \text{and} \quad \mathrm{k}_\perp \rho_\mathrm{i} \sim \mathcal{O}(1), \tag{4.1}$$

where ω is a characteristic fluctuation frequency, Ω_0 is the ion gyro frequency, $k_\parallel$ and $k_\perp$ are the inverse parallel and perpendicular characteristic fluctuation length scales respectively; ϕ is the electric potential and T_e is the electron temperature; ρ_i denotes the thermal ion gyroradius and L is a typical equilibrium length scale. This implies that the lowest order distribution function F_0 is slowly changing in space and time but also

$$\nabla F_0 \sim \nabla F_1 \tag{4.2}$$

where F_1 is the first order distribution function. Utilizing this ordering the Vlasov equation expressed in gyrokinetic coordinates $(\boldsymbol{X}, v_\parallel, \mu, \theta, t)$ (see Sec. 3.74) reads:

$$\frac{\partial}{\partial t}(F B_\parallel^*) + \nabla \cdot (\dot{\boldsymbol{X}} B_\parallel^* F) + \frac{\partial}{\partial v_\parallel}(\dot{v}_\parallel B_\parallel^* F) = 0, \tag{4.3}$$

where $\dot{\mu} = 0$ and $\partial_\theta F = 0$ has been used. $m^2 B_\parallel^* = m^2 B + \epsilon m^2 \frac{m}{q} v_\parallel \hat{\boldsymbol{b}} \cdot \nabla \times \hat{\boldsymbol{b}} + \mathcal{O}(\epsilon^2)$ denotes the volume element. We will only keep terms up to $\mathcal{O}(\epsilon^2)$

in the Vlasov equation and are therefore taking $B^*_\parallel = B$. Therefore only the $\mathcal{O}(\epsilon)$ correct gyrocenter velocity is sufficient

$$\dot{\boldsymbol{X}} = v_\parallel \hat{\boldsymbol{b}} + \epsilon \left[\frac{\mu}{qB} \hat{\boldsymbol{b}} \times \nabla B + \frac{m v_\parallel^2}{qB} (\nabla \times \hat{\boldsymbol{b}})_\perp + \frac{\hat{\boldsymbol{b}} \times \nabla \langle \phi \rangle}{B} \right] + \mathcal{O}(\epsilon^2), \quad (4.4)$$

where

$$\langle \phi \rangle = \frac{1}{2\pi} \oint d\theta \, \phi(\boldsymbol{X} + \boldsymbol{\rho}_0) \quad (4.5)$$

denotes the gyroaveraged electrostatic potential. In the above expression the particle position $\boldsymbol{x}$ is expressed only to lowest order in terms of the gyrokinetic coordinates $\boldsymbol{x} = \boldsymbol{X} + \boldsymbol{\rho}_0 + \mathcal{O}(\epsilon)$, where $\boldsymbol{X}$ is the gyrocenter and $\boldsymbol{\rho}_0 = \Omega^{-1}\sqrt{2\mu B/m} + \mathcal{O}(\epsilon)$ denotes the lowest order gyroradius.

The electrostatic Vlasov equation (4.3) is closed by the quasi-neutrality condition $\sum_\alpha q_\alpha n_\alpha(\boldsymbol{x}) = 0$, where

$$n_\alpha(\boldsymbol{x}, t) = \int d^3\boldsymbol{v} f_\alpha(\boldsymbol{x}, \boldsymbol{v}, t) \quad (4.6)$$

denotes the particle density. Expressed in gyrokinetic coordinates the quasi-neutrality condition (see Sec. 3.93) is

$$\sum_\alpha q_\alpha \int d^6 Z B \, \delta(\boldsymbol{r} - \boldsymbol{X} - \boldsymbol{\rho}_0) \big[1 + \frac{q_\alpha^2}{B} (\phi - \langle \phi \rangle) \frac{\partial}{\partial \mu} \big] F = 0 \quad (4.7)$$

The first term denotes the unperturbed charge contribution whereas the last term is the polarization due to the fluctuating electric potential ϕ. The last term is $\mathcal{O}(\epsilon)$. Therefore, it suffices to evaluate this term with the background distribution function which is assumed to be Maxwellian in μ. Using partial integration the quasi neutrality equation (4.7) then reads[34]

$$\sum_\alpha q_\alpha \big[\bar{N}_\alpha + \frac{1}{\sqrt[3]{2\pi}} \int d^3 k \, \frac{q_\alpha^2 N_{0\alpha}}{T_\alpha} (\Gamma_0 - 1) \phi_k \big] = 0 \quad (4.8)$$

where

$$\bar{N} = \int d^6 Z B \, F \delta(\boldsymbol{r} - \boldsymbol{X} - \boldsymbol{\rho}_0) = \int d\mu du d\theta B F(\boldsymbol{r} - \boldsymbol{\rho}_0) \quad (4.9)$$

denotes the gyroaveraged gyrofluid density, ϕ_k is the Fourier transformation of ϕ and $\Gamma_0(b) = J_0(b) e^{-b}$ is the zeroth order modified Bessel function; $b = k_\perp^2 \rho_0^2$.

The zeroth order fluid moment equation is obtained by taking gyrokinetic "velocity" space moments of the gyrokinetic Vlasov equation (4.3)

$$\frac{\partial}{\partial t} N + \nabla \cdot \left[\hat{\boldsymbol{b}} N U + \frac{P_\parallel}{qB} (\nabla \times \hat{\boldsymbol{b}})_\perp + \frac{P_\perp}{qB^2} \hat{\boldsymbol{b}} \times \nabla B + N \bar{\boldsymbol{u}}_E \right] = 0, \quad (4.10)$$

where the gyrofluid moments are

$$N = \|1\| = \int d\mu du d\theta B\, F \tag{4.11}$$

$$UN = \|v_\parallel\| = \int d\mu du d\theta B\, F v_\parallel \tag{4.12}$$

$$P_\perp = \|b\mu\| = \int d\mu du d\theta B\, F \mu B \tag{4.13}$$

$$P_\parallel = \|m v_\parallel^2\| = \int d\mu du d\theta B\, F m v_\parallel^2. \tag{4.14}$$

Note that the $\partial_{v_\parallel}$ part vanishes because F is assumed to vanish at infinity. The last term in Eq. (4.10) describes the gyroaveraged $\boldsymbol{E}\times\boldsymbol{B}$-drift

$$\bar{\boldsymbol{u}}_E = \frac{\hat{\boldsymbol{b}}\times\|\nabla\langle\phi\rangle\|}{NB}. \tag{4.15}$$

4.2.1 Closure

As with any fluid model the fluid hierarchy must be closed. We simply assume that the plasma is isothermal and that the pressure is isotropic $nT = p$, where n,T and p denote the usual particle density, temperature and pressure respectively. It is crucial to note that the particle fluid moments do not equal their gyrofluid counterparts. Even in the cold ion limit the gyrofluid fluid moments still carry finite inertia effects. However, the gyrofluid moments equals the particle moments to lowest order

$$\begin{aligned} n &= \int d^3\boldsymbol{v}\, f(\boldsymbol{r},\boldsymbol{v}) = \int d^3\boldsymbol{v} d^3\boldsymbol{x}\, f\delta(\boldsymbol{r}-\boldsymbol{x}) \\ &= \int d^6 Z B_\parallel^* F\delta(\boldsymbol{r}-\boldsymbol{x}(\boldsymbol{Z},t)) = \int d^6 Z B_\parallel^* F\delta(\boldsymbol{r}-\boldsymbol{X}-\boldsymbol{\rho}_0)+\mathcal{O}(\epsilon) \\ &= \int d^6 Z B_\parallel^* F\big[\delta(\boldsymbol{r}-\boldsymbol{X})+\boldsymbol{\rho}_0\cdot\nabla\delta(\boldsymbol{r}-\boldsymbol{X})+\frac{1}{2}\boldsymbol{\rho}_0\boldsymbol{\rho}_0:\nabla\nabla\boldsymbol{\rho}_0+\cdots\big]+\mathcal{O}(\epsilon) \end{aligned} \tag{4.16}$$

which shows using (4.2) and a similar calculation for T that $nT = p$ implies $NT = P + \mathcal{O}(\epsilon)$. The closure enters only $\mathcal{O}(\epsilon^2)$ terms in the gyrofluid continuity equation (4.10) and is therefore valid to $\mathcal{O}(\epsilon^2)$.

The gyroaveraging operators appearing in the gyroaveraged $\boldsymbol{E}\times\boldsymbol{B}$ drift (4.15) and in the quasi-neutrality equation (4.7) contain gyrofluid moments of infinite powers of μ. As pointed out in Ref. [88] one must be careful when choosing closures of the gyroaveraging operators in order to obtain a meaningful energy theorem; meaningful in the sense that the energy theorem should resemble the gyrokinetic counterpart. This can be done by choosing identical closures to identical operators. Therefore we must choose

identical closures for $\bar{N}$ in the quasi-neutrality condition Eq. (4.8) and for the gyroaveraged $\boldsymbol{E} \times \boldsymbol{B}$-drift Eq. (4.15).

First we choose a closure for Γ_0. Since the quasi-neutrality equation is a $\mathcal{O}(\epsilon)$ relation between the electric potential ϕ and the gyrofluid moments, it is consistent with the gyrokinetic ordering to evaluate this term assuming that the distribution function is Maxwellian $F \propto e^{-\mu B/T}$. Under this assumption $\Gamma_0 = J_0(b_t)e^{-b_t}$, where $b_t = k_\perp^2 \rho_t^2$ and the thermal gyroradius is defined as: $\rho_t = \sqrt{T/(\Omega^2 m)}$

Next we consider the closure of the gyroaveraged $\boldsymbol{E} \times \boldsymbol{B}$-drift (4.15). Writing the gyroaveraging operator in Fourier space

$$\langle \phi \rangle = \frac{1}{2\pi} \oint d\theta \, \phi(\boldsymbol{x}) = \frac{1}{\sqrt[3]{2\pi}} \int d^3k \, e^{-i\boldsymbol{k}\cdot\boldsymbol{X}} J_0(b) \phi_k \doteq J_0 \phi \tag{4.17}$$

where J_0 is the zeroth order Bessel function. The gradient of the gyroaveraged electric potential is

$$\nabla(J_0\phi) = J_0 \nabla\phi + \frac{\nabla B}{B} J_1 b \phi \tag{4.18}$$

where J_1 denotes the first order Bessel function. Taking a closer look at the moment of the gyroaveraged electric field

$$\|\nabla(J_0\phi)\| = \|\nabla J_0\|\phi + \nabla(\|J_0\|\phi) - (\nabla\|J_0\|)\phi \tag{4.19}$$

shows that if we choose $\|J_1\|$ such that the spatial dependence is only through B, the gradient and the moment integral commute[34]. Also, the gyroaveraging operator does not commute with the gyrofluid moment integrals. Evaluating the gyrofluid moment of J_0 assuming that the distribution function is Maxwellian $F \propto e^{-\mu B/T}$ we get

$$\|J_0\|_M = \exp(-\frac{b_t}{2}), \tag{4.20}$$

which has only spatial dependence through the magnetic field

$$\|\nabla(J_0\phi)\| = \nabla(\|J_0\|\phi). \tag{4.21}$$

We choose to use the 0/1 Padé approximation of $\|J_0\|_M$ in Eq. (4.20)

$$\|J_0\|_M \simeq \Gamma_1 = \frac{1}{1 + b/2} \tag{4.22}$$

which according to [34] has a better behavior than the full operator $\|J_0\|_M$ when comparing linear growth rates and instabillity thresholds calculated using kinetic codes. Also the 0/1 Padé approximation of Γ_0

$$\Gamma_0 = \frac{1}{1 + b} \tag{4.23}$$

behaves nicely and is therefore used for the sake of simplicity. We note that the 0/1 Padé approximations, especially Γ_1, should be used with care in the high $k_\perp \rho_0$ limit.

4.2.2 Gyrofluid equations

Having determined the closures we are now able to write down the gyrofluid equations. Neglecting the electron gyroradius $m_e \to 0$ we obtain the following equations for an electron and one ion species plasma

$$\frac{\partial}{\partial t} n_e + \boldsymbol{u}_E \cdot \nabla n_e = -n_e \mathcal{K}(\phi) + \frac{T_e}{e}\mathcal{K}(n_e) - \nabla_\parallel (n_e u_\parallel), \tag{4.24a}$$

$$\frac{\partial}{\partial t} N_i + \bar{\boldsymbol{u}}_E \cdot \nabla N_i = -N_i \mathcal{K}(\psi) - \frac{T_i}{e}\mathcal{K}(N_i) - \nabla_\parallel (N_i U_\parallel), \tag{4.24b}$$

$$\frac{eN_{i0}}{T_i}(\Gamma_0 - 1)\phi = n_e - \Gamma_1 N_i = \Omega_E, \tag{4.24c}$$

where the curvature operator is $\mathcal{K}(\cdot) = \nabla \cdot (\frac{1}{B}\hat{\boldsymbol{b}} \times \nabla \cdot)$ and the $\psi = \Gamma_1 \phi$ denotes the gyroaveraged electric potential. As we have derived no equation governing the parallel velocities, $u_\parallel$ and $U_\parallel$ are considered free parameters of the model.

4.3 Collisional dissipation and viscosity

Gyrokinetic theory and therefore also gyrofluid models do not describe collisional processes. However, collisions are important especially in the edge region where the transport time scale is typically longer than the collision time. Therefore collisional effects must be added to the model (4.24) in an ad hoc fashion. In the long wave length limit (LWL) $(k_\perp \rho_i)^3 \ll 1$ the gyrofluid equations resemble[89, 16, 9] the low frequency drift fluid equations[51]. Collisional effects enter the drift fluid equation in a natural way because the equations are derived from fluid models with collisional closures[14, 5, 6]. Given the gyrofluid/drift fluid correspondence it is therefore natural to add collisional effects to the gyrofluid models such that the correspondence is retained.

We also require that the diffusion is ambipolar. To lowest order the ion gyrocenter density describes the ion particle density, but at higher orders the gyrocenter density also describes the polarization of the plasma. It is this polarization part which through the polarization equation (4.24c) determines the local electrical potential. It is therefore crucial that the collisional damping terms added to the ion gyrocenter density equation (4.24b) only dissipates density and vorticity. Any small deviation from this requirement could potentially lead to artificial polarization. The calculations presented in this section are therefore also relevant in situations where the gyrofluid model is used to carry out numerical simulations of collisionless plasmas. Due to finite numerical resolution numerical codes are always forced to add artificial damping to the gyrofluid moment equations. This damping should not lead to hidden artificial polarization effects.

We consider the general fluid momentum equation []

$$mn[\frac{\partial}{\partial t} + \boldsymbol{u}\cdot\nabla]\boldsymbol{u} = -\nabla p - \nabla\cdot\pi - qn[\boldsymbol{E} + \boldsymbol{u}\times\boldsymbol{B}] + \boldsymbol{R} \tag{4.25}$$

where m denotes the mass, q denotes charge, n is the density, $\boldsymbol{u}$ is the fluid velocity, p is the scalar pressure and π is the off diagonal part of the pressure tensor, $\boldsymbol{E}$ and $\boldsymbol{B}$ denote the electric and magnetic fields respectively. $\boldsymbol{R}$ denotes the collisional resistivity. In the drift approximation the perpendicular part of the momentum equation is solved iteratively $\boldsymbol{u}_\perp = \boldsymbol{u}_\perp^{(0)} + \epsilon\boldsymbol{u}_\perp^{(1)} + \cdots$. $\boldsymbol{u}_\perp^{(0)} = \boldsymbol{u}_E + \boldsymbol{u}_D$, denote the $\boldsymbol{E}\times\boldsymbol{B}$ and diamagnetic drifts respectively. The second order drift $\boldsymbol{u}_\perp^{(1)} = \boldsymbol{u}_p + \boldsymbol{u}_\pi + \boldsymbol{u}_{\boldsymbol{R}}$, consist of the polarization drift $\boldsymbol{u}_p$ and drifts due to shear stress $\boldsymbol{u}_\pi$ and resistivity $\boldsymbol{u}_{\boldsymbol{R}}$.

In this way collisional resistivity and shear stress enter the continuity equation

$$\frac{\partial}{\partial t}n + \nabla\cdot\left(n\boldsymbol{u}_\perp^{(0)} + n\boldsymbol{u}_\perp^{(1)} + nu_\parallel\hat{\boldsymbol{b}}\right) = 0 \tag{4.26}$$

Linearizing the resistivity contribution we get

$$\nabla\cdot(n\boldsymbol{u}_R) = \chi\nabla_\perp^2 n, \tag{4.27}$$

reflecting ambipolar diffusion of density, where $\chi = p_0/(\sigma_\perp B_0^2)$. $\sigma_\perp = e^2 n\tau_e/m_e$ denotes the perpendicular conductivity and τ_e is the electron-ion collision frequency[14].

The shear stress contribution can be split into three parts $\pi = \pi^P + \pi^G + \pi^S$. π^P is due to collisions between particles moving along magnetic field lines. π^S describes collisions between particles orbiting different magnetic field lines. The characteristic momentum transport scale length is therefore proportional to the gyroradius, so even though the ion-ion collision frequency is $\mathcal{O}(\sqrt{\frac{m_e}{m_i}})$ times smaller than the electron-ion collision frequency, the ion contribution is dominant. Linearizing the ion part we get

$$\nabla\cdot(n\boldsymbol{u}_{\pi^S}) = \eta\nabla_\perp^4\phi^* \tag{4.28}$$

where $\phi^* = \phi + \frac{T_i n}{qn_0}$, $\eta = n_0\eta_1/(B_0^2 q)$ and the ion viscosity coefficient is $\eta_1 = \frac{3}{10}\frac{nT_i}{\omega_{ci}\tau_i}$. τ_i denotes the ion-ion collision time. The collisional viscosity is typically small compared to the resistivity but must be retained in the charge conservation equation because the ion and electron resistivities naturally cancel. Again, keeping only the lowest order fluid drifts the collisional viscosity enters the vorticity (charge conservation) equation as[51]

$$\frac{n_0}{\Omega_i B}\nabla\cdot\left[(\frac{\partial}{\partial t} + \boldsymbol{u}_E\cdot\nabla)\nabla_\perp\phi^*\right] = \eta\nabla_\perp^4\phi^* + \cdots. \tag{4.29}$$

In this way π^S provides momentum diffusion in the drift fluid vorticity equation. The last part of the shear stress tensor, the *gyroviscous* stress tensor π^G, is not related to collisions. It provides an FLR correction to the pressure due to spatial variations of the gyroradius. In the drift fluid vorticity equation Eq. (4.29) the *gyroviscosity* cancels the advection of momentum by the diamagnetic drift[51, 27].

When adding viscosity and dissipation to the gyrofluid model we require that the gyrofluid viscosity and dissipation effects are identical to the drift fluid counterparts in the LWL. We furthermore demand that the density dissipation is ambipolar. The reason why this is not a trivial task is due to the fact that the gyrocenter density N is a mixed quantity simultaneously describing particle density and polarization. Nonetheless, in the gyrofluid model we integrate this quantity in time and must therefore determine how gyrocenter dissipation should look like.

In order to do so we derive a "vorticity" like equation by inserting the quasi-neutrality condition (4.24c) into the electron continuity equation (4.24a), eliminating n_e, and subtract the ion continuity equation (4.24b)

$$\begin{aligned}\frac{d}{dt}\Omega^* - \frac{T_e+T_i}{e}\mathcal{K}(N_i) = -\Omega^*\mathcal{K}(\phi) + \frac{T_e}{e}\mathcal{K}(\Omega^*) - \frac{T_e+T_i}{e}\mathcal{K}(\tilde{\Gamma}_1 N_i)\\ +\tilde{\Gamma}_1(N_i\mathcal{K}(\tilde{\Gamma}_1\phi)) + \nabla_\parallel J_\parallel - \nabla_\parallel\big(\frac{J_{\parallel 0}}{eN_{i0}}\Omega^E\big) + \Lambda_e - \Lambda_i + \tilde{\Gamma}_1\Lambda_i\\ -\tilde{\Gamma}_1(\tilde{\Gamma}_1\boldsymbol{u}_E\cdot\nabla N_i)\end{aligned} \tag{4.30}$$

where $\Lambda_{e,i}$ denote the yet undetermined collisional terms in the electron and ion continuity equation respectively. We have defined

$$\tilde{\Gamma}_1 = \Gamma_1 - 1, \tag{4.31}$$

and have used that

$$nu_\parallel = \Gamma_1 NU + \frac{J_{0\parallel}}{T_i}(\Gamma_0 - 1)\phi \tag{4.32}$$

and we have defined the "FLR generalized" diamagnetic and $\boldsymbol{E}\times\boldsymbol{B}$ vorticity

$$\Omega^* = 2\tilde{\Gamma}_1 N + \Omega_E \tag{4.33}$$

where

$$\Omega_E = \frac{eN_{i0}}{T_i}(\Gamma_0 - 1)\phi \tag{4.34}$$

We have also defined the advective derivative

$$\frac{d}{dt} = \frac{\partial}{\partial t} + \boldsymbol{u}_E\cdot\nabla \tag{4.35}$$

$\Lambda_{i,e}$ denote the undetermined collision terms. The last term on the left hand side of (4.30) is the interchange drive due to the nonuniform background magnetic field. The interchange drive and the compression of the parallel current are the only non-FLR terms on the right hand side of the vorticity equation Eq. (4.30). The remaining terms describe FLR effects and do not enter the corresponding drift fluid vorticity equation.

We require that the collisional terms in the vorticity equation (4.30) do only dissipate the vorticity Ω^*

$$\Lambda_e - \Lambda_i + \tilde{\Gamma}_1 \Lambda_i = \eta \nabla_\perp^2 \Omega^* \tag{4.36}$$

If we for the electrons take the linearized collision term from drift fluid theory

$$\Lambda_e = \chi \nabla_\perp^2 n_e \tag{4.37}$$

where χ is the (Braginskii) collisional dissipation constant we find from (4.36) that the ion collisional dissipation is

$$\begin{aligned} \Lambda_i &= \Gamma_1^{-1}\Gamma_0 \big[\chi \nabla_\perp^2 n - \eta \nabla_\perp^2 \Omega^*\big] && (4.38)\\ &= \eta \nabla_\perp^2 N_i + (\chi - \eta)\Gamma_0 \nabla_\perp^2 N_i + (\chi - \eta)\Gamma_0 \Gamma_1^{-1} \nabla_\perp^2 \Omega_E && (4.39) \end{aligned}$$

This result has the interesting property that for Schmidt number $Sc = \eta/\chi = 1$

$$\Lambda_i^{Sc=1} = \chi \nabla_\perp^2 N_i \tag{4.40}$$

Therefore, when performing numerical calculations using the gyrofluid equations, diffusion of N_i does not imply artificial polarization effects.

In the long wave length limit the vorticity equation (4.30) is given as

$$\nabla \cdot \big(\frac{n_0}{\Omega B_0}\frac{d}{dt}\nabla \phi^*\big) = \frac{T_e + T_i}{e}\mathcal{K}(n) + \nabla_\parallel J_\parallel - \nabla_\parallel \big(\frac{J_{\parallel 0}}{\Omega_i^2 m_i}\nabla_\perp^2 \phi\big) + \frac{n_0}{B\omega_{ci}}\eta \nabla_\perp^4 \phi^*, \tag{4.41}$$

which resembles the linearized drift fluid vorticity equation[37]. The corresponding long wave length limit realization of Λ_i is given as

$$\begin{aligned} \Lambda_i^{LWL} &= \chi(1 + \rho_i^2 \nabla_\perp^2)\nabla_\perp^2 N_i - \eta \nabla_\perp^4 \phi^* + \chi \frac{N_{i0}}{\Omega_i B}\nabla_\perp^4 \phi \\ &= \chi(1 - b/2)\nabla_\perp^2 n - \frac{n_0}{B\omega_{ci}}\eta \nabla_\perp^4 \phi^*. \end{aligned} \tag{4.42}$$

The last term of (4.41) is identical to the linearized Braginskii[14] viscosity in (4.29).

4.4 Blob dynamics

In this section the gyrofluid model derived and analyzed in the previous section is employed to study the motion of isolated plasma blob structures in the scrape off layer region of a toroidal confined plasma. Motivated by temperature measurements in the edge/SOL region showing that the ion temperature generally exceeds the electron temperature $\tau \sim 1-10$[1, 104, 95, 97], we will investigate the influence ion temperature variations to the blob dynamics. In our model an ion temperature variation, generally speaking, has two consequences. First, the thermal energy of the ions is changed which therefore alters the total potential energy of the system. Secondly, the ion gyroradii are changed which potentially changes the influence of FLR effects. The influence of FLR effects is controlled by the ratio of the ion gyroradius to the characteristic length scale in the system $k_\perp \rho_i$. In order to separate these two effects a parameter scan varying the initial blob size and the ion temperature has been carried out. The remaining free parameters are held fixed at values that are characteristic for the SOL region. Furthermore, we neglect the parallel dynamics in order to simplify and isolate the finite ion temperature effects. This is reasonable when $\frac{u_\parallel / L_\parallel}{v_\perp / l} \ll 1$. If the filament expands along the magnetic fields lines at a speed comparable to c_s, this requirement is easily met. The simulations are therefore carried out on a drift plane perpendicular to the magnetic field with slab coordinates x and y having periodic boundary conditions.

The reduced model equations used in the numerical simulations are Bohm normalized

$$\boldsymbol{x} \to \frac{\boldsymbol{x}}{\rho_s}, \quad t \to \omega_{ci} t, \quad T_e \to \frac{T_e}{\mathcal{T}_e}, \quad n \to \frac{n}{\mathcal{N}}, \quad \phi \to \frac{e\phi}{\mathcal{T}_e}, \tag{4.43}$$

where $\rho_s = c_{s0}/\omega_{ci}$ is the hybrid thermal gyroradius in the cold ion limit, $c_{s0} = \sqrt{\mathcal{T}_e/m_i}$ is the corresponding cold ion sound speed, $\omega_{ci} = e\mathcal{B}/m_i$ denotes the gyrofrequency of a single charged ion at a characteristic magnetic field strength $\mathcal{B}$. $\mathcal{N}$ and $\mathcal{T}_e$ denote constant characteristic density and electron temperature respectively. We take the characteristic electron temperature $\mathcal{T}_e$ as the normalization of the ion temperature $\tau = T_i/\mathcal{T}_e$. The gradient of the inverse slab magnetic field is $\xi = \rho_s/R$, where R denotes the major radius of the toroidal plasma. Adding the collisional terms derived in section (4.3) to the gyrofluid equations (4.24), neglecting the parallel dynamics and assuming unity Schmidt number, we obtain the reduced model

equations used in this study,

$$\left[\frac{\partial}{\partial t} + \hat{\boldsymbol{z}} \times \nabla\phi \cdot \nabla\right] n = -\mathcal{C}(\phi) + \mathcal{C}(n) + D\nabla_\perp^2 n \tag{4.44a}$$

$$\left[\frac{\partial}{\partial t} + \hat{\boldsymbol{z}} \times \nabla(\Gamma_1\phi) \cdot \nabla\right] N = -\mathcal{C}(\psi) - \tau\mathcal{C}(N) + D\nabla_\perp^2 N \tag{4.44b}$$

$$\frac{1}{\tau}(\Gamma_0 - 1)\phi = n - \Gamma_1 N = \Omega_E \tag{4.44c}$$

where the normalized dissipation coefficient is $D = \chi/(\rho_{s0}^2\omega_{ci})$ and we have defined the curvature operator

$$\mathcal{C} = -\xi\frac{\partial}{\partial y} \tag{4.45}$$

where $\xi = \rho_e/R_0$; R_0 is the major radius of the toroidal plasma.

We note that the magnetic field in the advection of n_e and N_i is constant. This approximation is enforced by the periodic boundary conditions. In to order to retain mass conservation the compression of the $\boldsymbol{E} \times \boldsymbol{B}$-drift has been linearized in the electron (4.44a) and ion (4.44b) continuity equations. These changes should not change the overall blob dynamics because the blob evolution is dominated by interchange dynamics through the compression of the diamagnetic current in the vorticity equation (4.30), when $k_\perp\rho_i < 1$.

The density blobs are initialized as symmetric Gaussian structures δn sitting on a constant background n_0

$$n(t=0) = n_0 + A\exp\left(\frac{-\boldsymbol{x}^2}{2\sigma^2}\right) \tag{4.46}$$

We choose the initial condition such that the plasma is everywhere charge neutral $n_e(t=0) = n_i(t=0)$. From (4.24c) this implies that the initial ion gyrocenter density is given as

$$N(t=0) = \Gamma_1^{-1} n_e(t=0). \tag{4.47}$$

The density profiles at $x = 0$ in the vicinity of the blob are shown on Fig.4.1 which demonstrate the possibility of major local differences of the ion *gyrocenter* density and the electron *particle* density. Due to the assumption of quasi neutrality the global number density of ion gyrocenters and electron particles is the same. This can be seen by integrating the polarization equation (4.44c) assuming that the gyroaveraging operators equal unity at infinity.

Alternatively we could have used the initial condition $n(t=0) = N(t=0)$. The alternative initial condition is globally charge neutral but implies a nonzero initial vorticity distribution. In the absence of advection the diffusive solution on an infinite domain given the initial condition (4.46)

$$n^\infty(\boldsymbol{x}, t) = n_0 + \frac{A\sigma}{\sqrt{\sigma^2 + 2\chi t}}\exp\left[\frac{-\boldsymbol{x}^2}{2(\sigma^2 + 2\chi t)}\right] \tag{4.48}$$

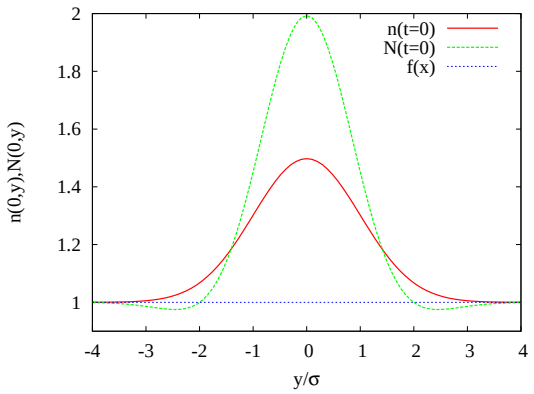

Figure 4.1: Electron n and ion gyrocenter density N poloidal profiles at $t = 0$ through the symmetry axes at $y = 0$, initial blob width $\sigma = 1$, ion temperature $\tau = 1$.

$\sigma = 5$

If we neglect the parallel dynamics in the long wave length vorticity equation Eq. (4.41) it is reasonable to assume that the the initial dynamics is dominated by interchange dynamics when the blob width σ is chosen such that $\rho_i^2/\sigma^2 < 1$. Balancing inertia with the interchange drive we obtain the ideal interchange rate

$$\gamma = \sqrt{\frac{g}{l}\frac{\delta n}{n_0}} \tag{4.49}$$

and the corresponding ideal perpendicular velocity

$$\frac{V_\perp}{c_s} = \sqrt{\frac{l}{R}\frac{\delta n}{n_0}} \tag{4.50}$$

where $g = c_s^2/R$ denotes the effective gravity, $c_s = \sqrt{p/\rho}$ is the acoustic speed, $p = p_e + p_i$ is the total particle pressure , $\rho = m_i n_i + m_e n_e$ denotes the total mass , Δn is a characteristic density perturbation, n_0 is the background density, R is the major radius and l denotes the characteristic length scale. Also, we define the Rayleigh number

$$\mathrm{Ra} = \frac{(T_e + T_i)l^3}{m_i R \chi \eta}\frac{\Delta n}{n_0}. \tag{4.51}$$

The Rayleigh number is the ratio of buoyancy to dissipative forces. In situations where FLR effects are important or even dominant in the vorticity equation Eq. (4.30) we cannot a priori expect that the characteristica of the general dynamics is well described by γ, $V_\perp$ and Ra simply because the interchange drive is not necessarily the dominating term in Eq. (4.30). In normalized units the ideal interchange rate is given as

$$\gamma = \sqrt{\frac{(1+\tau)\xi A}{\sigma}} \tag{4.52}$$

and the corresponding Rayleigh number

$$\mathrm{Ra} = \frac{\xi\sigma^3(1+\tau)A}{D^2}. \tag{4.53}$$

In many aspects the work presented here is an extension of earlier work where the blob dynamics was analyzed using a simplified two field interchange model[10, 43, 41]. When $\tau = 0$ the gyrofluid equations (4.44) are algebraically equivalent with the following set of equations

$$\left[\frac{\partial}{\partial t} + \hat{\boldsymbol{z}} \times \nabla\phi \cdot \nabla\right] n = -\mathcal{C}(\phi) + \mathcal{C}(n) + D\nabla_\perp^2 n, \tag{4.54a}$$

$$\left[\frac{\partial}{\partial t} + \hat{\boldsymbol{z}} \times \nabla\phi \cdot \nabla\right] \nabla_\perp^2\phi = \mathcal{C}(n) + D\nabla_\perp^2\nabla_\perp^2\phi, \tag{4.54b}$$

which resembles the two field interchange model used in previous contributions[43, 41, 10]. If the finite compression of the $\boldsymbol{E}\times\boldsymbol{B}$ and diamagnetic drifts are neglected the models are identical.

A quantitative measure of the dynamics of the "isolated" blob structures is the center of mass position subtracting the background level

$$x\boldsymbol{X}_C = (X_C, Y_C) = \frac{1}{M}\int d\boldsymbol{x}\, x(n-1) \tag{4.55}$$

where the total mass is defined as

$$M = \int d\boldsymbol{x}\,(n-1) \tag{4.56}$$

The corresponding center of mass velocity is

$$\boldsymbol{V}_C = \frac{d}{dt}\boldsymbol{X}_C \tag{4.57}$$

which is proportional to the convective flux

$$\mathrm{F}(t) = \int d\boldsymbol{x}\, n\boldsymbol{u}_E = M\boldsymbol{V}_C, \tag{4.58}$$

making the center of mass position $\boldsymbol{X}_C$ proportional to the time integrated flux

$$\mathrm{F}^{tot}(t) = \int_0^t dt\,\mathrm{F}(t) = M[\boldsymbol{X}_C(t) - \boldsymbol{X}_C(0)]. \tag{4.59}$$

4.4.1 FLR effects

The finite ion Larmor radius has two immediate consequences. First, due to the gyrotron motion ion gyrocenters are advected by an FLR averaged $\boldsymbol{E}\times\boldsymbol{B}$ velocity. In general the FLR averaging reduces the $\boldsymbol{E}\times\boldsymbol{B}$ particle

drift. Secondly, the ion gyrocenter charge contribution should be thought of as rings of charge. In the fluid description these effects are represented by the FLR averaged $\boldsymbol{E}\times\boldsymbol{B}$ advection in the ion gyrocenter density continuity equation (4.44b) and in the polarization equation (4.44c) respectively. FLR effects are therefore potentially able to alter the plasma polarization.

To gain insight into the impact of the FLR effects to the blob evolution we consider the LWL vorticity equation (4.41) (in normalized units)

$$\nabla\cdot\big(\frac{d}{dt}\nabla_\perp\phi^*\big)=(1+\tau)\mathcal{C}(n), \tag{4.60}$$

neglecting all parallel and collisional terms. Using the electron continuity equation (4.44a) the "diamagnetic vorticity" term can be rewritten as

$$\nabla\cdot\big(\frac{d}{dt}\nabla_\perp\tau n\big)=\frac{d}{dt}\frac{\rho_{ith}^2}{2}\nabla_\perp^2 n-\{\frac{\rho_{ith}^2}{2}\nabla_\perp^2\phi,n\}, \tag{4.61}$$

where we have introduced the bracket notation

$$\{n,\phi\}=\frac{\partial n}{\partial x}\frac{\partial\phi}{\partial y}-\frac{\partial n}{\partial y}\frac{\partial\phi}{\partial x}. \tag{4.62}$$

Eq.(4.61) demonstrates that the "diamagnetic vorticity" is indeed an FLR correction which originates from the FLR averaged $\boldsymbol{E}\times\boldsymbol{B}$ advection

$$(\Gamma_1\boldsymbol{u}_E)\cdot\nabla n=\{\phi,n\}+\{\frac{\rho_{ith}^2}{2}\nabla_\perp^2\phi,n\}+\cdots, \tag{4.63}$$

(recall that the Taylor expansion of the FLR averaging operator is: $\Gamma_1=1+\frac{1}{2}\rho_{ith}^2\nabla_\perp^2$) and the ring charge contribution to the charge balance

$$\frac{d}{dt}N\simeq\frac{d}{dt}\Gamma_1^{-1}n=\frac{d}{dt}(n-\frac{\rho_{ith}^2}{2}\nabla_\perp^2 n). \tag{4.64}$$

This also show that the drift fluid vorticity equation (4.29) contains the lowest order FLR effects.

Consider a blob which is initially charge neutral, $\phi=0$. The vorticity equation (4.60) shows that the only generator of vorticity in the initial phase is the finite compression of the diamagnetic current; the interchange drive. The compression of the diamagnetic current sets up a vorticity dipole as depicted on Fig.4.4.1. Rewriting Eq. (4.61)

$$\nabla\cdot\big(\frac{d}{dt}\nabla_\perp\tau n\big)=\rho_{ith}^2\{n,\nabla_\perp^2\phi\}-\rho_{ith}^2\{\nabla_\perp\phi,\nabla_\perp n\} \tag{4.65}$$

demonstrates that the in the LWL the "diamagnetic vorticity" term has two types of contributions. The first term shows that density acts as a stream function for the vorticity, i.e. vorticity is advected along the contour lines of n. This implies that vorticity is smeared out around the blob. Fig.4.3(a)

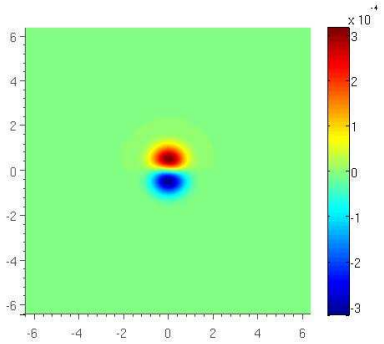

Figure 4.2: Contour plot of vorticity $\nabla_\perp^2 \phi$ after one ideal interchange time $t = \gamma^{-1}$. Initial blob width $\sigma = 10$, ion temperature $\tau = 1$, length scales are in units of σ.

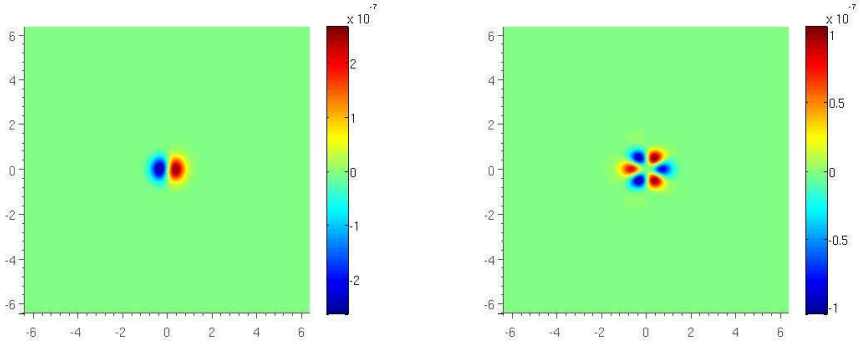

(a) (b)

Figure 4.3: Contour plots after one ideal interchange time $t = \gamma^{-1}$. Initial blob width $\sigma = 10$, ion temperature $\tau = 1$, length scales are in units of σ. (a) $-\rho_{ith}^2\{n, \nabla_\perp^2 \phi\}$ and (b) $-\rho_{ith}^2\{\nabla_\perp \phi, \nabla_\perp n\}$.

shows the contribution of this term after on ideal interchange time. If the system is in a state where this term dominates we should expect that the vorticity circulates around the blob. The last term contributes when the electric field $\boldsymbol{E} = -\nabla\phi$ and the gradient of the density are not parallel and is depicted on Fig.4.3(b). As long as the blob remains "blob shaped" the interchange drive setup a dipole in the electrical field, which implies that the second term in eq.(4.65) mix vorticity at the blob edge with vorticity in the blob core. We assume that both terms will be the main contributers to redistribution of vorticity as long as $k_\perp \rho_i < 1$. In the analysis of the numerical simulations, Sec.4.5, we further describe the implications of these terms.

4.4.2 Energy theorem

The conserved energy of the reduced model equations (4.44) are obtained by multiplying the electron continuity equations (4.44a) by $\big[\phi - n\big]$ and integrating over the domain

$$\int d\boldsymbol{x} \left[\phi \frac{\partial n}{\partial t} - \frac{1}{2}\frac{\partial}{\partial t}(n^2) - \big[\phi - n\big] D\nabla_\perp^2 n\right] = 0. \tag{4.66}$$

Similarly multiplying the ion continuity equation (4.44b) by $\big[\Gamma_1\phi + \tau N\big]$ and integrating over the domain gives

$$\int d\boldsymbol{x} \left[\Gamma_1\phi \frac{\partial N}{\partial t} + \frac{\tau}{2}\frac{\partial}{\partial t}(N^2) - \big[\Gamma_1\phi - \tau N\big] D\nabla_\perp^2 N\right] = 0, \tag{4.67}$$

Subtracting (4.66) and (4.67) gives the total conserved energy

$$\frac{d}{dt}(U_E + U_e + U_i) = U_\Lambda. \tag{4.68}$$

Using the polarization equation (4.44c) we identify the $\boldsymbol{E}\times\boldsymbol{B}$ energy

$$U_E = \int d\boldsymbol{x} \left[\Gamma_1\phi)\frac{\partial}{\partial t}N - \phi\frac{\partial}{\partial t}n\right] = \int d^3\boldsymbol{k}\, \frac{1}{2\tau}(1-\Gamma_0)|\phi_k|^2 \tag{4.69}$$

where we have used the hermiticity of Γ_1, ϕ_k denotes the Fourier transform of ϕ and $|\phi_k|^2 = \phi_k\phi_k^*$, where ϕ_k^* denotes the complex conjugate. As expected the generalized $\boldsymbol{E}\times\boldsymbol{B}$-energy (4.69) is identical to the $\boldsymbol{E}\times\boldsymbol{B}$-energy of linearized isothermal gyrokinetics[36]. The electron and ion thermal energies are

$$U_e = \int d\boldsymbol{x}\, n\ln n, \quad U_i = \int d\boldsymbol{x}\, N\tau \ln N, \tag{4.70}$$

and the energy loss due to viscosity and dissipation is given as

$$U_\Lambda = \int d\boldsymbol{x}\, D(\ln n\nabla^2 n + \ln N\nabla^2 N) + \int d\boldsymbol{k}\, \frac{D}{\tau}(1-\Gamma_0)k^2|\phi_k|^2, \tag{4.71}$$

where we have used the polarization equation (4.44c) to obtain the last term. The evolution of the individual energy parts is

$$\frac{d}{dt}U_E = \int d\boldsymbol{x}\left[n\mathcal{C}(\phi) + \tau N\mathcal{C}(\Gamma_1\phi)\right] + \int d\boldsymbol{k}\,\frac{D}{\tau}(\Gamma_0 - 1)k^2|\phi_k|^2, \quad (4.72a)$$

$$\frac{d}{dt}U_e = \int d\boldsymbol{x}\left[-n\mathcal{C}(\phi) + D\ln n\nabla^2 n\right], \quad (4.72b)$$

$$\frac{d}{dt}U_i = \int d\boldsymbol{x}\left[-\tau N\mathcal{C}(\Gamma_1\phi) + D\ln N\nabla^2 N\right]. \quad (4.72c)$$

The two first terms in (4.72a) and the first terms in (4.72b) and (4.72c) show the drive of $\boldsymbol{E}\times\boldsymbol{B}$-energy namely outward radial transport of thermal energy. The last term in (4.72a) describes the change of $\boldsymbol{E}\times\boldsymbol{B}$-energy due to viscosity. In the thermal energy equations (4.72b) and (4.72c) the last terms represent the change of energy due to dissipation. The fact that U_E only losses energy due to viscosity and thermal energy is only lost due to dissipation is a consistency check of the ad hoc collisional terms derived in the previous section.

4.5 Numerical results

In this section we present numerical solutions of the gyrofluid equations (4.44) using the Gaussian blob structure (4.46) and (4.47) as initial condition. Each species are individually isothermal but $\tau = T_i/T_e$ is varied. We investigate how the blob propagation is influenced by finite ion temperature effects. The influence of FLR effects is controlled by the ratio of the ion gyroradius to the characteristic length scale in the system $k_\perp\rho_i$. In the initial phase of the simulations the characteristic length scale is given by the blob amplitude and $k_\perp^{ini} \sim A/\sigma$. A parameter scan has been carried out varying the initial blob width σ and the ion temperature τ keeping the remaining free parameters (D, ξ, A) in the model fixed. The dissipation is held constant at $D = 10^{-3}$. In principle[14] $D \propto (1+\tau)$, but having chosen unity Schmidt number an ion temperature dependent dissipation would lead to complications as the viscosity constant does not have a similar ion temperature dependence. The blob amplitude is fixed at $A = 0.5$. This is in principle violating the validity of linearizing the compression of the $\boldsymbol{E}\times\boldsymbol{B}$-drift but test runs show that the linearization has no influence on the overall dynamic. The curvature constant is held fixed at $\xi = 5\times10^{-4}$. The free parameters corresponds to a plasma with the following characteristic parameters:

$$n_0 \approx 10^{19}\,\mathrm{m}^{-3} \quad T_e \approx 20\,\mathrm{eV}, \quad R \approx 1\,\mathrm{m}, \quad B \approx 1\,\mathrm{T}. \quad (4.73)$$

The numerical simulations have been carried out using a standard spectral method. Simulations with the given parameters is a challenging task.

Taking a closer look at the polarization equation (4.44c) shows that the characteristic spatial length scale of the equation is ρ_s, a length scale which in most cases must be resolved. Also, in order to minimize finite box size effects, mainly due to the slow spatial decay of ϕ, the simulation domain should be considerably larger than the blob size. In all simulations the ratio of box width L to the initial blob width σ is kept constant at $L/\sigma = 50$. In order to resolve the initial gradients test simulations have shown that the runs are only well converged when $\sigma/dx \sim 40$, where dx denotes the numerical grid resolution. This implies that most runs have required 2048^2 grid points in order to be well converged. The simulation time is in most simulations $30\,\gamma^{-1}$ which give typical computer runtime in the order of 1-2 weeks.

4.5.1 General blob evolution

Independent of blob width and ion temperature the blobs accelerate and move radially outwards as a consequence of a dipole in the vorticity field. The polarization is generated by the interchange drive which acts as to polarize the plasma when the magnetic field is inhomogeneous and the density perturbation persists. In Fig. 4.4 we present contour plots of two blobs that are initialized in the same way but are having different ion temperatures, in the top row $\tau = 0$ and in the bottom row $\tau = 3.0$. The first column show

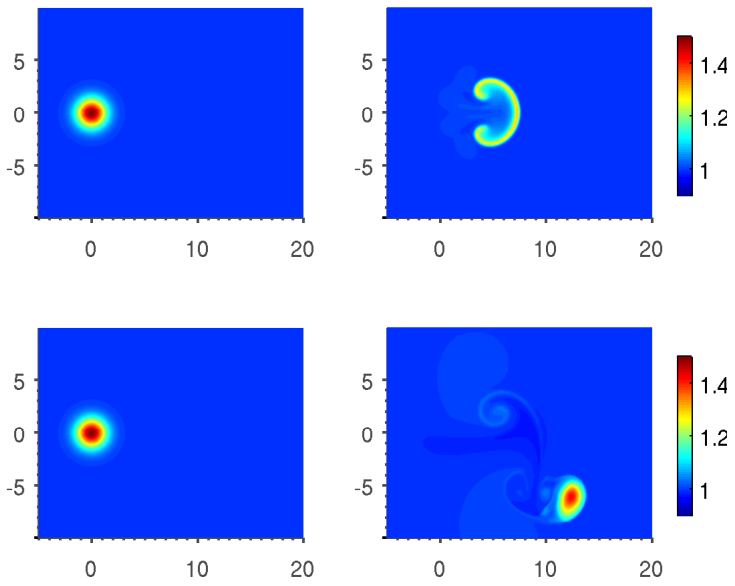

Figure 4.4: Spatial structure of density for two blobs with initial widths $\sigma = 5$. Length scales are normalized to initial blob width σ. In the top row $\tau = 0$, bottom row $\tau = 3$. First column $t = 0$, second column $t = 1250\omega_{ci}$.

the blobs as they where initialized and the second column show the blobs at $t = 1250\omega_{ci}$. We show this figure to demonstrate the main conclusion of the numerical simulations: at finite ion temperature the blobs travel further, faster, become more compact and have a different spatial density signature. The blob shape is similar to experimental observations[109, 93, 53] where the blobs are not mushroom shaped as in the cold ion limit. In the example shown in Fig. 4.4 we see that the finite ion temperature blob has moved approximately twice the distance of the cold ion blob. On the one hand, this should come as no surprise as an increased ion temperature naturally increase the thermal energy as well. On the other hand, one might have expected that the FLR averaging reduce the advection because the FLR correction in general reduce the $\boldsymbol{E} \times \boldsymbol{B}$-drift by which the ions are advected. This observation indicate that when FLR effects are taken into account the ideal interchange rate $\gamma \propto \sqrt{1+\tau}$ remains an appropriate scaling. Therefore, in the remaining part of this section we choose to normalize time to γ^{-1} (4.52) and length scales are normalized to the initial blob width σ.

Now, we give a more detailed presentation of the dynamical evolution of the blobs. Fig. 4.5,4.6,4.8,4.9 and 4.11 depict the dynamical evolution density n, electric potential ϕ, vorticity $\nabla_\perp^2\phi$ and radial $\boldsymbol{E} \times \boldsymbol{B}$-velocity $v_x = \hat{\boldsymbol{x}} \cdot \boldsymbol{u}_E$ of isolated blob structures, having different initial blob widths and ion temperature. Note that only a part of the simulation domain is shown. Table 4.1 summarize the initialization parameters of the simulations shown in Fig. 4.5-4.11. Despite the huge differences in Rayleigh number and

Figure #	τ	σ	$k_\perp^{ini}\rho_i$	Ra
4.5	0	2	0	2000
4.6	0	10	0	2.5×10^5
4.8	1	2	0.25	4000
4.9	1	10	0.05	5×10^5
4.11	7	5	0.26	2.5×10^5

Table 4.1:

$k_\perp^{ini}\rho_i$ it is evident that in this normalization blobs approximately travel the same distance per unit time; in normalized units. After $30\,\gamma^{-1}$ time units the blobs have approximately traveled ten times their initial width. However, a comparison of the contour plots show that the dynamical evolution changes dramatically when ion temperature and initial blob width are varied.

Cold ions

The dynamical evolution in the cold ion limit is special as $\rho_i = 0$, which imply that all FLR terms in the model (4.44) vanish. Therefore, $k_\perp\rho_i = 0$ at all times, leaving the initial width as the only parameter being varied. Recall

that in this limit the model is equivalent to the drift fluid equations (4.54). In the cold ion limit the numerical simulations show that the dynamical evolution has characteristic features independent of the initial width σ.

Simulations in the cold ion limit with initial widths $\sigma = 2, 10$, are presented in Fig. 4.5 and 4.6 respectively. The initial phase is characterized

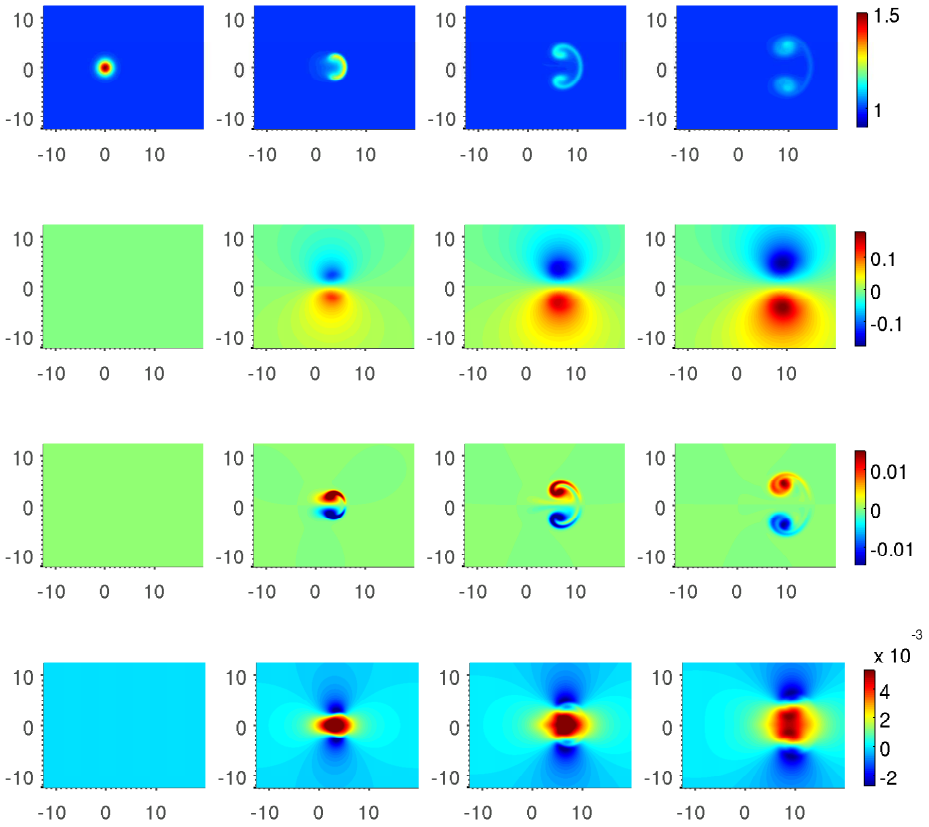

Figure 4.5: Ion temperature $\tau = 0$, initial blob width $\sigma = 2$, Rayleigh number $\mathrm{Ra} = 2000$. Spatial structure of density n (top row), electric potential ϕ (second row), vorticity $\nabla_\perp^2 \phi$ (third row) and radial $\boldsymbol{E} \times \boldsymbol{B}$-velocity v_x (bottom row). In all rows time increments $10\,\gamma^{-1}$ going from left to right. Axes are normalized with the initial blob width σ. Only a part of the simulation domain shown.

by a formation of a sharp density gradient at the leading edge as the blob is advected radially outwards. The sharp density gradient is followed by a trailing wake, a behavior which resembles the dynamics of a shock front. Comparing the spatial structure of density n and radial velocity v_x show that the maximal value of the velocity field lacks behind the density peak causing a steepening of the leading edge and the formation of a trailing

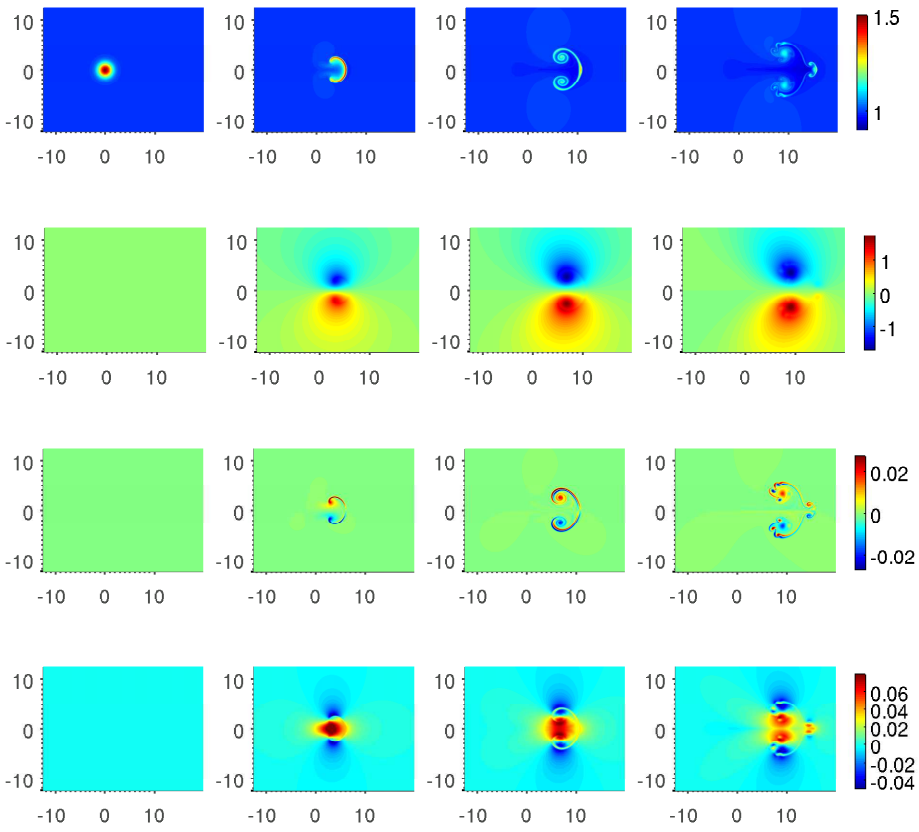

Figure 4.6: Ion temperature $\tau = 0$, initial blob width $\sigma = 10$, Rayleigh number $\mathrm{Ra} = 2.5 \times 10^5$. Spatial structure of density n (top row), electric potential ϕ(second row), vorticity $\nabla_\perp^2 \phi$ (third row) and radial $\boldsymbol{E}\times\boldsymbol{B}$-velocity v_x (bottom row). In all rows time increments $10\,\gamma^{-1}$ going from left to right. Axes are normalized with the initial blob width σ. Only a part of the simulation domain shown.

wake. Due to the smaller spatial scales when $\sigma = 2$, Fig. 4.5, dissipation and viscosity make the structure flatter and more smeared out in comparison to simulations at $\sigma = 10$, Fig. 4.6, where small scale structure evolves in all the vorticity and density fields. This can also be seen from the radial profiles

$$n_p(x,t) = \frac{1}{L_y}\int_0^{L_y} dy\,(n-1), \tag{4.74}$$

presented in Fig. 4.7. After the initial phase the density evolves into the

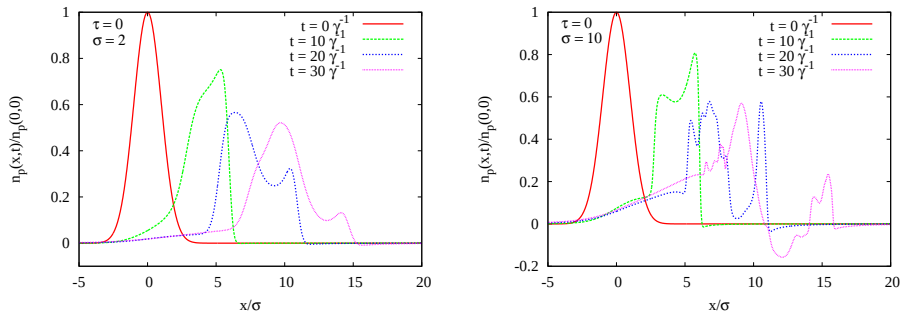

(a) (b)

Figure 4.7: Radial profiles of density n at zero ion temperature, initial widths are (a) $\sigma = 2$ and (b) $\sigma = 10$.

shape of a mushroom like cap where the tails of the cap eventually role up into two lobes. This behavior is due to poloidal gradients in the radial velocity field, advecting the the blob center ($y = 0$) faster than the blob edges. In the late evolution the leading front eventually vanish due to stretching and dissipation. As demonstrated in Ref.[41] especially the late evolution is sensible to the Rayleigh number. At higher Rayleigh numbers the lobes are unstable and the leading front can evolve into secondary plume structures. Through out the simulations the blobs are nearly symmetric around $y = 0$, which is a consequence of advecting electrons and ions by the same velocity. The spatial structure of the blob evolution at $\tau = 0$ is very similar to the results reported in Ref.[41] where a somewhat simpler model was used.

Finite ion temperature

At finite ion temperature the dynamical evolution depends no longer only on the initial blob width. As the ion temperature is finite so is the ion gyroradius. In the initial phase the characteristic scale length $k_\perp^{ini} = A/\sigma$ determines the strength of the FLR effects. At later times the influence of the FLR effects depends on the ion temperature and the initial blob width in a more complicated way. Two examples of the evolution of an

isolated blob where $\tau = 1$ are presented in Fig. 4.8 and Fig. 4.9, where the initial widths are $\sigma = 2$ and $\sigma = 10$ respectively. The corresponding Rayleigh numbers are: $\mathrm{Ra}(\sigma = 2) = 4000$ and $\mathrm{Ra}(\sigma = 10) = 0.5 \times 10^6$, and the initial length scales to ion gyroradii are: $k_\perp^{ini}\rho_i = 0.25$ for $\sigma = 2$ and $k_\perp^{ini}\rho_i = 0.05$ for $\sigma = 10$. A common feature of all finite ion temperature

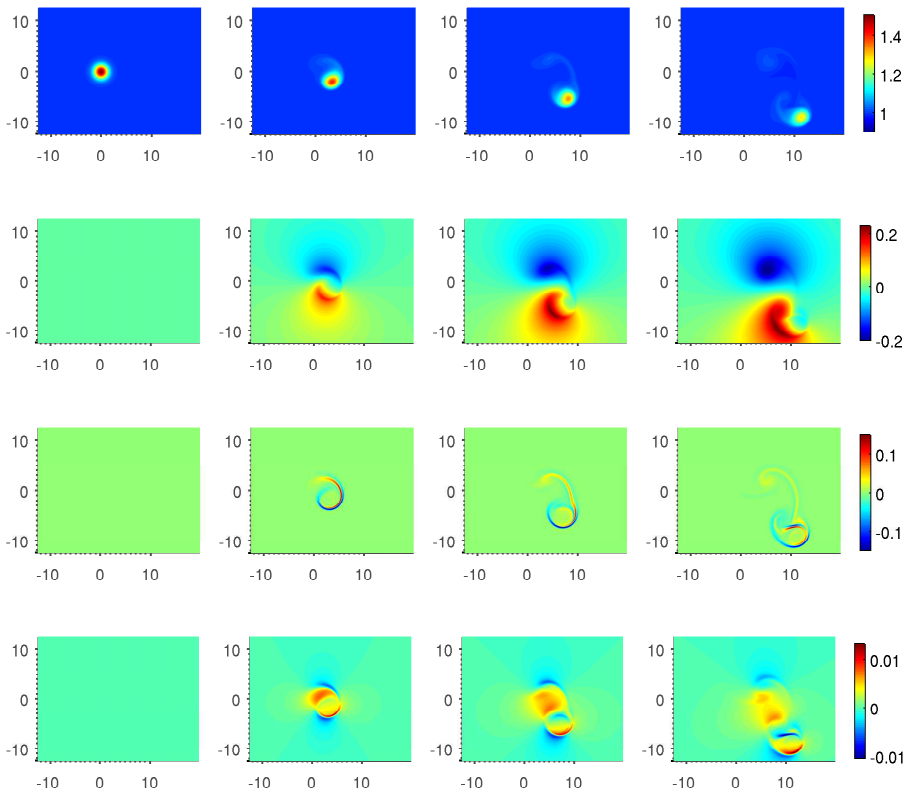

Figure 4.8: Ion temperature $\tau = 1.0$, initial blob width $\sigma = 2$, Rayleigh number $\mathrm{Ra} = 4000$. Spatial structure of density n (top row), electric potential ϕ(second row), vorticity $\nabla_\perp^2\phi$ (third row) and radial $\boldsymbol{E} \times \boldsymbol{B}$-velocity v_x (bottom row). In all rows time increments $10\,\gamma^{-1}$ going from left to right. Axes are normalized with the initial blob width σ. Only a part of the simulation domain shown.

simulations is the existence of a poloidal center of mass velocity. Contrary to the cold ion limit, no symmetry exists at $y = 0$. This is a consequence of the fundamental different gyrocenter drifts of ion and electrons. Almost independent of Rayleigh number it seems that when $k_\perp^{ini}\rho_i \gtrsim 0.05$ the FLR effects starts to play an important role. We observe that the blob structures get more compact when $k_\perp\rho_i$ is increased. Also, the formation of lobe like structures is reduced at increased $k_\perp\rho_i$. In other words, the blobs remain more blob shaped throughout the simulation when $k_\perp^{ini}\rho_i$ is increased. This

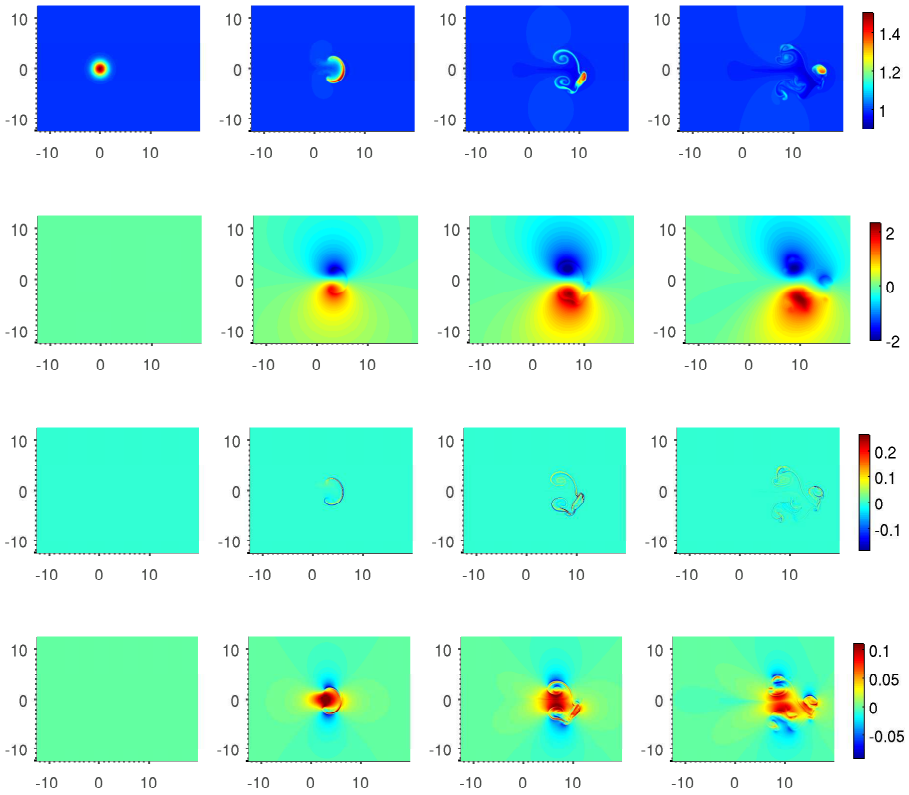

Figure 4.9: Ion temperature $\tau = 1$, initial blob width $\sigma = 10$, Rayleigh number $\mathrm{Ra} = 0.5 \times 10^6$. Spatial structure of density n (top row), electric potential ϕ(second row), vorticity $\nabla_\perp^2 \phi$ (third row) and radial $\boldsymbol{E}\times\boldsymbol{B}$-velocity v_x (bottom row). In all rows time increments $10\,\gamma^{-1}$ going from left to right. Axes are normalized with the initial blob width σ. Only a part of the simulation domain shown.

is a consequence of the FLR averaging which results in less peaked velocity profiles. Comparing the spatial structure of the velocity fields presented in Fig. 4.6 and Fig. 4.9, where $\tau = 0$ and $\tau = 1$ respectively, show that the radial velocities are much higher in the $\tau = 0$ case, even though the available ion free energy is three times smaller. The flatter velocity profile at finite ion temperature prevents the blob from getting sheared apart and results in an increased radial blob transport. When $k_\perp^{ini}\rho_i$ is relatively small ~ 0.05 the blob evolution in the initial phase, see Fig. 4.9, is similar to the corresponding cold ion evolution, see Fig. 4.6, but is not symmetric around $y = 0$ and has a more compact front and less density in the lobes. These effects can be ascribed to the formation of thin finger like vorticity structures in the vicinity of the blob front. The finger structures act as to smear out steep density and vorticity gradients. The amplitude of these finger structures in the vorticity field is stronger than the dipole structure generated by the interchange drive. The interchange vorticity dipole still exists as can be seen from the spatial structure of the electrical field (second row in Fig. 4.6) and the fact that the blob is advected radially outwards. In the vicinity of strong density gradients the vorticity is advected along the contour lines of density n, which is in agreement with the analytical discussion in section 4.4.1. In the later phase the structure size is smaller which make the FLR effects even more important. Therefore, the FLR effects gradually make the blob more compact and prevent the blob from leaving density behind and forming lobes.

At increased $k_\perp^{ini}\rho_i$ we observe that the dynamical evolution is altered dramatically. The simulation shown on Fig. 4.8 has a low Rayleigh number, $\mathrm{Ra}(\sigma = 2) = 4000$, but as $k_\perp^{ini}\rho_i = 0.25$, the FLR effects are strongly influencing the dynamics. The vorticity field is dominated by thin fingers circumferencing the density blob, which strongly reduce the amount of density leaving the advected blob structure. The increased blob coherence at increased $k_\perp^{ini}\rho_i = 0.25$ is also clearly found in the corresponding radial density profiles shown in Fig. 4.10. The radial profiles and the contour plots also show that the maximal density amplitude travels a shorter distance at increased $k_\perp^{ini}\rho_i$, but retains a high amplitude through out the simulation. The spatial position of the maximal density amplitude coincides with the blob structure except in some of the cold ion simulations where the maximal amplitude in the later phase is located in the rolled up lobes. The observation that increased $k_\perp^{ini}\rho_i$ implies higher blob amplitudes that travel shorter distances is not a simple result of Rayleigh number variation.

Fig. 4.11 show a simulation where $\tau = 7$ and $\sigma = 5$. With this choice of parameters the blob has the same Rayleigh number as the blob simulation shown on Fig. 4.6 where $\tau = 0$ and $\sigma = 10$. Comparing these simulations show that the FLR effects have a huge impact on the blob dynamics, ruling out that the differences are solely due to Rayleigh number variations.

The ratio of thermal ion gyroradius to the initial characteristic length

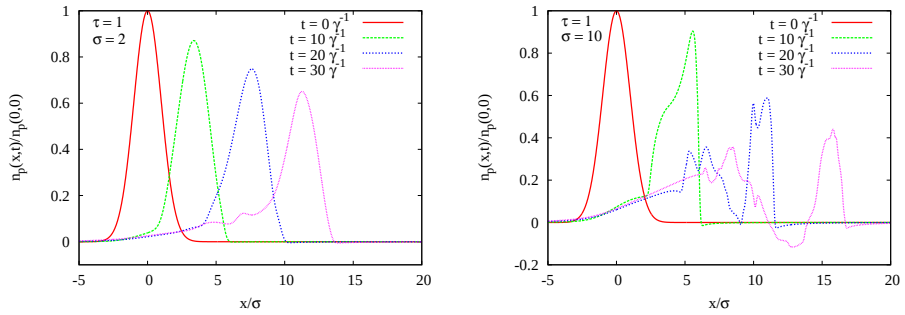

(a) (b)

Figure 4.10: Radial density profiles $n_p(x,t)$ for different ion temperatures at four different times.

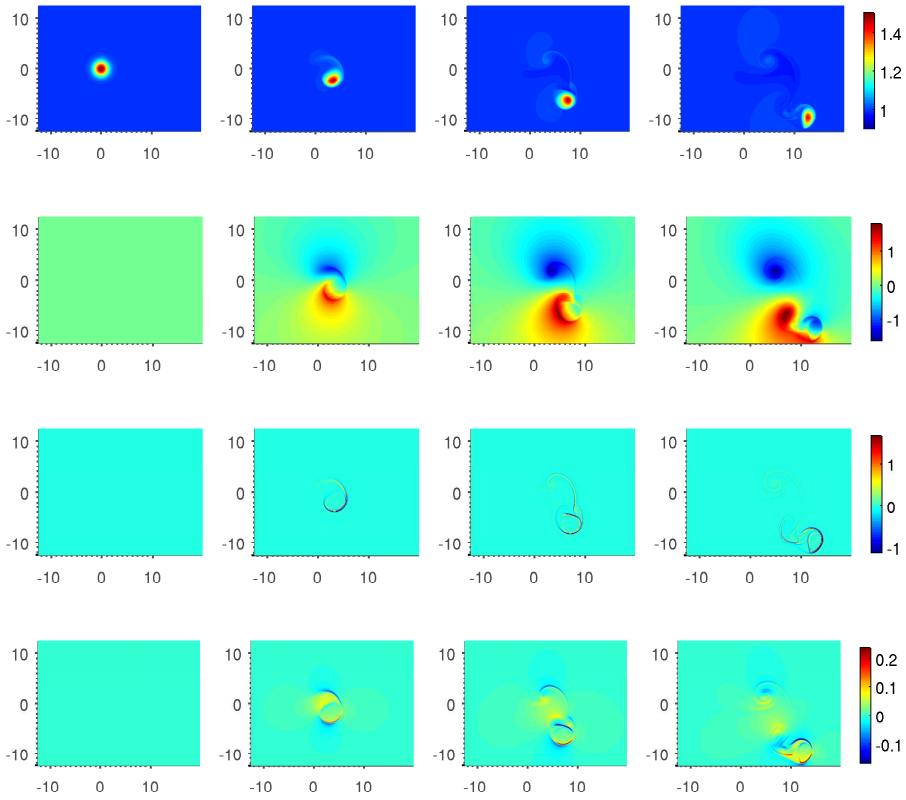

Figure 4.11: Ion temperature $\tau = 7$, initial blob width $\sigma = 5$, Rayleigh number $\mathrm{Ra} = 2.5 \times 10^5$. Spatial structure of density n (top row), electric potential ϕ(second row), vorticity $\nabla_\perp^2 \phi$ (third row) and radial $\boldsymbol{E}\times\boldsymbol{B}$-velocity v_x (bottom row). In all rows time increments $10\,\gamma^{-1}$ going from left to right. Axes are normalized with the initial blob width σ.

scale of the simulation shown in Fig. 4.11 is $k_{\perp}^{ini}\rho_i \simeq 0.26$, which is nearly identical to the corresponding ratio $k_{\perp}^{ini}\rho_i \simeq 0.25$, of the simulation shown in Fig. 4.8. The blob evolutions in these simulations are similar even though the corresponding Rayleigh numbers are significantly different, $\mathrm{Ra} = 2.5 \times 10^5$ and $\mathrm{Ra} = 4000$ respectively. Comparing the radial profiles, Fig. 4.10(a) and Fig. 4.12 , show that the blobs almost retain the initial shape and leave

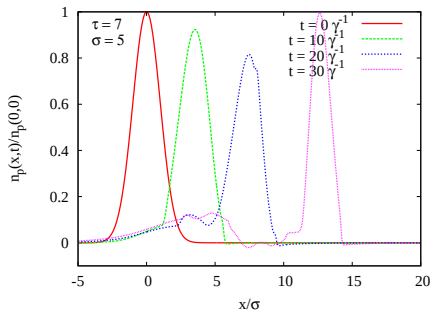

Figure 4.12: Radial density profiles $n_p(x,t)$ for $\tau = 7.0$ and initial width $\sigma = 5$.

almost no density behind. In Ref. [41] it was shown that when the Rayleigh number exceeds $\sim 10^4$, the dynamics enter an ideal regime where the radial flux is no longer influenced by Rayleigh number variations. A similar mechanism might explain the signatures of Rayleigh number invariance found in these simulations. We will return to this issue later.

4.5.2 Blob transport

Having presented an overview of the blob dynamics in the parameter range investigated in this chapter, we are now going quantify these observation. We will investigate the influence of ion temperature and initial blob width using the following measures. (1) The center of mass position and the corresponding velocity which are related to the total advective transport. The center of mass does not coincide with the position of the blob. (2) Instead, the maximal density amplitude is a good measure of the blob position. Therefore, we investigate the parametric dependence of the maximal amplitude as a function of time and the corresponding distance traveled by the blob. (3) The maximal amplitude does not express the density, and eventually thermal energy, carried by the blob. We measure the blob density transport and the blob compactness by following the integrated density in the vicinity of the blob center, defined as the position of the maximal density amplitude.

Center of mass The time evolution of the radial center of mass position is presented in Fig. 4.13 for blobs with different initial widths. First obser-

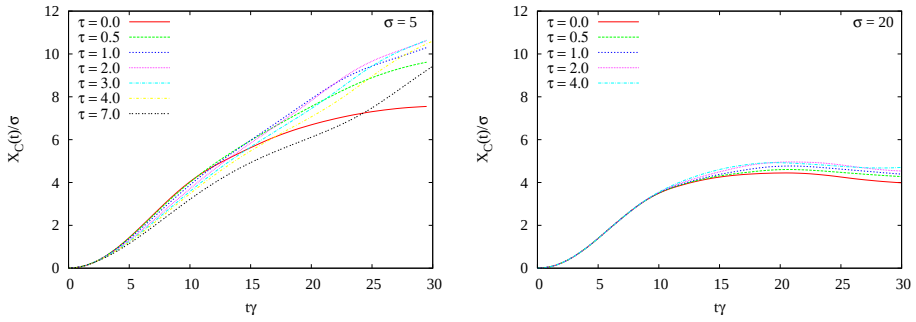

(a) (b)

Figure 4.13: Evolution of the radial center of mass position for different ion temperatures for blobs with initial width (a) $\sigma = 5$ and (b) $\sigma = 20$

vation made is that the center of mass of small blobs travel longer than the center of mass of big blobs, measured in initial blob widths. Secondly, at fixed initial blob width an increased ion temperature makes the blob travel longer. When $k_{\perp}^{ini}\rho_i \gtrsim 0.1 - 0.2$ the picture gets a little blurred. Taking a closer look at Fig. 4.13(a) reveal that at $\tau = 7.0$, which corresponds to $k_{\perp}^{ini}\rho_i \simeq 0.26$ the radial center of mass has traveled the shortest distance when $t < 25$ but catches up afterwards. This behavior is caused by the ion FLR effects. When the FLR effects strongly influence the dynamics the magnitude of the poloidal component of the advecting $\boldsymbol{E} \times \boldsymbol{B}$-drift gets comparable to the radial velocity component. Fig. 4.14 shows that the blobs

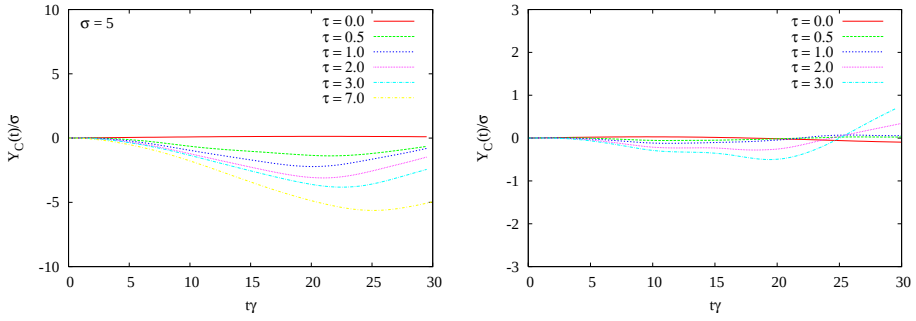

(a) (b)

Figure 4.14: Evolution of the poloidal center of mass position for different ion temperatures for blobs with initial width (a) $\sigma = 5$ and (b) $\sigma = 20$

have a significant poloidal center of mass velocity when $k_{\perp}^{ini}\rho_i \gtrsim 0.1 - 0.2$. We also observe that the poloidal center of mass position over time oscillates around $y = 0$, but the initial poloidal drift is always downwards.

In the initial phase a good scaling parameter of the radial distance traveled by the center of mass is $k_{\perp}^{ini}\rho_i$, which is demonstrated in Fig. 4.15(a).

At later times $t = 30\,\gamma^{-1}$, see Fig. 4.15(b), the high Rayleigh number blobs,

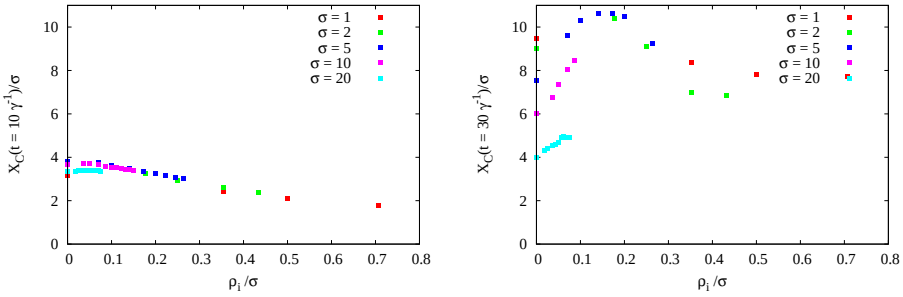

(a) (b)

Figure 4.15: Radial center of mass position at two different times as a function of $k_{\perp}^{ini}\rho_i$.

width $\sigma = 10, 20$, starts to deviate. Due to the high Rayleigh numbers and high advection velocities, big blobs are sheared apart leaving significant amounts of density behind. Fig.4.16 show the center of mass position as a function of Rayleigh number at $t = 30\,\gamma^{-1}$, clearly showing that the radial distance traveled by the center of mass decrease at high Rayleigh numbers.

In Ref. [41] using a simplified interchange model it was shown that when $\mathrm{Ra} \gtrsim 10^4$ the maximal center of mass velocity becomes Rayleigh number independent. In the gyrofluid model this ideal regime has not been found as shown in Fig. 4.17. Not even in the cold ion limit the result of Ref. [41] is reproduced. Apparently, retaining the compressional terms in the continuity equation (4.54a) must account for the differences in the scaling. It is also clear that at increased ion temperature the maximal center of mass velocity decrease. At increased ion temperature the radial center of mass velocity, shown in Fig.4.18, and acceleration get less peaked which is a consequence of the more coherent blobs at finite ion temperature. It is therefore no

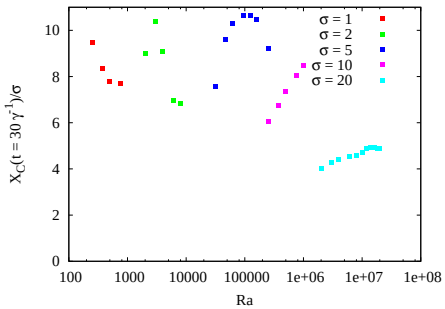

Figure 4.16: Center of mass position as a function of Rayleigh number at time $t = 30\,\gamma^{-1}$

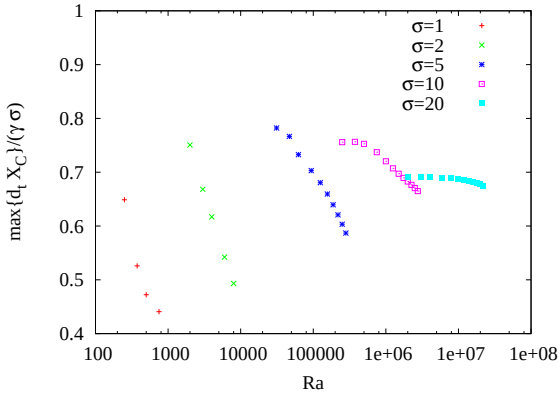

Figure 4.17: Maximal radial center of mass velocity as a function Rayleigh number.

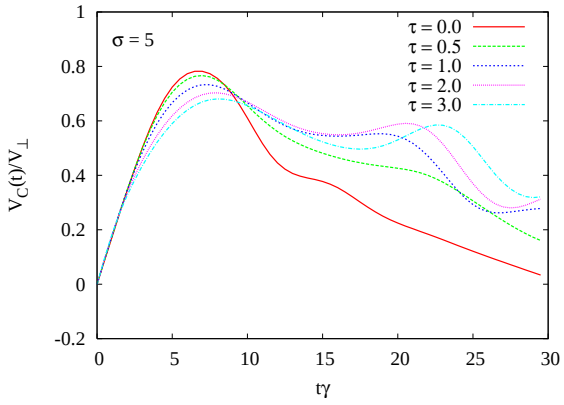

Figure 4.18: Radial center of mass velocity as a function of time for blobs with initial width $\sigma = 5$.

surprise that the maximal radial center of mass velocity depends on $k_\perp^{ini}\rho_i$ at finite ion temperature as depicted in Fig. 4.19 which demonstrate a decrease

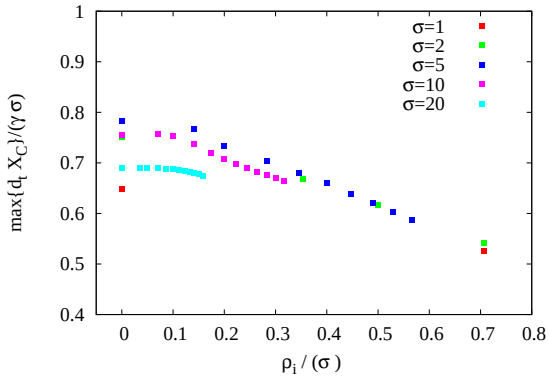

Figure 4.19: Maximal radial center of mass velocity as a function of the ratio of the thermal ion gyroradius ρ_{ith} to the initial blob width.

in the maximal center of mass velocity when $k_\perp^{ini}\rho_i$ increase which is in good agreement with the smeared out velocity field at finite ion temperature facilitated by the FLR averaging operators.

$X_{n_{max}}$ The center of mass position does not coincide with the blob. A better measure of the blob position is the position of the maximal density amplitude $X_{n_{max}}$. We observe that the blobs travel further at increased Rayleigh number Fig. 4.20(b) but travel shorter distances at increased $k_\perp^{ini}\rho_i$ as shown in Fig. 4.20(a). Big blobs are advected further than smaller blobs

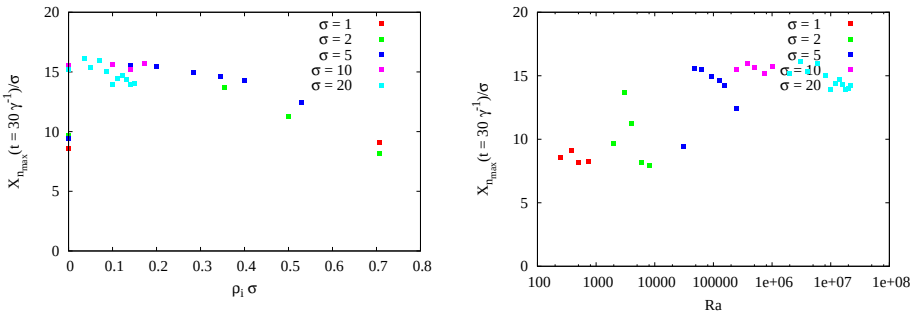

(a) (b)

Figure 4.20: Position of the maximal density amplitude at $t = 30\,\gamma^{-1}$ as a function of time at (a) ρ_i/σ and (b) Rayleigh number.

and increased ion temperature make the blobs travel shorter, all measured in units of the initial blob width. However, when Ra $\gtrsim 10^4$ the varitions are

no bigger than 20 %. Only in the cold ion limit these observations do not hold. In the special case of cold ions the distance traveled simply increase when the Rayleigh number is increased.

n_{max} In Fig. 4.21 we present the temporal evolution of the maximal amplitude n_{max} for different ion temperatures and initial widths. The amplitude

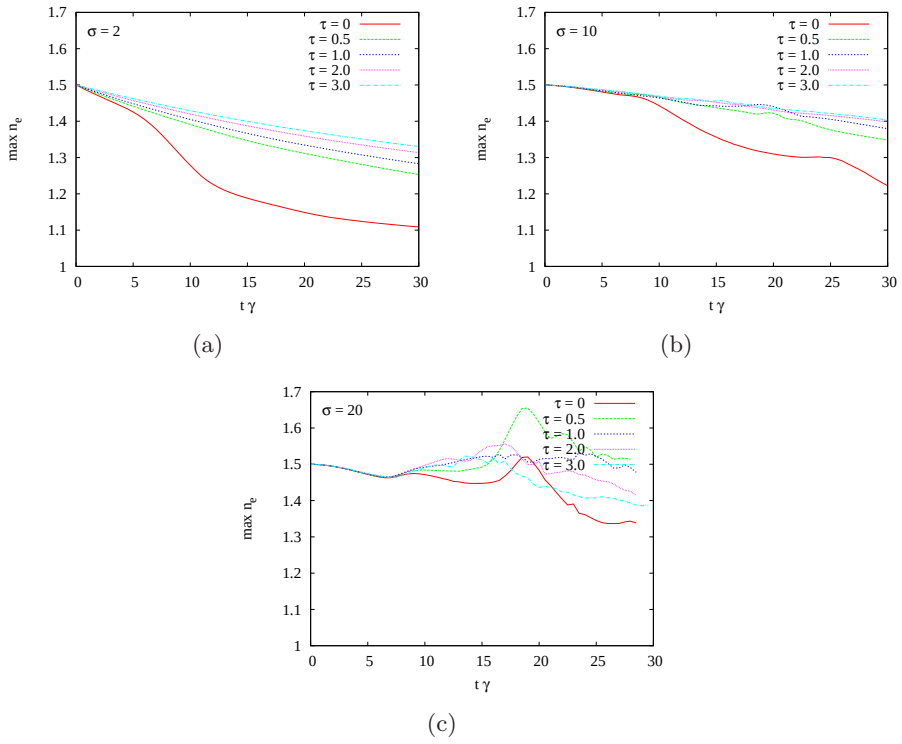

Figure 4.21: Maximal density amplitude as a function of time for different initial widths.

decay is due to dissipation and advection. Due to dissipation the amplitude decays faster for small blobs. Clearly, FLR effects has an important influence on the amplitude decay. When $\tau = 0$ the amplitude decrease faster except for very high Rayleigh numbers. As observed in Fig. 4.21(c) the violent blob evolution at high Rayleigh numbers even allows the maximal amplitude to exceed the initial amplitude. This is due to the high radial velocities lacking behind the position of the maximal amplitude. The observations are nicely summarized in Fig. 4.22. In the initial phase, Fig. 4.22(a), the amplitude decay is almost solely determined by dissipation and therefore the initial scale length σ. At Ra $\gtrsim 10^4$ the the amplitude decay seems to be independent of Rayleigh number, whereas in the later phase, Fig. 4.22(b) , where smaller scales are accessed the amplitude decay mainly depends on ion temperature.

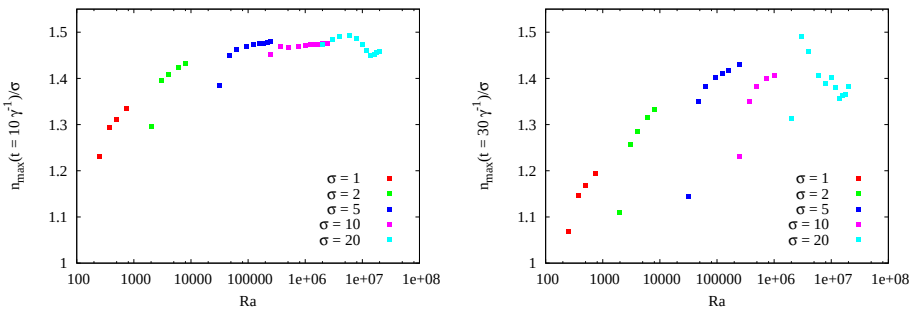

(a) (b)

Figure 4.22: Maximal density amplitude as a function of Rayleigh number at two different times (a) $t = 10\,\gamma^{-1}$ and (b) $t = 30\,\gamma^{-1}$.

The FLR effects prevent the blob from being sheared apart which eventually results in a slower amplitude decay.

Blob compactness From the evolution of maximal amplitude and center of mass alone we are not able to determine the density, and therefore thermal energy, carried by the blob. Therefore, we introduce the following quantity

$$I_C(t) = \frac{\int d\boldsymbol{x}\,(n-1)h}{\int d\boldsymbol{x}\,h n_{\text{init}}} \tag{4.75}$$

where

$$n_{\text{init}}(\boldsymbol{x}) = A \exp\left(\frac{-(\boldsymbol{x} - \boldsymbol{X}_{n_{max}})^2}{2\sigma^2}\right) \tag{4.76}$$

denotes the initial blob structure at position the position of the maximal density amplitude $\boldsymbol{X}_{n_{max}}$. h is a Heaviside function

$$h(\boldsymbol{x}) = \begin{cases} 0 & \text{if } (x - x_{\max})^2 + (y - y_{\max})^2 \geqq \sigma^2 \\ 1 & \text{if } (x - x_{\max})^2 + (y - y_{\max})^2 < \sigma^2, \end{cases} \tag{4.77}$$

centered at $\boldsymbol{X}_{n_{max}}$ having the width of the blob at $t = 0$. I_C integrate density in a ball of radius σ centered at $\boldsymbol{X}_{n_{max}}$ and is normalized such that $I_C(t = 0) = 1$. Imagine a situation where the initial blob is simply translated with no amplitude decay, I_C remains constant $I_C = 1$. Whereas if the blob is totally dissipated $I_C \to 0$.

Fig. 4.23(a) shows the time evolution of I_C at $\tau = 0$ for different initial blob widths. When the ions are cold the initial blob width has no big influence on the compactness. Only, the high Rayleigh number blob, $\sigma = 20$, has a significant lower compactness at $t = 30\,\gamma^{-1}$. At high Rayleigh numbers the

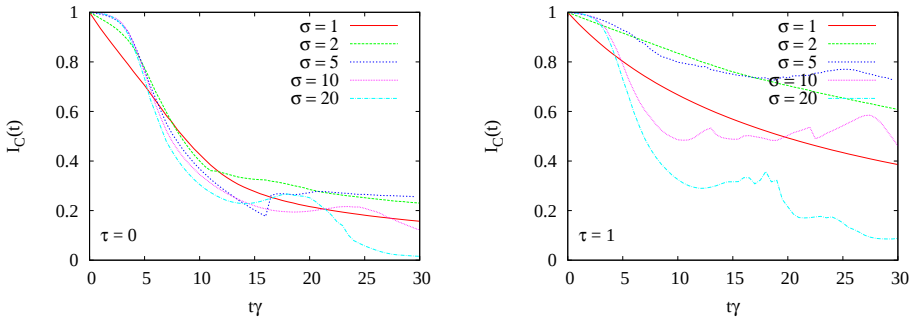

(a) (b)

Figure 4.23: I_C as a function of time for different initial blob widths σ at (a) $\tau = 0$ and (b) $\tau = 1$.

blob center is advected much faster than the blob "sides". The blob is therefore sheared in to many disconnected structures. When the ion temperature is finite the evolution of I_C is changed. The time evolution of I_C is presented in Fig. 4.23(b) for $\tau = 1$, demonstrating that when the initial blob width is increased, the blobs remain more compact and carry more density as they move radially outwards. The compactness of the blob increases when the initial blob width is decreased for medium, high Rayleigh number whereas the smaller blobs, $\sigma = 1, 2$, get less compact at decrease initial blob width due to the increased influence of dissipation. Fig. 4.24 show the time evolution of I_C at fixed initial blob width for different ion temperatures showing that the time evolution of I_C depends on the ratio of the thermal ion gyroradius to the initial length scale. As discussed in Sec.4.4.1 the FLR effects

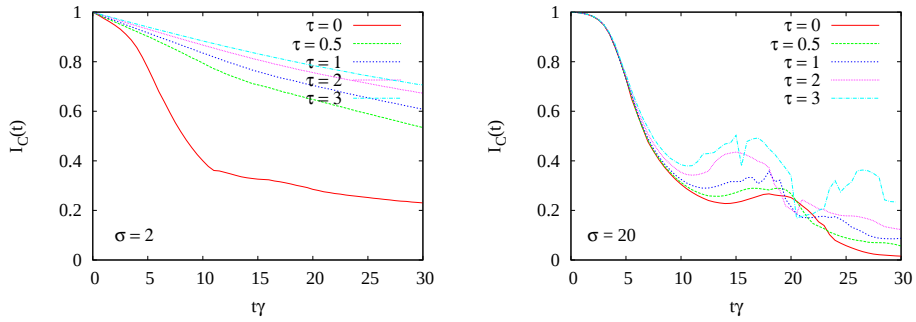

(a) (b)

Figure 4.24: I_C as a function of time for different ion temperatures for initial blob width (a) $\sigma = 2$ and (b) $\sigma = 20$.

mix vorticity at the blob center and edge which smear out the velocity field preventing the blob from being sheared and stretched apart. In Fig. 4.25,

we present the variation of I_C as a function of ρ_i/σ at two different times. In the medium and high Rayleigh number range, $\sigma = 5, 10, 20$, the blob

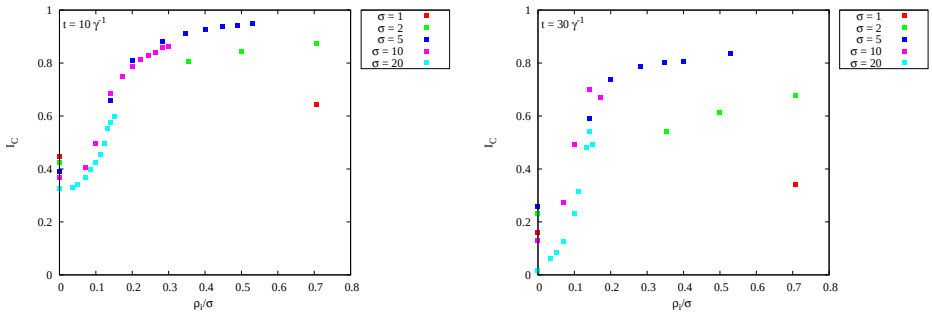

(a) (b)

Figure 4.25: I_C as a function of ρ_i/σ at two different times (a) $t = 10\,\gamma^{-1}$ and (b) $t = 30\,\gamma^{-1}$.

compactness seems to be independent of Rayleigh number variations in the initial phase, see Fig. 4.25(a). At all times a transition seems to appear when $\rho_i/\sigma \gtrsim 0.1$, where the blobs get significantly more compact. Above this limit the compactness seems nearly constant for the parameter range investigated here. Last, we observe that the compactness of relatively small blobs $\sigma = 2$ also benefit from the FLR effects. At $\tau = 1$ these small blobs triple the density carried by the blob.

4.6 Discussion

In the framework of the simple gyrofluid model the numerical simulations show that finite ion temperature has a strong impact on the dynamics of isolated blob structures. Finite ion temperature makes the blobs travel further, faster and makes the blobs carry more density along. There are however significant variations in the dynamical evolution which mainly depend on the ratio of the ion gyroradius to the initial blob width. We found that the total flux peaks when $\rho_i/\sigma \sim 0.1 - 0.2$, see Fig. 4.15(b). When Ra $\gtrsim 10^4$ measured in the initial blob width we also observed that the blobs travel almost the same distance, see Fig. 4.20(b), but the amount of plasma carried in the blobs changes drastically when $\rho_i/\sigma \gtrsim 0.1$. Below this critical value the blobs have almost lost all their initial density after having travelled 15 times their own initial width. Above this value the blobs carry $\sim 80\,\%$ of their initial density, see Fig. 4.25(b). If this threshold prevails in a more general setting where blobs are selfconsistently generated this would imply that a prefered blob size exists depending on the local ion temperature.

Experimental SOL temperature measurements report that $\tau \sim 1 - 10$[1,

104, 95, 97], but there seems to be no clear trend of whether τ increase or decrease going from the separatrix to the wall. If the treshold prevails one should expect to observe an increased average blob size at increased ion temperature. If that is the case one could try to reduce transport by lowering τ in the SOL region.

Finally, we observed that very high Rayleigh number blobs $\mathrm{Ra} \gtrsim 10^7$ are sheared apart due to strong gradient in the $\boldsymbol{E} \times \boldsymbol{B}$-velocity field unless τ is very high. This observation could be relevant in the process of understanding edge localized mode (ELM) filaments[83, 56]. The size in the perpendicular plane is in the range of $\sim 1-5\,\mathrm{cm}$ which in terms of the physical parameters on which the numerical simulations are based corresponds to $\sim 10-100\,\rho_\mathrm{s}$. Without FLR effects these blobs would not survive for long. This might indicate that the ion temperature in ELMs is much higher than the ion temperature of ordinary blobs.

4.7 Summary and future directions

An electrostatic, isothermal gyrofluid model has been derived. Collisional dissipation and viscosity has been added to the inherently collisionless gyrofluid model. This is not trivial because ion gyrocenter density describes ion density and polarizaton density. The collisional dissipation added to the ion gyrocenter equation takes a form which does not generate artificial polarization and allows for independent variations of collisional viscosity and dissipation. In the long wavelength limit the dissipation and viscosity terms resemble the corresponding terms in the finite ion temperature drift fluid equations. An analysis of the most important FLR terms in the model when $k_\perp \rho_i < 1$ has been carried out showing that the FLR correction acts as to redistribute the $\boldsymbol{E} \times \boldsymbol{B}$-vorticity leading to less peaked $\boldsymbol{E} \times \boldsymbol{B}$-velocity profiles.

Numerical simulations of isolated blob structures in the plane perpendicular to the magnetic field, where the parallel dynamics has been neglected, have been presented. A parameter scan of initial blob width and ion temperature show that finite ion temperature has a strong influence on the blob dynamics. The finite ion temperature blobs gets a spatial density structure which resembles experimental observation. This is not the case in the cold ion approximation. Finite ion temperature makes the blobs travel faster and further. To lowest order the blob speed is proportional to the cold ion soundspeed times the square root of the blob width times the squareroot of $(1+\tau)$. We observe that the maximal advective radial flux is found when $\rho_i/\sigma \sim 0.1-0.2$. We find that an increased Rayleigh number and decreased ρ_i/σ imply that blobs travel longer distances but that the variations are small when $\mathrm{Ra} \gtrsim 10^4$. The simulations also show that the decay of the blob amplitude is slower at increased ion temperature but again we find that vari-

ations are small when Ra $\gtrsim 10^4$. The most significant effects of finite ion temperature to the blob dynamics is a decreased loss of density as the blob moves radially outwards. When Ra $\gtrsim 10^4$ a threshold exist at $\rho_i/\sigma \gtrsim 0.1$ where we observe that the blob contains 5-10 times more density above the threshold than below. We also observe that small blobs Ra $< 10^4$ loose their density due to dissipation. Therefore, this threshold might imply that there exists a preferable blob size depending on the local ion temperature. Finally, the simulations show that bigger blobs Ra $\gtrsim 10^7$ are sheared apart by strong gradients in the velocity field.

4.7.1 Future directions

As a first step a parameter scan of blob amplitude should be carried out. Initially, this scan should be carried out using the model employd here, but eventually a nonlinearized model should be used. A natural extension of the work presented in this chapter is to employ a more complete gyrofluid model which accounts for the dynamical evolution of higher order gyrofluid moments, the parallel dynamics, sheath dissipation, neutrals, selfconsistent dissipation and viscosity coefficients and geometrical effects. The blobs are generated and advected in regions with strong pressure gradients. Therefore, one should investigate the blob dynamics in selfsustained turbulence. Investigations in a 2D slab setup which resembles the ESEL code[44] is ongoing.

We found that the ideal interchange rate provides a good time and velocity normalization, but it does not catch the details of the FLR effects. A more precise velocity scaling could possibly be obtained by applying an iterative procedure to the vorticity equation which would give corrections to the ideal interchange rate by balancing the FLR corrections appearing in the long wavelength limit vorticity equation. Analytic work in this direction is ongoing and give corrections to the ideal interchange rate which are $\propto \sqrt{T_i/\sigma^2}$.

The collisional dissipation and viscosity were added to the gyrofluid model in an ad hoc fashion. As a next step one should calculate the gyrofluid moment of the guidingcenter Landau collision operator derived by Brizard[17]. This task has been looked into and prelimnary investigations show that the same terms as the one added in this chapter would appear to lowest order.

Chapter 5

Conclusion

In this work two different extensions of the dynamical reduced Vlasov-Maxwell equations have been presented. An extension of the existing gyrokinetic theory to include time variations in the strong background electric field is presented (see Chap. 3). The derivation is based on a generalized gyrokinetic ordering by Hahm[48], which is relevant for edge turbulence in magnetically confined fusion plasmas. The results are shown in two versions of gyrokinetics (Hamiltonian and symplectic). From a variational principle fully electromagnetic Vlasov-Maxwell equations are derived, including a second Poisson equation associated with the background electric field, and the corresponding local energy theorem is derived explicitly. Taking terms quadratic in the fluctuation amplitude in the long wave length (drift kinetic) limit, we obtain equations that are numerically tractable. Several new terms are identified of which we emphasize the intrinsic magnetization current in the parallel Ampere equation and the polarization current which ensures conservation of polarization charge. A disadvantage of the gyrokinetic formalism is that in order not to include full finite Larmor radius effects effects the electromagnetic fields must be divided into high amplitude long wavelength and fluctuating short wavelength parts. This splitting makes simultaneous self-consistent solutions to both parts difficult (perhaps impossible).

As an alternative, second order guiding-center coordinates are derived using the phasespace Lie transform method, and the corresponding Vlasov-Maxwell equations are derived using a variational principle (see Chap. 2). In the guiding-center ordering strong $\boldsymbol{E} \times \boldsymbol{B}$-flows comparable to the thermal velocity are allowed, and the second order terms in the guiding-center Vlasov-Maxwell equations describe the lowest order finite Larmor radius corrections to the electromagnetic field. Therefore, second order Vlasov-Maxwell equations could be relevant for edge plasmas.

Finally, numerical simulations of the radial transport of isolated plasmas filaments in the scrape-off layer region are presented (see Chap. 4). A simple

two-dimensional gyrofluid model is employed and an appropriate collision operator is derived. The numerical simulations show that the transport strongly depends on the ratio of the thermal ion gyroradius to the size of the filament. When the ratio exceeds $\sim 0.1 - 0.2$ the transport is enhanced. Blobs having radillay travelled their own initial size ~ 15 times carry $\sim 80\,\%$ of their initial density above this threshold but only $\sim 20\,\%$ below.

Bibliography

[1] Adamek, Kocan, Panek, Gunn, Martines, Stockel, Ionita, Popa, Costin, Brotankova, Schrittwieser, and Van Oost. Simultaneous measurements of ion temperature by segmented tunnel and katsumata probe. *Contributions to Plasma Physics*, 48(5-7):395–399, 2008.

[2] H. Alfvén. On the motion of a charged particle in a magnetic field arkiv mat. astr. fysik, band 27 a, no. 22. *Arkiv Mat. Astr. Fysik*, 27 A(22):1, 1940.

[3] Y. Andrew, N. C. Hawkes, T. Biewer, K. Crombe, D. Keeling, E. de la Luna, C. Giroud, A. Korotkov, A. Meigs, A. Murari, I. Nunes, R. Sartori, T. Tala, and JET-EFDA Contributors. Evolution of the radial electric field in a jet h-mode plasma. *EPL (Europhysics Letters)*, 83(1):15003, 2008.

[4] G. Y. Antar, S. I. Krasheninnikov, P. Devynck, R. P. Doerner, E. M. Hollmann, J. A. Boedo, S. C. Luckhardt, and R. W. Conn. Experimental evidence of intermittent convection in the edge of magnetic confinement devices. *Phys. Rev. Lett.*, 87(6):065001, Jul 2001.

[5] R. Balescu. *Transport processes in plasmas vol. 1.* North-Holland, 1988.

[6] R. Balescu. *Transport processes in plasmas vol. 2.* North-Holland, 1988.

[7] Alfredo Baños. The guiding centre approximation in lowest order. *Journal of Plasma Physics*, 1(03):305–316, 1967.

[8] Paul M. Bellan. *Fundamentals of plasma physics.* Cambridge University Press, 1 edition, 2006.

[9] E. V. Belova. Nonlinear gyroviscous force in a collisionless plasma. *Phys. Plasmas*, 8(9):3936, 2001.

[10] N. Bian, S. Benkadda, J.-V. Paulsen, and O. E. Garcia. Blobs and front propagation in the scrape-off layer of magnetic confinement devices. *Physics of Plasmas*, 10(3):671–676, 2003.

[11] J. A. Boedo, D. Rudakov, and R. Moyer et al. *Phys. Plasmas*, 8:4626, 2001.

[12] J. A. Boedo, D. Rudakov, R. Moyer, S. Krasheninnikov, D. Whyte, G. McKee, G. Tynan, M. Schaffer, P. Stangeby, P. West, S. Allen, T. Evans, R. Fonck, E. Hollmann, A. Leonard, A. Mahdavi, G. Porter, M. Tillack, and G. Antar. Transport by intermittent convection in the boundary of the diii-d tokamak. *Physics of Plasmas*, 8(11):4826–4833, 2001.

[13] B. M. Boghosian. *Covariant Lagrangian Methods of Relativistic Plasma Theory.* PhD thesis, UNIVERSITY OF CALIFORNIA, DAVIS., 1987.

[14] Braginskii. Transport processes in a plasma. *Reviews of plasma physics*, Vol. 1, 1965.

[15] A. Brizard. Nonlinear gyrokinetic Maxwell-Vlasov equations using magnetic co-ordinates. *J. Plasma Physics*, 41:541–559, 1989.

[16] A. Brizard. Nonlinear gyrofluid description of turbulent magnetized plasmas. *Phys. Fluids B*, 4:1213, 1992.

[17] A. Brizard. A guiding-center fokker planck collision operator for nonuniform magnetic fields. *Phys. Plasmas*, 11(9):4429, 2004.

[18] A. J. Brizard. On the dynamical reduction of the Vlasov equation. *Communications in Nonlinear Science and Numerical Simulations*, 13:24–33, February 2008.

[19] A.J. Brizard and T.S. Hahm. Foundations of nonlinear gyrokinetic theory. *Reviews of modern physics*, 79:421–468, 2007.

[20] Alain J. Brizard. Nonlinear gyrokinetic Vlasov equation for toroidally rotating axisymmetric tokamaks. *Phys. Plasmas*, 2:459, 1995.

[21] Alain J. Brizard. Variational principle for nonlinear gyrokinetic Vlasov–Maxwell equations. *Physics of Plasmas*, 7(12):4816–4822, 2000.

[22] S. Brunner, M. Fivaz, T. M. Tran, and J. Vaclavik. Global approach to the spectral problem of microinstabilities in tokamak plasmas using a gyrokinetic model. *Physics of Plasmas*, 5(11):3929–3949, 1998.

[23] K. H. Burrell, E. J. Doyle, P. Gohil, R. J. Groebner, J. Kim, R. J. La Haye, L. L. Lao, R. A. Moyer, T. H. Osborne, W. A. Peebles, C. L. Rettig, T. H. Rhodes, and D. M. Thomas. Role of the radial electric field in the transition from l (low) mode to h (high) mode to vh (very

high) mode in the DIII-D tokamak. *Physics of Plasmas*, 1(5):1536–1544, 1994.

[24] Cary and Littlejohn. Noncanonical Hamiltonian mechanics and its application to magnetic field line flow. *Annals of Physics*, 151:1–34, 1983.

[25] John R. Cary. Lie transform perturbation theory for hamiltonian systems. *Physics Reports*, 79(2):129–159, 1981.

[26] H. Cendra, D. D. Holm, M. J. W. Hoyle, and J. E. Marsden. The Maxwell-Vlasov equations in Euler-Poincaré form. *Journal of Mathematical Physics*, 39:3138–3157, June 1998.

[27] Z. Chang and J. D. Callen. Generalized gyroviscous force and its effect on the momentum balance equation. *Phys. Fluids B.*, 4:1766, 1992.

[28] Dario Correa-Restrepo and Dieter Pfirsch. The electromagnetic gauge in the variational formulation of kinetic and other theories. *Journal of Plasma Physics*, 71, part 4:503–517, 2005.

[29] J.C. Cummings. PhD thesis, Princeton University, 1995.

[30] A. Deprit. Canonical transformations depending on a small parameter. *Celestial Mechanics*, 1:12–30, March 1969.

[31] R. L. Dewar. A Lagrangian theory for nonlinear wave packets in a collisionless plasma. *Journal of Plasma Physics*, 7:267–284, 1972.

[32] R. L. Dewar. Energy-momentum tensors for dispersive electromagnetic waves. *Australian Journal of Physics*, 30:533–+, November 1977.

[33] Andris M. Dimits. Gyrokinetic equations in an extended ordering. *Physics of Plasmas*, 17(5):055901, 2010.

[34] W. Dorland and G. W. Hammett. Gyrofluid turbulence models with kinetic effects. *Phys. Fluids B*, 5(3):812, 1993.

[35] Alex J. Dragt and John M. Finn. Lie series and invariant functions for analytic symplectic maps. *Journal of Mathematical Physics*, 17(12):2215–2227, 1976.

[36] Daniel H.E. Dubin et al. Nonlinear gyrokinetic equations. *Phys. Fluids*, 26(12):3524, 1983.

[37] A. Zeiler et al. Nonlinear reduced braginskii equations with ion thermal dynamics in toroidal plasma. *Phys. Plasmas*, 4:2134, 1997.

[38] R. J. Fonck, G. Cosby, R. D. Durst, S. F. Paul, N. Bretz, S. Scott, E. Synakowski, and G. Taylor. Long-wavelength density turbulence in the tftr tokamak. *Phys. Rev. Lett.*, 70(24):3736–3739, Jun 1993.

[39] Theodore Frankel. *The geometry of physics*. Cambridge University Press, 2003.

[40] E. A. Friemann and L. Chen. Nonlinear gyrokinetic equations for low-frequency electromagnetic waves in general plasma equilibria. *Physics of Fluids*, 25:502, 1982.

[41] O. E. Garcia, N. H. Bian, and W. Fundamenski. Radial interchange motions of plasma filaments. *Phys. Plasmas*, 13:82309, 2006.

[42] O E Garcia, N H Bian, V Naulin, A H Nielsen, and J Juul Rasmussen. *Phys. Scr.*, T122:104–124, 2006.

[43] O.E. Garcia, N. H. Bian, V. Naulin, A. H. Nielsen, and J. Juul Rasmussen. Mechanism and scaling for convection of isolated structures in nonuniformly magnetized plasmas. *Phys. Plasmas*, 12:90701, 2005.

[44] O.E. Garcia, V. Naulin, A. H. Nielsen, and J. Juul Rasmussen. Turbulence and intermittent transport at the boundary of magnetized plasmas. *Phys. Plasmas*, 12:62309, 2005.

[45] H. Goldstein, C. Poole, and J. Safko. *Classical Mechanics*. Addison Wesley, 2002.

[46] T. S. Hahm. Nonlinear gyrokinetic equations for turbulence in core transport barriers. *Phys. Plasmas*, 3(12):4658–4664, 1996.

[47] T. S. Hahm, W. W. Lee, and A. Brizard. Nonlinear gyrokinetic theory for finite-beta plasmas. *Physics of Fluids*, 31(7):1940–1948, 1988.

[48] T. S. Hahm, Lu Wang, and J. Madsen. Fully electromagnetic nonlinear gyrokinetic equations for tokamak edge turbulence. *Physics of Plasmas*, 16(2):022305, 2009.

[49] T.S. Hahm. Nonlinear gyrokinetic equations for tokamak microturbulence. *Phys. Fluids*, 31(9):2680, 1988.

[50] T.S. Hahm. private communication, 2008.

[51] F. L. Hinton and C. W. Horton. Amplitude limitation of a collisional drift wave instabillity. *Phys. Fluids*, 14(1):116, 1971.

[52] John David Jackson. *Classical Electrodynamics*. Number 20 August 2009. John Wiley and Sons, 1998.

[53] Noam Katz, Jan Egedal, Will Fox, Ari Le, and Miklos Porkolab. Experiments on the propagation of plasma filaments. *Phys. Rev. Lett.*, 101(1):015003, Jul 2008.

[54] Allan N. Kaufman. The electric dipole of a guiding center and the plasma momentum density. *Physics of Fluids*, 29(5):1736–1737, 1986.

[55] G. Kawamura and A. Fukuyama. Refinement of the gyrokinetic equations for edge plasmas with large flow shears. *Physics of Plasmas*, 15(4):042304, 2008.

[56] A. Kirk, H. R. Wilson, G. F. Counsell, R. Akers, E. Arends, S. C. Cowley, J. Dowling, B. Lloyd, M. Price, and M. Walsh. Spatial and temporal structure of edge-localized modes. *Phys. Rev. Lett.*, 92(24):245002, Jun 2004.

[57] L. D. Landau and E. M. Lifschitz. *Classical Mechanics*, volume 1. Pergamon Press, 3 edition, 1976.

[58] W. W. Lee. Gyrokinetic approach in particle simulation. *Phys. Fluids*, 26(2):556, 1983.

[59] Robert G. Littlejohn. Hamiltonian formulation of guiding center motion. *Phys. Fluids*, 24(9):1730, 1981.

[60] Robert G. Littlejohn. *J.Math. Phys*, 23(5):742, 1982.

[61] Robert G. Littlejohn. Variational principles of guiding center motion. *Journal of Plasma Physics*, 20:111–125, 1983.

[62] Robert G. Littlejohn. Geometry and guiding center motion. *Contemporary Mathematics*, 28:151, 1984.

[63] Robert G. Littlejohn. Phase anholonomy in the classical motion of charged particles. *Physical Review A*, 38(12):6034–6045, 1988.

[64] F.E. Low. A Lagrangian formulation of the Boltzmann-Vlasov equation for plasmas. *Proceedings of the Royal Society of London. Series A, Mathematical and Physical Sciences*, 248(1253):282–287, 1958.

[65] Jens Madsen. Second order guiding-center vlasov–maxwell equations. *Physics of Plasmas*, 17(8):082107, 2010.

[66] A. Mishchenko and A. Könies. A many-particle approach to the gyrokinetic theory. *Journal of Plasma Physics*, 73:757–772, October 2007.

[67] Alexey Mishchenko, Roman Hatzky, and Axel Könies. Conventional delta f-particle simulations of electromagnetic perturbations with finite elements. *Physics of Plasmas*, 11(12):5480–5486, 2004.

[68] Naoaki Miyato, Bruce D. Scott, Dafni Strintzi, and Shinji Tokuda. A modification of the guiding-centre fundamental 1-form with strong $\mathbf{E} \times \mathbf{B}$ flow. *Journal of the Physical Society of Japan*, 78(10):104501, 2009.

[69] A. I. Morozov and L. S. Solov'ev. Motion of charged particles in electromagnetic fields. *Reviews of Plasma Physics*, 2:201, 1966.

[70] R. A. Moyer, K. H. Burrell, T. N. Carlstrom, S. Coda, R. W. Conn, E. J. Doyle, P. Gohil, R. J. Groebner, J. Kim, R. Lehmer, W. A. Peebles, M. Porkolab, C. L. Rettig, T. L. Rhodes, R. P. Seraydarian, R. Stockdale, D. M. Thomas, G. R. Tynan, and J. G. Watkins. Beyond paradigm: Turbulence, transport, and the origin of the radial electric field in low to high confinement mode transitions in the diii-d tokamak. *Physics of Plasmas*, 2(6):2397–2407, 1995.

[71] V. Naulin. Turbulent transport and the plasma edge. *JOURNAL OF NUCLEAR MATERIALS*, 363:24–31, JUN 15 2007. 17th International Conference on Plasma-Surface Interactions in Controlled Fusion Devices, Hefei, PEOPLES R CHINA, MAY 22-26, 2006.

[72] V. Naulin. Turbulent transport and the plasma edge. *Journal of Nuclear Materials*, 363-365:24–31, 2007. Plasma-Surface Interactions-17.

[73] T. G. Northrop. *The Adiabatic Motion of Charged Particles*. Interscience, 1963.

[74] I. Nunes, M. Manso, F. Serra, L.D. Horton, G.D. Conway, A. Loarte, the ASDEX Upgrade, and CFN Reflectometry Teams. Density profile analysis during an elm event in asdex upgrade h-modes. *Nuclear Fusion*, 45(12):1550–1556, 2005.

[75] G. Van Oost et al. Multi-machine studies of the role of turbulence and electric fields in the establishment of improved confinement in tokamak plasmas. *Plasma Physics and Controlled Fusion*, 49:A29–A44, 2007.

[76] D. Pfirsch. New variational formulation of Maxwell-Vlasov and guiding center theories local charge and energy conservation laws. *Zeitschrift Naturforschung Teil A*, 39:1–8, January 1984.

[77] D. Pfirsch and P. J. Morrison. Local conservation laws for the Maxwell-Vlasov and collisionless kinetic guiding-center theories. *Phys. Rev. A*, 32(3):1714–1721, Sep 1985.

[78] H. Qin, R. H. Cohen, W. M. Nevins, and X. Q. Xu. Geometric gyrokinetic theory for edge plasmas. *Physics of plasmas*, 14:056110, 2007.

[79] H. Qin, W. M. Tang, W. W. Lee, and G. Rewoldt. Gyrokinetic perpendicular dynamics. *Phys. Plasmas*, 6(5):1575, 1999.

[80] M Reich, E Wolfrum, J Schweinzer, H Ehmler, L D Horton, J Neuhauser, and ASDEX Upgrade Team. Lithium beam charge exchange diagnostic for edge ion temperature measurements at the asdex upgrade tokamak. *Plasma Physics and Controlled Fusion*, 46(5):797–808, 2004.

[81] B. W. Rice, D. G. Nilson, K. H. Burrell, and L. L. Lao. Simultaneous measurement of q and e[sub r] profiles using the motional stark effect in high-performance diii-d plasmas (invited). *Review of Scientific Instruments*, 70(1):815–820, 1999.

[82] Rogers and Drake. Enhancement of turbulence in tokamaks by magnetic fluctuations. *Physical Review Letters*, 79(2):229–232, 1997.

[83] D L Rudakov, J A Boedo, R A Moyer, S Krasheninnikov, A W Leonard, M A Mahdavi, G R McKee, G D Porter, P C Stangeby, J G Watkins, W P West, D G Whyte, and G Antar. Fluctuation-driven transport in the diii-d boundary. *Plasma Physics and Controlled Fusion*, 44(6):717, 2002.

[84] P. H. Rutherford and E. A. Frieman. Drift instabilities in general magnetic field configurations. *Physics of Fluids*, 11(3):569–585, 1968.

[85] B Scott. Three-dimensional computation of drift alfvén turbulence. *Plasma Physics and Controlled Fusion*, 39(10):1635, 1997.

[86] B. Scott. The geodesic transfer effect on zonal flows in tokamak edge turbulence. *Physics Letters A*, 320(1):53–62, 2003.

[87] Bruce D Scott. Computation of electromagnetic turbulence and anomalous transport mechanisms in tokamak plasmas. *Plasma Physics and Controlled Fusion*, 45(12A):A385–A398, 2003.

[88] Bruce D. Scott. Free-energy conservation in local gyrofluid models. *Phys. Plasmas*, 12:102307, 2005.

[89] Bruce D. Scott. Nonlinear polarization and dissipative correspondence between low-frequency fluid and gyrofluid equations. *Physics of Plasmas*, 14(10):102318, 2007.

[90] Philippe L. Similon. Conservation laws for relativistic guiding-center plasma. *Physics Letters*, 112A(1,2):33–37, October 1985.

[91] Murray R. Spiegel and John Liu. *Schaum's Mathematical Handbook of Formulas and Tables*. Schaum Outlines. McGraw-Hill, 1999.

[92] H. Sugama. Gyrokinetic field theory. *Phys. Plasmas*, 7(2):466, 2000.

[93] J.L. Terry, N.P. Basse, I. Cziegler, M. Greenwald, O. Grulke, B. LaBombard, S.J. Zweben, E.M. Edlund, J.W. Hughes, L. Lin, Y. Lin, M. Porkolab, M. Sampsell, B. Veto, and S.J. Wukitch. Transport phenomena in the edge of alcator c-mod plasmas. *Nuclear Fusion*, 45(11):1321–1327, 2005.

[94] J.L. Terry, S.J. Zweben, K. Hallatschek, and B. LaBombard. Observations of the turbulence in the scrape-off-layer of alcator c-mod and comparisons with simulation. *Phys. Plasmas*, 10(5):1739, 2003.

[95] K. Uehara, T. Kawakami, H. Amemiya, K. Höthker, A. Cosler, and W. Bieger. Measurements of ion temperature and flow velocity using symmetric and asymmetric double probes in the boundary plasma of the jft-2m tokamak. *Nuclear Fusion*, 38(11):1665–1674, 1998.

[96] F. Wagner, G. Becker, K. Behringer, D. Campbell, A. Eberhagen, W. Engelhardt, G. Fussmann, O. Gehre, J. Gernhardt, G. v. Gierke, G. Haas, M. Huang, F. Karger, M. Keilhacker, O. Klüber, M. Kornherr, K. Lackner, G. Lisitano, G. G. Lister, H. M. Mayer, D. Meisel, E. R. Müller, H. Murmann, H. Niedermeyer, W. Poschenrieder, H. Rapp, H. Röhr, F. Schneider, G. Siller, E. Speth, A. Stäbler, K. H. Steuer, G. Venus, O. Vollmer, and Z. Yü. Regime of improved confinement and high beta in neutral-beam-heated divertor discharges of the asdex tokamak. *Phys. Rev. Lett.*, 49(19):1408–1412, Nov 1982.

[97] A.S. Wan, B. Lipschultz, F.S. McDermott, and J.L. Terry. The effect of icrf on the alcator c scrape-off layer plasma. *Journal of Nuclear Materials*, 162-164:292–299, 1989.

[98] F. W. Warner. *Foundations of Differentiable Manifolds and Lie Groups*, volume 94 of *Graduate texts in mathematics*. Springer-Verlag, 1994.

[99] B Weyssow and R. Balescu. Hamiltonian theory of guiding centre motion revisited. *J. Plasma Phys.*, 35:449, 1986.

[100] H.K. Wimmel. Kinetic guiding-center equations for the theory of drift instabilities an anomalous transport. *Physica Scripta*, 29:141–145, 1984.

[101] Inc. Wolfram Research. Mathematica edition: Version 5.0.

[102] Inc. Wolfram Research. *Mathematica Edition: Version 5.0*. Wolfram Research, Inc., 2003.

[103] A.J. Wooton, B.A. Carreras, and H. Matsumoto. Fluctuations and anomalous transport in tokamaks. *Phys. Fluids B*, 2(12):2879, 1989.

[104] G. S. Xu, V. Naulin, W. Fundamenski, J. Juul Rasmussen, A. H. Nielsen, and B. N. Wan. Intermittent convective transport carried by propagating electromagnetic filamentary structures in nonuniformly magnetized plasma. *Physics of Plasmas*, 17(2):022501, 2010.

[105] Huanchun Ye and Allan N. Kaufman. Self-consistent theory for ion gyroresonance. *Physics of Fluids B: Plasma Physics*, 4(7):1735–1753, 1992.

[106] Huanchun Ye and P.J. Morrison. Action principles for the Vlasov equation. *Phys. Fluids B.*, 4:771–777, 1992.

[107] L Zeng, G Wang, E J Doyle, T L Rhodes, W A Peebles, G R McKee, R Fonck, K H Burrell, M E Fenstermacher, J Boedo, and R Moyer. Dynamics of pedestal perturbations by elms and edge harmonic oscillations in diii-d. *Plasma Physics and Controlled Fusion*, 46(5A):A121–A129, 2004.

[108] Fulvio Zonca, Liu Chen, J. Q. Dong, and Robert A. Santoro. Existence of ion temperature gradient driven shear alfv[e-acute]n instabilities in tokamaks. *Physics of Plasmas*, 6(5):1917–1924, 1999.

[109] S. J. Zweben, D. P. Stotler, and J. L. Terry et al. *Phys. Plasmas*, 9:1981, 2002.

Appendix A

Appendix

A.1 Hamiltonian mechanics and symplectic geometry

In this appendix we give a resume of Hamiltonian mechanics formulated on a symplectic manifold. This presentation is focused on results. No proofs (almost) are given. The level of mathematical rigor is that of a (lazy) physicist. For a more concise presentation I strongly recommend the book: "The Geometry of Physics", by Theodore Frankel[39].

A.1.1 Poincaré one-form, symplectic two-form

First, we introduce some definitions. Let M denote the configuration space of a mechanical system , equipped with local coordinates q_i. The $2n$ dimensional phase space, i.e.. the cotangent bundle T^*M, has local *canonical* coordinates $q_1, ..., q_n, p_1, ..., p_n$. On T^*M we define the oneform

$$\hat{\gamma} = p_i dq_i, \tag{A.1}$$

and the symplectic two form (anti-symmetric two-tensor)

$$\omega = d\hat{\gamma} = dp_i \wedge dq_i, \tag{A.2}$$

where d denotes the exterior derivative. For a mechanical system we require that ω is nonsingular. Also from the definition we note that ω is closed, i.e.. $d\omega = 0$. In canonical coordinates ω can be written as

$$\omega = dp_i \wedge dq_i = \frac{\partial p_i}{\partial z_l}\frac{\partial q_i}{\partial z_m} dz_l \wedge dz_m, \tag{A.3}$$

thus the we identify the two form coordinate function as

$$\omega_{lm} = \frac{\partial p_i}{\partial z_l}\frac{\partial q_i}{\partial z_m}. \tag{A.4}$$

In arbitrary coordinates the Poincaré oneform can be written as

$$\hat{\gamma} = p_i dq_i = p_i \frac{\partial p_i}{\partial z_l} dz_l = \hat{\gamma}_l dz_l, \tag{A.5}$$

and the two-form

$$\omega = d(\hat{\gamma} dz_l) = \frac{\partial \hat{\gamma}_l}{\partial z_m} dz_m \wedge dz_l, \tag{A.6}$$

thus the lm entry in corresponding matrix Ω is

$$\Omega_{lm} = \frac{\partial \hat{\gamma}_m}{\partial z_l} - \frac{\partial \hat{\gamma}_l}{\partial z_m}. \tag{A.7}$$

Ω is the matrix of the *Lagrange bracket*.

A.1.2 Poisson brackets

The non-singularity of ω uniquely associates a vector field X_f to each function f on T^*M in the following way

$$\omega(X_f, \cdot) = -df. \tag{A.8}$$

X_f can be written in local coordinates z_i as

$$X_{f\,l} \frac{\partial}{\partial z_l} = -\Omega^{-1}_{lm} \frac{\partial f}{\partial z_m} \frac{\partial}{\partial z_l}, \tag{A.9}$$

where Ω^{-1} is the inverse coordinate matrix of the symplectic two form. The *Hamiltonian vector field*

$$\omega(X_H, \cdot) = -dH, \tag{A.10}$$

is defined in this way and the Hamiltonian (time independent) is constant along X_H

$$X_H(H) = dH(X_H) = -\omega(X_H, X_H) = 0. \tag{A.11}$$

The time evolution of a function f is therefore found to be (see Frankel p.148)

$$\dot{f} = \{f, H\} = -\omega(X_f, X_H) = i_{X_f} \circ i_{X_H} \circ \omega, \tag{A.12}$$

and the Poisson bracket is defined as

$$\{f, g\} = -\omega(X_f, X_g). \tag{A.13}$$

Given arbitrary local coordinates (z_i) the Poisson bracket can be written in matrix form in the following way using (A.9)

$$\{f, g\} = -\omega(X_f, X_g) = i_{X_f} \circ i_{X_g} \circ \omega = \Omega^{-1}_{mn} \frac{\partial f}{\partial z_m} \frac{\partial g}{\partial z_n} \tag{A.14}$$

From (A.8) it follows that the equations of motion can be written in terms of the Poincaré oneform. Written in local coordinates the vector field induced by ω reads

$$\begin{aligned} -dz_l = \omega(X_{z_l}, \cdot) &= \frac{\partial \gamma_k}{\partial z_m} dz_m \wedge dz_k(X_{z_{l_i}} \frac{\partial}{\partial z_i}, \cdot) \\ &= \frac{\partial \gamma_k}{\partial z_m} \delta_{mi} dz_k X_{z_{l_i}} - \frac{\partial \gamma_k}{\partial z_m} \delta_{ki} dz_m X_{z_{l_i}} \\ &= X_{z_{l_i}} (\frac{\partial \gamma_k}{\partial z_i} - \frac{\partial \gamma_i}{\partial z_k}) dz_k, \end{aligned} \tag{A.15}$$

thus $X_{z_l} = \Omega^{-1}_{li} \frac{\partial}{\partial z_i}$ and similarly the Hamiltonian vector field in local is given in local coordinates as

$$X_H = -\Omega^{-1}_{nm} \frac{\partial H}{\partial z_m} \frac{\partial}{\partial z_n}, \tag{A.16}$$

such that the equation of motion in local coordinates is

$$\dot{z}_l = i_{X_{z_l}} \circ i_{X_H} \circ \omega = -dz_l(X_H) = \Omega^{-1}_{lm} \frac{\partial H}{\partial z_m}. \tag{A.17}$$

This can be written in an even more fancy notation

$$\mathcal{L}_{X_H} z_l = X_H(z_l) = X_{Hn} \frac{\partial}{\partial z_n} z_l = \Omega^{-1}_{ln} \frac{\partial H}{\partial z_n}., \tag{A.18}$$

where $\mathcal{L}_{X_H}$ denotes the Lie derivative along the vector field X_H, which when acting on functions is nothing but the directional derivative as in the equation above. The Lie derivative can be viewed as a generalization of the directional derivative and is defined on tensors and differential forms.

A.1.3 Equations of motion from a variational approach

Now we show that the Poincaré oneform and the symplectic twoform naturally arise from a variational principle. The Poincaré one-form on $T^*M \times \mathbb{R}$ in local coordinates is defined as

$$\gamma = p_i dq_i - H(q,p,t)dt = p_i \frac{\partial q_i}{\partial z_l} dz_l - H dt = \hat{\gamma}_l dz_l - H(z,t)dt. \tag{A.19}$$

We seek the curve in $T^*M \times \mathbb{R}$ that provides us with an extremum(minimum) of the functional, the action

$$S = \int \gamma, \tag{A.20}$$

provided that the variations of (z_i, t) vanishes at the endpoints. A variation of the action S reads

$$\begin{aligned}\delta S &= \int \delta\gamma_l dz_l + \gamma_l \delta dz_l - \delta H dt - H\delta dt \\ &= \int \delta z_m \frac{\partial \gamma_l}{\partial z_m} dz_l - \frac{\partial \gamma_l}{\partial z_m} dz_m \delta z_l - \frac{\partial \gamma_l}{\partial t} dt \delta z_l + d(\gamma_l \delta z_l) - \delta z_m \frac{\partial H}{\partial z_m} dt \\ &= \int \delta z_m \Big\{ (\frac{\partial \gamma_l}{\partial z_m} - \frac{\partial \gamma_m}{\partial z_l}) dz_l - \frac{\partial \gamma_m}{\partial t} dt - \frac{\partial H}{\partial z_m} dt \Big\}. \end{aligned} \tag{A.21}$$

thus for arbitrary variations δz and δt vanishing at the endpoints we obtain the equations of motion when $\delta S = 0$

$$\begin{aligned}&\frac{dz_l}{dt}\omega_{ml} - \frac{\partial \gamma_m}{\partial t} - \frac{\partial H}{\partial z_m} = 0 \Rightarrow \\ &\frac{dz_l}{dt}\omega_{ml}\omega^{-1}_{im} = \frac{dz_i}{dt} = \omega^{-1}_{im}\big(\frac{\partial \gamma_m}{\partial t} + \frac{\partial H}{\partial z_m}\big) = \{z_i, z_m\}\frac{\partial \gamma_m}{\partial t} + \{z_i, H\}. \end{aligned} \tag{A.22}$$

The physicists notion of *extended phasespace* is a little different from the mathematical definition. In many text physicists texts on Hamiltonian mechanics extended phasespace refer to an actual extension of the phasespace by an energy like variable h conjugated to the time coordinate t. In this extended phasespace the time coordinate is treated on equal footing with the other coordinates. The energy coordinate h is taken to the value of the Hamiltonian H such that the dynamical evolution take place on the subspace $H - h = 0$. The time evolution is then parametrized by an unphysical parameter τ. The Poincaré oneform in this formalism is then defined as

$$\gamma^E = \gamma_i dz_i - h dt - (H - h) d\tau = \gamma^E_a dz_a - \mathcal{H} d\tau. \tag{A.23}$$

A variation of the corresponding action gives

$$\begin{aligned}\delta S &= \int \frac{\partial \gamma^E_a}{\partial z_b} \delta z_b dz_a - \frac{\partial \gamma^E_a}{\partial z_b} dz_b \delta z_a - \frac{\partial \mathcal{H}}{\partial z_a} \delta z_a d\tau \\ &= \int \delta z_b \Big((\frac{\partial \gamma^E_a}{\partial z_b} - \frac{\partial \gamma^E_b}{\partial z_a}) dz_a - \frac{\partial \mathcal{H}}{\partial z_b} d\tau \Big) \end{aligned} \tag{A.24}$$

which for arbitrary variations vanishing at the endpoints imply the equations of motion

$$\frac{dz_a}{d\tau}\omega^E_{ba}\omega^{E-1}_{cb} = \frac{dz_c}{d\tau} = \omega^{E-1}_{cb}\frac{\partial \mathcal{H}}{\partial z_b} = \{z_c, \mathcal{H}\}_E, \tag{A.25}$$

This demonstrates the advantage of the physicists extended phasespace formalism because we are able to write the equation of motion simply by inverting the coordinate matrix of the corresponding symplectic two-form. If we write out this result explicitly (i,j,l are from 1..6 and a,b,c are 1..6 plus t

and h) we obtain the equation of motion of the time coordinate by choosing $b = h$ in (A.25)

$$\frac{\partial \gamma_a^E}{\partial h} dz_a - \frac{\partial \mathcal{H}}{\partial h} d\tau = 0 \rightarrow \frac{\partial t}{\partial \tau} = 1, \tag{A.26}$$

showing that the curve parameter equals the real time up to a constant. Now choosing $z_b = z_i$ we get

$$\begin{aligned} (\frac{\partial \gamma_a^E}{\partial z_i} - \frac{\partial \gamma_i}{\partial z_a}) dz_a - \frac{\partial \mathcal{H}}{\partial z_i} d\tau = \\ -\frac{\partial \gamma_i}{\partial t} dt + (\frac{\partial \gamma_j}{\partial z_i} - \frac{\partial \gamma_i}{\partial z_j}) dz_j - \frac{\partial H}{\partial z_i} d\tau = 0 \Rightarrow \\ \frac{dz_j}{dt} \omega_{ij} = \frac{\partial \gamma_i}{\partial t} + \frac{\partial H}{\partial z_i} \end{aligned} \tag{A.27}$$

showing that the extended phasespace formalism leads to the same equations of motion as in the usual phasespace (A.22).

These manipulations demonstrate advantages of this modern formalism. From the Poincaré oneform we can deduce the two-form which is in fact the Lagrange brackets, the Poisson brackets and therefore the equations of motion and lastly we obtain the equations of motion by defining the action from the Poincaré oneform. Also, as we show in the next section, the symplectic two-form equips the phasespace with a volumeform from which the volume element, the determinant of the Jacobian, can be obtained. In some sense having the oneform and you have all the information you need.

A.1.4 Liouville and Vlasov

It can be shown that the symplectic two form ω on a $2n$ dimensional manifold M, defines a $2n$ volume form ω^n on M[39]. In local coordinates the coordinate function of the volume form equals the determinant of the Jacobian of a coordinate transformation going from canonical coordinates to arbitrary coordinates $(z_1, \cdots, z_{2n})$

$$\omega^n = \rho dz_1 \wedge \cdots \wedge dz_{2n} = \mathrm{Det}(\frac{\partial q, p}{\partial z}) dz_1 \wedge \cdots \wedge dz_{2n}. \tag{A.28}$$

First, lets establish that the symplectic twoform is constant along a Hamiltonian flow

$$\mathcal{L}_{\boldsymbol{X_H}} \omega = (i_{\boldsymbol{X}_H} \circ d + d \circ i_{\boldsymbol{X}_H}) \omega = i_{\boldsymbol{X}_H} \circ d^2 \omega - d \circ dH = 0 \tag{A.29}$$

The Lie derivative is distributive so we get

$$\mathcal{L}_{\boldsymbol{X_H}} \omega^n = 0. \tag{A.30}$$

The "coordinate" function of ω^n is ρ. This expression can be rewritten

$$\begin{aligned}\mathcal{L}_{\boldsymbol{X_H}}\omega^n &= d\circ i_{\boldsymbol{X}_H}\omega^n \\ &= d\sum_r(-1)^{r-1}\rho dz_1\wedge dz_2\wedge\cdots\wedge i_{\boldsymbol{X}_H}dz_r\wedge\cdots\wedge dz_{2n} \\ &= d\sum_r(-1)^{r-1}\rho X_{H_r}dz_1\wedge dz_2\wedge\cdots\wedge\widehat{dz_r}\wedge\cdots\wedge dz_{2n} \\ &= \sum_r(-1)^{r-1}\frac{\partial(\rho X_{H_r})}{\partial z_l}dz_l\wedge dz_1\wedge dz_2\wedge\cdots\wedge\widehat{dz_r}\wedge\cdots\wedge dz_{2n} \\ &= \sum_r\frac{\partial(\rho X_{H_r})}{\partial z_l}dz_1\wedge dz_2\wedge\cdots\wedge dz_r\wedge\cdots\wedge dz_{2n} \qquad (A.31)\end{aligned}$$

starting out from canonical coordinates $(y_1,\cdots,y_{2n})$ the volume form reads $\omega_c^n = dy_1\wedge\cdots\wedge dy_{2n}$. Changing variables

$$\begin{aligned}\omega_c^n &= dy_1\wedge\cdots\wedge dy_{2n} \\ &= \mathrm{Det}(\frac{\partial y}{\partial z})dz_1\wedge\cdots\wedge dz_{2n} \\ &= \rho dz_1\wedge\cdots\wedge dz_{2n} \qquad (A.32)\end{aligned}$$

So what we in fact have proven is (see eq. A.17)

$$\frac{\partial}{\partial z_a}(\rho\dot{z}_a) = 0, \qquad (A.33)$$

the Liouville theorem.

A.2 Lie transform

In this appendix we give a short introduction to the Lie transform method. Throughout this section d denotes the differential (pushforward) and δ denotes pullback[98]. I am not a mathematician so do not expect mathematical rigor. A good introduction to differential geometry is the book "The Geometry of Physics", written by T. Frankel[39].

Let $m\in M$ be a point in the $2n$ dimensional differentiable manifold M and let x be a coordinate map(chart) defined in a neighborhood around m. Let $G\in\mathbb{R}^{2n}_{\boldsymbol{x}(m)}$ be the vector field that generates the coordinate transformation. Notice, that the vectorfield is not in the tangentbundle as we want to change coordinates. We want to obtain new coordinates $\boldsymbol{y}$ by the going along the flow of G for a fixed time ϵ

$$y = \phi^\epsilon(x). \qquad (A.34)$$

Where the flow $\phi^\epsilon(x)$ along G is defined by

$$\frac{d}{d\epsilon}\phi(\epsilon,x) = G(y). \qquad (A.35)$$

In general a function $f \in C^\infty(\mathbb{R}^{2n})$ transforms in local coordinates under a coordinate transformation $x \to y$ as

$$f(x) = f(\phi^{-\epsilon}(y)) = F(y). \tag{A.36}$$

Thus

$$\frac{d}{d\epsilon}F(y(x,\epsilon)) = \frac{\partial f}{\partial x_i}\frac{\partial \phi^{-\epsilon}}{\partial \epsilon} = -\boldsymbol{G}(f). \tag{A.37}$$

We formally Taylor expand F around $\epsilon = 0$

$$\begin{aligned} F(y(x,\epsilon))\Big|_{y,xfixed} =& F(\epsilon) = \sum_n \frac{\epsilon^n}{n!}\frac{\partial^n F}{\partial \epsilon^n}\Big|_{\epsilon=0} \\ =& \exp(-\epsilon G) f(\phi^{-\epsilon}(y))\Big|_{\epsilon=0} = \exp(-\epsilon \mathcal{L}_G) f(y). \end{aligned} \tag{A.38}$$

The vectorfield is therefore the generator of the coordinate transformation. Similarly, a vectorfield $v \in T(\mathbb{R}^{2n})$ transforms according to

$$v_x = v_i \frac{\partial}{\partial x_i} = v(\phi^{-\epsilon}(y))\frac{\partial y_j}{\partial x_i}\frac{\partial}{\partial y_j} = V_j(y)\frac{\partial}{\partial y_j} = V_y = d\phi^{-\epsilon}(V_{\phi^\epsilon(x)}), \tag{A.39}$$

thus

$$\frac{d}{d\epsilon}\Big|_{\epsilon=0} V = \frac{d}{d\epsilon}\Big|_{\epsilon=0} d\phi^{-\epsilon}(V_{\phi^\epsilon(x)}) = \mathcal{L}_G V, \tag{A.40}$$

where $\mathcal{L}_G V$ denotes the Lie derivative of the vector V along G. The last equality is in fact the "official" definition of the Lie derivative of V along G[98]. Actually, the Lie derivative of a function f along a vectorfield G is simply the directional derivative $G(f) = \mathcal{L}_G(f)$, so the transformation of a function (A.38) can be expressed in terms of the Lie derivative. Again, we formally Taylor expand V around $\epsilon = 0$

$$V(y) = \sum_n \frac{\epsilon^n}{n!}\frac{\partial^n V}{\partial \epsilon^n}\Big|_{\epsilon=0} = \exp(\epsilon \mathcal{L}_G) v(x). \tag{A.41}$$

We can apply the same procedure to a differential oneform $\omega \in T^*(\mathbb{R}^{2n})$, which transforms as

$$\omega(x) = \omega(\phi^{-\epsilon}(y)) = \Omega(y). \tag{A.42}$$

Evaluated on a vector $v \in T_x(\mathbb{R}^{2n})$ and a function $f \in C^\infty(\mathbb{R}^{2n})$ we get

$$\begin{aligned} \omega(x)(v)(f) =& \omega(\phi^{-\epsilon}(y))(v)(f) = \omega(\phi^{-\epsilon}(y)(v)(f) \\ =& \omega(\phi^{-\epsilon}(y))(v(f(\phi^{-\epsilon}(y))) = \delta\phi^{-\epsilon}(\omega_{\phi^{-\epsilon}(y)})(v)(f), \end{aligned} \tag{A.43}$$

and therefore

$$\frac{d}{d\epsilon}\Big|_{\epsilon=0}\Omega(y) = \frac{d}{d\epsilon}\Big|_{\epsilon=0}\delta\phi^{-\epsilon}(\omega_{\phi^{-\epsilon}(y)}) = \mathcal{L}_{-G}\omega(x) = -\mathcal{L}_G\omega(x), \tag{A.44}$$

where the last equality holds because the Lie derivative is a derivation. We formally Taylor expand the expression

$$\Omega(y) = \sum_n \frac{\epsilon^n}{n!} \frac{\partial^n \Omega}{\partial \epsilon^n}\Big|_{\epsilon=0} = \exp(-\epsilon \mathcal{L}_G)\omega(x). \tag{A.45}$$

These definitions are practical because once the transformation is defined we automatically know how various geometric objects are transformed. In practical applications it turns out that it more flexible to carry out a series[35, 25] of Lie transformations

$$y = \prod_{i=1}^{\infty} \exp(-\epsilon^i \mathcal{L}_{G_i})x. \tag{A.46}$$

Applying this to the a oneform we obtain the hierachy used throughout this thesis

$$\Gamma_0 = \gamma_0 + dS_0, \tag{A.47a}$$
$$\Gamma_1 = \gamma_1 - \mathcal{L}_{\boldsymbol{G_1}}\gamma_0 + dS_1, \tag{A.47b}$$
$$\Gamma_2 = \gamma_2 - \mathcal{L}_{\boldsymbol{G}_1}\gamma_1 + \frac{1}{2}\mathcal{L}^2_{\boldsymbol{G}_1}\gamma_0 - \mathcal{L}_{\boldsymbol{G}_2}\gamma_0 + dS_2, \tag{A.47c}$$
$$\Gamma_3 = \gamma_3 - \frac{1}{6}\mathcal{L}^3_{\boldsymbol{G}_1}\gamma_0 + \frac{1}{2}\mathcal{L}^2_{\boldsymbol{G}_1}\gamma_1 - \mathcal{L}_{\boldsymbol{G}_1}\gamma_2 - \mathcal{L}_{\boldsymbol{G}_2}\gamma_1 - \mathcal{L}_{\boldsymbol{G}_3}\gamma_0 + dS_3. \tag{A.47d}$$

The amount of work can be substancially reduced by inserting lower order identities into the higher order ones

$$\Gamma_0 = \gamma_0 + dS_0, \tag{A.48a}$$
$$\Gamma_1 = \gamma_1 - \mathcal{L}_{\boldsymbol{G_1}}\gamma_0 + dS_1, \tag{A.48b}$$
$$\Gamma_2 = \gamma_2 - \mathcal{L}_{\boldsymbol{G}_2}\gamma_0 - \frac{1}{2}\mathcal{L}_{\boldsymbol{G}_1}(\gamma_1 + \Gamma_1) + dS_2, \tag{A.48c}$$
$$\Gamma_3 = \gamma_3 - \mathcal{L}_{\boldsymbol{G}_1}\gamma_2 - \mathcal{L}_{\boldsymbol{G}_3}\gamma_0 - \mathcal{L}_{\boldsymbol{G}_2}\Gamma_1 + \frac{1}{3}\mathcal{L}^2_{\boldsymbol{G}_1}(\gamma_1 + \frac{1}{2}\Gamma_1) + dS_3. \tag{A.48d}$$

A.3 Gyroaverage in guiding-center theory

Here we consider the second order physical terms in the guiding-center oneform

$$\frac{m\mu}{2q}\hat{\boldsymbol{b}}(\hat{\boldsymbol{b}} \cdot \nabla \times \hat{\boldsymbol{b}}) \cdot d\boldsymbol{X} - \frac{m\mu}{2q}\hat{\boldsymbol{b}} \cdot \nabla \times \boldsymbol{D}dt \tag{A.49}$$

A definition of the curl operator is

$$\hat{\boldsymbol{b}} \cdot \nabla \times \boldsymbol{D}(\boldsymbol{X}) = \lim_{A \to 0} \frac{\oint_C \boldsymbol{D} \cdot d\boldsymbol{l}}{A} \tag{A.50}$$

where $C = \partial A$ is the positively oriented boundary curve of an arbitrary surface with area A.

Lets pick an specific curve $\boldsymbol{X} + \boldsymbol{\rho} = \boldsymbol{X} + \boldsymbol{\rho}(\boldsymbol{X}, \theta)$, inserting this into the definiton

$$\hat{\boldsymbol{b}} \cdot \nabla \times \boldsymbol{D}(\boldsymbol{X}) = \lim_{\rho \to 0} \frac{\int_0^{2\pi} \boldsymbol{D}(\boldsymbol{X} + \boldsymbol{\rho}) \cdot \frac{\partial \boldsymbol{\rho}}{\partial \theta} d\theta}{\rho^2 \pi} \tag{A.51}$$

we see that the terms resemble some sort of gyroaveraging.

Doing some algebra it turns out that($\frac{\partial}{\partial t}\boldsymbol{A} = 0$)

$$\hat{\boldsymbol{b}} \cdot \nabla \times \boldsymbol{D} = \frac{1}{B}\nabla_\perp^2 \phi + \nabla_\perp \phi \cdot \nabla B^{-1} + \frac{1}{B}\hat{\boldsymbol{b}} \cdot \nabla \hat{\boldsymbol{b}} \cdot \nabla_\perp \phi \tag{A.52}$$

where $\nabla_\perp^2 = \nabla \cdot \nabla_\perp$. The first term therefore describes the lowest order FLR correction to the electric potential, ie the fact that the potential changes along the gyroorbit. The second describes that the orbit radius changes during the orbit and the third term arise because the perpendicular plane is wiggling during the orbit because the direction of the magnetic field is changing. This expression is different from the "normal" one encountered in the gyrokinetic formalism. Here the spatial dependence of the gyroorbit through $(\boldsymbol{B}_0, \boldsymbol{E}_0)$ is neglected. This is somewhat natural because the gyroaverage is performed on quantities with small amplitudes but with short wavelengths $k_\perp \rho_i \sim 1$. This neglection is taking place when the generating function of the Lie transform S_1 is determined, but usually also when actually doing the gyroaverage. There the spatial dependence is usually neglected. Here I mean the n-point average method and the Bessel function representation. The n-point method averaged over a perfect "ring" whereas the Bessel function representation neglects the spatial depence of ρ in order to avoid a cumbersome convolution. Not saying that something is wrong with the gk gyroaverage. It is simply an integral over θ. The point is that as it stand it is different from the "true" average which follows the particle for one characteristic time period $\sim \Omega^{-1}$.

Instead we could try do define a gyroaverage which does not fix $\boldsymbol{X}$. A

gyroaverage that I should look something like (fixing $\mu = \text{const}$)

$$\langle \phi(\boldsymbol{x}) \rangle = \frac{\int_C ds\, \phi}{\int_C ds} = \frac{\int_0^{\Omega^{-1}} dt\, \phi(\boldsymbol{x}) \|\dot{\boldsymbol{x}}\|}{\int_0^{\Omega^{-1}} dt \|\dot{\boldsymbol{x}}\|}$$

$$= \frac{1}{\int_0^{\Omega^{-1}} dt \|\dot{\boldsymbol{\rho}}\|} \int_0^{2\pi} d\theta \frac{1}{2\pi\Omega(\boldsymbol{\rho})} \phi(\boldsymbol{\rho}(t))[c_\perp - \boldsymbol{G}(\boldsymbol{c}_\perp)]$$

$$= \frac{1}{\int_0^{\Omega^{-1}} dt \|\dot{\boldsymbol{\rho}}\|} \int_0^{2\pi} d\theta \frac{1}{2\pi} (\Omega^{-1}(0) + \boldsymbol{\rho} \cdot \nabla \Omega^{-1}(0))$$

$$[\phi(0) + \rho \cdot \nabla\phi(0) + \frac{1}{2}\boldsymbol{\rho}\boldsymbol{\rho} : \nabla\nabla\phi(0)]$$

$$c_\perp(0, \mu, \theta, t)(1 - \frac{B}{2}\rho \cdot \nabla B^{-1})$$

$$= \phi + \frac{B\rho^2}{4} \nabla B^{-1} \cdot \nabla_\perp \phi + \frac{\rho^2}{4} (\mathbf{1} - \hat{\boldsymbol{b}}\hat{\boldsymbol{b}}) : \nabla\nabla\phi = \phi + \hat{\boldsymbol{b}} \cdot \nabla \times \boldsymbol{D} \qquad \text{(A.53)}$$

where a Galilean transformation $y = x - Wt$ has been carried out.

Risø DTU is the National Laboratory for Sustainable Energy. Our research focuses on development of energy technologies and systems with minimal effect on climate, and contributes to innovation, education and policy. Risø has large experimental facilities and interdisciplinary research environments, and includes the national centre for nuclear technologies.

Risø DTU
National Laboratory for Sustainable Energy
Technical University of Denmark

Frederiksborgvej 399
PO Box 49
DK-4000 Roskilde
Denmark
Phone +45 4677 4677
Fax +45 4677 5688

www.risoe.dtu.dk